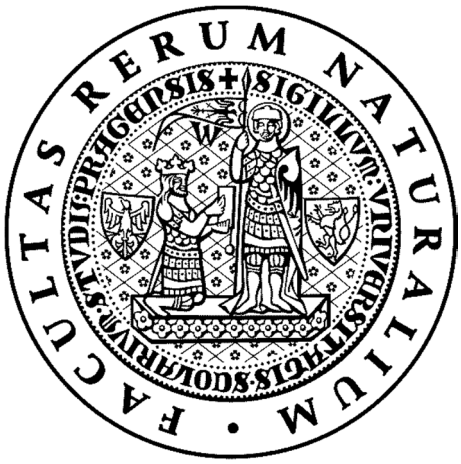
**Charles University in Prague**

**Faculty of Science**

Department of Physical chemistry

Ph.D. study program: Physical chemistry




**Adriana Bäumlová, MSc.**

# Struktura PI4-kinázy

# The crystal structure of PI4-kinase

DISSERTATION THESIS

Scientific Supervisor: Dr. Evžen Bouřa

Praha/Prague 2016

This dissertation describes my original work except where acknowledgement is made in the text. It is not substantially the same as any work that has been, or is being submitted to any other university for any degree, diploma or any other qualification.

Prague, 29. 4. 2016 …….....……..

Adriana Bäumlová, MSc.

# Acknowledgements

First and most I would like to thank my supervisor Evžen Bouřa for giving me an opportunity to work on this challenging and intriguing project. I am also grateful for his patient guidance during this project and provided help and support.

Special thanks belong to all my present and past colleagues for creating a friendly and warm-hearted atmosphere within the lab, for the coffee breaks that were full of fun and amusement and also for an unforgettable time spent together during lunch and our trips to Upa and the Synchrotron. Namely, I would like to thank Jan Tykvart for being my lab mentor during my time in the Konvalinka lab; Monika Sivá, Barbora Vorlová and Lucie Peclinovská for being more friends than colleagues and for cheering me up when needed; Anna Dubánková and Dominika Chalupská for dealing with problems with an extremely positive attitude and for making me laugh every day and finally to Martin Klíma and Jan Šilhán for their tremendous willingness to help and inspiring ideas. I am glad I could be a part of such an amazing collective.

Last but not least, I thank my family for their unceasing encouragement and support and to my boyfriend Juraj for his patience and care.

# Table of contents


1 Abstract ..... 5
2 Abstrakt ..... 7
3 Introduction ..... 9
3.1 Phosphoinositides ..... 9
3.1.1 Golgi complex ..... 10
3.1.1.1 Non-vesicular trafficking ..... 11
3.1.1.2 Vesicular trafficking ..... 12
3.1.2 Plasma membrane ..... 13
3.1.2.1 Signal transduction ..... 13
3.1.2.2 Endocytosis ..... 15
3.1.3 Endosomal trafficking ..... 15
3.1.4 Autophagy ..... 16
3.1.5 Pathogens and host phosphoinositides ..... 17
3.2 Human phosphatidylinositol 4-kinases (EC:2.7.1.67) ..... 19
3.2.1 PI4-kinase type IIIα (PI4K IIIα) ..... 20
3.2.1.1 Gene and protein isoforms ..... 20
3.2.1.2 Protein ..... 20
3.2.1.2.1 Localisation ..... 20
3.2.1.2.2 Structure ..... 21
3.2.1.2.3 Function ..... 22
3.2.2 PI4-kinase type IIIβ (PI4K IIIβ) ..... 25
3.2.2.1 Gene and protein isoforms ..... 25
3.2.2.2 Protein ..... 26
3.2.2.2.1 Localisation ..... 26
3.2.2.2.2 Structure ..... 26
3.2.2.2.3 Biological function ..... 28
3.2.3 PI4-kinases type II ..... 30
3.2.3.1 Gene and protein isoforms ..... 30
3.2.3.2 Protein ..... 31
3.2.3.2.1 Localisation ..... 31
3.2.3.2.2 Structure ..... 31
3.2.3.2.3 Function ..... 32
4 Aims of the study ..... 34
5 Publications ..... 35
5.1 The Crystal Structure of the Phosphatidylinositol 4-Kinase IIα ..... 36
5.2 The High-Resolution Crystal Structure of Phosphatidylinositol 4-Kinase IIβ and the Crystal Structure of Phosphatidylinositol 4-Kinase IIα Containing a Nucleoside Analogue Provide a Structural Basis for Isoform-Specific Inhibitor Design. ..... 38
5.3 Highly Selective Phosphatidylinositol 4-Kinase IIIβ Inhibitors and Structural Insight into Their Mode of Action ..... 49
6 Discussion ..... 61
6.1 Structural characterisation of PI4-kinases type II ..... 88
6.2 Highly selective PI4K IIIβ inhibitors ..... 91
7 Conclusion ..... 93
8 Abbreviations ..... 94

# 1 Abstract

Phosphatidylinositol 4-kinases (PI4K/PI4-kinases) catalyse the production of phosphatidylinositol 4-phosphate (PtdIns4P), the first step in the generation of higher phosphoinositides. PtdIns4P is an essential precursor in the production of second messengers, Ins(1,4,5)$P_3$ and diacylglycerol, in a receptor activated phospholipase C signalling pathway. Moreover, PtdIns4P itself regulates conserved compartment-specific biological processes, mainly via recruiting a broad spectra of effector proteins. Because PI4-kinases have a central position in PtdIns4P synthesis on a surface of intracellular membranes, they are implicated in a wide range of PtdIns4P-induced processes such as lipid transport and metabolism, intracellular trafficking processes and cargo sorting, membrane and cytoskeleton remodelling events, signal transduction and many others. In mammals, two types of PI4-kinases were identified: type II and type III. Both types do not bear high sequence similarity to each other and, therefore, they possess diverse biochemical properties. In order to elucidate their structural relationship to other lipid kinases, structural analysis is highly demanded. The structural characterisation of individual PI4-kinases could also clarify the catalytic mechanism of PtdIns4P synthesis. Furthermore, information about the architecture of the active site could provide the basis for isoform-specific inhibitor design that would be potentially important in human medicine since the selective blocking of enzymatic activity would eliminate phagocytic engulfment of several pathogenic bacteria or block replication of plus sense single strand RNA viruses (+RNA). Altogether, the structural characterisation of each of individual isoforms, preferably in complex with a regulatory molecule, was still not achieved. However, such structural information would help to elucidate structural aspects of fundamental biological processes and structural requirements for viral and pathogen replication.

The studies reported in this thesis provide the structural and functional characterisation of both type II PI4-kinases and PI4K IIIβ. The high-resolution crystal structures of individual isoforms revealed their overall fold and domain organisation and confirmed a bi-lobal character of the C-terminally localised catalytic domain in all three variants. Co-crystallization of PI4-kinases with physiological substrates defined the ATP binding pocket but no crystals were obtained in complex with inositol or inositol 1-phosphate. However, the binding cavity for phosphatidylinositol (PtdIns) was identified

based on docking and modelling. Interestingly, a new lateral hydrophobic pocked was found as a putative regulatory site in the case of the type II PI4-kinases. The overall fold of these proteins also confirmed the structural diversity between type II and III PI4-kinases. Whilst type III PI4-kinases are rather more similar to PI3-lipid kinases, type II PI4-kinases share higher similarity with protein kinases. The crystal structures in complex with potent isoform-specific inhibitors were also obtained. The structural details of the active site in complex with isoform-specific inhibitors helped us to fully understand the inhibition mechanism and provided information needed for specific drug design.

# 2 Abstrakt

Fosfatidylinositol 4-kinázy (PI4K/PI4-kinázy) katalyzují produkci fosfatidylinositol 4-fosfátu (PtdIns4P), první krok v tvorbě vyšších fosfoinositidů. Fosfatidylinositol 4-fosfát je esenciálním prekurzorem pro tvorbu druhých poslů, fosfatidylinositol(1,4,5)trifosfátu a diacylglycerolu, které vznikají v signalizační dráze zahájené receptorem aktivovanou fosfolipázou C. Kromě toho fosfatidylinositol 4-fosfát reguluje procesy specificky se odehrávající v buněčných kompartmentech a to prostřednictvím vazby širokého spektra efektorových molekul na membránu. Jelikož PI4-kinázy mají ústřední pozici v tvorbě fosfatidylinositol 4-fosfátu probíhající na povrchu intracelulárních membrán, jsou tímto způsobem zodpovědné za procesy zprostředkované fosfatidylinositol 4-fosfátem jako například transport lipidů a jejich metabolizmus, transportní procesy v buňce a řízení transportovaného nákladu, remodelace membrán a cytoskeletu, přenos signálu do buňky a mnoho jiných. U savců byly identifikovány dva druhy PI4-ináz: typu II a typu III. Tyto typy kináz si nejsou sekvenčně podobné, a proto mají odlišné biochemické vlastnosti. Abychom objasnili strukturní příbuznost PI4-ináz, je zapotřebí strukturní analýzy. Strukturní charakterizace jednotlivých PI4-kináz by taktéž umožnila objasnit mechanizmus katalýzy vzniku fosfatidylinositol 4-fosfátu. Informace o aktivním místě by navíc mohly být využity při navrhování inhibitorů specifických pro PI4-kinázy, což by mělo potenciální využití v medicíně. Selektivní blokování enzymové aktivity by totiž eliminovalo vstup patogenních bakterií fagocytózou a inhibovalo replikaci virů s pozitivní jednovláknovou RNA (+RNA). Strukturní charakterizace jednotlivých izoforem, přednostně v komplexu s její regulační molekulou, nebyla doposud provedena. Získané informace by přitom pomohly ozřejmit strukturní aspekty základních biologických dějů a rovněž by osvětlili strukturní nároky virů či bakteriálních patogenů pro jejich replikaci.

Studie popsané v této práci poskytují strukturní i funkční charakterizaci PI4-kináz typu II a PI4-kinázy IIIβ. Krystalové struktury jednotlivých forem objasnily celkové uspořádání molekul a organizaci jednotlivých domén a současně potvrdily přítomnost N a C laloku v C-terminální části katalytické domény u všech tří variant. Krystalizace PI4-kináz s fyziologickými substráty odhalila ATP vazebné místo, avšak krystaly v komplexu s inositolem a inositol 1-fosfátem se nepodařilo získat. Proto bylo vazebné místo pro fosfatidylinositol určeno na základe dokovacích studií a molekulárního modelování. Ve struktuře PI4-kináz typu II byla překvapivě objevena také nová laterální hydrofobní kapsa-potenciální regulační místo. Celkové uspořádaní u všech tří proteinů taktéž potvrdilo

strukturní odlišnosti mezi typem II a typem III PI4-kináz. Zatímco typ III PI4-kináz je mnohem víc podobný PI3-kinázám, typ II PI4-kináz se podobá protein kinázám. Kromě struktur PI4-kináz s ATP byly vyřešeny také krystalové struktury v komplexu s inhibitory specifickými pro dané kinázy. Strukturní detaily aktivního místa s navázaným inhibitorem nám umožnily plně porozumět inhibičnímu mechanizmu a poskytly informace potřebné pro návrh specifických léčiv.

# 3 Introduction

## 3.1 Phosphoinositides

Phosphoinositides represent only a small fraction of cellular phospholipids but they control fundamental biological processes, most notably intracellular membrane trafficking, cytoskeleton remodelling and receptor-mediated signal transduction. Phosphoinositides, as structural lipids, maintain organelle integrity but also serve as a precursor for signalling molecules. Phosphoinositides represent all phosphorylated derivatives of phosphatidylinositol. In biology only position 3, 4 and 5 of the inositol ring can be phosphorylated giving rise to seven distinct phosphoinositide species. The reversible production of individual phosphoinositides is catalysed through the finely tuned action of phosphatidylinositol phosphatases and kinases. Each of the seven phosphoinositides has a unique subcellular distribution within the cell and hence provides constitutive signal for maintaining organelle identity. The steady state enrichment of phosphatidylinositol (4,5)-bisphosphate (PtdIns(4,5)$P_2$) is a hallmark of the plasma membrane [1,2], phosphatidylinositol 3-phosphate (PtdIns3P) is an endosomal marker [3,4], phosphatidylinositol 4-phosphate (PtdIns4P) marks the Golgi complex [5,6] and phosphatidylinositol (3,5)-bisphosphate (PtdIns(3,5)$P_2$) is a marker of multivesicular (late) endosomes (see Figure 1.) [7]. The individual phosphoinositides in lipid membranes are specifically recognised by peripheral membrane proteins which have a specific function at a given membrane such as to propagate signal further downstream to cellular effectors. The specific recruitment of effector molecules to a certain membrane containing a specific phospholipid is mediated via its recognition by the lipid-binding domain. Distinct lipid-binding domains such as PH, PX, FYVE, ENTH, FERM bind different phosphoinositide head groups [8]. Since most members of lipid-binding domain family exhibit low affinity and selectivity for a certain lipid (with notable exception being the PtdIns4P binding domains of SidC and SidM [9,10]), their additional stabilisation by cooperative binding to membrane-resident proteins, often to small GTPases from the Rab and Arf families, is needed [11].

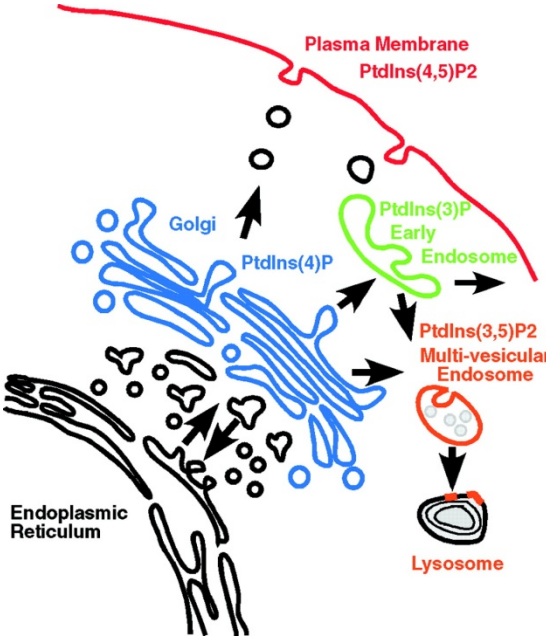



**Figure 1.: Intracellular distribution of phosphoinositides in mammalian cells.**
The localisation of different phosphoinositides are coloured for their identification. PtdIns4P is predominantly localised in the Golgi complex and partially at the plasma membrane where it serves as a precursor of PtdIns(4,5)$P_2$. Phosphatidylinositols phosphorylated at the 3$^{rd}$ and additionally at the 5$^{th}$ position were visualised primarily in the endosomal system. Taken from [12].

### 3.1.1 Golgi complex

The Golgi is a central regulatory organelle responsible for vesicle-mediated cargo transport within the cell [13]. Furthermore, this compartment plays a well defined role in lipid biosynthesis and in glycolipid maturation. PtdIns4P was observed as a key molecule implicated in Golgi membrane biogenesis and vesicular trafficking events in the *trans*-Golgi network (TGN). Its production in the Golgi complex is tightly coordinated by dynamic localisation of kinases that generates PtdIns4P (phosphatidylinositol 4-kinase IIIβ {PI4K IIIβ}, phosphatidylinositol 4-kinase IIα {PI4K IIα}) and phosphoinositide phosphatases (Sac1 and Sac2) that consume it [14,15]. The primary residence of Sac1 is the endoplasmic reticulum (ER) and the early cisternae of the Golgi complex (*cis*-Golgi) while PI4K IIIβ is localised throughout all the Golgi. This evidence suggests the upward gradient of PtdIns4P across the Golgi complex, ranging from *cis*-Golgi to the TNG [15–17].

#### 3.1.1.1 Non-vesicular trafficking

The Golgi-localised PtdIns4P is employed in sphingolipid and cholesterol biosynthesis through recruitment of lipid transfer proteins (CERT, FAPP2, OSBP, ORP9L) (see Figure 2.). Lipid transfer proteins recognise PtdIns4P via a specific PtdIns4P-binding domain called plecstrin homology (PH) domain [11]. The synthesis of sphingolipid is initiated in the ER where the condensation of serine with palmitoyl-coenzyme A occurs leading to additional reactions to generate ceramide [18]. The ceramide transfer protein (CERT) then binds ceramide via its START domain and transfers it from the ER to the TGN where ceramide is converted into sphingomyelin (SM). The ER to Golgi transfer of ceramide depends on the ability of CERT to bind the Golgi-localised PtdIns4P via its PH domain and the ER-localised VAMP ((vesicle-associated membrane protein) associated protein)-A or VAMP-B via its FFAT motif. The Golgi interacting PH domain and ER interacting FFAT motif at the opposite end of CERT facilitate simultaneous binding of two distinct membranes and the non-vesicular transport of ceramide across inter-organelle contact sites [19,20]. Ceramide transport and SM synthesis are controlled in a phosphorylation/dephosphorylation manner. The phosphorylation of CERT by protein kinase D (PKD) inhibits the interaction of PH domain with PtdIns4P, thereby reducing SM synthesis [21].

In addition to SM synthesis, ceramide can be processed further via its conversion to glucosylceramide (GlcCer) and then to glycosphingolipids. The conversion of ceramide to GlcCer takes place on a cytosolic leaflet of the early Golgi compartments from which GlcCer is transferred to an inner leaflet of the late Golgi compartments where its maturation to glycosphingolipids occurs. Glucosylceramide transfer protein FAPP2 (four-phosphate adaptor protein 2) was identified as a lipid transfer protein solely responsible for GlcCer flipping [22]. However, the exact machinery of GlcCer transport through the Golgi and its translocation across the lipid bilayer is so far unknown. FAPP2 as well as other lipid transfer proteins are recruited at the Golgi membrane in a PtdIns4P-dependent manner [23].

There are two other lipid transfer proteins, oxysterol-binding protein (OSBP) and OSBP-related protein (ORP). Both proteins possess similar structural elements to CERT that consist of a PH domain and FFAT motif. In addition, OSBP and ORP contain an

oxysterol/cholesterol-binding domain which indicates their involvement in sterol transport machinery between the ER and the Golgi complex [24,25].

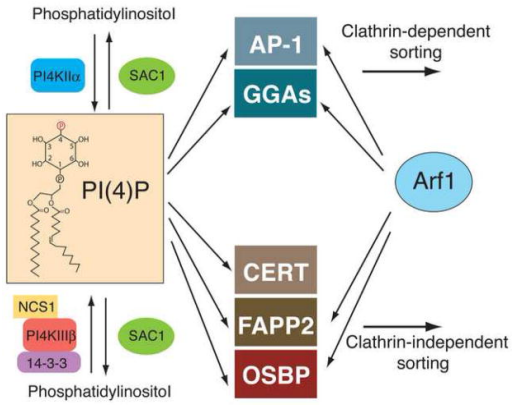



**Figure 2.: Schematic representation of PtdIns4P effectors.**
Two distinct types of PtdIns4P effectors are recruited to the Golgi membrane. The first group of proteins, represented by CERT, FAPP2 and OSBP, transfer lipids among different compartments in a non-vesicular manner and, therefore, they are involved in clathrin-independent cargo sorting. On the other hand, coat adaptor proteins AP-1 and GGAs promote clathrin-dependent TGN-endosomal trafficking via direct interaction with clathrin molecules. These transport processes are regulated in a PtdIns4P- and Arf1-dependent manner. Taken from [26].

### 3.1.1.2 Vesicular trafficking

Cargo vesicular transport from the Golgi complex to the plasma membrane (PM) or to the endosomal compartments (anterograde trafficking) is a highly regulated process in which PtdIns4P plays a prominent role. PtdIns4P is crucial for cargo sorting and packaging into the secretory granules and for membrane rearrangement that drives vesicle budding [27]. In the yeast model, it was shown that inactivation of the yeast homolog of PI4K IIIβ (Pik1) blocked anterograde trafficking from the Golgi. Moreover, the function of PtdIns4P in this process was described in the yeast model for the first time [28].

In yeast, vesicle budding events during post-Golgi transport to the PM are mediated by PtdIns4P and the Rab family of GTPases. The recruitment of guanidine nucleotide exchange factor to PtdIns4P in the Golgi membranes with co-incident binding of small GTPases triggers a dynamic cascade of Rab GTPases and PtdIns4P interactions that promotes vesicle budding and consequent vesicle liberation to the cytosol [29–31]. However, prior to post-Golgi vesicle fusion with the PM, vesicle tethering to exocyst complex is needed. This step is tightly controlled at the PtdIns4P level. It was shown that vesicular-bound guanidine nucleotide exchange factor Sec2 interacts with exocyst but only in the absence of PtdIns4P [32]. These findings present an evidence for the gradual

decrease of PtsIns4P content toward reaching the PM. The mechanism by which PtdIns4P is diminished from secretory vesicles still remains elusive. On the other hand, in humans, FAPP1 but not FAPP2 regulates cargo export from the Golgi destinated for the plasma membrane localisation [33]. FAPP1 is the only known PtdIns4P and Arf1 binding effector with functions in both vesicular and non-vesicular trafficking.

In contrast to TGN-PM trafficking, transport between the TGN and endosomes is mediated via clathrin-coated vesicles (CCVs). PtdIns4P together with small GTPase Arf1 are necessary for efficient recruitment of clathrin adaptors such as adaptor protein 1 (AP-1), γ-ear containing ADP-ribosylation factor binding protein 2 (GGA2) and the Epsin-related (EpsinR) protein to the *trans*-Golgi membranes (see Figure 2.) [34]. The coincident binding of coat adaptor proteins (AP-1, GGA2) to PtdIns4P and Arf1 together with cargo sorting motif recognition represents the driving force in CCVs biogenesis [27,35,36].

During intracellular vesicular trafficking all membranes are subjected to remodelling events which alter membrane curvature [37]. Membrane deformation could be mediated by lipid modifying enzymes or lipid transfer enzymes. In yeast, it was proposed that Drs2 flippase alters membrane curvature by translocating positively charged aminophospholipids from the luminal to the cytosolic leaflet thus generating a charge asymmetry in the membrane [38]. Drs2 flippase activity is strongly dependent on PtdIns4P synthesis by Pik1 (a yeast homolog of PI4K IIIβ) [39]. Also lipid transfer proteins FFAP1 and FFAP2 are involved in a membrane deformation. The precise mechanism by which FFAPs proteins control vesicle biogenesis in not completely understood, however, some structural studies suggest that upon PtdIns4P recognition by PH domain, a hydrophobic wedge of this domain is inserted into the cytosolic leaflet thus inducing membrane deformation [40].

### 3.1.2 Plasma membrane

#### 3.1.2.1 Signal transduction

In a canonical signalling pathway, an extracellular signal is transferred inside the cell by a series of sequential reactions. The initial step of signal transduction involves receptor activation caused by a conformational change upon ligand binding. Receptor stimulation then leads to phospholipase C (PLC) activation and the generation of two second messengers, soluble $Ins(1,4,5)P_3$ and diacylglycerol (DAG) captured by the

membrane. The released Ins(1,4,5)$P_3$ binds to specific receptors located in the ER and causes an influx of $Ca^{2+}$ into the cytosol [41,42]. The elevated level of $Ca^{2+}$ is then taken up into the mitochondria where it can stimulate metabolic enzymes or initiate apoptosis [43]. The other second messenger, DAG, activates members of protein kinase C family or contributes to the regulation of some ion channels [44,45]. The regulation of PLC activation depends on a constant replenishment of the PtdIns(4,5)$P_2$ pool at the PM. A steady state concentration of PtdIns(4,5)$P_2$ is maintained primarily by a large pool of PtdIns4P at the PM. This pool can be replenished in three ways. Firstly, PtdIns4P can be produced *in situ* by PI4K IIIα, secondly, this lipid can be delivered to the cell surface in vesicles derived from the Golgi complex and recycling organelles and thirdly, PtdIns4P can be replenished via PM-ER contact sites [46–48].

In addition to the signalling events, PtdIns(4,5)$P_2$ influences actin remodelling processes important for pathogen-mediated phagocytosis [49].

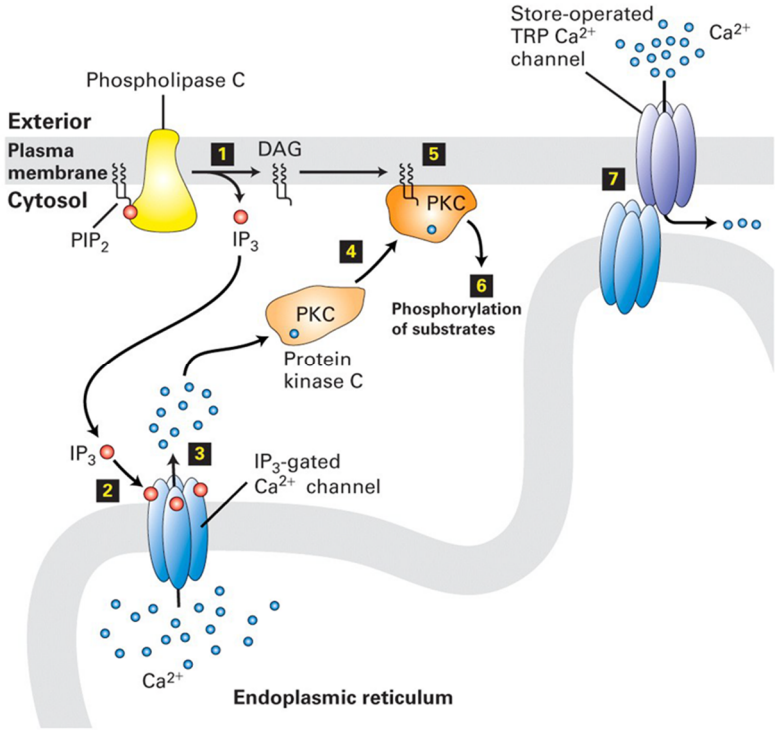



**Figure 3.: Signal transduction into the cell.**
The membrane-localised phosphatidylinositol 4,5-bisphosphate ($PIP_2$) is hydrolysed by the G-protein-stimulated phospholipase C yielding second messengers, diacylglycerol (DAG) and phosphatidylinositol (1,4,5) trisphosphate ($IP_3$). Second messengers mobilise the intracellular storage of $Ca^{2+}$ and hence modulate further downstream signalling pathways or $Ca^{2+}$-responsive proteins. Taken from [50].

### 3.1.2.2 Endocytosis

PtdIns4P participates not only in a signal transduction but also in the regulation of endosomal trafficking in response to receptor stimulated endocytosis. The strength and duration of the cellular response to a given extracellular stimuli depends on receptor-ligand retrieval back to the plasma membrane. Clathrin-mediated endocytosis represents the major pathway for signal uptake induced by the internalization of a ligand-bound cell surface receptor inside the cell and its recycling back to the plasma membrane in a ligand-free state. PtdIns4P is required as a precursor to PtdIns(4,5)$P_2$ in clathrin-dependent budding processes [51]. The essential role of PtdIns(4,5)$P_2$ in this process was proved by direct binding with clathrin adaptors (AP-108, AP-2, EpsinR). All these interactions promote clathrin self-assembly by driving or stabilising membrane remodelling events. AP-180-PtdIns(4,5)$P_2$ interaction is important for the formation of a clathrin lattice on a cytosolic face of the plasma membrane [52,53]. Dual recognition of AP-180 and PtdIns(4,5)$P_2$ by the clathrin adaptor complex AP-2 together with cargo selection promote clathrin-coated pit formation [53]. Finally, EpsinR binds to AP-2 and the clathrin molecules thus terminating the assembly of clathrin coated vesicles (CCVs) [54]. After vesicle fissions from the donor PM, CCVs undergo uncoating prior to their delivery to the target membrane (endosomes) during which the clathrin adaptors are released back into the cytosol to be reused. Uncoating of CCVs is triggered by synaptojanin-mediated dephosphorylation of PtdIns(4,5)$P_2$ into PtdIns4P which in cooperation with endophilin causes dissociation of the CCV-forming complex [55,56].

## 3.1.3 Endosomal trafficking

The major regulatory phospholipid in endosomal trafficking and autophagy is PtdIns3P, a marker of early endosomes [57]. Its further phosphorylation at the 5$^{th}$ position of the inositol ring promotes the endocytosed cargo to be processed, in particular, in the endosomal-lysosomal degradation pathway [58].

Myotubularin (MTM) and myotubularin-related (MTMR) lipid phosphatases together with phosphatidylinositol 3-kinases (PI3K) and phosphatidylinositol-3-phosphate 5-kinases (PIKfyve/ PI5PK) maintain the turnover of PtdIns3P and PtdIns(3,5)$P_2$ in endosomal compartments (early, late, recycling endosomes). Recently, Ketel *et al.* showed that catalytic inactivation of MTM1 and MTMR1 impaired recycling of the TfR cell surface receptor from endosomes back to the PM. In MTM-depleted cells, elevated level of

PtdIns3P was detected. Co-depletion of PtdIns3P and MTM restored TfR exocytosis from endosomes. In addition, Ketel *et al.* revealed that hydrolysis of PtdIns3P by phosphatidylinositol 3-phosphatase MTM1 accompanied by PtdIns4P production (PI4K IIα) are necessary for recruitment of proteins responsible for tethering and subsequent fusion of recycling endosomes with the plasma membrane [48]. PtdIns3P conversion to PtdIns4P facilitates cargo exit from endosomes and its return to the plasma membrane (see Figure 4.).

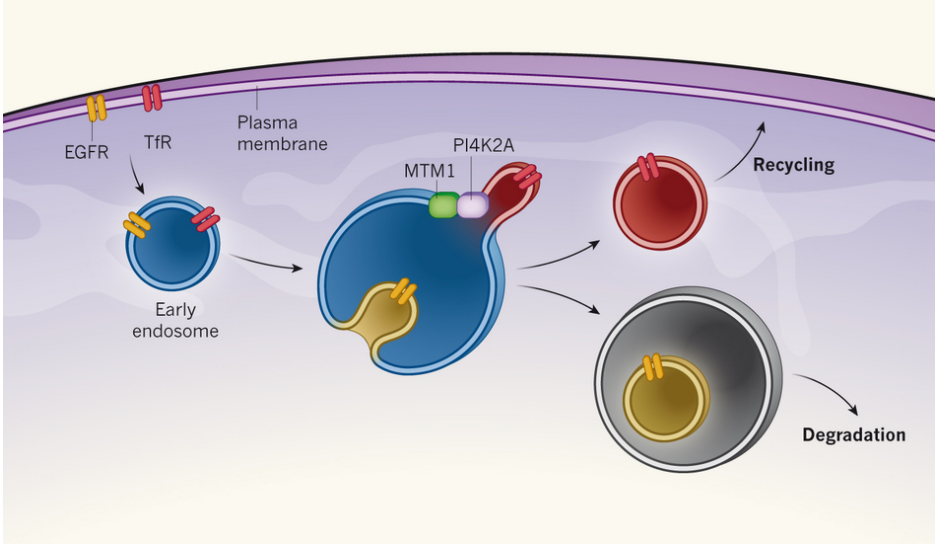



**Figure 4.: Cartoon representation of an endocytosed receptor and its further derivatization into recycling or late endosomes.**
The clathrin coated pits harbouring the internalised receptors are fused with the membrane of early endosomes enriched with PtdIns3P (indicated in blue). Another modification of this lipid determines whether or not the internelised cargo will be recycled back to the plasma membrane or undergo degradation. The PtdIns3P conversion to PtdIns(3,5)$P_2$ (yellow membrane) defines the membrane region or vesicle designated for degradation. On the other hand, replacement of PtdIns3P to PtdIns4P (red membrane) by the dual action of MTM1 and PI4K IIα directs this organelle back to the membrane. Taken from [59].

### 3.1.4 Autophagy

Quite recently the PI4K IIα enzymatic activity was found to be implicated in autophagy machinery [60]. Autophagy is an intracellular degradation system important for removing misfolded or aggregated proteins, eliminating damaged organelles (mitochondria, ER, peroxisomes) and pathogens and also for maintaining cell integrity and homeostasis during nutrient starvation and stress conditions [61,62]. Autophagy utilises a series of tethering and fusion reactions of autophagic vesicles with different intracellular membranes to assure cargo degradation. Autophagosome biogenesis consists of phagophore formation, elongation and sealing of the membrane to generate a double

membrane compartment. The exact composition of phagophores are not precisely known but it is assumed that they originate from the lipid bilayer of ER, ER exit sites, ER-mitochondria contact sites, trans-Golgi and endosomes [63–68]. Phagophores with trapped cytoplasmic components expand to autophagosomes which subsequently mature to autolysosomes by fusing with the late endosomes and lysosomes (see Figure 5.). The lysosomal proteases then promote the degradation of autophagosomal content [64,69].

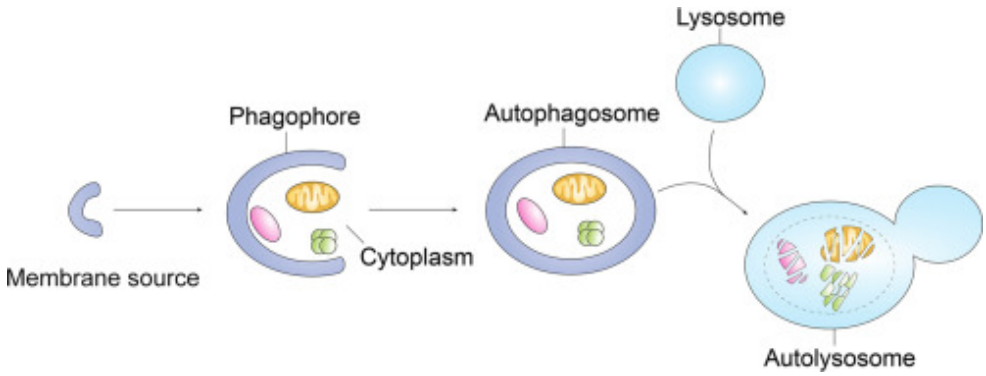



**Figure 5.: Autolysosome formation.**
The phagophore membrane encloses the cytosolic proteins and organelles to form an immature autophagosome. The autophagosome subsequently fuses with the lysosome to generate a mature autolysosome where the internal material is degraded. Taken from [70].

Autophagy is a highly regulated process in which many critical factors belong to ATGs (autophagy related proteins) family [71]. The γ-aminobutyric acid receptor-associated protein (GABARAP), one of the ATG proteins, recruits PI4K IIα to the autophagosomes to generate PtdIns4P *in situ*. Deficiency of PtdIns4P caused by GABARAP depletion blocks autophagososme-lysosome fusion and results in abnormally large autophagosomes. Taken together, the late stage of autophagy is under the control of the GABARAP-PI4K IIα-PtdIns4P interactome and depletion of even one of these components leads to autophagosomal failure [60].

### 3.1.5 Pathogens and host phosphoinositides

Phosphoinositides are attractive targets for many pathogens to invade the host cell and modify lipid homeostasis in order to alter organelle identity and membrane trafficking events. Most of the pathogens are internalised into the host cell in membrane-derived compartments (phagosomes) similar to vacuolar organelles where they are protected from the host immune system. Upon cell entry, most pathogens follow the endosomal-lysosomal

pathway. During this pathway the phagosome maturates to a phagolysosome which should lead to digestion of the trapped microbe. However, many pathogens have developed strategies to control pathogen-containing vacuole maturation to sustain their survival [72]. Another way pathogens can enter into the cell is injection of the virulence factors across the host membrane via a pathogen secretion system. Inserted virulence factors subsequently rearrange cytoskeleton and membrane morphology to enable pathogen uptake. Importantly, many of the virulence factors are either phosphoinositides effectors or phosphoinositides-metabolising enzymes [73].

*Listeria monocytogenes* utilises the effector molecule In1B to activate host PI3-kinase and to produce PtdIns3P subsequently blocking phagosomal maturation [74]. Furthermore, this molecule is also capable of recruiting PI4K IIα/β to the phagosomes. Knockdown of PI4K IIα/β inhibits *Listeria* engulfment but the exact mechanism of PI4K IIα/β -mediated action on phagosomal membrane remains to be established [75].

*Legionela pneumophila* exploits a completely different mechanism to block lysosomal fusion with pathogen-containing vacuoles. *Legionela* employs SidC and SidM proteins to assure the maturation of the plasma membrane-derived *Legionela*-containing vesicles (LCV) to ER-like compartments. SidC and SidM bind to PtdIns4P pool on *Legionela*-containing vesicles [9,10] and facilitate recruitment of the ER-derived secretory vesicles at the early stage of LCV formation and ER-resident proteins at the late stage to form a favourable environment for bacterial replication [76,77]. Therefore, PtdIns4P is a key lipid involved in SidC/SidM-mediated remodelling of the phagosomal membrane [10].

PtdIns4P, as a critical membrane component, tightly regulates fundamental biological processes established at intracellular membranes. This regulation is achieved through the scaffolding role of PtdIns4P and its spatio-temporal redistribution. The steady state enrichment of this lipid defines the organelle integrity while the recruitment of specific effectors (membrane coats, microtubule and actin motors, tethering factors, accessory proteins for GTPases, enzymes) controls lipid biogenesis, trafficking processes and the maturation of intracellular vesicles and organelles. The maturation with respect to the alteration of lipid environment provides the organelle plasticity necessary for organelle efficient functioning. However, the organelle plasticity can be harnessed by bacterial pathogens or viruses by various methods for their invasion into the cell and establishment of the replication niche. Subverting the organelle identity due to the loss of control over the lipid-synthesising and lipid-modifying enzymes has been heavily documented in a variety

of human pathologies. Although the physiological relevance of PtdIns4P is steadily expanding, there are still some fragmentary areas that need to be investigated in more detail to provide true comprehensive insight into PtdIns4P biology.

## 3.2 Human phosphatidylinositol 4-kinases (EC:2.7.1.67)

PI4-kinases account for only a small fraction of lipid kinases but play an important role in lipid signalling and maintaining lipid homeostasis. PI4-kinases convert PtdIns to PtdIns4P by phosphorylating the inositol head group at the 4$^{th}$ position. PtdIns4P was initially considered merely an intermediate in the production of second messengers (PtdIns(1,4,5)$P_3$ and DAG) and higher phosphoinositides. However, as more attention was paid to PI4-kinases, PtdIns4P emerged as a key regulatory molecule in vesicular trafficking, lipid transport and metabolism (see Section 1.). Additionally, PI4-kinases were identified as essential host factors for +RNA viruses.

In eukaryotes, PI4-kinases are categorised into two major classes, type II and III. Further molecular characterisation revealed two isoforms in each family (PI4K IIα and IIβ also known as PI4K2A and PI4K2B; and PI4K IIIα and IIIβ also known as PI4KA and PI4KB). Although PI4-kinases catalyse the same reaction in different membrane compartments, they utilise diverse strategies to associate to the location of their action. PI4-kinases type II are tightly associated with membranes via their palmitoyl anchor, whereas type III are soluble peripheral membrane proteins which are recruited to the membrane via additional interaction with their binding partners. Recent crystal structures of three out of four PI4-kinases shed some light on their mechanism of membrane association and also revealed the structural similarity between type III PI4-kinases to PI3-lipid kinases in contrast to type II which were found to be more similar to protein kinases than to lipid kinases. The individual types of PI4-kinases can be also easily distinguished from each other based on their sensitivity towards adenosine (PI4K type II) or Wotmannin (PI4K type III). The location of PI4-kinases activity encompasses diverse cellular compartments, in particular, PI4K IIIα is predominantly localised to the plasma membrane and ER, PI4K IIIβ to the Golgi and type II PI4-kinases are localised in the endosomal system.

### 3.2.1 PI4-kinase type IIIα (PI4K IIIα)

#### 3.2.1.1 Gene and protein isoforms

The gene encoding for PI4K IIIα (PI4KA) contains 57 exons and is located on human chromosome 22, in locus 22q11.2 which is known for its genetic instability. Transcription of the PI4KA gene gives rise to two splice variants annotated in GenBank as GI:4505807 for isoform1 and GI:155030226 for isoform 2 [78]. A shorter form (isoform 1) was cloned as the first mammalian PI4-kinase from cDNA isolated from human placenta which encodes 854 amino acid-long protein with a predicted molecular weight 97 kDa [79]. However, the endogenous existence of a shorter variant on the protein level has never been confirmed. Furthermore, this N-terminally truncated variant was shown to be catalytically inactive in *in vitro* experiments [78]. The full length variant (isoform 2) was firstly cloned from rat brain cDNA encoding 2041 amino acid-long protein with a predicted molecular mass 210-230 kDa [80].

#### 3.2.1.2 Protein

##### 3.2.1.2.1 Localisation

PI4K IIIα is predominantly localised to the ER but its significant pool was also immunostained on a cytoplasmic leaflet of the PM [47,81]. It was shown that PI4K IIIα is concentrated at PM patches where it forms the complex with EFR3B and TTC7B [82]. EFR3B and TTC7B are human analogues of yeast scaffolding proteins (Efe3p, Ypp1p) which recruit Stt4 (a yeast orthologue of PI4K IIIα) to the PM [83]. The bipartite NLS (nuclear localisation signal) and NES (nuclear export signal) sequence motifs at the N-termini of PI4K IIIα leads to the expectation that this protein could also be distributed in the nucleus and the nucleolus. This speculation was supported by the recent research of Kakuk *et al*. [84,85]. A high expression level of PI4K IIIα was also detected in the brain, especially on cisternae of the ER and atypical membranes surrounding the outer mitochondrial membrane or on multivesicular bodies [86].

#### 3.2.1.2.2 Structure

The crystal structures of almost all PI4-kinases were published recently [87–89]. PI4K IIIα is the only PI4-kinase with a three-dimensional structure that remains to be solved. The computationally predicted domain organisation of PI4K IIIα described a putative SRC homology 3 (SH3) domain and a Pro-rich region at the very end of the N-terminus [80,90,91]. Both, the SH3 domain and the Pro-rich region are characteristic motifs of proteins participating in signal transduction. Furthermore, within the N-terminal half of the protein a Leu-rich nuclear export signal (NES) followed by a bipartite nuclear localisation signal (NLS) are predicted [92]. The C-terminal part of the protein contains a highly conserved catalytic domain that bears high sequence similarity to PI3-kinases. Preceding the catalytic domain, a lipid kinase unique (LKU) domain typical for type III PI4-kinases and PI3-kinases is predicted. A PH domain was mistakenly predicted between the catalytic and the LKU domain [79]. The compelling work of Harak *et al*., that used experiment guided modelling, provided new insight into PI4K IIIα domain organisation. Harak *et al*. described two new functional domains in the C-terminal part of the protein. The first one encompassing residues 1101-1535 is predicted to be mostly helical and is therefore termed the helical domain. This domain can be further divided into three individual subdomains (DI, DII, DIII). The whole helical domain structurally corresponds to the helical domain of PI4K IIIβ. A second region, composed of residues 1536-1723, is designated as the armadillo repeat (ARM) domain and includes predicted LKU domain. Furthermore, the predicted PH domain is replaced with the N-lobe of the catalytic domain in Harak´s model (see Figure 6.) [93].

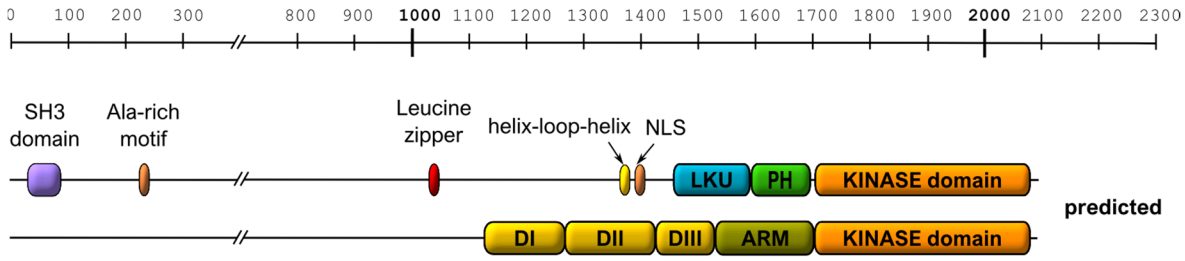



**Figure 6.: Schematic representation of the predicted domain organisation of PI4K IIIα.**
NLS refers to nuclear localisation signal, LKU- lipid kinase domain; PH- plecstrin homology domain; ARM- armadillo repeat domain; SH3- SRC homology 3 domain; DI, DII, DIII- individual subdomains of helical domain. The scale at the top refers to amino acid number.

Additionally, multiple sequence alignments and homology-based molecular modelling were used for a detailed characterisation of the catalytic domain. Based on this strategy, two conserved cysteine (Cys1839, Cys1843) residues were found among all the orthologues of human PI4K IIIα. In human PI4K IIIβ, cysteine residues are replaced with serine and proline (in human PI4K IIIβ: Cys1839-Ser592, Cys1843-Pro597). In comparison with human PI3-kinases, the cysteine residues in their catalytic core are replaced with valine, isoleucine or tyrosine. In the predicted three-dimensional structural model, the cysteine residues are localised in a flexible loop connecting the N- and C-terminal lobes at ATP binding site. This makes them promising regulatory residues in the enzymatic activity of PI4K IIIα. Furthermore, the occurrence of a third cysteine residue (Cys1796) adjacent to Cys1839 and Cys1843 was also described. Mutagenesis analysis of individual cysteine residues revealed that a Cys1839Ser mutation did not affect the enzymatic activity while the mutations of Cys1796Pro/Ser render the protein inactive [94].

In order to elucidate the complete mechanism of PtdIns4P catalysis and the residues involved in this process as well as the correct domain organisation, the crystal structure of PI4K IIIα is highly demanded.

#### 3.2.1.2.3 Function

Very little is known so far about the precise function of PI4K IIIα on cellular membranes. Since PI4K IIIα is localised at the ER and the PM, it is assumed that PI4K IIIα is the enzyme responsible for the generation of the PtdIns4P pool on these organelles [95]. Additionally, the study of Shoji-Kawaguchi *et al.* showed that the acidic character of PtdIns, PtdIns4P, PS and PA in the nucleus has a great impact on the activity of some DNA polymerases. However, whether nuclear-localised PI4K IIIα is responsible for this effect is questionable [96].

Intensive studies focusing on the functional and structural relevance of PI4K IIIα in cell physiology has been enhanced by the identification of type III PI4-kinases as essential host factors in hepatitis C virus (HCV) replication. The involvement of PI4K IIIα in the HCV life cycle makes this protein a promising target for pharmacological intervention.

HCV, a member of Flaviviridae family, is a single strand plus sense RNA virus (+RNA). Its genome is represented by an uncapped RNA molecule flanked by non-translated regions (NTRs) [97]. The internal ribosome entry site (IRES) and two microRNA-122 binding sites needed for further RNA processing were mapped into the HCV genome (see Figure 7.) [98–100]. Genome translation results in a polyprotein

precursor whose cleavage mediated by viral and host proteases gives rise to three structural proteins, a small hydrophobic protein and six non-structural proteins (see Figure 7.) [101,102].

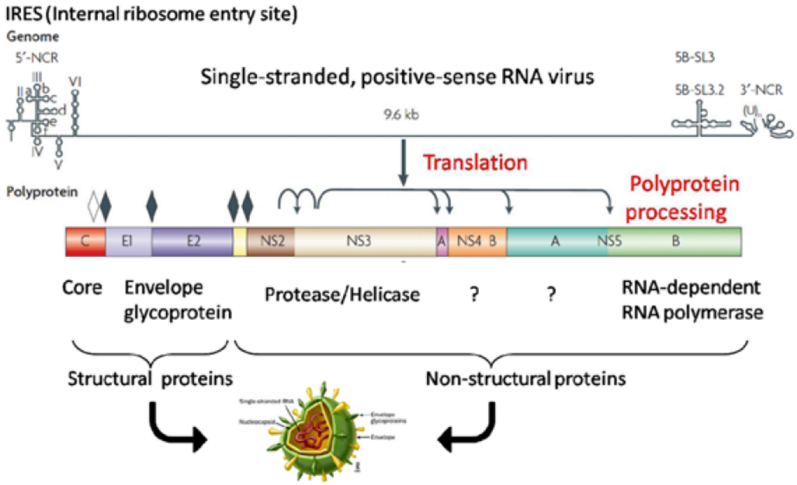



**Figure 7.: Schematic representation of the HCV genome.**
The HCV genome contains non-translated regions (NTR) and a single open reading frame. The internal ribosome entry site (IRES)-mediated translation yields a 3000 amino acid- long polyprotein. This polyprotein precursor is further processed by viral and host proteases into both structural and non-structural (NS) proteins at the ER membrane. Structural proteins are responsible for virus particle assembly while non-structural proteins are involved in RNA genome replication. Taken from [103].

In general, the HCV life cycle is a highly complex multi-step process which needs to be completed as quickly and efficiently as possible upon host cell entry or else the virus would be eliminated by the host immune system. To effect this, HCV utilises host cellular membranes to modulate their lipid environment in favour of viral replication. Furthermore, HCV utilises the host secretory and trafficking pathways for assembly and export of its virions [104]. In HCV infected cells, discrete membrane platforms with highly enriched PtdIns4P microenvironments were detected [105–109]. These invaginated membrane structures called membranous webs (MWs) provide not only platforms for efficient RNA synthesis but also a protective environment against innate immunity [110]. The generation of the MWs is driven by a rearrangement of pre-existing organelle complexes. In the case of HCV, the MWs are derived from the ER membrane [105]. The PtdIns4P depletion from unique multivesicular structures observed in infected liver cells significantly decrease HCV replication efficiency which indicates that PtdIns4P is indispensable for HCV RNA synthesis [109,111,112]. The precise role of PtdIns4P in the viral replication machinery is not known but it seems that HCV takes advantage of normal physiological functions of PtdIns4P. Its biochemical properties (including the ability to be exchanged for cholesterol

[113]) and its scaffolding role are the most important ones. The acidic character of PtdIns4P in ER-derived platforms leads to a charge redistribution and perturbation of the membrane curvature [114]. The presence of positive and negative membrane curvatures has already been observed in HCV infected cells [115]. Independently from the electrostatic character of PtdIns4P, this lipid is also efficiently recognised by diverse effector proteins. These proteins could easily be harnessed by the virus to modulate lipid composition and the membrane architecture or even to concentrate viral or host proteins indispensable for viral replication. In particular, oxysterol binding protein (OSBP) was shown to bind to PtdIns4P via its PH domain and shuttle cholesterol to the MWs thus assisting in maintaining membrane three-dimensional architecture. The lipid transfer function of OSBP is not only exploited by HCV as it has been described to be vital to encephalomyocarditis virus replication as well [116].

In ordered to understand this complex biological phenomenon in detail, the elucidation of the exact mechanism by which PtdIns4P is involved in HCV replication and MWs formation as well as the identification of host and viral proteins involved in these processes are required.

Therefore, extensive siRNA library screenings were carried out to identify the host cellular factors needed for the HCV life cycle [108,112,117–119]. Interestingly, PI4K IIIα together with PI4K IIIβ were identified as major host factors of the HCV life cycle. Since PI4K IIIα synthesises PtdIns4P on the ER membrane [95], it was necessary to determine its role in MWs formation. The inhibitor treatment as well as siRNA-mediated knockdown displayed a potent anti-HCV replication effect and a serious defect in the MWs architecture [108,109,111,112]. In addition, it was shown that PI4K IIIα co-localised with the viral non-structural NS5A protein in immunofluorescent staining [112]. The co-immunoprecipitation studies together with yeast two hybrid system study confirmed the direct interaction between PI4K IIIα and HCV NS5A [108,109,111,120]. Since viral NS5A binds membrane via its amphipathic helix, there is a possibility of NS5A playing a role in PI4K IIIα recruitment to the MWs. Furthermore, this interaction not only determines the localisation of PI4K IIIα but also stimulates its enzymatic activity *in vitro* which could be an explanation for the elevated level of PtdIns4P in HCV infected cells [108,111]. The interaction site of NS5A to PI4K IIIα was mapped to the C-terminus of domain I of NS5A. However, contrary data were published for an interacting area of PI4K IIIα [121]. Lim *et al*. described amino acids 400-600 as responsible for NS5A binding [122] but on the other hand PI4K IIIα with 1101 amino acids truncated from the N-terminus was still able to co-

precipitate with NS5A. In spite of the great effort to define the region involved in PI4K IIIα-NS5A interaction, the binding interface of PI4K IIIα has still not clearly been assigned [93].

The role of PI4K IIIβ in HCV replication is still highly controversial. The silencing of both isoforms resulted in a reduction of HCV replication due to the decreased level of PtdIns4P in HCV replicon cells [107,119]. However, siRNA-induced negative effect on HCV replication was stronger in the case of PI4K IIIα. In contrary to PI4K IIIα, up-regulated PI4K IIIβ was not able to rescue the viral phenotype [117]. Therefore, PI4K IIIβ must have a different role in the HCV life cycle than in HCV replication. It is also possible that the different genotypes of HCV utilise either PI4K IIIα or PI4K IIIβ for their replication. That would explain the contradictory results obtained by the different laboratories.

HCV has evolved skilful strategies to interfere with host lipid metabolism, thereby providing its uncontrolled replication. More than 170 million people suffer from acute or chronic liver diseases due to insufficient anti-viral therapy [123]. Therefore, the development of more potent anti-viral drugs with low cytotoxic effect is required. As a promising strategy seems to be targeting both viral and host factors in order to avoid the development of viral resistance. For these reasons the identification of host factors essential for HCV replication machinery is desirable.

## 3.2.2 PI4-kinase type IIIβ (PI4K IIIβ)

### 3.2.2.1 Gene and protein isoforms

The gene encoding for PI4K IIIβ (PI4KB) is localised on chromosome 1, locus 1q21. 2.4 kbp full-length cDNA that encodes the 801 amino acid-long protein with a predicted size of 92 kDa was obtained by screening of cDNA libraries from the heart and the placenta. The observed molecular weight of PI4K IIIβ was distinct from the predicted one. The antibodies raised against PI4K IIIβ and size-exclusion chromatography confirmed the existence of 110 kDa protein [124]. Another splice variant with 15 amino acids inserted was described by Balla *et al*. [125]. Furthermore, Suzuki *et al*. and Saito *et al*. detected other slightly different cDNA with sizes of 3.6 kbp and 4.8 kbp. The corresponding proteins contained 816 and 828 amino acids, respectively, and they differed only in the presence of 12 N-terminal amino acids [126,127].

### 3.2.2.2 Protein

#### 3.2.2.2.1 Localisation

PI4K IIIβ is primarily a Golgi complex-resident enzyme [95,128]. The small GTP-binding protein Arf1 and yeast Frq1 (the yeast homolog of human neuronal calcium sensor-1 (NCS-1)) were proposed to facilitate targeting of PI4K IIIβ to the Golgi complex [128,129]. Unlike Frq1, human NCS-1 is not primarily localised to the Golgi and, therefore, it is unlikely that NCS-1 could target PI4K IIIβ to the Golgi [130]. Instead, the Golgi resident ACBD3 (acyl-CoA binding domain containing 3) was proposed to recruit PI4K IIIβ to the Golgi membranes. siRNA knockdown of ACBD3 led to cytoplasmic localisation of PI4K IIIβ [131]. Moreover, we showed that ACBD3 can recruit PI4K IIIβ to virtually any membrane both *in vivo* and *in vitro*. For instance, if ACBD3 is forced to be localised to the mitochondria it recruits PI4K IIIβ to the mitochondria. This interaction was also characterised at the atomic level using protein NMR [132]. Like PI4K IIIα, PI4K IIIβ was also found on the surface of the nuclear envelope as well as on the mitochondrial and the ER membranes in neuronal cells [86,133]. Its function on these compartments is still under investigation.

#### 3.2.2.2.2 Structure

Domain organisation of PI4K IIIβ was described to be almost similar to PI4K IIIα based on primary sequence alignment and computational domain/motif prediction programmes. Based on this prediction, PI4K IIIβ should contain a C-terminally localised catalytic domain, an LKU domain and an N-terminal Pro-rich motif. Adjacent to the C-terminus of the LKU domain is predicted to be a Hom2 region characteristic only of PI4K IIIβ and its yeast homolog. This region was identified as a putative Rab11-binding site. A Ser-rich segment with several phosphorylation sites should precede the Hom2 region (see Figure 8.) [134]. A putative binding site of the PI4K IIIβ recruiter, yeast Frq1, is predicted between the LKU domain and the Ser-rich motif [134].

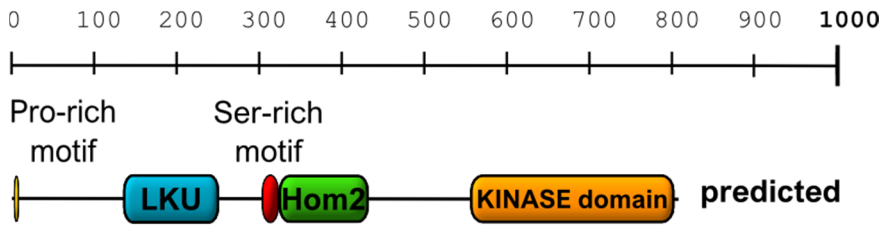



**Figure 8.: Schematic representation of the predicted domain organisation of PI4K IIIβ.**
The LKU in blue refers to a lipid kinase unique domain; Hom2 region is in green with a putative Rab11-binding site and the catalytic domain is depicted in orange. The scale at the top refers to the amino acid number.

It was only in 2014 that, structural information for PI4K IIIβ in complex with Rab small GTPase was released (see Figure 9.). Since the N-terminal part of the protein is unstructured, the N- and C-terminally truncated variant with a loop deletion was crystallized. In comparison with the domain organisations based on computational predictions and the literature, new domain boundaries were established. It was discovered that the bi-lobal catalytic domain is much larger than the predicted one was. The Hom2 region is replaced with the N-lobe of the catalytic domain while a helical domain comprising the Rab11-binding site replaced the LKU domain [135].

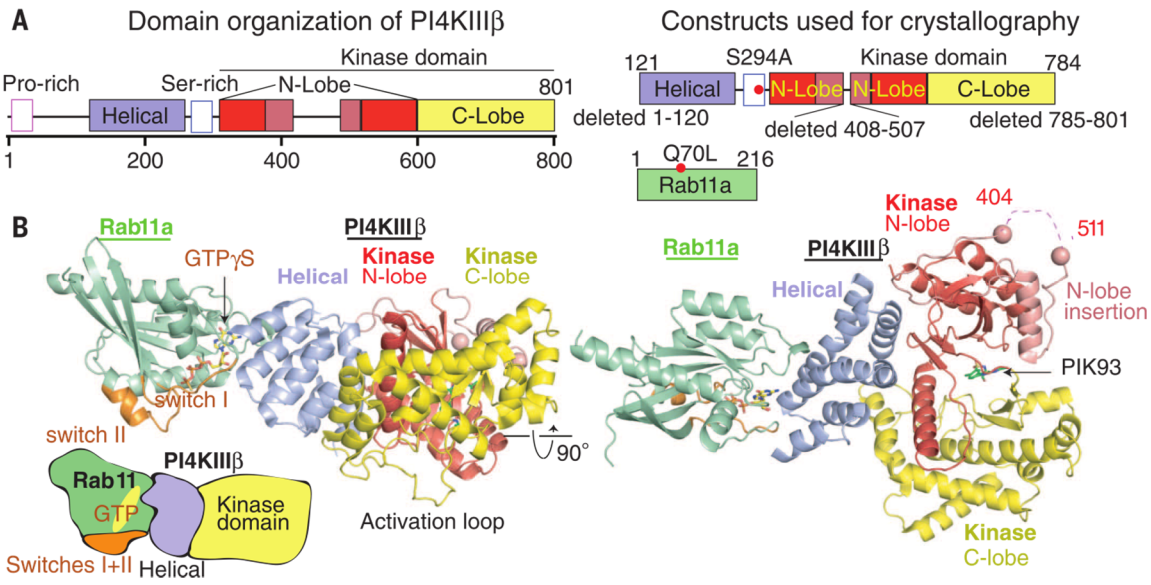



**Figure 9.: The crystall structure of human PI4K IIIβ in complex with Rab 11a (Q70L)-GTPγS and inhibitor Pik93.**
**Panel A:** Domain organisation of full-length PI4K IIIβ and PI4K IIIβ in complex with Rab11a used for crystallization studies. **Panel B**: Cartoon representation of the overall fold of this complex. Taken from [135].

#### 3.2.2.2.3 Biological function

PI4K IIIβ is a major producer of PtdIns4P pools at the Golgi complex. However, it also maintains the integrity of this organelle and regulates Golgi-localised processes such as lipid metabolism or anterograde trafficking. Specific interactions of multiple effector molecules (CERT, FAPP, OSBP) to PtdIns4P [22,23,136] are employed in these processes thus providing a regulatory step easily affected by modulating the lipid kinase activity.

Phosphorylation is a second most prevalent post-translation modification after glycosylation and has a tremendous regulatory impact on the activity of many enzymes. Therefore, it has been suggested that also the enzymatic activity of PI4K IIIβ could be modulated by phosphorylation. Eight putative phosphorylation sites together with several protein kinases responsible for particular phosphorylations were identified [92]. The effect of individual phosphorylation on PI4K IIIβ function is not clearly proved except for phosphorylation at Ser294 which has been suggested to enhance the enzymatic activity of PI4K IIIβ [137]. This activated state is further stabilised by the interaction with a scaffolding protein 14-3-3 which binds PI4K IIIβ only upon phosphorylation at Ser294 [138]. In the Golgi complex, PI4K IIIβ is phosphorylated at Ser294 by protein kinase D (PKD) which is recruited to this membrane via interaction with DAG. DAG is a side product in sphingomyelin synthesis, a process tightly regulated by PI4K IIIβ [18,20]. Therefore, the coordination of PKD and PI4K IIIβ action seems to be a potential regulatory loop in sphingomyelin metabolism. Additionally, phosphorylation not only affects the lipid kinase activity but also protein localisation. For instance, PI4K IIIβ phosphorylated at Ser496 and Thr504 was detected in the nucleus while phosphorylation at Ser266 and Ser258 localises PI4K IIIβ to the Golgi [92,139].

PI4K IIIβ seems to be another crucial lipid kinase hijacked by some of the myriad +RNA viruses. PI4K IIIβ has emerged as a vital host factor required for enterovirus 71, Achi virus, bovine cobuvirus, poliovirus, coxsackievirus, human rhinovirus and SARS coronavirus replication [131,140–142]. Different strategies are employed by these viruses in a functional replication complex assembly which originates from the Golgi membranes with the highest steady state level of PtdIns4P lipid.

In enteroviral replication, membrane-bound enteroviral 3A protein modulates the PtdIns4P pool on "replication organelles" via recruitment of PI4K IIIβ (see Figure 10.) [107,141,143]. It was suggested that PI4K IIIβ is recruited to the Golgi membranes via interaction with a small GTPase Arf1 [128] whose functional state is influenced by GBF1

guanidine nucleotide exchange factor [144]. In enterovirus infected cells these interactions result in greater levels of PI4K IIIβ membrane recruitment which leads to a conventional subversion of Golgi architecture and secretory vesicles disassembly [145]. The organelle disassembly is further exploited by viral proteins for building up a new replication microenvironment. As a consequence of the Golgi membrane disruption, host immune system viral invader recognition is impeded due to blocking of MHC proteins and cytokines trafficking [107]. In general, these replication platforms serve as docking sites for viral and host proteins to promote efficient RNA synthesis. Enteroviral RNA polymerase RdRp $3D^{pol}$ was described to selectively bind to PtdIns4P over other lipids components presented in membranes (see Figure 10.) [107]. However, controversially, the PtdIns4P binding site is not known and further canonical PtdIns4P binding domains (PH domain, ENTH domain) have not been identified yet [107].

Independently from enteroviruses, Aichi virus utilises different mechanisms to hijack host PI4K IIIβ to secure a PtdIns4P enriched membrane environment. In Achi virus-infected cells, PI4K IIIβ is recruited to the Golgi membrane via series of subsequent interactions among ACBD3, viral protein and PtdIns4P (see Figure 10.) [131,142]. ACBD3 is recruited to the Golgi membrane via giantin recognition in non-infected cells [146] while in a more advanced state of viral infection the giantin can be replaced with any of the five non-structural viral proteins (2B, 2BC, 2C, 3A, 3AB) [131]. The giantin-ACBD3 interaction turned out to be crucial for maintaining Golgi integrity since its replacement with viral protein results in cytoplasmic dispersion of the Golgi compartment in the form of sequestered invaginated membrane structures [131]. Whether viral 3D RNA polymerase preferentially binds to PtsIns4P in membranous webs to generate a functional replication complex is still not known. However, in contrast to HCV RNA polymerase, a direct interaction between PI4K IIIβ-RdRp $3D^{pol}$ or PI4K IIIβ-3D has yet to be discovered.

Overall, the mechanism by which PI4K IIIβ is hijacked by viral proteins has been outlined for some viruses, thereby providing an alternative approach to combat multiple viral infections. However, further structural studies have been necessitated for mapping host-viral interactions sites which could be potentially targeted.

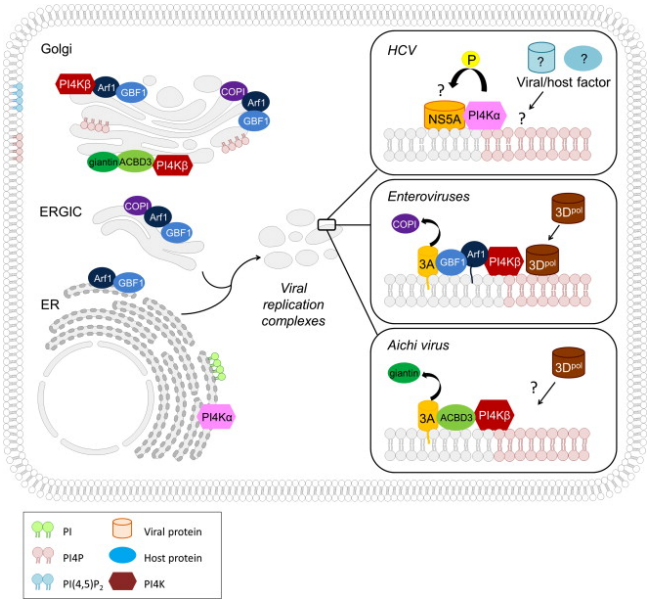



**Figure 10.: Schematic representation of different strategies to hijack human PI4 kinases type III.**
In the top right panel PI4K IIIα is recruited to the MWs by direct interaction with viral non-structural protein NS5A. In the middle right panel myristoylated enteroviral 3A protein recruits PI4K IIIβ to the replication platform via interaction with small GTPase Arf1 and its GBF1 guanidine nucleotide exchange factor. The bottom right panel depicts recruitment of PI4K IIIβ by Achi-virus 3A protein via cooperative interaction with ACBD3. Taken from [147].

## 3.2.3 PI4-kinases type II

### 3.2.3.1 Gene and protein isoforms

Different approaches have been attempted in order to obtain DNA sequences coding for the α and β isoforms of PI4-kinases type II. Since reverse transcription together with EST data base searching provided a partial cDNA or incomplete ORF, the first clones of individual isoforms were obtained from proteolytic fragments derived from individual proteins isolated from membrane rafts [148,149]. Different tryptic peptides were used for multiple sequence assignment to assemble overlapping sequences. Upon gene sequence recognition, the localisation of PI4K2A and PI4K2B genes were mapped to chromosome 10, locus 10q24 and chromosome 4, locus 4p15.2, respectively. The 1437 bp-long ORF for the α isoform and 1443 bp-long ORF for the β isoform encode 54 kDa proteins that is in a good agreement with the expected molecular weight [149]. In yeast, both the α and β isoforms are represented by only one gene termed Lsb6 [150] while *Arabidopsis thaliana* contains eight genes coding for ubiquitously expressed variants of PI4K type II [151]. Furthermore, the yeast orthologue Lsb6 was found to be dispensable for yeast survival but

the yeast orthologues of type III PI4-kinases, Pik1(PI4K IIIβ) and Stt4 (PI4K IIIα), are essential [152–154].

### 3.2.3.2 Protein

#### 3.2.3.2.1 Localisation

A novel type of PI4 kinases was discovered serendipitously when testing the function of lipid rafts. An elevated level of ATP hydrolysing activity was observed during this experiment and its further examination led to identification of type II PI4 kinases. Following experiments with recombinant proteins confirmed that both isoforms behave as integral membrane proteins in spite of a missing transmembrane segment [149,155]. A detailed sequence analysis identified the presence of a cysteine-rich motif which can serve as a putative palmitoylation site. Mutating this motif to serine residues reduced the kinase activity and converted the tightly membrane-anchored kinase to a peripherally bound protein. Although this motif is also conserved in the β isoform, a vast majority of this protein is retained as a cytoplasmic pool and its membrane association was demonstrate to be a tightly regulated process [155–157].

Membrane bound forms of PI4K type II were found in the ER, the TGN, endosomes and in lesser amounts at the plasma membrane either at basal conditions (PI4K IIα) or after the platelet-derived growth factor stimuli (PI4K IIβ) [148,157].

#### 3.2.3.2.2 Structure

A limited proteolysis and computational sequence analysis was employed to identify the minimum fragment responsible for the enzymatic activity and potentially novel structural domains or motifs in type II PI4-kinases [158]. Sequence analysis revealed a cluster of cysteine residues in the catalytic region of both isoforms whereas a diverse N-terminal area contained a highly acidic region in the β isoform and a proline-rich region in the α isoform. Recently solved crystal structures of both the α and β isoforms confirmed the bi-lobed C-terminal catalytic domain with the ATP binding site positioned between the N- and C- lobes (see Figure 11.) [87–89]. Surprisingly, a second ATP binding site was found in a lateral hydrophobic pocket of the C-lobe in PI4K IIα (see Figure 11.) [87,88]. The overall fold of both isoforms is highly conserved and, therefore, only the disordered N-terminal region makes these proteins structurally distinguishable.

#### 3.2.3.2.3 Function

The TGN- and endosomal-localised type IIα kinase regulates trafficking processes via recruitment of coat adaptors proteins AP-1 and AP-3 to the Golgi and endosomal PtdIns4P lipids [27,159]. Furthermore, PI4K IIα is implicated in EGF receptor endosomal-mediated degradation [160] and synaptic vesicle biogenesis [161]. PI4K IIα was also identified to play a role in modulating the Wnt signalling pathway. Wnt3a protein up-regulates PI4K IIα activity in a Dvl- and Fz-dependent manner. Dishevelled (Dvl), a cytosolic protein recruited to Wnt3a-bound Frizzled (Fz) receptors, forms a complex with PI4K IIα and PIP5K I to stimulate PtdIns(4,5)$P_2$ production. An increased amount of this lipid is required for phosphorylation-induced LRP6 aggregation and the final β-catenine stabilisation [162,163]. The enzymatic activity of PI4K IIα can be modulated not only by interaction with Dvl protein in a positive manner but also by tight association with Itch-E3 ubiquitin ligase in the opposite way. Once the PI4K IIα-Itch complex is formed, PI4K IIα-mediated PtdInd(4,5)$P_2$ production is decreased and ubiquitin-dependent endosomal degradative sorting of internalised Fz receptors is promoted. Therefore, Itch-E3 ubiquitin ligase represents a negative regulator of the canonical Wnt signalling pathway [164]. Additionally, PI4K IIα together with PI4K IIIβ control LIMP-2-mediated GBA transport to the lysosomes [165]. β-glucocerebrosidase (GBA) is a lysosomal enzyme responsible for hydrolysing glucosylceramide and, therefore, a defect in this metabolic pathway leads to glucosylceramide accumulation and causes the lysosomal storage disorder known as Gaucher disease. Lysosomal delivery of this enzyme is highly dependent on its recruitment to the LIMP-2 receptor (lysosomal integral membrane protein type 2) and on the catalytic activity of PI4K IIα and PI4K IIIβ. In order to distinguish the role of each kinase in GBA lysosomal transport, depletion of the enzymatic activity or of the protein itself was carried out. Treatment of PI4K IIIβ with isoform-specific inhibitor revealed that PI4K IIIβ is responsible for proper sorting of the LIMP-2/GBA complex from the Golgi since its inactivation prevented exit of this complex. On the other hand, siRNA targeting PI4K IIα resulted in enlarged LIMP-2 positive endosomes thus implicating it in the trafficking steps between the late endosomes and the lysosomes. Collectively, dysfunction of both PI4K IIα and PI4K IIIβ blocks post-Golgi trafficking events and causes missorting of GBA enzyme, thereby contributing to Gaucher´s disease [165].

In contrast, no specific function was described for PI4K IIβ.

As mentioned previously, PI4K IIα is a constitutively membrane bound protein whilst PI4K IIβ is distributed between membranes and the cytosol. It was shown that membrane association makes these proteins catalytically active while a cytosolic form is inactive [155–157]. Therefore, in the cell there is a large pool of inactive PI4K IIβ isoform which can be converted to the active form following exposure to the appropriate stimuli. Jung *et al*. proposed the model of stimulus-dependent activation of PI4K IIβ. The key regulatory molecule in this model is molecular chaperon Hsp90 which associates only with the cytosolic form of PI4K IIβ and protects it from proteasomal degradation. In response to the stimuli, released PI4K IIβ is recruited to the membrane in a yet unidentified mechanism where it is further palmitoylated and activated [166].

As any other lipid kinases, type II PI4-kinases must be membrane bound to access their substrate. Therefore, palmitoylation seems to be the main regulatory mechanism of type II PI4K activation. Palmitoylation itself is cholesterol dependent and, therefore, the cholesterol level can modulate the lipid kinase activity indirectly by affecting membrane composition and fluidity [167]. Moreover, the enzymatic activity of PI4K IIα was shown to be sensitive to calcium [168] and adenosine inhibition [155].

# 4 Aims of the study

**Specific research aims:**

1. To structurally and functionally characterise type II PI4-kinases using X-ray crystallography. To define and juxtapose the active sites and individual residues responsible for cooperative ATP and phosphatidylinositol binding of both isoforms. To evaluate the overall kinase fold and domain organisation. To outline membrane association and kinase orientation with respect to the phospholipid bilayer. To compare the structural similarity of type II PI4-kinases with type III PI4-kinases.

2. To attempt crystallization with a series of ATP-derived inhibitors. To select reasonably soluble inhibitors and initiate their co-crystallization studies with PI4-kinases type II and PI4K IIIβ. To optimise the crystal growth and quality and conduct X-ray diffraction analysis. To outline the inhibition mechanism at the atomic level.

# 5 Publications

## Publications included in dissertation thesis

**1 "The Crystal Structure of the Phosphatidylinositol 4-Kinase IIα."**

Baumlova A, Chalupska D, Różycki B, Jovic M, Wisniewski E, Klima M, Dubankova A, Kloer D, Nencka R, Balla T and Boura E. *EMBO Rep.* **15,** 1085–1092 (2014)

**2. "The High-Resolution Crystal Structure of Phosphatidylinositol 4-Kinase IIβ and the Crystal Structure of Phosphatidylinositol 4-Kinase IIα Containing a Nucleoside Analogue Provide a Structural Basis for Isoform-Specific Inhibitor Design."**

Klima M, Baumlova A, Chalupska D, Hřebabecký H, Dejmek M, Nencka R and Boura E. *Acta Crystallog D Biol Crystallog.* **71,** 1555–1563 (2015).

**3. "Highly Selective Phosphatidylinositol 4-Kinase IIIβ Inhibitors and Structural Insight into Their Mode of Action."**

Mejdrová I, Chalupská A, Kögler M, Šála M, Plačková P, Baumlova A, Hřebabecký H, Procházková E, Dejmek M, Guillon R, Strunin D, Weber J, Lee G, Birkus G, Mertlíková-Kaiserová H, Boura E and Nencka R. *J Med Chem.* **58,** 3767–3793 (2015)

## Publication not included in dissertation thesis

**"Structural Insights and in Vitro Reconstitution of Membrane Targeting and Activation of Human PI4KB by the ACBD3 Protein."**

Klima M, Tóth DJ, Hexnerova R, Baumlova A, Chalupska A, Tykvart J, Rezabkova L, Senqupta N, Man P, Dubankova A, Humpolickova J, Nencka R, Veverka V, Balla T and Boura E. *Sci Rep.* **6,** 23641 (2016)

1.

## 5.1 The Crystal Structure of the Phosphatidylinositol 4-Kinase IIα

**Background**

PI4K IIα is the most active enzyme from all four mammalian PI4-kinases and, therefore, is responsible for about 50% of the overall PtdIns4P turnover on cell membranes. Since PI4K IIa is a constitutively membrane bound protein, its enzymatic activity is modulated indirectly by changing the lipid composition and affecting the enzyme diffusion in the phospholipid bilayer. The functional role of PI4K IIα in a cell physiology is not fully understood but it was shown that PI4K IIα is involved in TGN and endosomal trafficking processes [27,36,159], neuronal vesicular sorting [161], microbial pathogenicity [75] and Wnt signalling pathway which is implicated in embryonic and bone development, tumorigenesis, neurogenesis and in lipid and glucose metabolism [162,163]. Additionally, dysfunction of this protein was detected in Alzheimer´s disease [169,170] and also leads to a metabolic disorder known as Gaucher´s disease [165].

Considering the emerging role of PI4KIIa in diverse intracellular processes and its inadequate structural and functional characterisation, an X-ray determined crystal structure would help to elucidate the mechanism of PtdIns4P synthesis and regulation of its functional state, which when coupled together, would obviously be a useful tool for isoform-specific inhibitor design.

**Summary**

We solved the crystal structure of PI4K IIα in complex with its physiological substrate ATP at 2.8 Å resolution using MR-SAD method (see Figure 11.). Structural analysis revealed the presence of the N- and C-lobe with the ATP binding site positioned in between. The crystal structure also enabled us to define the residues in the ATP binding site. Their importance for catalytic activity was verified using mutagenesis analysis. Surprisingly, a second ATP molecule was identified in the C-lobe of the catalytic domain. Since mostly hydrophobic residues define this site, we termed it as the lateral hydrophobic pocket. Unfortunately, we were not able to obtain crystals with inositol or inositol-1-phosphate bound. Therefore, docking studies were performed to identify a putative phosphatidylinositol pocket. Additionally, the membrane binding mode of PI4K IIα was outlined based on MD-simulation and mutagenesis analysis. Different structural aspects such as the overall protein fold, presence of the lateral hydrophobic pocket, localisation of

the ATP binding site and distribution of electrostatic potential were taken into account in identifying the regions responsible for membrane association.

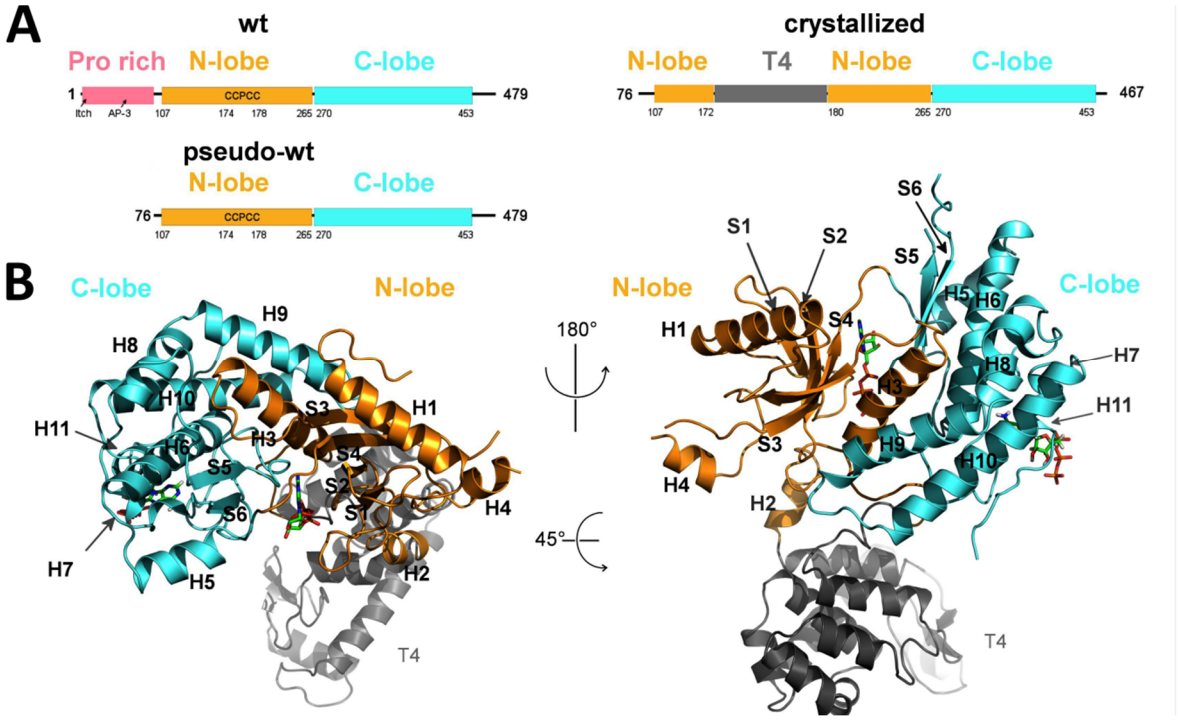



**Figure 11.: The crystal structure of PI4K IIα.**
**Panel A:** depicts a domain organisation of the individual constructs used for crystallization trials or biochemical studies**. Panel B:** shows cartoon representation of the overall PI4K IIα structure with bound ATP. The N- and C-lobes are coloured in orange and cyan, T4 lysozyme in grey and ATP is shown in stick representation.

## My contribution

I expressed and purified constructs of PI4K IIα without T4 lysozyme or with differently positioned T4 lysozyme and carried out the crystallization trials. I performed the mutagenesis experiments and expressed and purified individual mutants of PI4K IIα. I analysed the impact of the mutated residues in the active site as well as in the lateral hydrophobic pocket on enzymatic activity using *in vitro* kinase assay. I participated in X-ray data collection.

Scientific Report

TRANSPARENT PROCESS

EMBO reports

# The crystal structure of the phosphatidylinositol 4-kinase IIa

Adriana Baumlova[1], Dominika Chalupska[1], Bartosz Różycki[2], Marko Jovic[3], Eva Wisniewski[3], Martin Klima[1], Anna Dubankova[1], Daniel P Kloer[4], Radim Nencka[1], Tamas Balla[3] & Evzen Boura[1,*]

## Abstract

Phosphoinositides are a class of phospholipids generated by the action of phosphoinositide kinases with key regulatory functions in eukaryotic cells. Here, we present the atomic structure of phosphatidylinositol 4-kinase type IIa (PI4K IIa), in complex with ATP solved by X-ray crystallography at 2.8 Å resolution. The structure revealed a non-typical kinase fold that could be divided into N- and C-lobes with the ATP binding groove located in between. Surprisingly, a second ATP was found in a lateral hydrophobic pocket of the C-lobe. Molecular simulations and mutagenesis analysis revealed the membrane binding mode and the putative function of the hydrophobic pocket. Taken together, our results suggest a mechanism of PI4K IIa recruitment, regulation, and function at the membrane.

Keywords crystal structure; kinase; membrane; Monte Carlo simulations; phosphatidyl inositol
Subject Categories Membrane & Intracellular Transport; Structural Biology
DOI 10.15252/embr.201438841 | Received 27 March 2014 | Revised 6 August 2014 | Accepted 7 August 2014

## Introduction

The importance of inositol lipids in many aspects of eukaryotic biology has now been widely recognized [1]. As phosphorylation products of phosphatidylinositol (PI), they are generated by a plethora of enzymes that phosphorylate specific positions of the inositol ring, yielding the seven known inositol lipid isomers [1]. These lipids control membrane dynamics lipid distribution, ion channels, transporters, and intracellular signaling among emerging roles in viral entry and replication [1]. Phosphorylation of PI at the 4-position by PI 4-kinases (PI4Ks) and subsequently by phosphatidylinositol 4-phosphate (PI4P) 5-kinases has been recognized as the major route of PI(4,5)P2 synthesis [2]. Although PI(4,5)P2 is one of the best studied phosphoinositides with connections to a number of plasma membrane-linked processes [1], it is increasingly evident that its precursor, PI4P plays independent and critical regulatory roles in various membrane compartments, most notably in the plasma membrane [3], Golgi [4], and late endosomes/lysosomes [5–7]. The recent identification of PI4P as a key phosphoinositide required for the replication of a number of RNA viruses [8] has drawn attention to the significant gaps in our understanding of the biogenesis of this lipid by PI4K enzymes at the molecular level.

PI4P is made by four distinct PI4K enzymes in mammals [9], all of which have homologues in lower eukaryotes [10]. The highest PI4K activity associated with isolated membranes is attributed to the so-called type II enzymes that are tightly membrane-bound and require detergents to be extracted from membranes [11]. In contrast, type III PI4Ks are peripherally membrane associated soluble proteins whose recruitment to membranes involves interaction with other protein [9]. Bioinformatics analysis revealed that the catalytic domains of type III PI4Ks show high homology to the PI3Ks and PI-kinase-related protein kinases, whereas type II PI4Ks form a distinct family [12,13]. Additionally, the biology of type III PI4Ks has been explored primarily by elegant yeast studies where the larger PI4K IIIa enzyme (and the yeast orthologue, Stt4p) is mostly responsible for the synthesis of the PM pool of PI4P, whereas PI4K IIIb (or its yeast orthologue, Pik1p) mostly functions in the Golgi and post-Golgi compartments [10]. Mammalian type II PI4Ks (alpha and beta) are proteins whose membrane association and activity is highly dependent on palmitoylation [14,15], and they are present in the PM and in a number of endomembrane compartments including the TGN and early and late endosomes [5,16,17]. Type II PI4K enzymes are tightly linked to vesicular trafficking by contributing to the recruitment of the clathrin adaptors AP1, AP3, some GGAs, and VAMP3 [6,17–19] and are particularly important for the lysosomal targeting of EGF receptors [5] or enzymes of sphingolipid metabolism [7]. The activity of the PI4K IIa enzyme is regulated by cholesterol [20], which also affects the palmitoylation and localization of the protein [21].

The dissimilarity of the type II PI4Ks to any other kinase families has presented difficulties in gaining any reliable insight into the structure of these molecules. Here, we present the X-ray structure of

1 Institute of Organic Chemistry and Biochemistry AS CR, Prague, Czech Republic
2 Institute of Physics, Polish Academy of Sciences, Warsaw, Poland
3 Section on Molecular Signal Transduction, Program for Developmental Neuroscience, NICHD, NIH, Bethesda, MD, USA
4 Syngenta, Jealott's Hill Internation Research Centre, Bracknell, UK
*Corresponding author. Tel: +420 220 183 465; Fax: +420 220 183 578; E-mail: boura@uochb.cas.cz

a 2014 The Authors

the PI4K IIa at 2.8 Å resolution. The structure provides a critical template for this unique family of type II PI4K enzymes. The structure, which revealed non-typical kinase fold and an unexpected hydrophobic pocket with a second ATP bound, will greatly facilitate further study of these proteins and allow targeted manipulation of their interactions with regulatory components.

## Results and Discussion

### PI4K IIa crystal structure

The proline-rich N-termini of the enzyme contains physiologically important binding sites for ubiquitin ligase Itch [22] and clathrin adaptor complex 3 [6] but is predicted to be disordered, and its deletion does not affect the kinase activity [23]. Since this N-terminus lowers solubility and expression yields of the recombinant enzyme, it was omitted in the constructs used for biochemical analysis (called here pseudo-wt). For crystallographic analysis, additional 12 residues at the C-terminus were deleted and the palmitoylated LCCPCCF motif was replaced with T4 lysozyme to increase solubility and to improve crystallization properties (Fig 1A). We obtained crystals that diffracted to 2.8 Å and belonged to the orthorhombic $P2_12_12$ space group with one molecule per asymmetric unit. The structure was subsequently solved by MR-SAD and refined to $R_{work}$ = 21.15% and $R_{free}$ = 25.11%. (Table 1). The first ordered residue in the structure was $R^{101}$, and the last one was $A^{454}$. We were able to trace the entire chain from $R^{101}$ to $A^{454}$ except for two short disordered loops between residues $S^{231}$ – $I^{251}$ and $Y^{318}$ – $D^{331}$. The structure revealed a non-typical kinase fold that could be divided into the N-lobe and C-lobe with the ATP binding groove between (Fig 1B and C, detailed Fig 2A). The N-lobe consists of four helices (H1-H4) packed around a core of four small antiparallel b-sheets (S1-S4). The C-lobe has two b-sheets closely surrounded by helices H5, H6, and H7. Helices H8, H9, and H10 are packed in a 'roof' arrangement above both lobes and represent the most distant part of the kinase from the membrane. Surprisingly, the structure revealed another ATP molecule bound in a lateral hydrophobic pocket partly supported by the H11 helix (Fig 1B, Supplementary Fig S2) (detailed Fig 2B). While this study was under review, a structural study of PI4K IIIb that has a more typical PI-kinase fold was published [24]. Superimposition of the whole kinase domains of PI4K IIa and PI4K IIIb (Fig 1D) showed that only helix H3 of the N-lobe can be superimposed on the corresponding regions of the

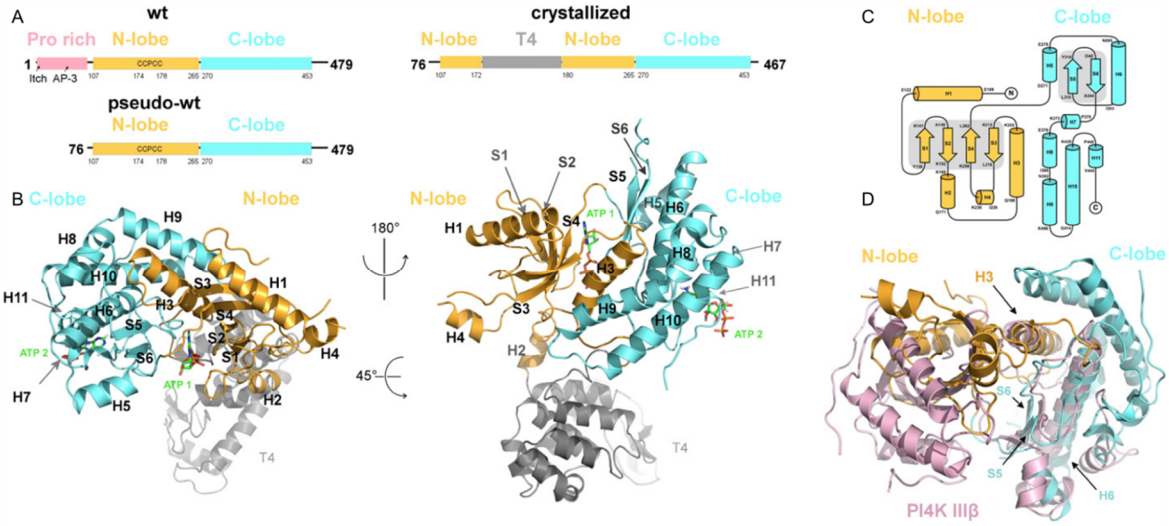



Figure 1. The overall fold of PI4K IIa.

A Wt, pseudo-wt, and crystallized PI4K IIa. Binding sites for ubiquitin ligase Itch and AP3 are shown within the proline rich of the wt enzyme (left). The N-terminus is deleted in the pseudo-wt construct (lower left) used for biochemical assays. In the crystallized construct (right), the last 12 residues are deleted as well and the palmitoylated CCPCC motif is replaced with T4 lysozyme.

B Overall fold of PI4K IIa. On the left, view oriented to show the ATP binding pocket localized between the N- and C-lobes. On the right, view rotated 180° and tilted to place T4 lysozyme in the back. The kinase has 11 a-helices (numbered H1–H11), H1 to H4 are located in the N-lobe, where they surround two pairs of antiparallel b-sheets (S1–S4). A pair of b-sheets (S5, S6) in the C-lobe is closely surrounded by helices H5, H6, and H7, while the helices H8, H9, and H10 form a 'roof'. A second ATP is bound in a lateral hydrophobic pocket of the C-lobe that is partially supported by helix H11. The palmitic acid residues would occupy the loop that is replaced by the T4 lysozyme. The N-lobe is depicted in orange, the C-lobe in cyan, the T4 lysozyme in gray.

C Topology plot of PI4K IIa. The enzyme's N-lobe consists of four a-helices and four b-sheets, and the C-lobe is composed of seven a-helices and two b-sheets. The color code is as in (A).

D Superimposition of PI4K IIa and PI4K IIIb. Only helix H3 of the N-lobe can be superimposed on the corresponding regions of the PI4K IIIb typical kinase domain. On the other hand, from the C-lobe helix H6 and sheets S5, S6 superimpose well. The N-lobe and C-lobe of PI4K IIa are in orange and cyan, respectively. The PI4K IIIb kinase domain is shown in pink.


a 2014 The Authors

Table 1. Statistics of crystallographic data collection and refinement

| Data collection | | |
|---|---|---|
| Crystal | Native PI4K IIa | SeMet PI4K IIa |
| Space group | $P2_12_12$ | $P2_12_12$ |
| Cell dimension | a = 104.8 Å, b = 79.5 Å, c = 78.7 Å | a = 102.3 Å, b = 79.5 Å, c = 79.1 Å |
| X-ray source | BESSY ID 14-2 | BESSY ID 14-1 |
| Wavelength, Å | 0.91841 | 0.97984 |
| Resolution, Å | 36.84–2.77 (2.87–2.77) | 49.16–3.00 (3.10–3.00) |
| No. of unique reflections | 16256 (1631) | 13505 (1325) |
| I/r (I) | 12.45 (2.02) | 10.99 (3.07) |
| $R_{merge}$ | 15.9 | 20.9 |
| Data completeness, % | 93.87 (95.77) | 99.92 (98.95) |
| Multiplicity | 5.8 | 12.9 |
| Refinement | | |
| $R_{work}$, % | | 21.15 (27.10) |
| $R_{free}$, % | | 25.11 (36.45) |
| Number of non-hydrogen atoms | | 3975 |
| Protein residues | | 484 |
| rms bond angle deviation, ° | | 0.013 |
| rms bond angle deviation, Å | | 1.46 |
| Average B-factor | | 58.30 |
| Ramachandran (outliers/favored) | | 0.21%/97% |

Numbers in parentheses refer to the highest resolution shell of the respective dataset.

PI4K IIIb typical kinase domain. However, helix H6 and sheets S5, S6 of the C-lobe can be superimposed on the corresponding regions of the PI4K IIIb typical kinase domain. The dissimilarity of the N-lobes and the similarity of the C-lobes become apparent when the superimpositions are done separately for each lobe (Supplementary Fig S1 C and D). Comparison of the structures of PI4K IIa and of its closest structural relative found in a search of Protein Data Bank (Supplementary Fig S1A)—the cell translocating kinase A (ctkA), a Ser/Thr kinase from Helicobacter pylori [25]—shows a possible evolutionary connection between the type II PI4Ks and Ser/Thr protein kinases.

In summary, the structure of the PI4K IIa serves as a template for the type II PI4K enzymes. It reveals a non-typical kinase fold and an unexpected hydrophobic pocket with a second ATP bound. Its flattened fold brings the catalytic center close to the membrane-anchored substrate [26] with the c-phosphate of the ATP pointing directly to the lipid membrane (Fig 3A).

## The ATP binding groove

The catalytic ATP binding groove lies between the N- and C-lobes (Fig 1B). ATP is held in position by hydrogen bonds with side chains of residues $K^{152}$, $S^{137}$, $D^{346}$, and with the protein backbone (Fig 2A). Mutagenesis analysis (Fig 2C) showed that residues defining the ATP binding site (e.g. $S^{134}$, $V^{150}$, $I^{345}$) are important for catalytic activity, whereas mutation of a residue further away ($F^{139}A$) has no significant impact on activity. We also show that the residue $K^{152}$ making direct hydrogen bond with the a-phosphate is indispensable for catalytic activity. Since the $D^{308}$ is too far away from the ATP, the known $D^{308}A$ kinase dead mutation can be only explained by $D^{308}$ being part of the inositol binding pocket and/or being important for positioning a water molecule for catalysis. Unfortunately, we were unable to get crystal structure with inositol or inositol-1-P bound. However, modeling suggests that inositol can be fitted without structural or energetic constraints in a pocket in close vicinity to the ATP's c-phosphate (Fig 3C).

## Membrane binding mode of PI4K IIa

Molecular simulations show that when the kinase is tightly bound to the membrane, the ATP molecule, located in the catalytic site between the N- and C-lobes, points directly toward the lipid bilayer. Notably, the lateral hydrophobic pocket is then exposed toward the lipid bilayer (Fig 3A). This suggests that it could bind a hydrophobic ligand present within the lipid membrane in the physiological environment. In a second group of solutions obtained in our simulations, the kinase is in a 'loose' state where it is tethered to the membrane only by the four palmitoyl groups, the segment between $K^{165}$ and $K^{172}$, and the lateral hydrophobic pocket (Supplementary Fig S3C). This, probably non-physiological, second configuration is described and discussed in more detail in the Supplementary Information.

To test our model, we chose two residues at the predicted membrane interface ($N^{163}$, $R^{275}$) and two control residues ($N^{249}$, $V^{339}$) predicted not to interact with the membrane for mutational analysis. As predicted, the mutations $N^{163}A$ or $R^{275}A$ significantly lowered the kinase activity, whereas the mutations $N^{249}A$ or $V^{339}A$ had no effect (Fig 3B). In addition, when the segment 165-KWTKWLQK-172 that is predicted most important for membrane binding was mutated to alanines, the kinase became inactive (Fig 3B). However, even though that the mutants expressed at the same level as wild-type enzyme both in mammalian and in bacterial cells and that the recombinant mutant proteins behaved as wild-type during size exclusion chromatography, we cannot completely rule out that the mutants had somewhat lower kinase activity due to folding problems.

Based on these data, we propose that the enzyme is kept at the membrane by multiple interactions: First, its palmitoylation plays a very important role. Second, the amphipathic segment 165-KWTKWLQK-172 adjacent to the palmitoylation sites also makes a significant contribution, probably through immersion of hydrophobic residues into the membrane with the basic residues interacting with the phosphorylated lipid head group—a common theme among membrane binding proteins [27,28]. Third, a hydrophobic pocket with $W^{359}$ and $W^{368}$ also helps aligning the enzyme with the membrane. The last contributing regions identified are helices H5 and H7. The impact of the latter interactions on enzymatic activity is exaggerated in assays using recombinant enzymes that are not palmitoylated when expressed in bacteria (Fig 3). This explains why the combined mutations of $W^{359}$ and $W^{368}$ only partially reduced the activity of the enzyme purified from mammalian cells or assayed in the cells in situ (Fig 4).

[a] 2014 The Authors

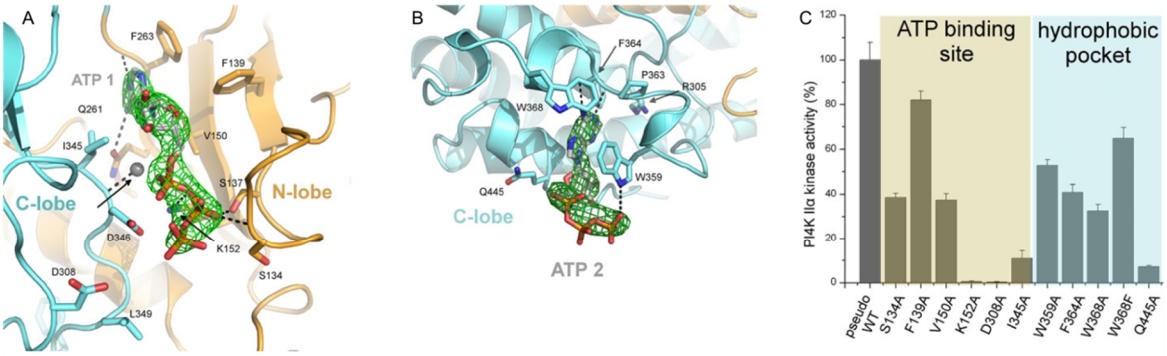



Figure 2. Detailed view and mutagenesis analysis of ATP binding sites.

A Detailed view of the ATP binding pocket. Hydrogen bonds between ATP and residues $S^{137}$, $K^{152}$, $Q^{261}$, $D^{346}$ as well as hydrogen bonds with a coordinated water molecule and protein backbone shown as dotted black lines. The catalytically important residue $D^{308}$ surprisingly does not form a direct contact with ATP as it is spaced 4.55 Å away from the ATP's closest c-phosphate oxygen. The unbiased $F_o$-$F_c$ map contoured at 2 sigma is shown around the ATP molecule. The protein backbone is shown in cartoon representation, N-lobe colored in orange, C-lobe in cyan. ATP and side chains of selected residues are shown in stick representation and colored according to elements. Oxygen is shown in red, nitrogen in blue, phosphor in orange, kinase carbon atoms are colored according to domain assignment, and ATP's carbons are in silver. Water molecule is shown as a sphere. Hydrogen atoms are not shown.

B Detailed view of the lateral hydrophobic binding pocket of the C-lobe. The pocket is formed by the hydrophobic residues $W^{359}$, $F^{364}$, $W^{368}$ with some help of $P^{363}$. The adenine ring forms only two hydrogen bonds with the protein backbone, a third hydrogen bond is formed between the $W^{359}$ indole ring and the c-phosphate of ATP. The unbiased $F_o$-$F_c$ map contoured at 2 sigma is shown around the ATP molecule. The figure is colored as in (A).

C Mutagenesis analysis of the ATP binding site and the hydrophobic pocket. Selected residues of the ATP binding site were mutated to alanines, and the kinase activity was measured in vitro using recombinant proteins and the luminescent ADP-Glo kinase assay [35]. The luminescence signal was normalized to the pseudo-wt activity. The mutation of all the tested residues of the ATP binding site had profound effect on the kinase activity with the exception of $F^{139}$ that is not in close vicinity of the ATP. The most profound effect was the mutations of $K^{152}$ and $D^{308}$. Similarly, all mutations tested in the hydrophobic pocket had profound effect. Noteworthy, the mutations $W^{368}$A had a two times stronger phenotype than mutation $W^{368}$F presumably because phenylalanine is also a hydrophobic residue albeit not as much as a tryptophan residue.

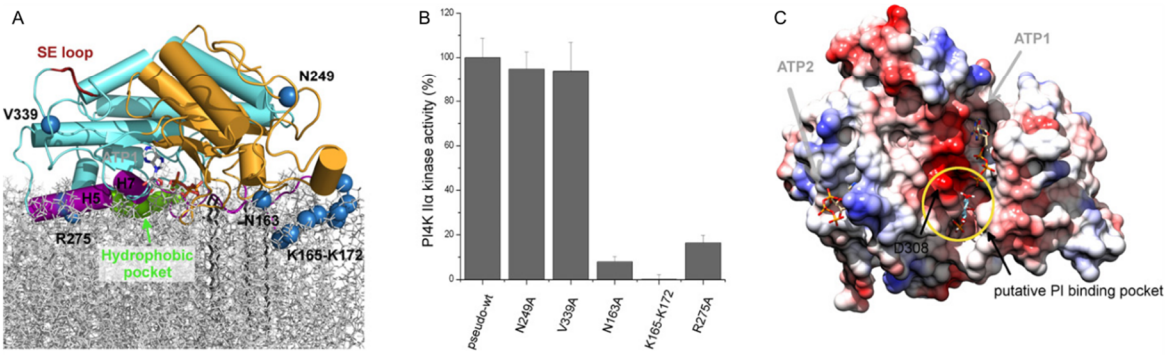



Figure 3. Membrane binding mode of PI4K IIa.

A Simulation-based model of PI4K IIa on the lipid bilayer. The kinase is bound to the membrane by several regions of the kinase that include helices H5 and H7 (highlighted in violet), the lateral hydrophobic pocket and the entire flexible segment between $Pro^{164}$ and $Asp^{182}$, which contains the four palmitoylated Cys residues. These regions are in direct contact with the lipid membrane, and the c-phosphate of the ATP points toward the membrane. Residues selected for mutagenesis analysis are highlighted as blue spheres. The hydrophobic pocket is highlighted in green and the surface exposed (SE) loop in red.

B Mutagenesis analysis of the membrane binding model. Two residues predicted not to contact the membrane ($V^{339}$ and $N^{249}$), two residues predicted to be important for membrane binding ($N^{163}$ and $R^{275}$) and the entire $K^{165}$–$K^{172}$ membrane binding segment were chosen for in vitro mutagenesis analysis using recombinant and the luminescent ADP-Glo kinase assay. The luminescence signal was normalized to the pseudo-wt activity. While the mutations $V^{339}$A or $N^{249}$A had no effect on the kinase activity, both mutations $N^{163}$A and $R^{275}$A had significant effect and when the entire membrane binding segment $K^{165}$–$K^{172}$ was mutated to alanines, the kinase was inactive.

C The inositol binding pocket. Docking studies with inositol-1-P identified a putative PI binding pocket. The catalytically important aspartate residue $D^{308}$ does not directly contact the ATP, instead it is a part of the putative PI binding pocket. The surface of the kinase is colored accordingly to electrostatic potential. ATPs and inositol-1-P are shown in stick representation.


a 2014 The Authors

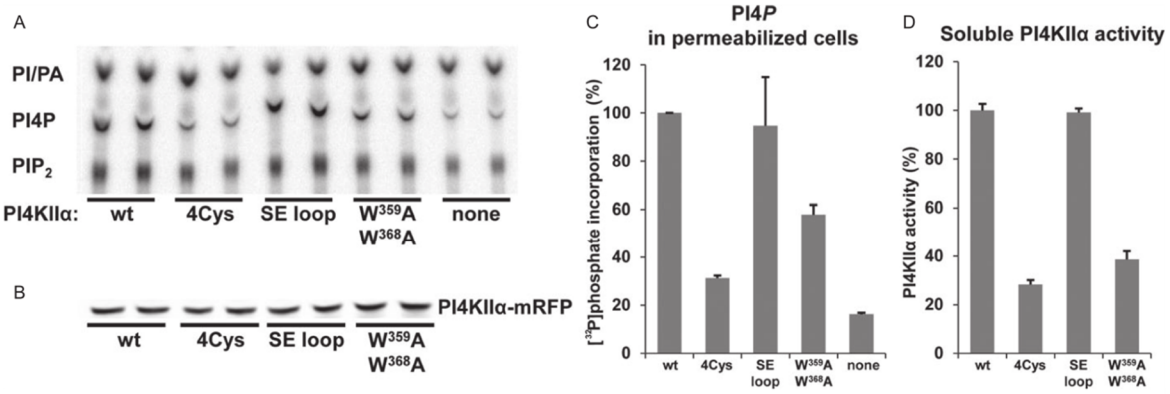



Figure 4. Kinase activity of human PI4KIIa mutants assayed in situ and in solution.

A COS-7 cells transfected with the indicated PI4KIIa-RFP plasmids were pretreated with 10 I M wortmannin (Wm) to inhibit the endogenous type III PI 4-kinases, then permeabilized with digitonin and incubated with [c-$^{32}$P]ATP and Wm for 15 min prior to phospholipid extraction. Shown is a representative TLC autoradiogram.

B Western blot showing the expression levels of PI4KIIa-RFP constructs used in (A).

C Quantification of phosphoinositide levels from two in situ PI4KIIa experiments shown in (A) performed in duplicate. Shown are grand averages Æ range.

D Characterization of kinase activities of PI4KIIa-mRFP mutants affinity-purified from COS-7 cells. ADP-Glo luminescence signal was normalized to the wild-type activity after subtracting the background signal detected from untransfected cells. Shown are means Æ SEM from triplicate measurements obtained in two experiments.

## The hydrophobic pocket

An intriguing feature of the solved structure is the hydrophobic pocket located at the C-lobe that is occupied by a second ATP molecule. It is predominantly formed by W$^{359}$, F$^{464}$, and W$^{368}$ residues with some help from P$^{363}$ (Fig 2B). In this pocket, the ATP molecule is stabilized by only two hydrogen bonds to the backbone of residues F$^{452}$ and Y$^{453}$, a third hydrogen bond is formed between the c-phosphate and the nitrogen of the W$^{359}$ indole ring. It is likely that the second ATP is found in the structure only because of the lack of a more suitable hydrophobic ligand in the crystallization condition. In the real cellular environment, at the surface or within the lipid bilayer, other, more suitable hydrophobic ligands could be presented. It is tempting to speculate that the recruitment or activity of the kinase is regulated by a ligand presented on the membrane suitable for binding to the hydrophobic pocket. The hydrophobic pocket could sterically accommodate the head group of several phospholipids, including the inositol ring of PI and cholesterol that has been implied in the control of PI4K IIa palmitoylation and activity is cholesterol (Supplementary Fig S2) [20,21]. To address its functional relevance, we performed mutagenesis studies. We used permeabilized cells expressing the various mutant enzymes to assay the enzyme activity in its natural environment. We compared the double mutant within the hydrophobic pocket (mutation W$^{359,368}$A) with the 4Cys palmitoylation-deficient mutant (the palmitoylated motif CCPCC is mutated to SSPSS) and with an additional mutant in which a surface exposed (SE) hydrophobic loop not predicted to be important for membrane binding in our simulations was mutated (332-WVVV-335 mutated to 332-SAAA-335) (Fig 4). We found that the palmitoylation-deficient 4Cys mutant showed the strongest impairment in kinase activity in both the permeabilized cell (Fig 4C) and in vitro assay (Fig 4D). No major effect was observed when the solvent exposed hydrophobic loop was mutated. Mutations within the hydrophobic pocket facing the membrane significantly reduced but did not eliminate the kinase activity. It is noteworthy that mutations W$^{359}$A or W$^{368}$A in the bacterially expressed and thus non palmitoylated pseudo-wt protein (Fig 2C) showed stronger impairment of kinase activity than the double mutant W$^{359,368}$A expressed in the mammalian cells. Since the latter proteins is palmitoylated, these results suggest that the hydrophobic pocket is important for membrane binding or proper positioning and its importance becomes critical when the enzyme lacks palmitoylation. We also tested the localization of the mutant enzyme and found no obvious difference compared to wild-type except for the 4Cys mutation, which made a larger fraction of the enzyme cytoplasmic and enhanced the localization in the plasma membrane (Supplementary Fig S4). Further studies are in progress in cellular systems to address whether these mutations change the cholesterol requirement of the enzyme or if there is any specific lipid ligand that interacts with this site. However, the fact that these mutants show reduced activity even by the in vitro assays against lipid micelles suggests that this site may be promiscuous in its membrane interaction.

## Concluding remarks

Taken together, our results provide structural information on PI4P synthesis at the Golgi or other membranes. They explain how the PI4K IIa interacts with the membrane. The existence of a hydrophobic pocket facing the membrane can form the structural basis for recruitment or regulation of the enzymatic activity of PI4K IIa by a membrane components. While this study was under review, another structural study on PI4K IIa was published [29]. Zhou and colleagues used a different approach and obtained crystals in which the two PI4KIIa molecules in the asymmetric unit pack one against each other at the putative membrane binding surface leaving the hydrophobic pocket empty. Nevertheless, the major findings of the two

a 2014 The Authors

studies are in good agreement. While Zhou et al found that mutation of the $W^{359}$ and $W^{368}$ residues completely eliminated the enzymatic activity, our studies showed only a reduction. This difference may be due to the fact that they tested the effects of their mutations only with the recombinant protein expressed in bacteria in which all cysteines were already mutated. Our analysis using enzymes assayed in intact cells should be more informative in this respect. Regardless of these small differences, the structural information obtained here should help design further studies and aid rational drug design to better understand the roles of these enzymes in the control of trafficking and signaling in eukaryotic cells.

## Materials and Methods

### Plasmid construction, protein expression, and purification

PI4KIIa-mRFP was prepared from the previously described PI4KIIa-GFP construct [30] by replacing the entire GFP coding sequence with that coding the mRFP. Human PI4KIIa residues 76–479 was cloned into pRSFD vector (Novagen) with a N-terminal 6xHis tag followed by a GB1 solubility tag and TEV protease cleavage site using restriction cloning. Mutations were generated using the QuikChange kit (Stratagene) or the Phusion Site-Directed Mutagenesis Kit (Thermo Scientific). For crystallographic studies, the cysteine-rich motif LeuCysCycProCycCycPhe (residues 173–179) was replaced by a GlyThrGly linker followed by T4 lysozyme using the QuikChange kit (Stratagene) and the last 12 amino acids were deleted. The resulting protein had improved solubility and crystallization properties.

The proteins were expressed in E. coli BL21 Star and purified using affinity, anion exchange, and size exclusion chromatography as usual in our laboratory [31–33] and are detailed in the Supplementary Information.

### Crystallization and data collection

Before setting up crystallization drops, PI4K IIa was supplemented with ATP and $MgCl_2$. The crystals grew in 2 days, belonged to the $P2_12_12$ space group and diffracted to 2.77 Å resolution. The structure was solved using MR-SAD with T4 lysozyme as a search model and the anomalous signal from SeMet containing crystals as detailed in the Supplementary Information. The structure was refined to $R_{work}$ = 21.15% and $R_{free}$ = 25.11%.

### Replica Exchange Monte Carlo simulations

To efficiently sample physical configurations of the membrane-bound kinase, we used a coarse-grained model developed to simulate proteins both on membranes and in solution [34]. The detailed description of the coarse-grained model and simulation procedures are in the Supplementary Information. Briefly, we performed Replica Exchange Monte Carlo simulations with soft harmonic restrains imposed on the z-coordinates of the four palmitoylated Cys residues to mimic their attachment to the membrane. We analyzed the resulting 10,000 configurations as described in Supplementary Information and identified the residues that contribute to membrane interactions.

### Docking studies

The docking runs were performed in AutoDock Vina using the default scoring function. The 3D structures of the docked molecules were built using ACD/ChemSketch 12.01 (www.acdlabs.com), and the geometry was optimized with MOPAC2012 (www.OpenMOPAC.net) using PM7 method. Further details are in the Supplementary Information.

### Cell culture

COS-7 cells were cultured in Dulbecco's modified Eagle's medium (DMEM) supplemented with 10% fetal bovine serum (FBS), 100 U/ml of penicillin, and 100 l g/ml of streptomycin. COS-7 cells seeded on 12-well plates were transfected for 24 h with PI4KIIa-mRFP constructs using Lipofectamine 2000 (Life Technologies, Carlsbad, CA).

### In situ PI4KIIa kinase assay

Transfected COS-7 cells were incubated for 10 min in complete medium containing 10 l M wortmannin, followed by incubation in permeabilization medium containing 110 mM KCl, 10 mM NaCl, 5 mm MgCl2, 20 mM Hepes at pH 7.4, 2 mM EGTA, 0.05% bovine serum albumin, 15 l g/ml digitonin, 0.3 mM ATP, 12.5 l Ci/ml [c-$^{32}$P]ATP at 37°C, in the presence of 10 l M wortmannin. Reactions were terminated after 15 min using perchloric acid (5% final concentration). Inositol lipids were then extracted, separated by thin layer chromatography, and quantitated by phosphorimaging as described previously [30].

### In vitro soluble PI4KIIa kinase assay

Lysates from COS-7 cells transiently transfected with PI4KIIa-mRFP constructs were prepared as previously described before [35]. Lysates were then incubated for 1 h with streptavidin-conjugated Dynabeads (Life Technologies, Carlsbad, CA), prebound with biotin-conjugated anti-RFP antibody (Rockland, Gilbertsville, PA). PI4KIIa-bound Dynabeads were washed and subjected to ADP-Glo kinase assay as described [35]. Recombinant proteins were used in the ADP-Glo kinase assay at 85 nM concentration. Details are stated in the Supplementary Information.

### Data deposition

The crystallography, atomic coordinates, and structure factors have been deposited in the RCSB Protein Data Bank, www.pdb.org (accession code 4PLA).

Supplementary information for this article is available online:
http://embor.embopress.org

## Acknowledgements

Crystallographic data were collected at ESRF beamlines ID 14-4 and ID-23-1 and at beamlines 14-1 and 14-2 operated by the Helmholtz-Zentrum Berlin (HZB) at the BESSY II electron storage ring. This project was supported by MarieCurie FP7-PEOPLE-2012-CIG, project number 333916 (to E.B.), by Project InterBioMed LO1302 from Ministry of Education of the

 a 2014 The Authors

Czech Republic, and by the Academy of Sciences Czech Republic (RVO: 61388963). The work of B.R. was supported by the Polish National Science Centre Grant No. 2012/05/B/NZ1/00631. The work of M.J., E.W., and T.B. is supported by the intramural research program of the Eunice Kennedy Shriver National Institute of Child Health and Human Development of the NIH, Bethesda, MD, USA.

### Author contributions

AB, DC, MJ, MK, AD, EW performed experiments. BR performed computer simulations. BR, DPK, RN, TB, and EB analyzed data. TB and EB wrote the manuscript. EB designed the study.

### Conflict of interest

The authors declare that they have no conflict of interest.

## References

1. Balla T (2013) Phosphoinositides: tiny lipids with giant impact on cell regulation. Physiol Rev 93: 1019 – 1137
2. Berridge MJ, Irvine RF (1984) Inositol trisphosphate, a novel second messenger in cellular signal transduction. Nature 312: 315 – 321
3. Hammond GRV, Fischer MJ, Anderson KE, Holdich J, Koteci A, Balla T, Irvine RF (2012) PI4P and PI(4,5)P-2 are essential but independent lipid determinants of membrane identity. Science 337: 727 – 730
4. D'Angelo G, Vicinanza M, Wilson C, De Matteis MA (2012) Phosphoinositides in Golgi complex function. Subcell Biochem 59: 255 – 270
5. Minogue S, Waugh MG, De Matteis MA, Stephens DJ, Berditchevski F, Hsuan JJ (2006) Phosphatidylinositol 4-kinase is required for endosomal trafficking and degradation of the EGF receptor. J Cell Sci 119: 571 – 580
6. Craige B, Salazar G, Faundez V (2008) Phosphatidylinositol-4-kinase type II alpha contains an AP-3-sorting motif and a kinase domain that are both required for endosome traffic. Mol Biol Cell 19: 1415 – 1426
7. Jovic M, Kean MJ, Szentpetery Z, Polevoy G, Gingras AC, Brill JA, Balla T (2012) Two phosphatidylinositol 4-kinases control lysosomal delivery of the Gaucher disease enzyme, beta-glucocerebrosidase. Mol Biol Cell 23: 1533 – 1545
8. Altan-Bonnet N, Balla T (2012) Phosphatidylinositol 4-kinases: hostages harnessed to build panviral replication platforms. Trends Biochem Sci 37: 293 – 302
9. Minogue S, Waugh MG (2012) The phosphatidylinositol 4-kinases: don't call it a comeback. Subcell Biochem 58: 1 – 24
10. Strahl T, Thorner J (2007) Synthesis and function of membrane phosphoinositides in budding yeast, Saccharomyces cerevisiae. Biochim Biophys Acta 1771: 353 – 404
11. Carpenter CL, Cantley LC (1996) Phosphoinositide kinases. Curr Opin Cell Biol 8: 153 – 158
12. Barylko B, Gerber SH, Binns DD, Grichine N, Khvotchev M, Sudhof TC, Albanesi JP (2001) A novel family of phosphatidylinositol 4-kinases conserved from yeast to humans. J Biol Chem 276: 7705 – 7708
13. Minogue S, Anderson JS, Waugh MG, dos Santos M, Corless S, Cramer R, Hsuan JJ (2001) Cloning of a human type II phosphatidylinositol 4-kinase reveals a novel lipid kinase family. J Biol Chem 276: 16635 – 16640
14. Barylko B, Mao YS, Wlodarski P, Jung G, Binns DD, Sun HQ, Yin HL, Albanesi JP (2009) Palmitoylation controls the catalytic activity and subcellular distribution of phosphatidylinositol 4-kinase II{alpha}. J Biol Chem 284: 9994 – 10003
15. Jung G, Wang J, Wlodarski P, Barylko B, Binns DD, Shu H, Yin HL, Albanesi JP (2008) Molecular determinants of activation and membrane targeting of phosphoinositol 4-kinase IIbeta. Biochem J 409: 501 – 509
16. Balla A, Tuymetova G, Tsiomenko A, Varnai P, Balla T (2005) A plasma membrane pool of phosphatidylinositol 4-phosphate is generated by phosphatidylinositol 4-kinase type-III alpha: studies with the PH domains of the oxysterol binding protein and FAPP1. Mol Biol Cell 16: 1282 – 1295
17. Wang YJ, Wang J, Sun HQ, Martinez M, Sun YX, Macia E, Kirchhausen T, Albanesi JP, Roth MG, Yin HL (2003) Phosphatidylinositol 4 phosphate regulates targeting of clathrin adaptor AP-1 complexes to the Golgi. Cell 114: 299 – 310
18. Wang J, Sun HQ, Macia E, Kirchhausen T, Watson H, Bonifacino JS, Yin HL (2007) PI4P promotes the recruitment of the GGA adaptor proteins to the trans-Golgi network and regulates their recognition of the ubiquitin sorting signal. Mol Biol Cell 18: 2646 – 2655
19. Jovic M, Kean MJ, Dubankova A, Boura E, Gingras AC, Brill JA, Balla T (2014) Endosomal sorting of VAMP3 is regulated by PI4K2A. J Cell Sci doi: 10.1242/jcs.148809
20. Waugh MG, Minogue S, Chotai D, Berditchevski F, Hsuan JJ (2006) Lipid and peptide control of phosphatidylinositol 4-kinase IIalpha activity on Golgi-endosomal Rafts. J Biol Chem 281: 3757 – 3763
21. Lu D, Sun HQ, Wang H, Barylko B, Fukata Y, Fukata M, Albanesi JP, Yin HL (2012) Phosphatidylinositol 4-kinase IIalpha is palmitoylated by Golgi-localized palmitoyltransferases in cholesterol-dependent manner. J Biol Chem 287: 21856 – 21865
22. Mossinger J, Wieffer M, Krause E, Freund C, Gerth F, Krauss M, Haucke V (2012) Phosphatidylinositol 4-kinase IIalpha function at endosomes is regulated by the ubiquitin ligase Itch. EMBO Rep 13: 1087 – 1094
23. Barylko B, Wlodarski P, Binns DD, Gerber SH, Earnest S, Sudhof TC, Grichine N, Albanesi JP (2002) Analysis of the catalytic domain of phosphatidylinositol 4-kinase type II. J Biol Chem 277: 44366 – 44375
24. Burke JE, Inglis AJ, Perisic O, Masson GR, McLaughlin SH, Rutaganira F, Shokat KM, Williams RL (2014) Structures of PI4KIIIbeta complexes show simultaneous recruitment of Rab11 and its effectors. Science 344: 1035 – 1038
25. Kim do J, Park KS, Kim JH, Yang SH, Yoon JY, Han BG, Kim HS, Lee SJ, Jang JY, Kim KH et al (2010) Helicobacter pylori proinflammatory protein up-regulates NF-kappaB as a cell-translocating Ser/Thr kinase. Proc Natl Acad Sci USA 107: 21418 – 21423
26. Rao VD, Misra S, Boronenkov IV, Anderson RA, Hurley JH (1998) Structure of type IIbeta phosphatidylinositol phosphate kinase: a protein kinase fold flattened for interfacial phosphorylation. Cell 94: 829 – 839
27. Hurley JH, Boura E, Carlson LA, Rozycki B (2010) Membrane budding. Cell 143: 875 – 887
28. Boura E, Hurley JH (2012) Structural basis for membrane targeting by the MVB12-associated beta-prism domain of the human ESCRT-I MVB12 subunit. Proc Natl Acad Sci USA 109: 1901 – 1906
29. Zhou Q, Li J, Yu H, Zhai Y, Gao Z, Liu Y, Pang X, Zhang L, Schulten K, Sun F et al (2014) Molecular insights into the membrane-associated phosphatidylinositol 4-kinase IIalpha. Nat Commun 5: 3552

a 2014 The Authors

30. Balla A, Tuymetova G, Barshishat M, Geiszt M, Balla T (2002) Characterization of type II phosphatidylinositol 4-kinase isoforms reveals association of the enzymes with endosomal vesicular compartments. J Biol Chem 277: 20041 – 20050
31. Rezabkova L, Boura E, Herman P, Vecer J, Bourova L, Sulc M, Svoboda P, Obsilova V, Obsil T (2010) 14-3-3 protein interacts with and affects the structure of RGS domain of regulator of G protein signaling 3 (RGS3). J Struct Biol 170: 451 – 461
32. Boura E, Rezabkova L, Brynda J, Obsilova V, Obsil T (2010) Structure of the human FOXO4-DBD-DNA complex at 1.9 A resolution reveals new details of FOXO binding to the DNA. Acta Crystallogr D Biol Crystallogr 66: 1351 – 1357
33. Nemecek D, Boura E, Wu W, Cheng N, Plevka P, Qiao J, Mindich L, Heymann JB, Hurley JH, Steven AC (2013) Subunit folds and maturation pathway of a dsRNA virus capsid. Structure 21: 1374 – 1383
34. Kim YC, Hummer G (2008) Coarse-grained models for simulations of multiprotein complexes: application to ubiquitin binding. J Mol Biol 375: 1416 – 1433
35. Tai AW, Bojjireddy N, Balla T (2011) A homogeneous and nonisotopic assay for phosphatidylinositol 4-kinases. Anal Biochem 417: 97 – 102

 a 2014 The Authors

## 5.2 The High-Resolution Crystal Structure of Phosphatidylinositol 4-Kinase IIβ and the Crystal Structure of Phosphatidylinositol 4-Kinase IIα Containing a Nucleoside Analogue Provide a Structural Basis for Isoform-Specific Inhibitor Design.

**Background**

Currently, PI4K IIβ is the least well-understood PI4-kinase when considering function and regulation. *In vitro* experiments indicate that PI4K IIβ possesses less enzymatic activity than the α isoform in spite of having the same palmitoylation motif affecting their lipid kinase activity. From a structural point of view, it is known that the first 100 amino acids at the N-terminus of PI4K IIβ are distinct from the N-termini of PI4K IIα while the C-terminal part is highly homologous having 58% identity and 75% homology [148]. This makes PI4K IIβ the closest homologue of PI4K IIα. Since the crystal structures of PI4K IIα and PI4K IIIβ have already been solved, we were interested in the extent to which PI4K IIβ possesses the same or similar catalytic residues that preserve the architecture of the active site. We hoped that a high resolution crystal structure could also reveal the crucial structural dissimilarities that could be used for the design of isoform specific inhibitors.

In addition, a series of nucleotide analogues were prepared in Dr. Nencka´s laboratory. We decided to test their inhibitory efect against type II PI4-kinases and to perform co-crystallization studies with type II PI4-kinases in order to obtain the starting point for isoform specific inhibitor design.

**Summary**

The DNA construct of PI4K IIβ used for crystallization was designed based on the crystal structure of PI4K IIα. Subsequently, crystallization trials and optimization of the crystal quality were performed and the final crystals were subjected to X-ray diffraction analysis. The solved crystal structure of PI4K IIβ at 1.9 Å resolution confirmed a highly similar overall fold with PI4K IIα and highly conserved residues in the active site (see Figure 12A.). However, large conformational changes were found in the lateral hydrophobic pocket (see Figure 12B.). These changes were induced by crystal packing, but, nevertheless, they still document high flexibility of the individual hydrophobic residues forming the lateral pocket.

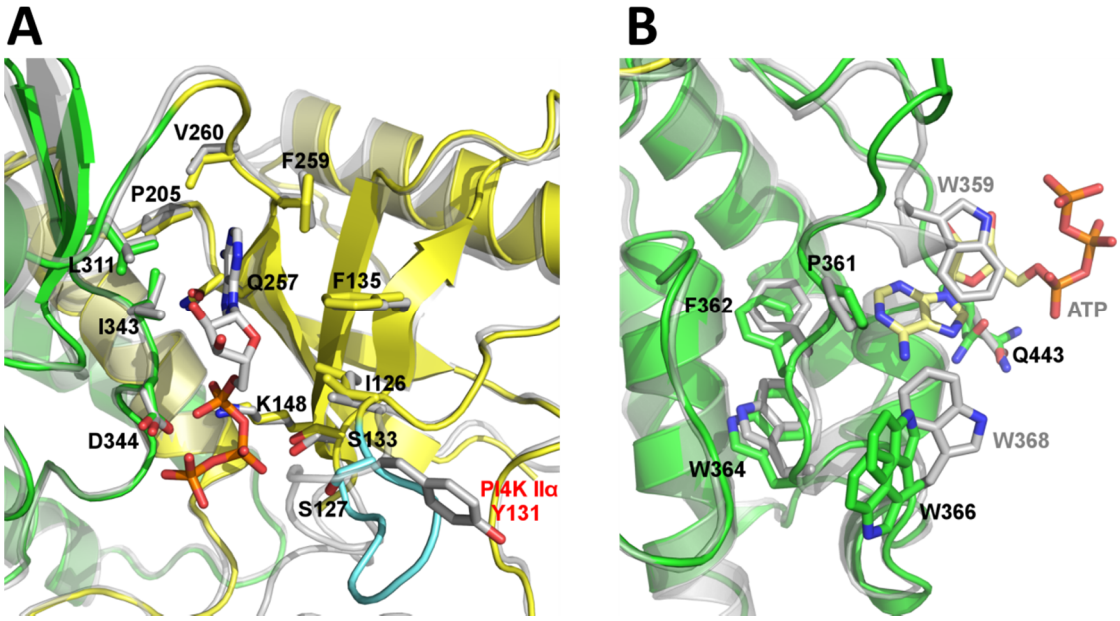



**Figure 12.: Superposition of ATP binding sites and lateral hydrophobic pockets of PI4K IIα and IIβ.** **Panel A:** Comparison of ATP binding pockets. The protein backbone is depicted in cartoon representation while ATP and the residues involved in ATP binding are shown in stick representation. PI4K IIα is coloured in grey and the N- and C-lobes of PI4K IIβ are coloured in yellow and green, respectively. The disordered loop of PI4K IIβ consisting of Ser127-Gly132 is coloured in cyan. Differently oriented PI4K IIα Tyr131 corresponding to PI4K IIβ Ser127 is highlighted in red. **Panel B:** Comparison of the lateral hydrophobic pockets is in the same representation and coloured as in panel A.

In a second part of this project, crystallization trials with a series of nucleotide analogues derived from adenosine were performed with both isoforms. However, only co-crystallization of PI4K IIα with MD59 provided well diffracted crystals (2.6 Å resolution). As expected, MD59 occupied the position of ATP adenine ring in the active site as it is an adenosine analogue (see Figure 13.). The inhibition profiles of nucleotide analogues against PI4K IIα were also tested using the luminescent ADP-Glo kinase assay. MD59 from all tested inhibitors displayed the highest potency toward PI4K IIα and there were no significant concurrent inhibition of PI4K IIIβ observed.

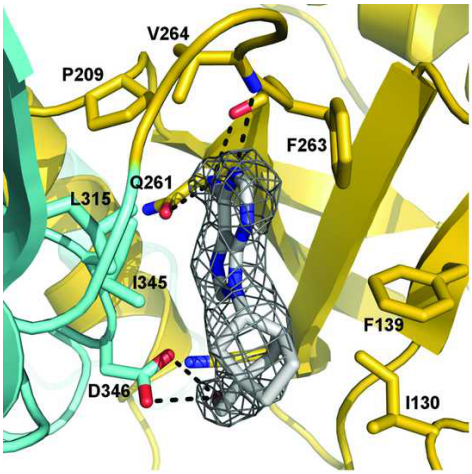



**Figure 13.: Detailed view of the ATP binding site of PI4K IIα with bound inhibitor MD59 from a series of adenosine analogues.**
The protein backbone is depicted in cartoon representation with the N-lobe coloured in yellow and the C-lobe coloured in cyan. MD59 and the side chains of selected residues are shown in stick representation and coloured according to elements: oxygen-red; nitrogen-blue and carbon-grey. The unbiased $F_o$-$F_c$ map contoured at 3$\sigma$ is shown around MD59. Hydrogen bonds between MD59 and amino acids residues are shown as dotted black lines.

## My contribution

I expressed and purified the recombinant proteins used for the biochemical experiments. I tested the inhibitory effect of the compounds synthesised in Dr. Nencka´s group against PI4K IIα and PI4K IIIβ using the luminescent ADP-Glo kinase assay.

CrossMark

electronic reprint

BIOLOGICAL
CRYSTALLOGRAPHY

ISSN: 1399-0047
journals.iucr.org/d

# The high-resolution crystal structure of phosphatidylinositol 4-kinase II$\beta$ and the crystal structure of phosphatidylinositol 4-kinase II$\alpha$ containing a nucleoside analogue provide a structural basis for isoform-specific inhibitor design

**Martin Klima, Adriana Baumlova, Dominika Chalupska, Hubert Hřebabecký, Milan Dejmek, Radim Nencka and Evzen Boura**

*Acta Cryst.* (2015). D**71**, 1555–1563

IUCr Journals
CRYSTALLOGRAPHY JOURNALS ONLINE

Copyright © International Union of Crystallography

Author(s) of this paper may load this reprint on their own web site or institutional repository provided that this cover page is retained. Republication of this article or its storage in electronic databases other than as specified above is not permitted without prior permission in writing from the IUCr.

For further information see http://journals.iucr.org/services/authorrights.html

BIOLOGICAL CRYSTALLOGRAPHY
ISSN 1399-0047

# The high-resolution crystal structure of phosphatidylinositol 4-kinase IIβ and the crystal structure of phosphatidylinositol 4-kinase IIα containing a nucleoside analogue provide a structural basis for isoform-specific inhibitor design

**Martin Klima, Adriana Baumlova, Dominika Chalupska, Hubert Hřebabecký, Milan Dejmek, Radim Nencka and Evzen Boura***

Department of Biochemistry, Institute of Organic Chemistry and Biochemistry, Flemingovo nam. 2, 166 10 Prague, Czech Republic. *Correspondence e-mail: boura@uochb.cas.cz

Received 26 March 2015
Accepted 18 May 2015

Edited by Z. Dauter, Argonne National Laboratory, USA

**Keywords:** phosphatidyl inositol; kinase; crystal structure; ATP; inhibitor.

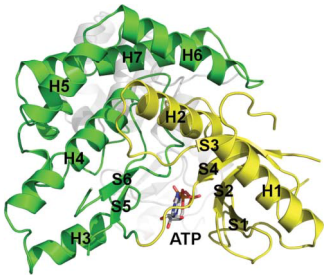
**PDB references**: phosphatidylinositol 4-kinase IIβ, 4wtv; phosphatidylinositol 4-kinase IIα, complex with nucleotide analogue, 4yc4

**Supporting information**: this article has supporting information at journals.iucr.org/d

Phosphatidylinositol 4-phosphate (PI4P) is the most abundant monophosphoinositide in eukaryotic cells. Humans have four phosphatidylinositol 4-kinases (PI4Ks) that synthesize PI4P, among which are PI4K IIβ and PI4K IIα. In this study, two crystal structures are presented: the structure of human PI4K IIβ and the structure of PI4K IIα containing a nucleoside analogue. The former, a complex with ATP, is the first high-resolution (1.9 Å) structure of a PI4K. These structures reveal new details such as high conformational heterogeneity of the lateral hydrophobic pocket of the C-lobe and together provide a structural basis for isoform-specific inhibitor design.

## 1. Introduction

Phosphatidylinositol 4-phosphate (PI4P) is the most abundant monophosphoinositide in the eukaryotic cell. PI4P, together with other phosphoinositides (PIPs), regulates many cellular processes, including vesicle trafficking, cell signalling, autophagy and cell survival, and has been implicated in the pathogenesis of many human diseases (Balla, 2013; Tan & Brill, 2014; Wang *et al.*, 2012; Waugh, 2015). Furthermore, PI4P is a key lipid marker of the Golgi and TGN, plays an important role in cell signalling and serves as a precursor for polyphosphoinositides (Balla, 2013; Tan & Brill, 2014). Humans have four phosphatidylinositol 4-kinases (PI4Ks) that synthesize PI4P. The type III PI4Ks (PI4K IIIα and PI4K IIIβ) are soluble cytoplasmic proteins that share homology with PI3Ks and are recruited to membranes transiently *via* protein–protein interactions (Wu *et al.*, 2014; Sasaki *et al.*, 2012; Greninger *et al.*, 2012). Conversely, the type II PI4Ks (PI4K IIα and PI4K IIβ) are active only when palmitoylated and anchored in the membrane. PI4K IIα is the most active PI4K and is almost exclusively localized to membranes as a consequence of its palmitoylation (Barylko *et al.*, 2001). PI4K IIβ is localized in the cytoplasm, where it is stabilized by the Hsp90 chaperone (Jung *et al.*, 2011) and translocates to the plasma membrane in response to activated Rac (Balla *et al.*, 2002; Wei *et al.*, 2002). Both type II and type III PI4Ks are important players in vesicular trafficking (Jović *et al.*, 2012; Burgess *et al.*, 2012). They contribute to the recruitment of the clathrin adaptor complexes AP1 and AP3 (Craige *et al.*, 2008), regulate the endosomal sorting of VAMP3 (Jović *et al.*, 2014) and are




© 2015 International Union of Crystallography



electronic reprint

important for EGF receptor targeting to the lysosome (Minogue *et al.*, 2006).

Recent crystal structures of PI4K II$\alpha$ and PI4K III$\beta$ (Baumlova *et al.*, 2014; Zhou *et al.*, 2014; Burke *et al.*, 2014) have emphasized the structural similarity of the type III PI4Ks to other lipid kinases such as PI3Ks and revealed that the type II enzymes are rather more similar to protein Ser/Thr kinases [for example, the cell translocating kinase A (CtkA) from *Helicobacter pylori*; Kim *et al.*, 2010]. Type III PI4Ks have recently been identified as essential host factors for the replication of single-strand positive-sense RNA (+RNA) viruses (Berger *et al.*, 2009; Altan-Bonnet & Balla, 2012). Type II PI4Ks, on the other hand, are exploited by intracellular bacteria such as *Legionella pneumophila* and *Chlamydia trachomatis* (Moorhead *et al.*, 2010; Weber *et al.*, 2006) and play a role in the Wnt signalling pathway (Qin *et al.*, 2009), a pathway that is often upregulated in cancer. As a result, PI4Ks are considered to be a pharmacological target. Potent and isoform-selective inhibitors would be a great tool to further dissect the biological role of each PI4K family member and, in addition, would be potentially useful in human medicine. Unfortunately, no specific inhibitors of type II PI4Ks are yet available. High-resolution crystal structures are very useful tools for inhibitor design. The previously solved structures of PI4Ks (PI4K II$\alpha$ and PI4K III$\beta$) have been obtained in the resolution range 2.8–3.3 Å and PI4K II$\alpha$ has only been crystallized with ATP or ADP. Here, we present the crystal structure of PI4K II$\beta$ solved at 1.9 Å resolution (the first high-resolution structure of a PI4K) and the structure of PI4K II$\alpha$ containing a bound nucleoside analogue. The structures reveal details of ATP binding, show the conformation heterogeneity of the allosteric hydrophobic pocket and provide a structural basis for nucleoside scaffold-based inhibitor design.

## 2. Materials and methods

### 2.1. Protein expression and purification

Pseudo wild-type (pseudo-wt) PI4K II$\alpha$ (UniProt code Q9BTU6) and the crystallographic construct were expressed

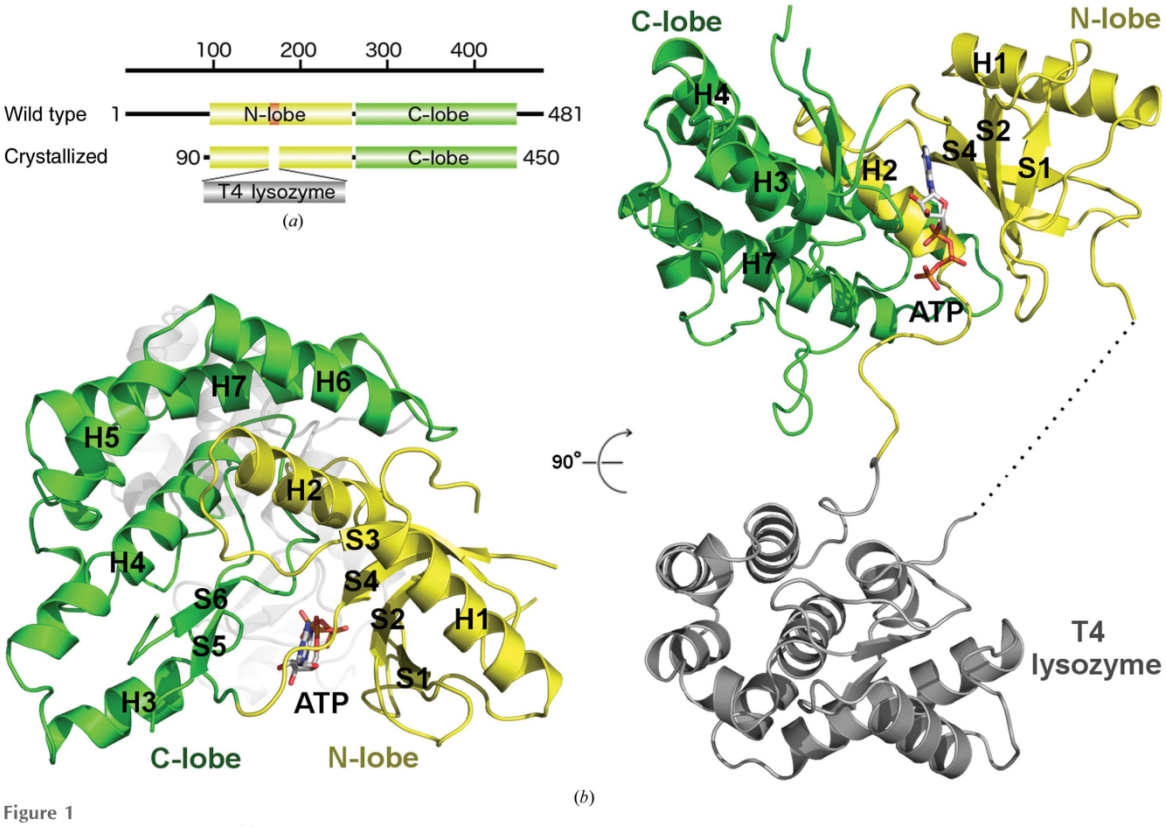



**Figure 1**
The overall fold of PI4K II$\beta$. (*a*) Schematic representation of wild-type PI4K II$\beta$ and the chimeric construct used for crystallization. The N-lobe and C-lobe of PI4K II$\beta$ are shown in yellow and green, respectively; the palmitoylated cysteine-rich motif of PI4K II$\beta$ is shown in orange and the T4 lysozyme in grey. (*b*) Overall fold of PI4K II$\beta$. The protein backbone is shown as a cartoon representation. The N-lobe is depicted in yellow, the C-lobe in green and the T4 lysozyme in grey. In the left panel, the front view is shown, in which the N-lobe, the C-lobe and the ATP-binding groove in between are emphasized; in the right panel, the view is rotated by 90° to place the T4 lysozyme at the bottom. The kinase is composed of seven $\alpha$-helices numbered H1–H7 and six $\beta$-sheets numbered S1–S6.


electronic reprint

**Table 1**
Data collection and processing.

Values in parentheses are for the outer shell.

| Crystal | PI4K II$\beta$ | PI4K II$\alpha$ + MD59 |
|---|---|---|
| Diffraction source | MX14.1 beamline, BESSY II | MX14.1 beamline, BESSY II |
| Wavelength (Å) | 1.28272 | 0.918409 |
| Temperature (K) | 100 | 100 |
| Detector | Pilatus 6M | Pilatus 6M |
| Crystal-to-detector distance (mm) | 375.7 | 647.3 |
| Rotation range per image (°) | 0.2 | 0.1 |
| Total rotation range (°) | 240 | 110 |
| Exposure time per image (s) | 0.8 | 0.5 |
| Space group | $P4_12_12$ | $P2_12_12$ |
| Unit-cell parameters (Å, °) | $a$ = 106.01, $b$ = 106.01, $c$ = 214.53, $\alpha = \beta = \gamma$ = 90 | $a$ = 79.41, $b$ = 103.77, $c$ = 78.11, $\alpha = \beta = \gamma$ = 90 |
| Resolution range (Å) | 47.52–1.90 (1.97–1.90) | 49.07–2.58 (2.67–2.58) |
| Total No. of reflections | 1704172 (165811) | 75199 (4056) |
| No. of unique reflections | 96773 (9513) | 20124 (1535) |
| Completeness (%) | 99.98 (99.94) | 95.77 (74.15) |
| Multiplicity | 17.6 (17.4) | 3.7 (2.6) |
| $\langle I/\sigma(I)\rangle$ | 17.40 (1.95†) | 15.98 (2.36) |
| $R_{r.i.m.}$‡ (%) | 10.5 (156.2) | 7.14 (40.4) |
| Overall $B$ factor from Wilson plot (Å$^2$) | 36.26 | 43.95 |

† It has been shown that including data with mean $I/\sigma(I) < 2.0$ leads to improved maps (Karplus & Diederichs, 2012). The *XDSAPP* program (Krug *et al.*, 2012) suggested a 1.83 Å resolution cutoff. We decided to be more conservative and cut the data at 1.9 Å resolution, leading to $I/\sigma(I) = 1.95$ in the highest resolution shell. Please note that $I/\sigma(I) = 2$ at 1.94 Å resolution. ‡ The $R_{r.i.m.}$ value was estimated by multiplying the conventional $R_{merge}$ value by the factor $[N/(N-1)]^{1/2}$, where $N$ is the data multiplicity.

**Table 2**
Structure solution and refinement.

Values in parentheses are for the outer shell.

| Crystal | PI4K II$\beta$ | PI4K II$\alpha$ + MD59 |
|---|---|---|
| Resolution range (Å) | 47.52–1.90 (1.97–1.90) | 49.07–2.58 (2.67–2.58) |
| Completeness (%) | 99.98 (99.94) | 95.77 (74.15) |
| No. of reflections, working set | 91934 | 19117 |
| No. of reflections, test set | 4839 | 1007 |
| Final $R_{work}$ (%) | 21.01 (28.60) | 21.52 (29.58) |
| Final $R_{free}$ (%) | 24.20 (33.16) | 25.48 (42.87) |
| No. of non-H atoms | | |
| Total | 7387 | 3943 |
| Protein | 7011 | 3882 |
| Ligand | 62 | 46 |
| Water | 277 | 3 |
| R.m.s. deviations | | |
| Bonds (Å) | 0.009 | 0.012 |
| Angles (°) | 1.04 | 1.63 |
| Average $B$ factors (Å$^2$) | | |
| Protein | 41.80 | 60.10 |
| Ligands | 43.60 | 67.33 |
| Solvent | 39.40 | 61.50 |
| Ramachandran plot | | |
| Most favoured (%) | 97 | 96 |
| Outliers (%) | 0 | 0 |

and purified as described previously (Baumlova *et al.*, 2014) as was the PI4K III$\beta$ (Burke *et al.*, 2014). The gene for full-length PI4K II$\beta$ (amino-acid sequence 1–481; UniProt code Q8TCG2) does not significantly express in bacteria. Therefore, we omitted the N-terminal part that is predicted to be disordered and is not important for the catalytic activity of the kinase (Jung *et al.*, 2008). PI4K II$\beta$ 90–481 was cloned into the first cassette of the pRSFD vector (Novagen) with an N-terminal 6×His tag followed by the GB1 solubility tag and the TEV protease-cleavage site. However, our attempts to express this construct of PI4K II$\beta$ produced only low yields that were contaminated with Hsp70 and Hsp90 chaperones which were difficult to remove, suggesting that the protein had folding complications. As a result, we employed the same strategy that produced well diffracting crystals of the PI4K II$\alpha$ enzyme: we truncated the C-terminus, which is flexible and thus impedes crystallization (Różycki & Boura, 2014), and we inserted T4 lysozyme instead of the cysteine-rich motif 169-VCCPCCF-175 of PI4K II$\beta$ that corresponds to the 173-LCCPCCF-179 motif of the PI4K II$\alpha$ enzyme. The resulting construct PI4K II$\beta$ 90–450 with a T4 insertion was expressed at high levels and could be purified to homogeneity (see below) but did not crystallize. Therefore, we had to screen the T4 insertion boundaries. All constructs with changed boundaries were expressed, but only the construct in which the sequence 166-VHKVCCPCCF-175 was replaced by T4 lysozyme (Fig. 1*a*) produced diffraction-quality crystals.

The cysteine-rich loop 166-VHKVCCPCCF-175 was replaced by T4 lysozyme using the QuikChange kit (Stratagene). The protein was purified using an affinity and size-exclusion chromatography procedure previously developed in our laboratory (Nemecek *et al.*, 2013; Boura *et al.*, 2010). Briefly, the protein was expressed in *Escherichia coli* BL21 Star cells. The bacterial cells were lysed in lysis buffer [50 m*M* Tris pH 8, 300 m*M* NaCl, 3 m*M* $\beta$-mercaptoethanol ($\beta$-ME), 40 m*M* imidazole, 10% glycerol] and the lysate was incubated with Ni–NTA resin (Macherey–Nagel) and extensively washed with lysis buffer. The protein was eluted with lysis buffer supplemented with imidazole (300 m*M*). The tags were removed with TEV protease and the protein was further purified using size-exclusion chromatography with a Superdex 200 column (GE Healthcare) in SEC buffer (10 m*M* MES pH 6.5, 200 m*M* NaCl, 3 m*M* $\beta$-ME). Proteins were concentrated to 5.4 mg ml$^{-1}$ and stored at −80°C. The protein concentration was estimated using theoretical extinction coefficients (90 300 for PI4K II$\alpha$ with a T4 insertion and 88 190 for PI4K II$\beta$ with a T4 insertion) calculated using the *PROTEIN CALCULATOR* web server (http://protcalc.sourceforge.net/).

### 2.2. Crystallization and crystallographic analysis

For the crystallization trials, the PI4K II$\beta$ 90–450 enzyme with a T4 insertion was supplemented with ATP (5 m*M*) and $MgCl_2$ (2 m*M*). Crystals grew in 2 d at 291 K in a sitting drop consisting of a 1:1 mixture of the protein solution and well solution [100 m*M* MES–imidazole pH 6.5, 10%(*w*/*v*) PEG 4000, 20%(*v*/*v*) glycerol, 20 m*M* 1,6-hexanediol, 20 m*M* 1-butanol, 20 m*M* 1,2-propanediol, 20 m*M* 2-propanol, 20 m*M* 1,4-butanediol, 20 m*M* 1,3-propanediol] as summarized in Supplementary Table S1. The crystals were flash-cooled in liquid nitrogen and analysed on the MX14.1 beamline at BESSY II using a Pilatus 6M detector. They diffracted to 1.9 Å resolution and belonged to the tetragonal space group $P4_12_12$.



electronic reprint

For the crystallization trials with the MD59 nucleoside analogue, the PI4K IIα enzyme with a T4 insertion was supplemented with MD59 (2 m*M*) and ADP (0.5 m*M*). Crystals grew in 2 d at 291 K in a sitting drop consisting of a 1:1 mixture of protein solution and well solution [100 m*M* HEPES pH 7.0, 10%(*w*/*v*) PEG 4000, 10%(*v*/*v*) 2-propanol] as summarized in Supplementary Table S1. The crystals were cryoprotected in well solution supplemented with 20%(*v*/*v*) glycerol and flash-cooled in liquid nitrogen. They diffracted to 2.6 Å resolution and belonged to space group $P2_12_12$.

The crystallographic data sets were collected from single cooled crystals. Data were integrated and scaled using *XDS* (Kabsch, 2010); the data quality is summarized in Table 1. The structure was solved by molecular replacement (MR) using *Phaser* (McCoy *et al.*, 2007) from the *CCP*4 package (Winn *et al.*, 2011). The structure of PI4K IIα with a T4 insertion (PDB entry 4pla; Baumlova *et al.*, 2014) was used as a search model. The ligands were placed using *Coot* (Debreczeni & Emsley, 2012) and the structures were refined in *PHENIX* (*xyz* coordinates, real-space and rotamers but no TLS or NCS; Adams *et al.*, 2010) as summarized in Table 2. Structural figures were generated in *PyMOL* (Schrödinger). The atomic coordinates were deposited in the Protein Data Bank (http://www.pdb.org) under accession codes 4wtv for PI4K IIβ and 4yc4 for PI4K IIα complexed with MD59.

### 2.3. *In vitro* kinase assay

*In vitro* kinase activity was measured using a standard procedure (Tai *et al.*, 2011). Briefly, reactions were carried out in a total volume of 5 µl in a 384-well plate format by mixing three stock solutions: 1 µl of the pseudo-wt PI4K IIα (the T4 insertion renders the enzyme inactive) or PI4K IIIβ enzyme (final concentration 100 n*M*) in kinase buffer (20 m*M* Tris pH 7.5, 5 m*M* $MgCl_2$, 0.2% Triton X-100, 0.1 mg ml$^{-1}$ BSA, 2 m*M* DTT), 1 µl of PI in kinase buffer (50 µ*M* final concentration) and 1 µl of the small molecule at the desired concentration. The reaction was started by adding 2 µl of ATP in kinase buffer (final concentration 100 µ*M*). The reaction was carried out for 60 min at room temperature (295 K) and the amount of hydrolyzed ATP was measured according to the manufacturer's protocol (5 µl of ADP/GloTM Reagent was added to terminate the kinase reaction and deplete the remaining ATP, and 10 µl of Kinase Detection Reagent was then added to simultaneously convert ADP to ATP and to allow the newly synthesized ATP to be measured by the luciferase/luciferin

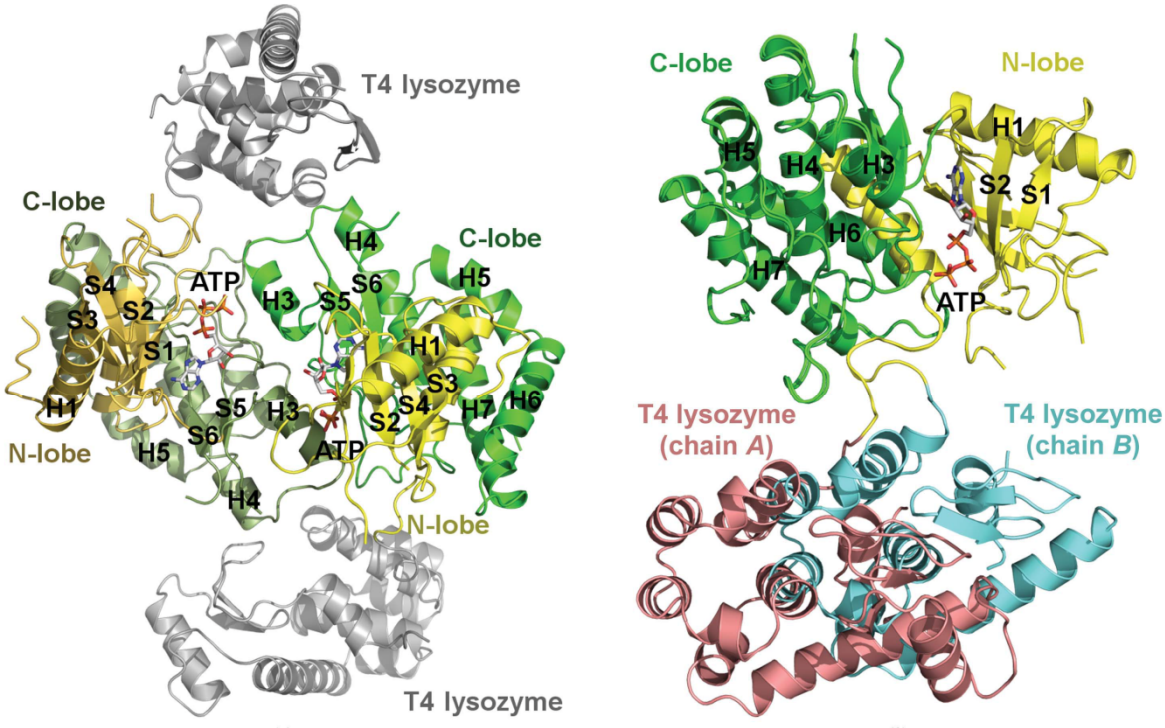



**Figure 2**
The asymmetric unit content. (*a*) The crystals contained two molecules of PI4K IIβ per asymmetric unit. The N-lobe and C-lobe of PI4K IIβ are shown in yellow and green, respectively. The T4 lysozyme is shown in grey. The second molecule is coloured in the same way except that darker tones are used. (*b*) Superposition of chain *A* and chain *B* according to the kinase domain of the chimeric PI4K IIβ/T4 construct reveals that the two copies of T4 lysozyme in the asymmetric unit are differently tilted with respect to the kinase domain. The N-lobe and C-lobe of PI4K IIβ are shown in yellow and green, respectively. The T4 lysozyme from chain *A* and chain *B* is shown in salmon and cyan, respectively.


electronic reprint

reaction). Luminiscence was measured using a Tecan Infinite M 1000 plate reader.

### 2.4. Chemical synthesis of the inhibitors MD59 and AdeN3

Compounds MD59 and AdeN3 were prepared according to previously reported procedures (Dejmek *et al.*, 2015; Anglin *et al.*, 2012) as detailed in the Supporting Information.

## 3. Results and discussion

### 3.1. The structure of PI4K II$\beta$

The overall fold of PI4K II$\beta$ (Fig. 1*b*) is highly similar to the fold of PI4K II$\alpha$ (they superpose with an r.m.s.d. of 1.12 Å; see Supplementary Fig. S1), which would be expected given the primary-sequence similarity: the major differences are localized to the disordered N-termini, which were not included in the crystallized construct, whereas the kinase domain is conserved (Supplementary Fig. S2). The kinase domain can be divided into N-terminal and C-terminal lobes. The N-lobe of PI4K II$\beta$ consists of two $\alpha$-helices (H1–H2) surrounding four small antiparallel $\beta$-sheets (S1–S4). The C-lobe consists of two $\alpha$-helices (H3–H4) surrounding two antiparallel $\beta$-sheets (S5–S6) located proximally to the ATP-binding groove, and another three $\alpha$-helices (H5–H6) located more distally and forming a scaffold for the catalytically active part of the kinase and/or providing its allosteric regulation. The catalytic site with ATP bound is localized between the lobes and is formed mainly by both stretches of antiparallel $\beta$-sheets mentioned above and their neighbourhood. The asymmetric unit contained two molecules of PI4K II$\beta$ (Fig. 2*a*). Interestingly, they contained differently tilted T4 lysozymes (Fig. 2*b*), probably owing to crystal contacts, yet the conformation of the enzyme remained the same. This fact further supports the current evidence that the insertion of T4 lysozyme instead of a disordered loop does not influence the conformation of the molecule with the insertion (Zou *et al.*, 2012; Rosenbaum *et al.*, 2007).

### 3.2. Conformational heterogeneity of the lateral hydrophobic pocket

A lateral hydrophobic pocket important for the activity of the PI4K II$\alpha$ enzyme was identified during structural analysis (Baumlova *et al.*, 2014; Zhou *et al.*, 2014). Comparison of the hydrophobic pocket conformation of PI4K II$\beta$ with both previously published structures of PI4K II$\alpha$ (Fig. 3) reveals its high conformational heterogeneity, especially of tryptophan residues Trp366 and Trp357. While the observed conformations may be affected by crystal packing, they still confirm the flexibility of this pocket. These findings structurally support its hypothesized function: to promiscuously bind hydrophobic ligands present within the lipid bilayer. Notably, the surface-exposed hydrophobic side chain of residue Trp357 (corresponding to Trp359 in PI4K II$\alpha$) is not resolved in our structure, highlighting its flexibility. Surface-exposed hydrophobic

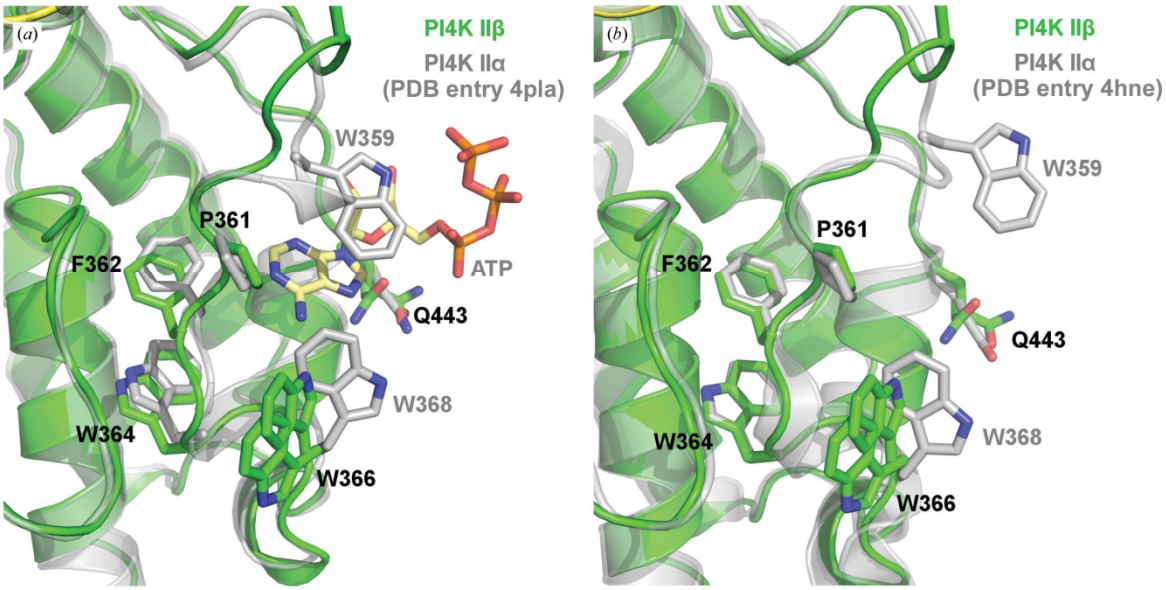



**Figure 3**
Comparison of the lateral hydrophobic pockets of PI4K II$\alpha$ and PI4K II$\beta$. (*a*) Detailed view of the lateral hydrophobic pocket of PI4K II$\alpha$ (PDB entry 4pla) superposed with the corresponding region of PI4K II$\beta$. The protein backbone is shown in cartoon representation, the C-lobe of PI4K II$\alpha$ is coloured grey and the C-lobe of PI4K II$\beta$ is coloured green. ATP bound to PI4K II$\alpha$ and the side chains of selected residues are shown in stick representation and coloured according to element: oxygen, red; nitrogen, blue; phosphorus, orange. Kinase C atoms are colored according to their domain assignment and the ATP C atoms are shown in light yellow. H atoms are not shown. (*b*) Detailed view of the lateral hydrophobic pocket of PI4K II$\alpha$ (PDB entry 4hne; Zhou *et al.*, 2014) superposed with the corresponding region of PI4K II$\beta$ in the same representation and coloured as in (*a*).



electronic reprint

residues are rare in proteins, and in the case of membrane-binding proteins they often serve as anchors to the membrane (Boura & Hurley, 2012; Boura *et al.*, 2012) and are one possible method by which proteins can induce membrane curvature (Hurley *et al.*, 2010; Różycki *et al.*, 2012). We thus propose that Trp357 is such an anchor. This is supported by the fact that when the corresponding residue in PI4K IIα is mutated the catalytic activity is impaired (Baumlova *et al.*, 2014) and by the blue shift of the internal tryptophan residues upon liposome binding observed in the case of the PI4K IIα enzyme (Zhou *et al.*, 2014).

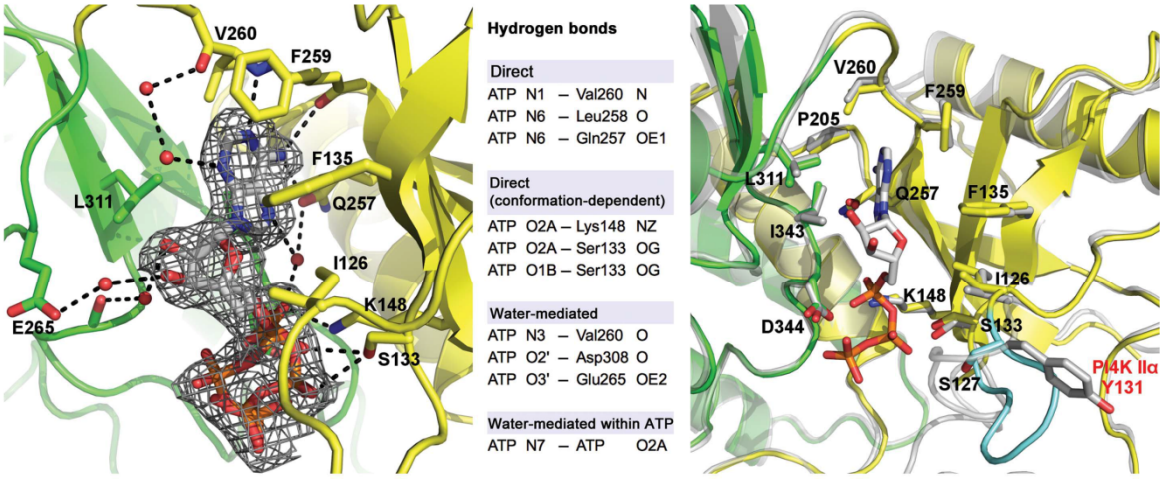
### 3.3. The catalytic site of PI4K IIβ and its comparison with previous PI4K structures

One of the main goals of this study was to obtain detailed structural information about the catalytic site for the future design of inhibitors specific for type II PI4Ks. Owing to the high resolution that we obtained, we were able to precisely model the ATP in the catalytic site (Fig. 4). The ATP is held in place by a complex network of hydrogen bonds to residues of both the N-lobe and C-lobe, as summarized in Fig. 4(*a*). ATP was observed in two alternative conformations that mainly differ in the position of the β-phosphate, which forms hydrogen bonds to Ser133 only in the major conformation (occupancies of 72 and 54% for the two molecules in the asymmetric unit); these hydrogen bonds are absent in the alternative conformation.

### 3.4. Towards nucleoside-based inhibitors specific for type II PI4Ks

Specific inhibitors of type III PI4Ks have been described (Bianco *et al.*, 2012; van der Schaar *et al.*, 2013; Mejdrova *et al.*, 2015), but no inhibitors of type II enzymes have been reported. This represents a major shortcoming, as such inhibitors would be a good tool to elucidate the function of type II enzymes in cell cultures. In addition, both PI4K IIβ and PI4K IIα are part of the Wnt signalling pathway, a pathway that is often upregulated in cancer, and PI4K IIα is exploited by several intracellular bacteria; therefore, specific inhibitors would have medical importance.

It has been known for decades that type II but not type III PI4Ks are inhibited by adenosine and calcium (Balla, 1998), suggesting that an adenosine scaffold would be an appropriate starting point for type II-specific inhibitor design. Thus, we decided to screen our series of adenosine analogues for their inhibitory activities. We found that compound MD59 (Fig. 5*a*) exhibited moderate inhibitory activity against type II PI4Ks comparable to but better than that of adenosine and other adenosine-based compounds but had no significant activity against the typical type III PI4Ks (Fig. 5*b*). These results suggest that inhibitors that share nucleoside-based scaffolds




(*a*) (*b*)

**Figure 4**
The catalytic site. (*a*) Detailed view of the ATP-binding pocket. The protein backbone is shown in cartoon representation; the N-lobe is coloured yellow and the C-lobe is coloured green. ATP and side chains of selected residues are shown in stick representation and coloured according to element: oxygen, red; nitrogen, blue; phosphorus, orange. The kinase C atoms are coloured according to their domain assignment and the ATP C atoms are shown in silver. Four water molecules are shown as spheres; H atoms are not shown. The unbiased $F_o - F_c$ map contoured at 3σ is shown around the ATP molecule. Hydrogen bonds between ATP, the amino-acid residues and selected water molecules are shown as dotted black lines. Two alternative conformations of the triphosphate moieties of ATP are presented. (*b*) Comparison of the ATP-binding pockets of PI4K IIα and PI4K IIβ. The protein backbone is shown in cartoon representation; PI4K IIα is coloured grey, the N-lobe of PI4K IIβ is coloured yellow and the C-lobe of PI4K IIβ is coloured green. ATP bound to PI4K IIβ and the side chains of selected residues are shown in stick representation and are coloured according to element: oxygen, red; nitrogen, blue; phosphorus, orange. The kinase C atoms are colored according to their domain assignment and ATP C atoms are shown in silver. H atoms are not shown. The poorly ordered loop Ser127–Gly132 of PI4K IIβ is coloured cyan and the PI4K IIα Tyr131 with a different orientation compared with the homologous PI4K IIβ Ser127 is highlighted in red.


electronic reprint

also share the same mechanism of action and are capable of inhibiting the atypical type II PI4Ks but not the typical type III PI4Ks (Fig. 5*b*).

To obtain detailed insight into the function of MD59, we sought to solve the crystal structure of MD59 bound to a type II PI4K. We tried both the PI4K II$\alpha$ and PI4K II$\beta$ isoforms and succeeded in obtaining crystals with the PI4K II$\alpha$ isoform. Initially, the crystals diffracted poorly; we hypothesized that the poor diffraction is owing to a missing ligand in the lateral pocket of the C-lobe. Previously, we have shown that a

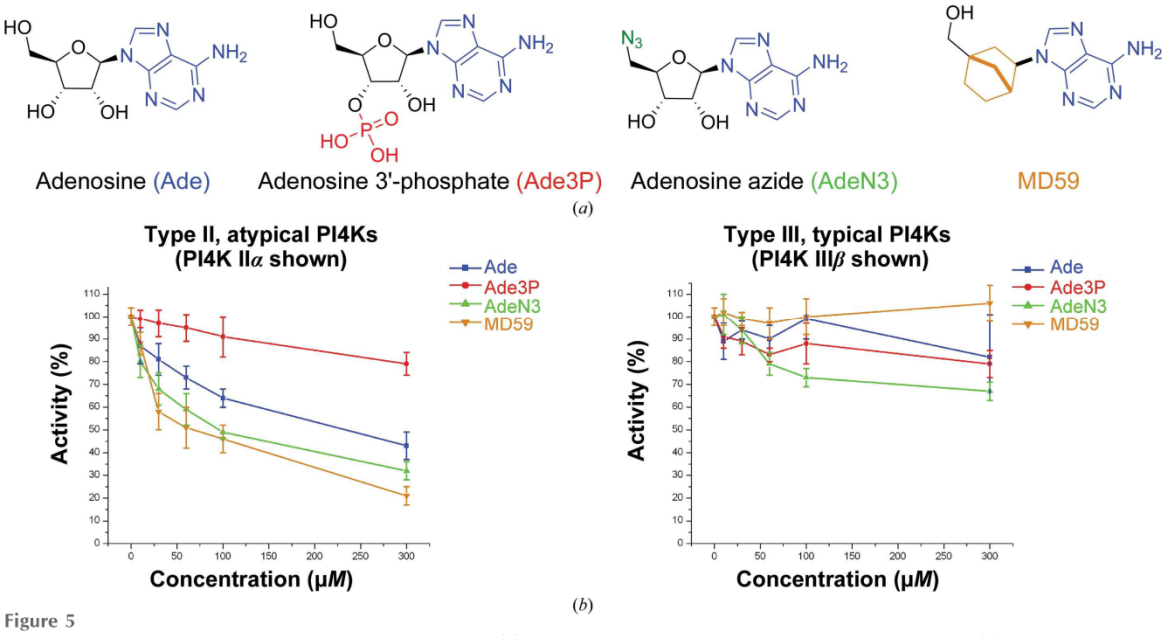



**Figure 5**
Inhibition of PI4Ks by selected nucleosides and their analogues. (*a*) Chemical formulae of the nucleosides and analogues used. (*b*) Inhibitory activity of selected nucleosides and analogues against type II and type III PI4Ks.

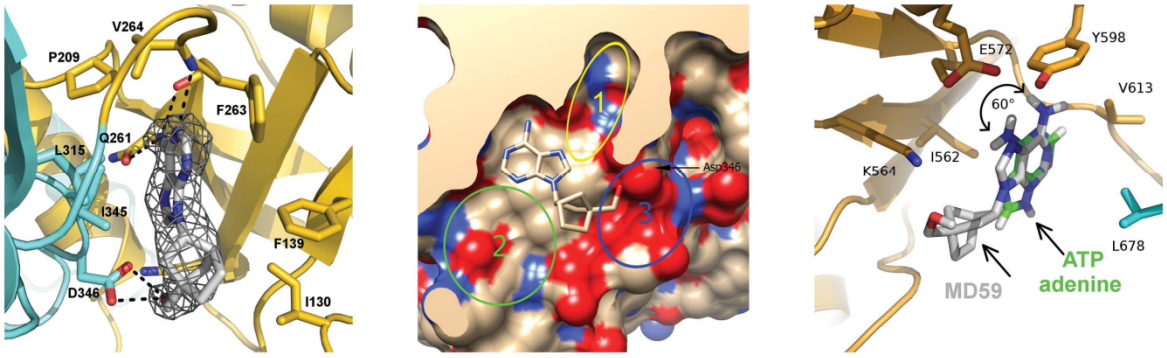



**Figure 6**
Inhibition of PI4Ks by MD59. (*a*) Detailed view of the MD59 inhibitor bound in the ATP-binding pocket of PI4K II$\alpha$. The protein backbone is shown in cartoon representation; the N-lobe is coloured aquamarine and the C-lobe is coloured gold. MD59 and the side chains of selected residues are shown in stick representation and coloured according to element: oxygen, red; nitrogen, blue. Kinase C atoms are coloured according to domain assignment and the C atoms of MD59 are shown in silver. H atoms are not shown. The unbiased $F_o - F_c$ map contoured at 3$\sigma$ is shown around the MD59 molecule. Hydrogen bonds between MD59 and the amino-acid residues are shown as dotted black lines. (*b*) Exploitable pockets in the vicinity of MD59. Design strategies for novel PI4K inhibitors should utilize the three pockets identified in the crystal structure of the PI4K II$\alpha$ enzyme with MD59. The narrow deep pocket 1 might be effectively filled with a linear substituent. Significant space for modification is opened in pocket 2, which is formed mostly by lipophilic residues. The interaction of Asp346 with pocket 3 seems to be essential for adequate affinity of the ligand for the kinase and should be exploited preferably by ionic interaction. (*c*) MD59 docked into PI4K III$\beta$. MD59 was docked into PI4K III$\beta$ in the same orientation as that in which it interacts with PI4K II$\alpha$. However, superposition with the ATP adenine ring reveals that it is rotated by 60° and that its hydroxyl group cannot form hydrogen bonds to any residue. The N-lobe of PI4K III$\beta$ is shown in orange and the C-lobe is shown in cyan. MD59 C atoms are coloured grey and C atoms of the ATP adenine ring are coloured green.



electronic reprint

nucleotide is capable of binding to this pocket (Baumlova *et al.*, 2014); thus, we included ADP in the crystallization condition. To prevent ADP from competing with MD59, we added ADP at a low concentration (0.5 m*M*) while keeping the concentration of MD59 high (2 m*M*). The resulting crystals diffracted to 2.6 Å resolution (albeit with some anisotropy) and density for MD59 was clearly visible (Fig. 6*a*). The side chain of Asp346 has changed conformation to form hydrogen bonds to the hydroxyl group of MD59 (Fig. 6*a*, Supplementary Fig. S3*a*); notably in this conformation it would clash with the $\alpha$-phosphate of ADP. To further confirm that the ligand density is not from the sterically similar ADP molecule, we built ADP instead of MD59 in the same conformation as reported by Zhou and coworkers (Supplementary Figs. S3*b* and S3*c*). Our structure clearly has no density for phosphates, which were well visible in previously reported structures of PI4K II$\alpha$ (Baumlova *et al.*, 2014; Zhou *et al.*, 2014).

The structure revealed three pockets in the proximity of MD59 (numbered 1, 2 and 3 in Fig. 6*b*) that could be exploited for the design of highly selective and potent inhibitors of type II PI4Ks. Since pocket 1 appears to be narrow, a linear substituent such as acetylene may be suitable to attach to the adenine ring to appropriately fill this space. In addition, a large aromatic substituent either on the adenylyl or ribosyl ring could fill pocket 2 and a charged group (for example amidine or guanidine) attached to the ribosyl ring could fill pocket 3.

We have shown above that nucleoside scaffold-based inhibitors only inhibit the atypical type II PI4Ks (Fig. 5*b*). To understand why, we took advantage of the structure of PI4K III$\beta$ bound to ATP that we have recently solved (Mejdrova *et al.*, 2015). We have docked MD59 in the PI4K III$\beta$ in the same orientation that it has when bound to PI4K II$\alpha$ (Fig. 6*c*). Docking revealed that the MD59 adenine ring would be rotated by 60° compared with the ATP adenine ring and thus unable to form the key hydrogen bonds to Glu572 and Lys564. The MD59 hydroxyl group that is important for inhibition of type II kinases also does not form any hydrogen bonds to the type III kinase. Previously, we have prepared highly selective inhibitors against PI4K III$\beta$ (Mejdrova *et al.*, 2015); we now show that inhibitors with a nucleoside scaffold only inhibit the atypical type II PI4Ks and are thus the perfect starting point for isoform-specific inhibitor design.

Structural analysis of the catalytic sites of PI4K II$\alpha$ and PI4K II$\beta$ (Fig. 4*b*) revealed only a few differences, implying that the design of an inhibitor discriminating between the II$\alpha$ and II$\beta$ isoenzymes would be rather difficult. One difference potentially useful for isoform-specific inhibitor design is the orientation of residue Ser127 of PI4K II$\beta$, which corresponds to Tyr131 in the PI4K II$\alpha$ enzyme. Neither Ser127 nor Tyr131 contact ATP directly, but are in close proximity. A PI4K II$\alpha$-specific inhibitor must have a group that is capable of interaction with the aromatic ring of Tyr131, for example a small aromatic ring ($\pi$-stacking) or an –SH, –S*R* or positively charged group, whereas a PI4K II$\beta$-specific inhibitor must have a bulky non-aromatic group that would sterically interfere with Tyr131 but would be capable of hydrogen bonding to Ser127.

Taken together, our results provide a structural basis for the design of specific inhibitors of type II PI4Ks.

## Acknowledgements

The project was supported by the Academy of Sciences Czech Republic (RVO: 61388963), by the Marie Curie FP7-PEOPLE-2012-CIG project No. 333916, by the Grant Agency of the Czech Republic, grant Nos. 15-21030Y and 15-09310S, and by Project InterBioMed LO1302 from the Ministry of Education of the Czech Republic. We thank HZB for the allocation of synchrotron-radiation beamtime. The research leading to these results has received funding from the European Community's Seventh Framework Programme (FP7/2007-2013) under BioStruct-X (grant agreement No. 283570). We are grateful to Lenka Klouckova for technical assistance.

## References

Adams, P. D. *et al.* (2010). *Acta Cryst.* D**66**, 213–221.
Altan-Bonnet, N. & Balla, T. (2012). *Trends Biochem. Sci.* **37**, 293–302.
Anglin, J. L., Deng, L., Yao, Y., Cai, G., Liu, Z., Jiang, H., Cheng, G., Chen, P., Dong, S. & Song, Y. (2012). *J. Med. Chem.* **55**, 8066–8074.
Balla, T. (1998). *Biochim. Biophys. Acta*, **1436**, 69–85.
Balla, T. (2013). *Physiol. Rev.* **93**, 1019–1137.
Balla, A., Tuymetova, G., Barshishat, M., Geiszt, M. & Balla, T. (2002). *J. Biol. Chem.* **277**, 20041–20050.
Barylko, B., Gerber, S. H., Binns, D. D., Grichine, N., Khvotchev, M., Südhof, T. C. & Albanesi, J. P. (2001). *J. Biol. Chem.* **276**, 7705–7708.
Baumlova, A., Chalupska, D., Różycki, B., Jovic, M., Wisniewski, E., Klima, M., Dubankova, A., Kloer, D. P., Nencka, R., Balla, T. & Boura, E. (2014). *EMBO Rep.* **15**, 1085–1092.
Berger, K. L., Cooper, J. D., Heaton, N. S., Yoon, R., Oakland, T. E., Jordan, T. X., Mateu, G., Grakoui, A. & Randall, G. (2009). *Proc. Natl Acad. Sci. USA*, **106**, 7577–7582.
Bianco, A., Reghellin, V., Donnici, L., Fenu, S., Alvarez, R., Baruffa, C., Peri, F., Pagani, M., Abrignani, S., Neddermann, P. & De Francesco, R. (2012). *PLoS Pathog.* **8**, e1002576.
Boura, E. & Hurley, J. H. (2012). *Proc. Natl Acad. Sci. USA*, **109**, 1901–1906.
Boura, E., Ivanov, V., Carlson, L. A., Mizuuchi, K. & Hurley, J. H. (2012). *J. Biol. Chem.* **287**, 28144–28151.
Boura, E., Rezabkova, L., Brynda, J., Obsilova, V. & Obsil, T. (2010). *Acta Cryst.* D**66**, 1351–1357.
Burgess, J., Del Bel, L. M., Ma, C.-I. J., Barylko, B., Polevoy, G., Rollins, J., Albanesi, J. P., Krämer, H. & Brill, J. A. (2012). *Development*, **139**, 3040–3050.
Burke, J. E., Inglis, A. J., Perisic, O., Masson, G. R., McLaughlin, S. H., Rutaganira, F., Shokat, K. M. & Williams, R. L. (2014). *Science*, **344**, 1035–1038.
Craige, B., Salazar, G. & Faundez, V. (2008). *Mol. Biol. Cell*, **19**, 1415–1426.
Debreczeni, J. É. & Emsley, P. (2012). *Acta Cryst.* D**68**, 425–430.
Dejmek, M. *et al.* (2015). *Bioorg. Med. Chem.* **23**, 184–191.
Greninger, A. L., Knudsen, G. M., Betegon, M., Burlingame, A. L. & DeRisi, J. L. (2012). *J. Virol.* **86**, 3605–3616.
Hurley, J. H., Boura, E., Carlson, L. A. & Różycki, B. (2010). *Cell*, **143**, 875–887.
Jović, M., Kean, M. J., Dubankova, A., Boura, E., Gingras, A. C., Brill, J. A. & Balla, T. (2014). *J. Cell Sci.* **127**, 3745–3756.
Jović, M., Kean, M. J., Szentpetery, Z., Polevoy, G., Gingras, A. C., Brill, J. A. & Balla, T. (2012). *Mol. Biol. Cell*, **23**, 1533–1545.


electronic reprint

Jung, G., Barylko, B., Lu, D., Shu, H., Yin, H. & Albanesi, J. P. (2011). *J. Biol. Chem.* **286**, 12775–12784.
Jung, G., Wang, J., Wlodarski, P., Barylko, B., Binns, D. D., Shu, H., Yin, H. L. & Albanesi, J. P. (2008). *Biochem. J.* **409**, 501–509.
Kabsch, W. (2010). *Acta Cryst.* D**66**, 125–132.
Karplus, P. A. & Diederichs, K. (2012). *Science*, **336**, 1030–1033.
Kim, D. J. *et al.* (2010). *Proc. Natl Acad. Sci. USA*, **107**, 21418–21423.
Krug, M., Weiss, M. S., Heinemann, U. & Mueller, U. (2012). *J. Appl. Cryst.* **45**, 568–572.
McCoy, A. J., Grosse-Kunstleve, R. W., Adams, P. D., Winn, M. D., Storoni, L. C. & Read, R. J. (2007). *J. Appl. Cryst.* **40**, 658–674.
Mejdrova, I. *et al.* (2015). *J. Med. Chem.* **58**, 3767–3793.
Minogue, S., Waugh, M. G., De Matteis, M. A., Stephens, D. J., Berditchevski, F. & Hsuan, J. J. (2006). *J. Cell Sci.* **119**, 571–581.
Moorhead, A. M., Jung, J.-Y., Smirnov, A., Kaufer, S. & Scidmore, M. A. (2010). *Infect. Immun.* **78**, 1990–2007.
Nemecek, D., Boura, E., Wu, W., Cheng, N., Plevka, P., Qiao, J., Mindich, L., Heymann, J. B., Hurley, J. H. & Steven, A. C. (2013). *Structure*, **21**, 1374–1383.
Qin, Y., Li, L., Pan, W. & Wu, D. (2009). *J. Biol. Chem.* **284**, 22544–22548.
Rosenbaum, D. M., Cherezov, V., Hanson, M. A., Rasmussen, S. G. F., Thian, F. S., Kobilka, T. S., Choi, H.-J., Yao, X.-J., Weis, W. I., Stevens, R. C. & Kobilka, B. K. (2007). *Science*, **318**, 1266–1273.
Różycki, B. & Boura, E. (2014). *J. Phys. Condens. Matter*, **26**, 463103.
Różycki, B., Boura, E., Hurley, J. H. & Hummer, G. (2012). *PLoS Comput. Biol.* **8**, e1002736.
Sasaki, J., Ishikawa, K., Arita, M. & Taniguchi, K. (2012). *EMBO J.* **31**, 754–766.
Schaar, H. M. van der *et al.* (2013). *Antimicrob. Agents Chemother.* **57**, 4971–4981.
Tai, A. W., Bojjireddy, N. & Balla, T. (2011). *Anal. Biochem.* **417**, 97–102.
Tan, J. & Brill, J. A. (2014). *Crit. Rev. Biochem. Mol. Biol.* **49**, 33–58.
Wang, K., Yang, Z., Liu, X., Mao, K., Nair, U. & Klionsky, D. J. (2012). *J. Biol. Chem.* **287**, 37964–37972.
Waugh, M. G. (2015). *Biochim. Biophys. Acta*, **1851**, 1066–1082.
Weber, S. S., Ragaz, C., Reus, K., Nyfeler, Y. & Hilbi, H. (2006). *PLoS Pathog.* **2**, e46.
Wei, Y. J., Sun, H. Q., Yamamoto, M., Wlodarski, P., Kunii, K., Martinez, M., Barylko, B., Albanesi, J. P. & Yin, H. L. (2002). *J. Biol. Chem.* **277**, 46586–46593.
Winn, M. D. *et al.* (2011). *Acta Cryst.* D**67**, 235–242.
Wu, X., Chi, R. J., Baskin, J. M., Lucast, L., Burd, C. G., De Camilli, P. & Reinisch, K. M. (2014). *Dev. Cell*, **28**, 19–29.
Zhou, Q., Li, J., Yu, H., Zhai, Y., Gao, Z., Liu, Y., Pang, X., Zhang, L., Schulten, K., Sun, F. & Chen, C. (2014). *Nature Commun.* **5**, 3552.
Zou, Y., Weis, W. I. & Kobilka, B. K. (2012). *PLoS One*, **7**, e46039.


electronic reprint

## 5.3 Highly Selective Phosphatidylinositol 4-Kinase IIIβ Inhibitors and Structural Insight into Their Mode of Action

**Background**

PI4-kinases type III play a pivotal role in the life cycle of +RNA viruses. Using the HCV and enteroviral model of RNA replication it was shown that viral proteins exploit different mechanisms to hijack type III PI4-kinases in order to modify the lipid environment and to build a platform for functional replication machinery. Inhibition of type III PI4-kinases seems to be a potential therapeutic target since the lipid kinase activity is indispensable for efficient viral replication. Therefore, structural insight into the complex of type III PI4-kinases with a potent isoform-specific inhibitor would be highly beneficial for anti-viral structure-based drug design.

**Summary**

PI4K IIIβ was used for co-crystallization experiments with ATP and a series of archetypical inhibitors. Two obtained crystal structures (see Figure 14.) provided important information to outline the mechanism of their action. Albeit the crystal structures of PI4K IIIβ in complex with ATP or selective inhibitor 49 were solved only at 3.5 Å and 3.3 Å resolutions, respectively, the electron density for the individual ligands was sufficient for their unambiguous placement. The superposition of both structures identified that compound 49 occupies the same place normally occupied by the ATP adenine ring and revealed conformational changes of individual residues involved in ligand binding (see Figure 14.). Overall structural information indicates that compound 49 interferes with adenosine ring in its binding into the active site thus blocking the course of PtdIns4P synthesis. In order to determine the inhibitory relevance of the different substituents in a series of these inhibitors, docking studies were performed as well. The results were used later to design more potent inhibitors.

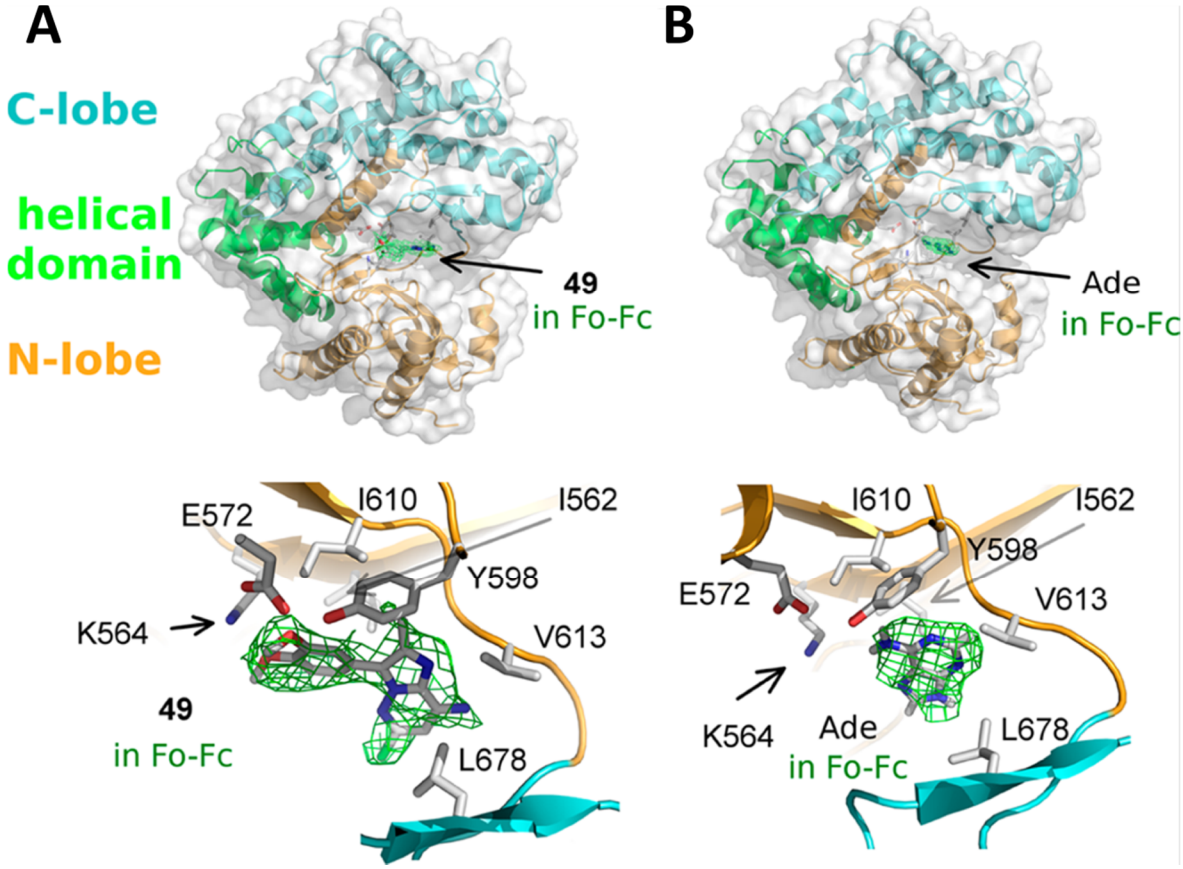



**Figure 14.: The crystal structures of inhibitor 49 and ATP bound to PI4K IIIβ.**
**Panel A:** The overall structure of PI4K IIIβ in complex with inhibitor 49 is depicted on top and a detailed view into the ATP binding site with inhibitor 49 is shown on the bottom. The unbiased Fo-Fc map contoured at 2σ is shown around 49 compound. The protein backbone is depicted in a cartoon representation with the N-lobe coloured in yellow, the C-lobe coloured in cyan and with the helical domain in green. Inhibitor 49 together with ATP and side chains of selected residues are shown in stick representation coloured according to elements: oxygen-red; nitrogen-blue and carbon in grey. **Panel B:** The overall fold of PI4K IIIβ in complex with an ATP molecule on the top and a detailed view of the binding pocket with an ATP bound molecule on the bottom. The adenine ring of ATP in the unbiased Fo-Fc map is contoured at 2σ.

## My contribution

I expressed and purified recombinant PI4K IIIβ. I participated in crystallization trials and in X-ray data collection.

Journal of Medicinal Chemistry

Article

pubs.acs.org/jmc

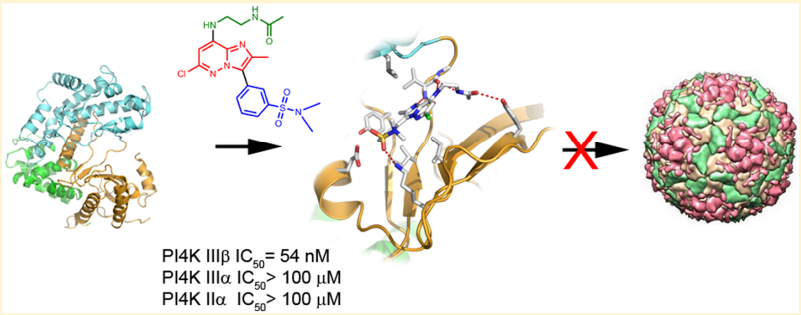
# Highly Selective Phosphatidylinositol 4-Kinase IIIβ Inhibitors and Structural Insight into Their Mode of Action

Ivana Mejdrová,[†,§] Dominika Chalupská,[†,§] Martin Kögler,[†,§] Michal Šála,[†] Pavla Plačková,[†] Adriana Baumlová,[†] Hubert Hřebabecký,[†] Eliška Procházková,[†] Milan Dejmek,[†] Rémi Guillon,[†] Dmytro Strunin,[†] Jan Weber,[†] Gary Lee,[‡] Gabriel Birkus,[‡] Helena Mertlíková-Kaiserová,[†] Evzen Boura,*[,†] and Radim Nencka*[,†]

[†]Institute of Organic Chemistry and Biochemistry, Academy of Sciences of the Czech Republic, v.v.i., Gilead Sciences & IOCB Research Centre, Flemingovo nám. 2, 166 10 Prague 6, Czech Republic

[‡]Gilead Sciences, Inc., 333 Lakeside Drive, Foster City, California 94404, United States

Supporting Information




**ABSTRACT:** Phosphatidylinositol 4-kinase IIIβ is a cellular lipid kinase pivotal to pathogenesis of various RNA viruses. These viruses hijack the enzyme in order to modify the structure of intracellular membranes and use them for the construction of functional replication machinery. Selective inhibitors of this enzyme are potential broad-spectrum antiviral agents, as inhibition of this enzyme results in the arrest of replication of PI4K IIIβ-dependent viruses. Herein, we report a detailed study of novel selective inhibitors of PI4K IIIβ, which exert antiviral activity against a panel of single-stranded positive-sense RNA viruses. Our crystallographic data show that the inhibitors occupy the binding site for the adenine ring of the ATP molecule and therefore prevent the phosphorylation reaction.

## INTRODUCTION

Phosphatidylinositol 4-phosphate (PI4P) is the most abundant monophosphoinositide in eukaryotic cell. It decorates the Golgi complex and trans-Golgi networks (TGN) and also has a role at the plasma membrane and endosomes.[1] In addition, PI4P is the precursor for the synthesis of other phosphoinositides, most notably phosphatidylinositol 4,5-bisphosphate ($PI(4,5)P_2$), the hallmark of the plasma membrane, and phosphatidylinositol 3,4,5-trisphosphate ($PI(3,4,5)P_3$), a key secondary messenger molecule. The synthesis of PI4P is carried out by phosphatidylinositol 4-kinases (PI4Ks).[2,3] Mammalian genomes contain two types of PI4Ks, type II (PI4K IIα and PI4K IIβ) and type III (PI4K IIIα and PI4K IIIβ) kinases that share homology with phosphatidylinositol 3-kinases (PI3Ks). Recently, crystal structures were solved for PI4K IIα[4,5] and for PI4K IIIβ.[6]

Type II PI4Ks are palmitoylated enzymes stably associated with the membrane. They are present at various endomembranes such as the TGN, early and late endosomes, as well as at the plasma membrane.[7,8] These enzymes are critical to intracellular trafficking[9,10] and interact with clathrin adaptor complexes (PI4K IIα with AP-3 and PI4K IIβ with AP1).[11,12] In contrast, type III kinases are soluble cytoplasmic proteins that are recruited to the membrane via protein−protein interactions. Efr, YPP1/TTC7, and TMEM150 direct the PI4K IIIα recruitment to the plasma membrane, where it is responsible for PI4P synthesis.[13,14] The Golgi resident proteins ACBD3 and GBF1/Arf recruit PI4K IIIβ to the Golgi,[15,16] where this enzyme is mostly responsible for the biogenesis of the Golgi pool of PI4P although type II PI4Ks also contribute to this pool.[17,18] The type III PI4Ks are essential host factors for a plethora of single-stranded positive-sense (ss(+)RNA) viruses[19] and are potential drug targets.

ss(+)RNA viruses hijack PI4Ks to produce membranous organelles (referred to as "membranous webs" or "replication

Received: December 15, 2014
Published: April 21, 2015

ACS Publications © 2015 American Chemical Society



DOI: 10.1021/acs.jmedchem.5b00499
J. Med. Chem. 2015, 58, 3767−3793

factories") highly enriched in PI4P, which facilitate the assembly of functional viral replication machinery. For example, the hepatitis C virus (HCV) hijacks both PI4K IIIα[20] and PI4K IIIβ,[21,22] whereas various members of the *Picornaviridae* family, including coxsackieviruses and rhinoviruses,[23−26] and those of the *Coronaviridae* family,[27] were shown to depend on PI4K IIIβ. In spite of the broad dependence on PI4Ks, several different molecular mechanisms of hijacking have recently been described. The NS5A protein of HCV directly binds to PI4K IIIα and stimulates its activity,[28] whereas the 3A protein of the Aichi virus hijacks PI4K IIIβ through interaction with its binding partner, the ACBD3 protein.[15] The recruitment of PI4K IIIβ to Coxsackievirus B3 replication factories occurs through an unknown mechanism that is independent of ACBD3.[29] PI4Ks are therefore potential drug targets as essential host factors for the replication of ss(+)RNA viruses. A possible impediment to these strategies, however, is that genetic inactivation of type III PI4Ks is detrimental for animals.[30,31] A window of possibility relies on the fact that RNA viruses require every bit of the cell's PI4K activity (and even up regulate PI4Ks) for replication, whereas partially compromised PI4K activity may be well tolerated in animals, especially if only for a short time period.[19] To clarify whether a therapeutic window exists for PI4K enzyme inhibition, potent and selective inhibitors of the PI4K enzymes are needed.

Although several potent inhibitors of PI4K type III enzymes have been discovered recently, most of them targeted PI4K IIIα.[32,33] The studies focused on PI4K IIIβ suffer from a lack of detailed structure−activity relationship (SAR) and structural data, which would allow for a better understanding of the mode of action of these compounds.[34−36]

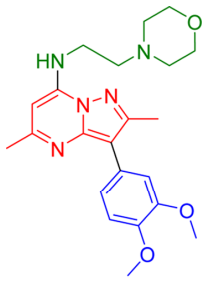
We present an extensive study on a broad series of novel PI4K IIIβ inhibitors. We show that these compounds are highly selective based on biochemical characterization. We also assess the effects of these inhibitors against selected viruses in cell-based assays. To gain detailed knowledge of the molecular details of their inhibitory mechanisms, we solved the crystal structures of PI4K IIIβ enzyme bound to an archetypical inhibitor and to ATP. These structures revealed the mechanism of PI4K IIIβ enzyme inhibition by these compounds at the atomic level.

## RESULTS

**Chemistry.** We prepared a series of 65 novel compounds based on the screening hit **2a** (T-00127-HEV1) discovered by Arita et al.[24] We sequentially modified all three parts of the molecule: the amine side chain 1 (Figure 1, in green), bicyclic central core (Figure 1, in red), and aromatic side chain 2 (Figure 1, in blue).

First, we focused on the effect of diverse modifications of the side chain 1 using the original pyrazolo[1,5-*a*]pyrimidine central core. Most of the derivatives were prepared starting from the compound **1**[37] by simple nucleophilic substitution (DIPEA, EtOH, 75 °C) of the chlorine atom at position 7 of the bicyclic central core (Scheme 1), which proceeds smoothly with high to excellent yields. An additional series of the inhibitors was prepared by derivatization of the ethyl-enediamino chain with various substituents (Scheme 2, compounds **3**−**9**). Analogous derivatives **10** and **11** were obtained by acetylation from appropriate starting materials **2f** and **2k**, respectively.

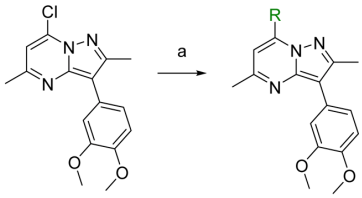
We also prepared compounds with sulfur and oxygen atoms instead of the NH-group at position 7 in order to investigate



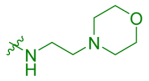
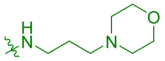
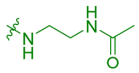
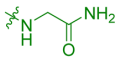
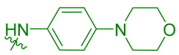
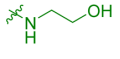
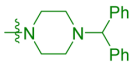
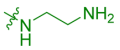
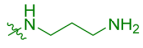
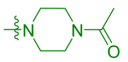
**2a** (T-00127-HEV1)

**Figure 1.** Screening hit as a model compound for SAR study.

**Scheme 1. Synthesis of C7-Modified Pyrazolopyrimidines**[a]



**1** **2a-l**

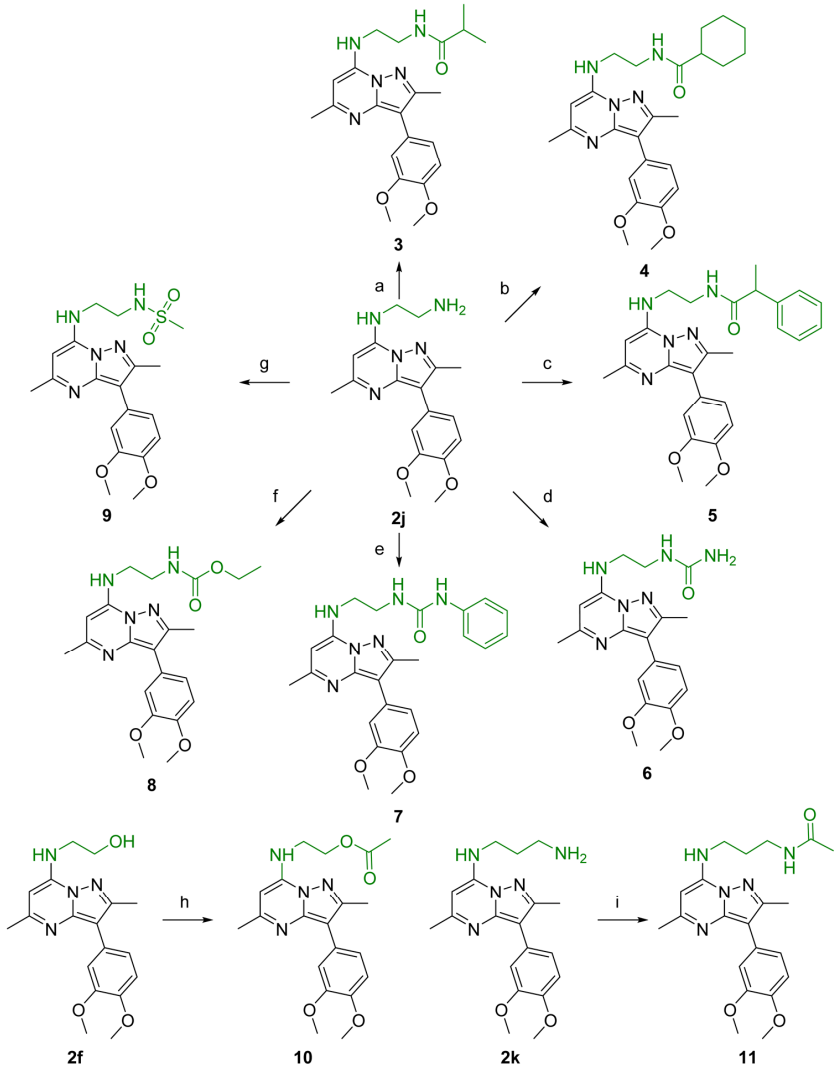
| Compnd | R | Yield |
|---|---|---|
| **2a** |  | 89% |
| **2b** |  | 80% |
| **2c** |  | 87% |
| **2d** |  | 82% |
| **2e** |  | 65% |
| **2f** |  | 88% |
| **2g** |  | 75% |
| **2h** |  | 77% |
| **2i** | $NH_2$ | 74% |
| **2j** |  | 91% |
| **2k** |  | 92% |
| **2l** |  | 90% |

[a]Reagents and conditions: (a) amine, EtOH, heating.



DOI: 10.1021/acs.jmedchem.5b00499
*J. Med. Chem.* 2015, 58, 3767−3793

**Scheme 2. Preparation of Various *N*-Modified Ethylenediamino Derivatives 3−11**[a]




[a]Reagents and conditions: (a) isobutyric acid, DCC, $CH_2Cl_2$, 0 °C to rt, 20 h, 74%; (b) cyclohexanecarbonyl chloride, $Et_3N$, $CH_2Cl_2$, 0 °C, 2 h, 72%; (c) 2-phenylpropionic acid, DCC, $CH_2Cl_2$, 0 °C to rt, 20 h, 81%; (d) KCNO, aq HCl·$H_2O$, MeOH, 50 °C, 40 h, 75%; (e) phenyl isocyanate, $CH_2Cl_2$, 24 h, 89%; (f) ClCOOEt, $Et_3N$, $CH_2Cl_2$, 0 °C, 1.5 h, 61%; (g) methanesulfonyl chloride, $Et_3N$, $CH_2Cl_2$, 0 °C, 5 h and rt 4 h, 83%; (h) $Ac_2O$, $Et_3N$, $CH_2Cl_2$, 0 °C, 20 h, 71%; (i) $Ac_2O$, aq $NaHCO_3$, $CHCl_3$, 0 °C, 80%.

the influence of putative hydrogen bond with the protein. The thio derivatives were prepared either by reaction with thiourea and subsequent alkylation with chloroethyl morpholine to obtain analogue **13** or by direct nucleophilic substitution using appropriate thiophenol yielding derivative **14**. The oxygen analogue **15** of the parent compound **2a** was prepared also by a nucleophilic substitution under basic conditions (NaH/DMF) (Scheme 3).

Second, we turned our attention to the modification of the central bicyclic core. We prepared analogues of the parent compound with imidazo[1,2-*a*]pyridine (**16**) (Scheme 4), imidazo[1,2-*b*]pyridazine (**17**) (Scheme 5), and pyrazolo[1,5-*a*][1,3,5]triazine (**18**) central core (Scheme 7).

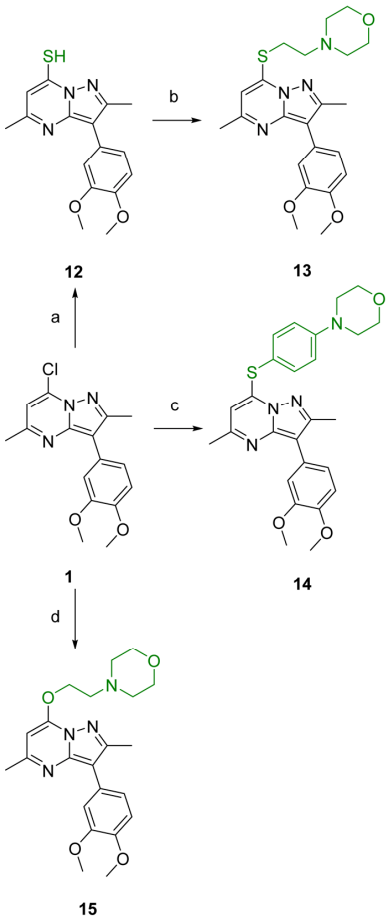
The synthesis of imidazo[1,2-*a*]pyridine derivative started from compound **19**,[38] which was easily iodinated using NIS (Scheme 4). Suzuki cross-coupling reaction followed by a microwave-assisted Hartwig−Buchwaldg reaction with 4-(2-aminoethyl)morpholine yielded the desired analogue **16**. However, this compound is surprisingly unstable and decomposes quite rapidly.

The preparation of the compound **17** started from dichloro derivative **22**.[39] Because the reactivity of the chlorine atoms differs significantly, treatment with 4-(2-aminoethyl)-morpholine afforded the desired monosubstituted product **23** in high yield. This compound was utilized for subsequent preparation of the methylated derivative **24** (Scheme 5). A number of diverse methylation reactions failed to give this



DOI: 10.1021/acs.jmedchem.5b00499
J. Med. Chem. 2015, 58, 3767−3793

**Scheme 3. Synthesis of C7-Modified Pyrazolopyrimidines**[a]




[a]Reagents and conditions: (a) thiourea, EtOH, reflux, 15 h, 85%; (b) 4-(2-chloroethyl)-morpholine hydrochloride, $K_2CO_3$, DMF, 77%; (c) 4-(morpholin-4-yl)benzenethiol, $K_2CO_3$, DMF, 43%; (d) 4-(2-hydroxyethyl)morpholine, NaH, DMF, 58%.

derivative. Finally, the transfer of a methyl group was accomplished by reacting compound **23** with DABAL-$Me_3$ (a reactive complex between one molecule of DABCO and two molecules of $AlMe_3$)[40] under Pd-catalyzed cross-coupling conditions. This way, key intermediate **24** was prepared in moderate 42% yield. Iodination and Suzuki coupling with 3,4-dimethoxyphenyl boronic acid afforded title compound **17** (Scheme 5).

Because compound **17** exerted interesting inhibitory activity in the PI4K III$\beta$ enzymatic assay, the preparation of analogues with modified substituents at position 6 was the logical further step. The derivative **23** served as a suitable precursor for the preparation of analogues bearing either a hydrogen or chlorine atom instead of the methyl group at this position (Scheme 5). The synthesis of the former derivative (**28**) was accomplished by simple hydrogenolysis followed by iodination and Suzuki reaction. The latter compound (**30a**) was obtained in the similar fashion without the hydrogenolysis step. In this case, we prepared also several other related derivatives with this structural pattern summarized in Scheme 6 using intermediate **29** subdued to Suzuki cross-coupling reactions.

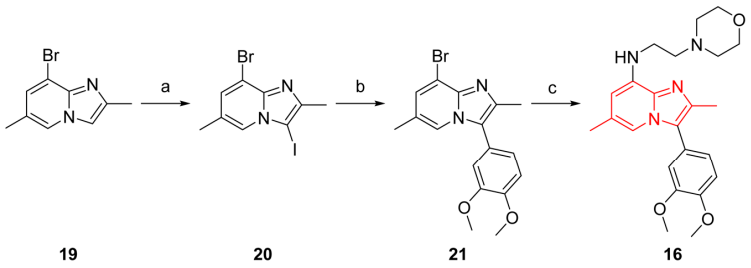
Derivative **32** with the last bicyclic core, pyrazolo[1,5-*a*][1,3,5]triazine, was obtained starting from bromide **31**[41] by cross-coupling reaction with 3,4-dimethoxyphenylboronic acid. Subsequent chlorination followed by immediate substitution of the chlorine atom with the appropriate amine afforded the desired analogue of **2a**, compound **18**, and derivative **33** (Scheme 7).

On the basis of our preliminary results from PI4K III$\beta$ assay, with respect to synthetic feasibility and potential metabolic decomposition, we selected 6-chloro-2-methylimidazo[1,2-*b*]-pyridazine as the most suitable central core and [2-(acetylamino)ethyl]amino group as side chain 1 for further optimization of the aromatic side chain 2. The key intermediate **35** for this study was prepared by iodination with NIS, giving compound **34** (Scheme 5), followed by selective nucleophilic substitution of the chlorine at position 8 with 2-amino-ethylacetamide.

Majority of compounds form the last series was prepared by Suzuki cross-coupling reaction starting from the compound **35** (Scheme 8).

Another subseries of derivatives modified in the aromatic side chain was prepared by derivatization of suitable precursors obtained by Suzuki couplings. First, we modified the amino group of the compound **36u**. In particular, we obtained a few acylated derivatives (**37**–**39**) either by reaction with acyl anhydrides or chlorides (Scheme 9). Subsequently, reaction with isopropylisocyanate afforded the substituted urea derivative **40** and the compounds **41** and **42** were prepared by reductive amination and alkylation of compound **36u**, respectively (Scheme 10).

**Scheme 4. Preparation of Bicyclic Analogue Imidazo[1,2-*a*]pyridine 16**[a]

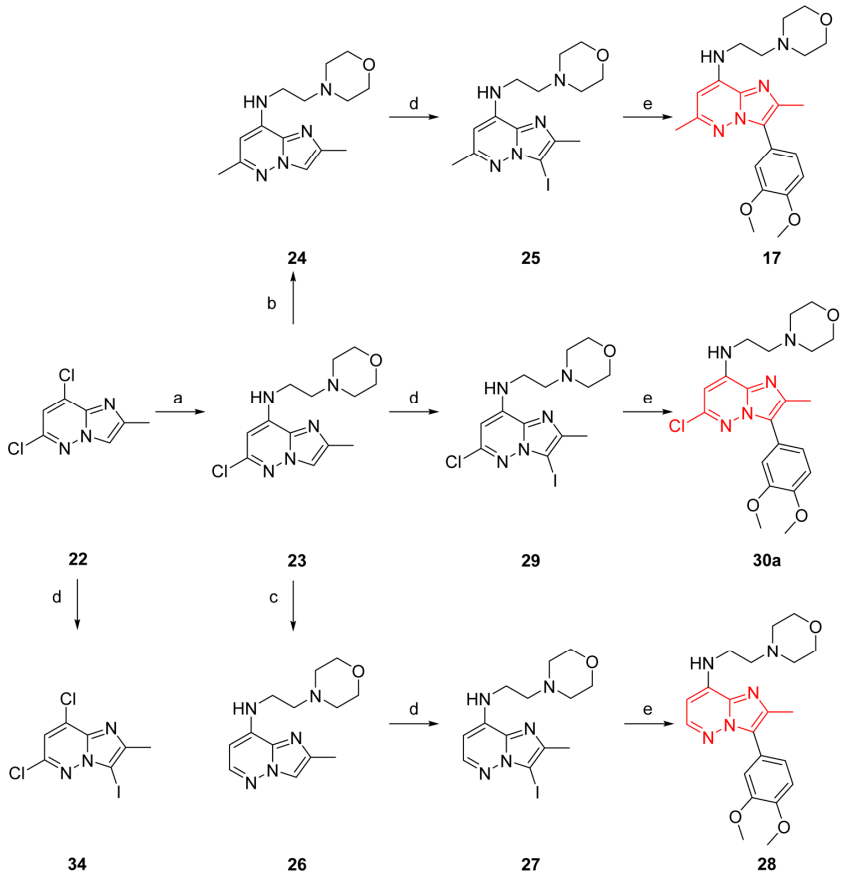



[a]Reagents and conditions: (a) NIS, DMF, rt, 30 min, yield 89%; (b) 3,4-dimethoxy-phenylboronic acid, Pd(dppf)$Cl_2$, $Na_2CO_3$, dioxane/$H_2O$ (4:1), 16 h, 60%; (c) 4-(2-aminoethyl)morpholine, $Pd_2(dba)_3$, MeDalPhos, *t*-ButONa, dioxane, MW, 30 min, 150 °C, 72%.



DOI: 10.1021/acs.jmedchem.5b00499
*J. Med. Chem.* 2015, 58, 3767−3793

Scheme 5[a]




[a]Reagents and conditions: (a) 4-(2-aminoethyl)morpholine, DIPEA, $CH_3CN$, 80 °C, sealed vessel, 16 h, 87%; (b) DABAL-$Me_3$, $Pd_2(dba)_3$, X-Phos, THF, rt to 80 °C, overnight, 42%; (c) $H_2$, Pd/C, THF:MeOH, rt, 21 h; (d) NIS, AcOH/$CH_2Cl_2$ or DMF, (49% for **25**, 41% for **27**, 41% for **29**, 95% for **34**); (e) 3,4-dimethoxyphenylboronic acid, $Pd(PPh_3)_4$, 1 M $K_2CO_3$, dioxane, 95 °C, overnight (60% for **17**, 83% for **28**, 77% for **30a**).

We also prepared 3-(3,4-dihydroxyphenyl) derivative **43** by the demethylation of **30a**, albeit in very low yield (Scheme 11). Reduction of the formyl functions in compounds **36e** and **36i** with $NaBH_4$ gave the corresponding hydroxymethyl derivatives **44** and **45**, respectively, in moderate yields.

To introduce highly polar group, the cyano moiety in compound **36h** was successfully reduced to the primary amine **46**, which was isolated as its hydrochloride salt.

The analogue of compounds **36a** with hydrogen instead of the chlorine atom at the position 6 of the imidazo[1,2-*b*]pyridazine core (**47**) was prepared by simple hydrogenolysis of **36a** (Scheme 12).

Finally, the derivative **49** was obtained by ammonolysis of compound **34** and subsequent Suzuki coupling as described in Scheme 12.

**Novel PI4K III$\beta$ Inhibitors and Their Antiviral Activity.** To characterize the potency of this series of inhibitors in vitro, we used the luminescent ADP-Glo kinase assay.[42] For the presentation of the biological activities of the whole series, we have selected 10 compounds which exerted the highest inhibitory activities against PI4K III$\beta$ in vitro (Figure 2).

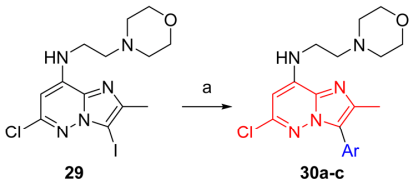
We found that the $IC_{50}$ values for the top 10 compounds were in the range of 50−130 nM against PI4K III$\beta$. Further, we determined whether the compounds were isoform specific for PI4K III$\beta$, a necessity for evaluating therapeutic potential. We have thus used the ADP-Glo kinase assay to measure the $IC_{50}$ values for two structurally and functionally related enzymes, PI4K III$\alpha$ and PI4K II$\alpha$. We found that none of the top 10 compounds inhibited PI4K III$\alpha$ and PI4K II$\alpha$ with an $IC_{50}$ less than 10 $\mu$M (These data are summarized in Table 1 for the top 10 compounds, and in Supplementary Results, Supporting Information, Table 2, for the remaining 55).

Next, we focused on determining the antiviral activity of the compounds. For this, we used an assay based on the virus-induced cytopathic effect in HeLa cells (in detail in Experimental Methods). We tested the activity of the compounds against two important members of the *Picornaviridae* family, Coxsackievirus B3 (CVB3), and human rhinovirus (HRV) and two distinct genotypes of HCV (*Flaviviridae*), genotype 1b and 2a. For each virus tested except for HCV 2a several of the compounds exhibited $IC_{50}$ values below 1 $\mu$M as summarized in Table 2 and Supporting Information, Table 3.

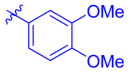
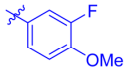


DOI: 10.1021/acs.jmedchem.5b00499
J. Med. Chem. 2015, 58, 3767−3793

**Scheme 6. Suzuki Cross-Coupling Reaction of Morpholino Ethyl Derivative 29**[a]

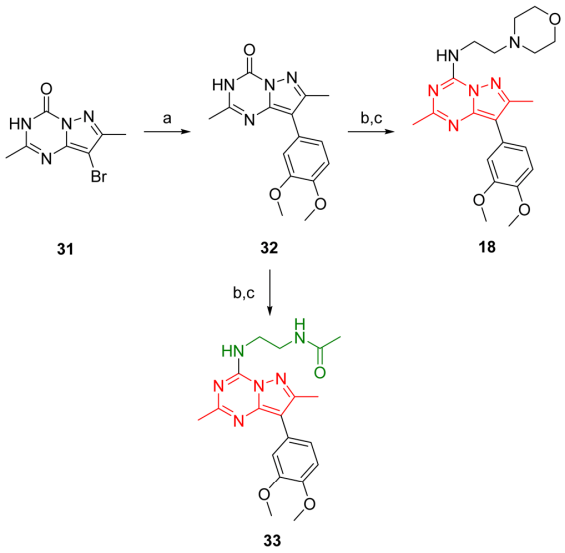



29 30a-c

| Compd | Ar | Yield |
|---|---|---|
| 30a |  | 77% |
| 30b |  | 76% |
| 30c |  | 56% |

[a]Reagents and conditions: (a) Ar-B(OH)$_2$, Pd(PPh$_3$)$_4$, 1 M K$_2$CO$_3$, dioxane, heating.

**Scheme 7. Synthesis of Pyrazolo[1,5-*a*][1,3,5]triazine Derivatives**[a]




[a]Reagents and conditions: (a) 3,4-dimethoxyphenylboronic acid, Pd(dppf)Cl$_2$, Na$_2$CO$_3$, dioxane/H$_2$O (4:1), 16 h, 60%; (b) POCl$_3$, dimethylaniline, 120 °C, 20 h; (c) amine, DCM, 0 °C−rt, 16 h (yields over two steps: 68% for **18**, 65% for **33**).

Although the correlation between the results from the enzymatic assay and the cell-based assay was not very tight, there was a clear rise in antiviral potency as PI4K III$\beta$ inhibitory activity increased. The sensitivity of various viruses to the inhibition of the PI4K III$\beta$ showed significant differences. The HCV genotype 1b displayed some sensitivity, whereas the effects of PI4K III$\beta$ inhibition on replication of HCV 2a were rather limited. The most potent compound in the series was derivative **36t**, which inhibited PI4K III$\beta$ with IC$_{50}$ = 54 nM and exerted significant effect in all cell-based assays. Derivative **36t** was the most active compound in HVC 2a assay (EC$_{50}$ = 10.6 $\mu$M) and the second most active against HCV1b (EC$_{50}$ = 0.087 $\mu$M). Furthermore, this compound showed strong protection against CVB3-induced cytopathic effects in HeLa cells with half-maximal effective concentration (EC$_{50}$) value of 145 nM. This compound was also evaluated in a panel of phosphatidylinositol 3-kinases (PI3K$\alpha$, PI3K$\beta$, PI3K$\delta$, and PI3K$\gamma$). None of these kinases was inhibited with IC$_{50}$ up to 10 $\mu$M.

**Structural Analysis of the Inhibition Mode of PI4K III$\beta$.** To determine how the inhibitors function at the atomic level, we solved the crystal structure of PI4K III$\beta$ either with an inhibitor or bound to ATP. We selected several inhibitors of archetypical chemical structure and reasonable solubility for crystallographic trials. The best crystals were obtained with inhibitor **49** but still diffracted only to 3.5 Å resolution. The structure was solved by molecular replacement using chain A of the crystal structure of PI4K III$\beta$ with Rab11 (PDB code: ID0L) without the PIK93 inhibitor to reduce bias. Because of the rather low resolution the unbiased $F_o - F_c$ map contoured at 3$\sigma$ did not provide enough information to unambiguously place the **49** inhibitor (Supporting Information, Figure 3). However, the density for the **49** inhibitor was clearly visible in the $F_o - F_c$ map contoured at 2$\sigma$ and allowed for unambiguous placement of the **49** inhibitor (Figure 3a). We have refined the structure to $R$ = 20.89% and $R_{free}$ = 25.16%. To confirm that the result of manual docking and refinement in Coot[43] is correct, we calculated the $R$ factors for a structure where the **49** inhibitor is rotated by 180° and refined into the $F_o - F_c$ density. The obtained values ($R$ = 21.19% and $R_{free}$ = 26.07%) are significantly worse and argue for correct placement of the ligand.

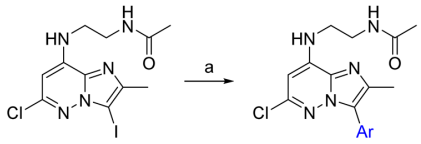
Crystals with ATP bound diffracted to 3.3 Å resolution, and the structure was solved in the same way as the structure with **49** inhibitor and refined to $R$ = 18.25% and $R_{free}$ = 24.41%. However, we did not observe density for the whole ATP molecule, only for the adenine ring (Figure 3b), despite the better resolution. We, therefore, concluded that the ribose ring and the three phosphate groups are disordered in our structure. The density for adenine at 3.3 Å, in principle, allows positioning the adenine ring in multiple orientations. To confirm that the best fit obtained in Coot[43] was the right solution, we compared the structure of PI4K III$\beta$ with the structure of PI4K II$\alpha$, where the ATP molecule is clearly resolved.[4] We have used the C-lobes of PI4K II$\alpha$ and PI4K III$\beta$ for superposition, taking advantage of the fact that they are structurally very similar. The superposition revealed that the adenine rings in both structures are in a similar orientation (Supplementary Figure 2), supporting the placement of the adenine ring in the presented structure.

Both **49** and the adenine ring lie in a binding canyon of PI4K III$\beta$ held in place by a combination of hydrophobic interactions and hydrogen bonds, water bridges surely also contribute (for instance, the hydroxyl group of Tyr$^{598}$ and the N6 of the adenine ring are in perfect distance and orientation for a water bridge), but water molecules were not modeled due to limited resolution of our crystal structures (Figure 4a,b). Superposition of the two structures revealed that compound **49** and the adenine ring occupy the same pocket (Figure 4c), suggesting that this family of inhibitors function by sterically blocking the

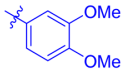
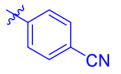
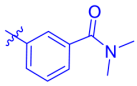
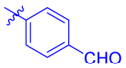
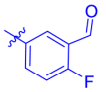
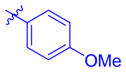
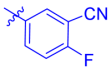
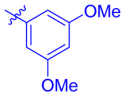
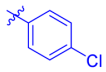
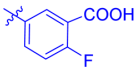
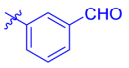
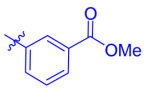
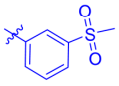
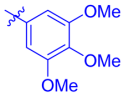
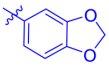
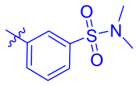
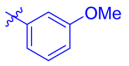
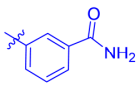
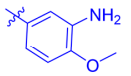


DOI: 10.1021/acs.jmedchem.5b00499
J. Med. Chem. 2015, 58, 3767−3793

**Scheme 8. Aryl Derivatives Prepared by Suzuki Coupling Reaction**[a]




35 36a-u

| Compd | Ar | Yield | Compd | Ar | Yield | Compd | Ar | Yield |
|---|---|---|---|---|---|---|---|---|
| **36a** |  | 97% | **36h** |  | 92% | **36o** |  | 78% |
| **36b** |  | 85% | **36i** |  | 91% | **36p** |  | 55% |
| **36c** |  | 60% | **36j** |  | 77% | **36q** |  | 73% |
| **36d** |  | 32% | **36k** |  | 40% | **36r** |  | 29% |
| **36e** |  | 82% | **36l** |  | 40% | **36s** |  | 57% |
| **36f** |  | 96% | **36m** |  | 40% | **36t** |  | 65% |
| **36g** |  | 96% | **36n** |  | 78% | **36u**[b] |  | 80% |

[a]Reagents and conditions: (a) Ar−B(OH)$_2$, Pd(PPh$_3$)$_4$, K$_2$CO$_3$, dioxane/H$_2$O (4:1), 95 °C, 16 h. [b]Pinacol ester of boronic acid was used as reagent.

binding of the ATP's adenine ring rather than the phosphate moiety and therefore interfering with the course of the reaction.

The *N*-lobe is colored in orange, the C-lobe in cyan, and the helical domain and the $F_o - F_c$ map in green. In the detailed view, carbon atoms are colored silver, nitrogen in blue, chlorine in green, and oxygen in red.

**Docking Study of the Inhibitors.** We performed docking studies with selected inhibitors to determine putative parts of the inhibitor that could be further modified to enhance the affinity to the enzyme and to explain the results of our structure−activity relationship (SAR) study at the atomic level. The results of our docking study largely explain the outcomes of the SAR study.The conformation of **36t** with the lowest predicted energy fits into the enzyme's ATP binding site and forms three hydrogen bonds with Val$^{613}$ in the hinge region (Figure 4d). The amide oxygen of this residue forms two hydrogen bonds with both nitrogen moieties of side chain 1. The hydrogen atom bound to amide nitrogen of Val$^{613}$ interacts with nitrogen atom of the inhibitor's central bicyclic core, which facilitates effective interaction with the enzyme (Figure 4d). Two additional hydrogen bonds with residues Tyr$^{400}$ and Lys$^{564}$ are responsible for the effect of the sulfonamide moiety (the aromatic side chain) and importance of the amide oxygen atom (the amine side chain), respectively.

## DISCUSSION

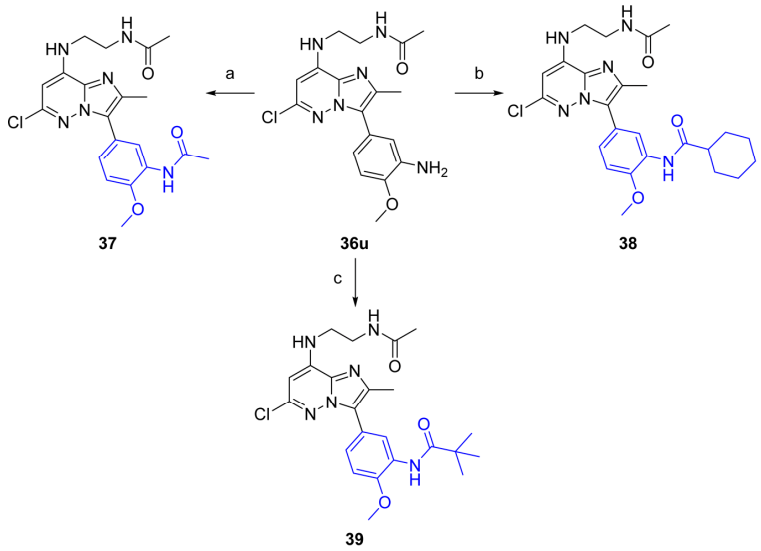
Selective inhibitors of PI4K III$\beta$ are critically needed as PI4K III$\beta$ is a promising target for development of broad-spectrum antiviral agents for treatment of diseases caused by viral pathogens such as SARS, MERS, HCV, and HRV. Furthermore, effective inhibitors of this class of enzymes can serve as much-needed tools to understand various processes connected with membrane signaling and mechanisms of membrane trafficking in numerous cellular structures. Therefore, such compounds can revolutionize the treatment of viral diseases and sharpen our knowledge of cell biology of organelles.

We show that substitution of all three moieties (amine side chains, bicyclic central core, and aromatic side chain) on the parent molecule has significant impact on the activity of this family of inhibitors (Figure 5). Our study suggests that for substitutions the most suitable side chains at position 1 (the amino side chain) are the 2-aminoethyl acetate and the 2-aminoethylacetamide groups. Because the ester substituent is most likely metabolically unstable, we focused our efforts on



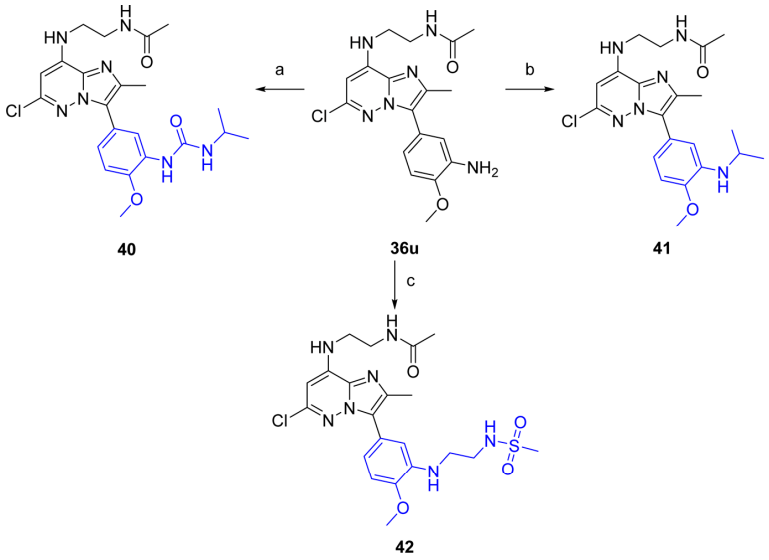
DOI: 10.1021/acs.jmedchem.5b00499
J. Med. Chem. 2015, 58, 3767−3793

**Scheme 9. Acylated Derivatives Preparation**[a]




[a]Reagents and conditions: (a) $Ac_2O$, DIPEA, $CH_2Cl_2$, 0 °C, 92%; (b) cyclohexanoyl chloride, DIPEA, $CH_2Cl_2$, 0 °C, 63%; (c) pivaloyl chloride, DIPEA, $CH_2Cl_2$, 0 °C, 48%.

**Scheme 10. Preparation of Derivatives with Substituted Aromatic Part of the Molecule**[a]



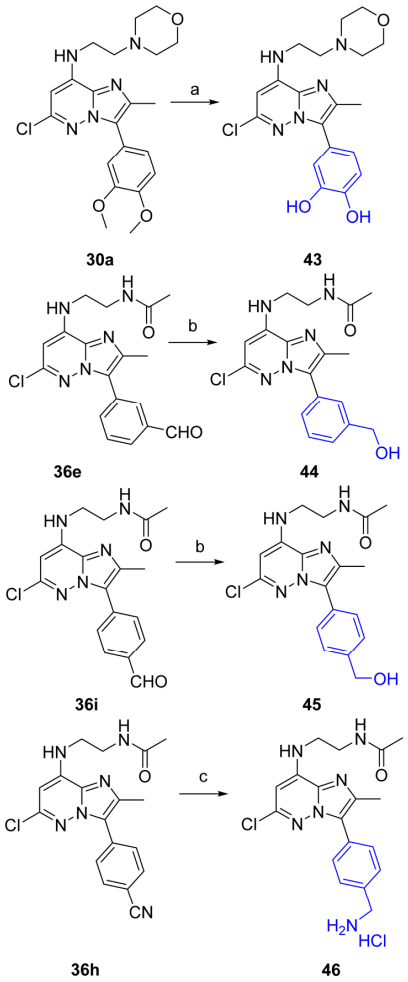

[a]Reagents and conditions: (a) acetone, $NaBH_3CN$, MeOH, 76%; (b) isopropylisocyanate, THF, 6 h, reflux, 86%; (c) *N*-(2-chloroethyl)-methanesulfonamide, $K_2CO_3$, toluene, 90 °C, 45%.

the amide and the central core of the molecule. These optimizations revealed two important factors: First, simple scaffold hopping significantly influences the activity, thus the derivatives with imidazo[1,2-*b*]pyridazine exert higher potency than the members of pyrazolo[1,5-*a*]pyrimidine series, whereas the compounds with other central cores possess lower affinity toward PI4K III*β*. Second, small variations of the substituent at position 6 of both imidazo[1,2-*b*]pyridazine and pyrazolo[1,5-*a*]pyrimidine core do not significantly affect the activity. Generally, hydrogen, methyl, and chlorine atoms were all tolerated, with only marginal differences in their inhibitory activities. We subsequently screened a large series of compounds, with aromatic side chain 2 modified to investigate the most suitably decorated arene moiety. Although derivatives with the dimethoxybenzene group were among the most potent inhibitors, the phenyl groups bearing a strong hydrogen bond acceptor, such as sulfonamide or aldehyde, at the meta position relative to the central core significantly contributed to the



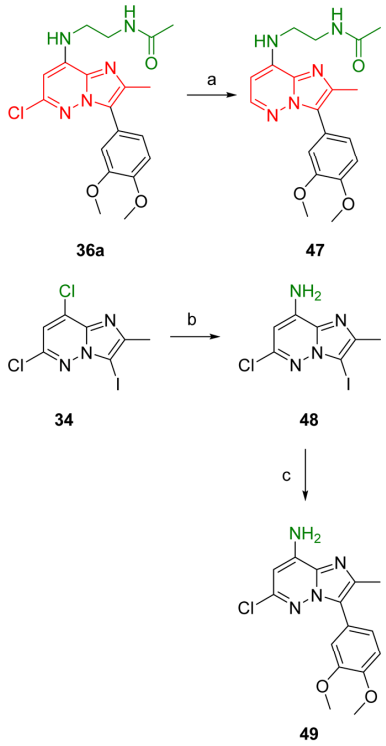
DOI: 10.1021/acs.jmedchem.5b00499
*J. Med. Chem.* 2015, 58, 3767−3793

Scheme 11. Modification of the Aromatic Side Chain[a]




[a]Reagents and conditions: (a) $BBr_3$, $CH_2Cl_2$, −78 °C to rt, overnight, 13%; (b) $NaBH_4$, MeOH/$CH_2Cl_2$, rt, 1 h, 30% for **33** and 40% for **34**; (c) (i) $H_2$ (3.5 bar), Raney-Ni, $NH_3$/EtOH, rt, overnight, (ii) HCl/$Et_2O$, $CH_2Cl_2$, 0 °C, 71%.

Scheme 12. Preparation of Derivatives 47 and 49[a]




[a]Reagents and conditions: (a) $H_2$ (5 bar), $Pd(OH)_2$/C, $Et_3N$, THF:MeOH (1:1), 63%; (b) $NH_3$/EtOH, MW, 140 °C, 1.5 h, 77%; (c) (3,4-dimethoxyphenyl)boronic acid, $Pd(PPh_3)_4$, 1 M $K_2CO_3$, dioxane, 90 °C, overnight, 80%.

enhanced affinity toward the enzyme. Using this approach, we identified a number of novel inhibitors of PI4K III$\beta$ with the most interesting compound being **36t** with $IC_{50}$ = 54 ± 15 nM. This compound displayed antiviral activity against members of both the *Picornaviridae* and the *Filoviridae* families, with activities being in the nanomolar level for CVB3 and HCV 1b and in micromolar level for HRVM and HCV 2a. The results in both enzymatic and antiviral cell-based assays showed the clear superiority over the starting hit T-00127-HEV1 (**2a**).

Very recently, the first crystal structure of PI4K III$\beta$ in complex with a nonselective lipid kinase inhibitor, PIK93 was solved by Burke et al.[6,44] Our extensive synthetic studies yielding a set of molecular tools now allowed us to solve the structure of PI4K III$\beta$ bound to a potent and selective molecule, namely compound **49**, which possesses a significantly different structure than PIK93. In addition, we were able to obtain a crystal structure with a bound ATP even though a significant part of the ATP molecule is disordered in the structure, probably because it would be stabilized by the catalytically important C-terminus of the enzyme, which impedes crystallization and thus is missing in the crystallized construct.[6] This crystal structure suggests the correct orientation and electrostatic interactions of the adenine moiety in the hinge region. The superposition of the structure with **49** and ATP clarifies the precise mode of action of this type of inhibitors. They compete with the natural binding site for ATP adenine ring, preventing the binding of ATP and hence inhibiting the lipid phosphorylation reaction. The crystal structures also suggest that the binding of the inhibitor causes conformational changes in the ATP binding site. In particular, residues $Glu^{572}$ and $Lys^{564}$ seem in closer proximity when binding ATP due to a weak electrostatic interaction. However, when the inhibitor **49** is bound, the $Lys^{564}$ residue adopts a conformation that allows for an effective hydrogen bond with one of the methoxy groups of the inhibitor's aromatic side chain. Our docking studies suggest that this interaction can be exploited for the design of inhibitors with significantly enhanced affinity toward the enzyme as demonstrated in the example of the most active compound, **36t**. In the case of compound **36t**, the lysine residue $Lys^{564}$ is significantly attracted by the strongly electronegative oxygen atom of the sulfonamide moiety. The docking studies support the importance of the amide side chain, which can significantly elevate the enthalpic contribution to the interaction of the



DOI: 10.1021/acs.jmedchem.5b00499
J. Med. Chem. 2015, 58, 3767−3793

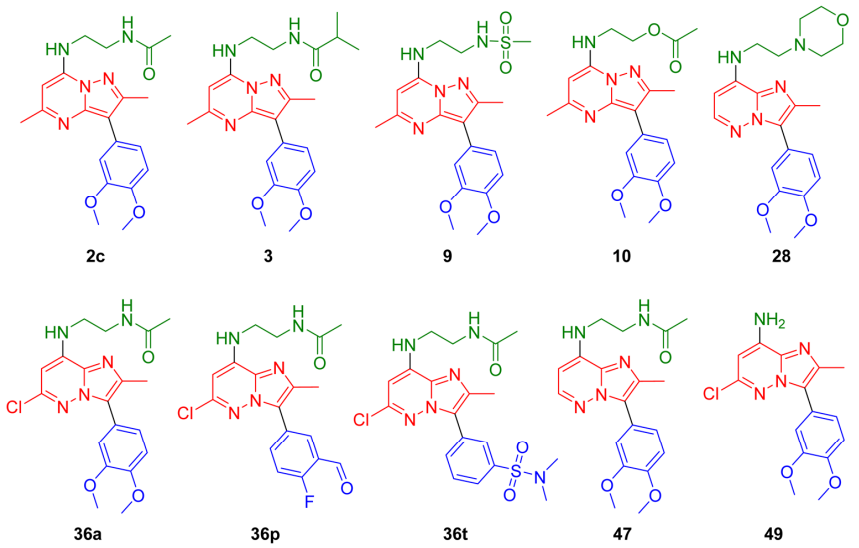



**Figure 2.** Structures of the selected subseries of inhibitors. The amine side chains are in green, bicyclic central core in red, and aromatic side chain in blue.

**Table 1. Inhibitory Activity of Selected Compounds against Members of PI4K Family**

| compd | PI4K IIIβ $IC_{50}$ (μM) | PI4K IIIα $IC_{50}$ (μM) | PI4K IIα $IC_{50}$ (μM) |
|---|---|---|---|
| **2c** | 0.070 ± 0.020 | 59.45 ± 0.06 | >100 |
| **3** | 0.120 ± 0.010 | 62.14 ± 0.84 | >100 |
| **9** | 0.120 ± 0.010 | 29.31 ± 0.96 | >100 |
| **10** | 0.067 ± 0.009 | 29.52 ± 3.40 | >100 |
| **28** | 0.093 ± 0.012 | 27.46 ± 2.47 | >100 |
| **36a** | 0.090 ± 0.011 | 82.67 ± 18.64 | >100 |
| **36p** | 0.089 ± 0.003 | >100 | >100 |
| **36t** | 0.054 ± 0.015 | >100 | >100 |
| **47** | 0.092 ± 0.006 | 33.67 ± 0.49 | >100 |
| **49** | 0.083 ± 0.025 | >100 | >100 |
| T-00127-HEV1[a] | 0.150 ± 0.010 | 74.55 ± 3.08 | ≥100 |

[a]References 24, 26.

enzyme and inhibitor. While we cannot explain the specificity of our compounds against PI4K IIIα on the structural level as the PI4K IIIα crystal structure is not available, we can explain why the prepared compounds do not inhibit PI4K IIα. The structural superposition of these two enzymes (Supporting Information, Figure 3) reveals that from the two most critical residues for inhibitor binding (K564 and E572) only the glutamate is conserved.

## CONCLUSION

In conclusion, we present highly potent inhibitors of PI4K IIIβ with excellent selectivity. The most active compound, **36t** ($IC_{50}$ = 54 nM), possesses outstanding selectivity against both the most homologous enzyme, PI4K IIIβ, and the nonhomologues enzyme, the PI4K IIα that catalyzes the same reaction. This compound has high potential as exquisite chemical biology tool for efficient studies of PI4Ks in cells and in animal models as well as an excellent starting point in the search for broad-spectrum antiviral agents against ss(+)RNA viruses and potential therapeutics of other human diseases. Through our crystallographic and computational studies, we revealed the molecular mechanism of the inhibitors and their disruption of

**Table 2. Antiviral Activity against Selected ss(+)RNA Viruses**

| compd | CVB3 $EC_{50}$ (μM) | HRVM $EC_{50}$ (μM) | HCV 1b $EC_{50}$ (μM) | HCV 2a $EC_{50}$ (μM) | HeLa $CC_{50}$ (μM) |
|---|---|---|---|---|---|
| **2c** | 1.23 ± 0.03 | 2.9 ± 0.1 | 1.03 ± 1.17 | >44 | >50 |
| **3** | 11.0 ± 0.1 | 1.62 ± 0.04 | 1.21 ± 0.22 | >44 | >50 |
| **9** | 1.43 ± 0.01 | 3.0 ± 0.1 | 0.91 ± 0.44 | 42.5 ± 0.5 | >50 |
| **10** | 0.86 ± 0.08 | 1.38 ± 0.05 | 0.96 ± 0.67 | >44 | >50 |
| **28** | 0.50 ± 0.07 | 0.88 ± 0.10 | 0.37 ± 0.06 | 17.9 ± 0.1 | >50 |
| **36a** | 0.75 ± 0.03 | 1.09 ± 0.14 | 0.29 ± 0.07 | 31.8 ± 0.2 | >50 |
| **36p** | >50 | 24.3 ± 0.1 | 5.3 ± 0.1 | 13.6 ± 0.1 | >50 |
| **36t** | 0.145 ± 0.034 | 1.03 ± 0.35 | 0.087 ± 0.067 | 10.6 ± 0.1 | >50 |
| **47** | 0.28 ± 0.04 | 2.9 ± 0.1 | 0.36 ± 0.09 | 27.9 ± 0.2 | >50 |
| **49** | 0.023 ± 0.004 | 0.89 ± 0.10 | 0.21 ± 0.09 | 26.5 ± 0.21 | 1.75 ± 0.17 |
| T-00127-HEV1[a] | 3.38 ± 0.05 | 2.5 ± 0.1 | 1.03 ± 0.12 | >44 | >50 |
| MK-0608[b] | ND | 5.1 ± 1.5 | 0.21 ± 0.07 | 0.21 ± 0.10 | >50 |

[a]References 24, 26. [b]7-Deaza-2′-C-methyladenosine (MK-0608), ref 36.



DOI: 10.1021/acs.jmedchem.5b00499
J. Med. Chem. 2015, 58, 3767−3793

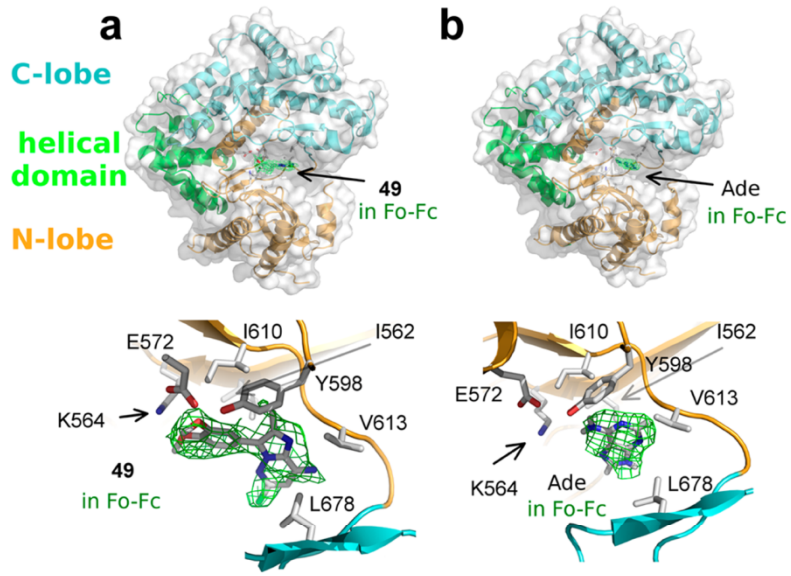



**Figure 3.** Crystal structures of **49** and ATP bound to PI4K III$\beta$. (a) Compound **49** in the unbiased $F_o - F_c$ map contoured at 2$\sigma$. Top: view on the whole enzyme. Bottom: detailed view of the binding pocket. (b) The adenine ring of the ATP in the unbiased $F_o - F_c$ map contoured at 2$\sigma$. Top: view on the whole enzyme. Bottom: detailed view of the binding pocket.

ATP binding. Finally, we explain the role of their structural features for interaction with PI4K III$\beta$.

## EXPERIMENTAL METHODS

**Synthesis of Novel Inhibitors.** *General Chemical Procedures.* Melting points were determined on a Büchi melting point B-540 apparatus. Microwave syntheses were carried out in a CEM Discover instrument with a single0-mode cavity and focused microwave heating (microwave power supply 0−300 W, 1 W increments, sealed vessel mode, pressure range 0−20 bar). NMR spectra were measured on a Bruker Avance II-600 and/or Bruker Avance II-500 instruments (600 or 500.0 MHz for $^1$H and 150 or 125 MHz for $^{13}$C) in hexadeuterodimethyl sulfoxide and referenced to the solvent signal ($\delta$ 2.50 and 39.70, respectively). Mass spectra were measured on a LTQ Orbitrap XL (Thermo Fischer Scientific) using electrospray ionization (ESI) and a GCT Premier (Waters) using EI. HPLC-MS spectra were obtained on a Shimadzu LCMS-2020 LC-MS. The elemental analyses (summarized in Supporting Information, Table 1) were obtained on a PerkinElmer CHN Analyzer 2400, series II Sys (PerkinElmer) and X-ray fluorescence spectrometer SPECTRO iQ II (SPECTRO Analytical Instruments, Germany). All of the compounds in the series had purity higher than 95% (determined either by elemental analysis or HPLC-MS). Column chromatography and thin-layer chromatography (TLC) were performed using Silica Gel 60 (Fluka) and Silufol Silica Gel 60 $F_{254}$ foils (Merck), respectively. Solvents were evaporated at 2 kPa and bath temperature 30−60 °C. The compounds were dried at 13 Pa and 50 °C.

*General Procedure for Introduction of the N-Substituent to Position 7.* Chloro derivative **1**[35] (150 mg, 0.47 mmol) was dissolved in ethanol (5 mL) and DIPEA (0.25 mL, 1.41 mmol) together with an appropriate amine (2 equiv). Reaction mixture was then stirred at 75 °C for 12 h (or until consumption of the starting material). Reaction mixture was then evaporated, and the residue was chromatographed (silica gel, 50 g) with an appropriate mobile phase and the solid was recrystallized.

*3-(3,4-Dimethoxyphenyl)-2,5-dimethyl-N-(2-morpholinoethyl)-pyrazolo[1,5-a]pyrimidin-7-amine (**2a**).* Mobile phase: ethyl acetate → ethyl acetate:toluene:acetone:ethanol (17:4:3:1). Crystallized from ethanol−water. Yield: 172 mg (89%); mp 170−170.5 °C. $^1$H NMR (500 MHz, $CDCl_3$) $\delta$ (ppm): 7.42 (d, $J_{2''-6''}$ = 2.0 Hz, 1H, H-2″), 7.23 (dd, $J_{6''-2''}$ = 2.0, $J_{6''-5''}$ = 8.3 Hz, 1H, H-6″), 6.96 (d, $J_{5''-6''}$ = 8.3 Hz, 1H, H-5″), 6.63 (t, $J_{NH-1'}$ = 5.0 Hz, 1H, NH), 5.78 (s, 1H, H-6), 3.95 (s, 3H, 3″-$OCH_3$), 3.91 (s, 3H, 4″-$OCH_3$), 3.78 (m, 4H, morph-$O(CH_2)_2$), 3.44 (q, $J_{1'-2'} = J_{1'-NH}$ = 5.7 Hz, 2H, H-1′), 2.75 (t, $J_{2'-1'}$ = 6.1 Hz, 2H, H-2′), 2.66 (s, 3H, 2-$CH_3$), 2.55 (m, 4H, morph-$N(CH_2)_2$), 2.50 (s, 3H, 5-$CH_3$). $^{13}$C NMR (125 MHz, $CDCl_3$) $\delta$ (ppm): 159.3 (C-5), 150.9 (C-2), 148.8 (C-3″), 147.2 (C-4″), 146.2 (C-3a), 145.7 (C-7), 126.1 (C-1″), 120.9 (C-6″), 112.4 (C-2″), 111.4 (C-5″), 107.0 (C-3), 85.3 (C-6), 66.9 (morph-$O(CH_2)_2$), 56.3 (C-2′), 55.9 (4″-$OCH_3$), 55.9 (3″-$OCH_3$), 53.3 (morph-$N(CH_2)_2$), 38.2 (C-1′), 25.3 (5-$CH_3$), 14.5 (2-$CH_3$). Anal. ($C_{22}H_{29}N_5O_3$) C, H, N. ESI MS, *m/z* (rel%): 412 (100) [M + H]. HRMS: calcd for [M + H], 412.23432; found, 412.23434.

*3-(3,4-Dimethoxyphenyl)-2,5-dimethyl-N-(3-morpholinopropyl)-pyrazolo[1,5-a]pyrimidin-7-amine (**2b**).* Mobile phase: ethyl acetate → ethyl acetate:toluene:acetone:ethanol (17:4:4:1). Crystallized from ethyl acetate. Yield 160 mg (80%); mp 105.5−116 °C. $^1$H NMR (500 MHz, $CDCl_3$) $\delta$ (ppm): 8.06 (t, $J_{NH-1'}$ = 4.6 Hz), 7.43 (d, $J_{2''-6''}$ = 1.9 Hz, 1H, H-2″), 7.23 (dd, $J_{6''-2''}$ = 1.9, $J_{6''-5''}$ = 8.2 Hz, 1H, H-6″), 6.96 (d, $J_{5''-6''}$ = 8.2 Hz, 1H, H-5″), 5.75 (s, 1H, H-6), 3.97−3.94 (m, 7H, 3″-$OCH_3$, morph-$O(CH_2)_2$), 3.91 (s, 3H, 4″-$OCH_3$), 3.49 (m, 2H, H-1′), 2.63−2.53 (m, 9H, H-3′, 2-$CH_3$, morph-$N(CH_2)_2$), 2.49 (s, 3H, 5-$CH_3$), 1.93 (pent, $J_{2'-1'} = J_{2'-3'}$ = 5.8 Hz, 2H, H-2′). $^{13}$C NMR (125 MHz, DMSO-$d_6$) $\delta$ (ppm): 159.3 (C-5), 150.7 (C-2), 148.8 (C-3′), 147.1 (C-4″), 146.2 (C-3a), 146.1 (C-7), 126.3 (C-1″), 120.9 (C-6″), 112.4 (C-2″), 111.4 (C-5″), 106.7 (C-3), 84.8 (C-6), 66.6 (morph-$O(CH_2)_2$), 58.0 (C-3′), 56.0 and 55.8 (4″-$OCH_3$ and 3″-$OCH_3$), 53.9 (morph-$N(CH_2)_2$), 42.3 (C-1′), 25.4 (5-$CH_3$), 24.0 (C-2′), 14.4 (2-$CH_3$). Anal. ($C_{23}H_{31}N_5O_3$) C, H, N. ESI MS, *m/z* (rel%): 426 (100) [M + H]. HRMS: calcd for [M + H], 426.24997; found, 426.24991.

*N-(2-((3-(3,4-Dimethoxyphenyl)-2,5-dimethylpyrazolo[1,5-a]-pyrimidin-7-yl)amino)ethyl)acetamide (**2c**).* Mobile phase: ethyl acetate → ethyl acetate:acetone:ethanol:$H_2O$ (20:3:1.2:0.8). Crystallized from ethyl acetate. Yield 156 mg (87%); mp 163−164 °C. $^1$H NMR (500 MHz, DMSO-$d_6$) $\delta$ (ppm): 8.06 (t, $J_{NH-2}$ = 5.6 Hz, 1H, NHCO), 7.76 (t, $J_{NH-1}$ = 6.2 Hz, 1H, 7′-NH), 7.41 (d, $J_{2''-6''}$ = 2.0 Hz, 1H, H-2″), 7.21 (dd, $J_{6''-2''}$ = 2.0, $J_{6''-5''}$ = 8.3 Hz, 1H, H-6″), 7.01 (d, $J_{5''-6''}$ = 8.3 Hz, 1H, H-5″), 6.08 (s, 1H, H-6′), 3.79 (s, 3H, 3″-$OCH_3$), 3.78 (s, 3H, 4″-$OCH_3$), 3.42 (m, 2H, H-1), 3.29 (m, 2H, H-2), 2.52 (s,



DOI: 10.1021/acs.jmedchem.5b00499
J. Med. Chem. 2015, 58, 3767−3793

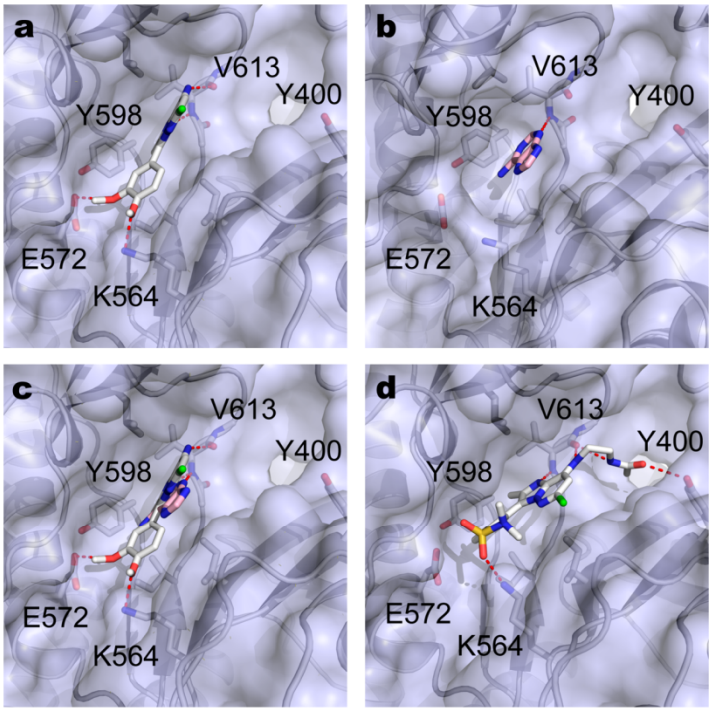



**Figure 4.** Structural insight into the inhibition of ATP approach to ATP binding site. (a) Compound **49** in the ATP binding site: the inhibitor appears to be strongly bound in the ATP binding site based on strong hydrogen bonds to amino acid residues Val$^{613}$, Lys$^{564}$, and Glu$^{572}$ and significant structural match with the binding canyon. (b) ATP bound to PI4K III$\beta$ (a detailed view into ATP binding site) residues Glu$^{572}$ and Lys$^{564}$ seem to be in close proximity, suggesting existence of electrostatic interaction between these two residues with opposite polarity; this conformation of the protein allows effective binding of the nucleobase due to extensive shape complementarity. (c) Superposition of ATP and **49** in the biding site, which clearly shows these two ligands occupy the same area of the enzyme and compete with each other at the ATP binding site. (d) Docking study of the most potent inhibitor in the study derivative **36t** fits nicely into the binding canyon of the enzyme, formed by numerous lipophilic residues. In particular, the aromatic side chain of the inhibitor stays in T-shape conformation to the Tyr$^{598}$, suggesting significant $\pi-\pi$ interaction. In comparison with the binding mode of **49**, compound **36t** seems to form a stronger hydrogen bond with Lys$^{564}$ and two additional hydrogen bonds with Val$^{613}$ and Tyr$^{400}$.

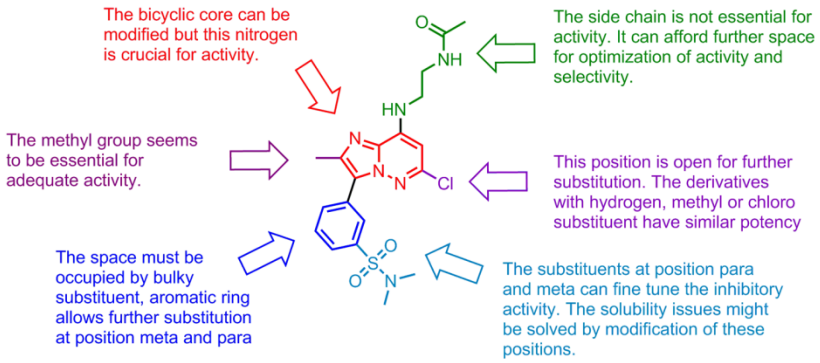



**Figure 5.** Schematic representation of the results of our SAR study.

3H, 2′-$CH_3$), 2.38 (s, 3H, 5′-$CH_3$), 1.80 (s, 3H, $COCH_3$). $^{13}$C NMR (125 MHz, DMSO-$d_6$) $\delta$ (ppm): 170.0 (CO), 158.8 (C-5′), 149.9 (C-2′), 148.7 (C-3″), 147.0 (C-4″), 146.1 and 146.2 (C-3a′ and C-7′), 126.3 (C-1″), 120.6 (C-6″), 112.7 (C-2″), 112.2 (C-5″), 105.6 (C-3′), 85.2 (C-6′), 55.8 and 55.7 (3″-$OCH_3$ and 4″-$OCH_3$), 41.1 (C-1), 38.2 (C-2), 25.1 (5′-$CH_3$), 22.8 ($COCH_3$), 14.7 (2′-$CH_3$). Anal. ($C_{20}H_{25}N_5O_3$·0.25$H_2O$) C, H, N. ESI MS, *m*/*z* (rel%): 384 (100) [M + H]. HRMS: calcd for [M + H], 384.20302; found, 384.20302.

*2-((3-(3,4-Dimethoxyphenyl)-2,5-dimethylpyrazolo[1,5-a]-pyrimidin-7-yl)amino)acetamide (**2d**).* Mobile phase: ethyl acetate → ethyl acetate:toluene:acetone:ethanol (17:4:4:1). Crystallized from ethyl acetate. Yield 137 mg (82%); mp 229.5−231 °C. $^1$H NMR (500 MHz, DMSO-$d_6$) $\delta$ (ppm): 7.67 (t, $J_{NH-CH_2}$ = 6.0 Hz), 7.57 (bs, 1H, $CONH_2$b), 7.41 (d, $J_{2'-6'}$ = 2.0 Hz, 1H, H-2′), 7.25 (bs, 1H, $CONH_2$a), 7.23 (dd, $J_{6'-2'}$ = 2.0, $J_{6'-5'}$ = 8.3 Hz, 1H, H-6′), 7.01 (d, $J_{5'-6'}$ = 8.3 Hz, 1H, H-5′), 5.88 (s, 1H, C-6), 3.96 (d, $J_{CH_2-NH}$ = 6.0 Hz,


DOI: 10.1021/acs.jmedchem.5b00499
J. Med. Chem. 2015, 58, 3767−3793

2H, $CH_2CO$), 3.79 (s, 3H, 3′-$OCH_3$), 3.78 (s, 3H, 4′-$OCH_3$), 2.53 (s, 3H, 2-$CH_3$), 2.38 (s, 3H, 5-$CH_3$). $^{13}C$ NMR (125 MHz, DMSO-$d_6$) $\delta$ (ppm): 170.0 ($CONH_2$), 158.8 (C-5), 150.0 (C-2), 148.7 (C-3′), 147.0 (C-4′), 146.2 (C-7), 146.0 (C-3a), 126.2 (C-1′), 120.6 (C-6′), 112.7 (C-2′), 112.2 (C-5′), 105.6 (C-3), 85.6 (C-6), 55.7 and 55.8 (3′-$OCH_3$ and 4′-$OCH_3$), 44.1 ($NHCH_2$), 25.1 (5-$CH_3$), 14.7 (2-$CH_3$). Anal. ($C_{18}H_{21}N_5O_3 \cdot 0.33H_2O$) C, H, N. ESI MS, $m/z$ (rel%): 356 (100) [M + H]. HRMS: calcd for [M + H], 356.17172; found, 356.17176.

*3-(3,4-Dimethoxyphenyl)-2,5-dimethyl-N-(4-morpholinophenyl)-pyrazolo[1,5-a]pyrimidin-7-amine (2e).* After 12 h, the same amount of the reagents was added and heating continued for another 12 h. Reaction mixture was cooled down, and product started to crystallize. Yield 140 mg (65%); mp 175.5−176 °C. $^1H$ NMR (500 MHz, $CDCl_3$) $\delta$ (ppm): 7.79 (bs, 1H, NH), 7.42 (d, $J_{2''-6''}$ = 2.0 Hz, 1H, H-2″), 7.28 (d, $J_{2'-3'}$ = 8.9 Hz, 2H, H-2′), 7.24 (dd, $J_{6''-2''}$ = 2.0, $J_{6''-5''}$ = 8.3 Hz, 1H, H-6″), 6.98 (d, $J_{3'-2'}$ = 8.9 Hz, 2H, H-3′), 6.97 (d, $J_{5''-6''}$ = 8.3 Hz, 1H, H-5″), 6.01 (s, 1H, H-6), 3.95 (s, 3H, 3″-$OCH_3$), 3.92 (s, 3H, 4″-$OCH_3$), 3.89 (m, 4H, morph-O($CH_2$)$_2$), 3.21 (m, 4H, morph-N($CH_2$)$_2$), 2.62 (s, 3H, 2-$CH_3$), 2.45 (s, 3H, 5-$CH_3$). $^{13}C$ NMR (125 MHz, $CDCl_3$) $\delta$ (ppm): 159.6 (C-5), 151.0 (C-2), 149.8 (C-4′), 148.9 (C-3″), 147.3 (C-4″), 146.3 (C-3a), 144.7 (C-7), 128.4 (C-1′), 125.9 (C-1″), 125.8 (C-2′), 121.0 (C-6″), 116.4 (C-3′), 112.5 (C-2″), 111.5 (C-5″), 107.4 (C-3), 86.4 (C-6), 66.8 (morph-O($CH_2$)$_2$), 56.0 and 55.9 (3″-$OCH_3$ and 4″-$OCH_3$), 49.2 (morph-N($CH_2$)$_2$), 25.4 (5-$CH_3$), 14.4 (2-$CH_3$). Anal. ($C_{26}H_{29}N_5O_3$) C, H, N. ESI MS, $m/z$ (rel %): 460 (100) [M + H]. HRMS: calcd for [M + H], 460.23432; found, 460.23434.

*2-((3-(3,4-Dimethoxyphenyl)-2,5-dimethylpyrazolo[1,5-a]-pyrimidin-7-yl)amino)ethanol (2f).* Mobile phase: ethyl acetate. Crystallized from ethyl acetate. Yield 142 mg (88%); mp 183.5−184 °C. $^1H$ NMR (600 MHz, DMSO-$d_6$) $\delta$ (ppm): 7.48 (t, $J_{NH-2}$ = 6.1 Hz, 1H, NH), 7.42 (d, $J_{2''-6''}$ = 2.0 Hz, 1H, H-2″), 7.22 (dd, $J_{6''-2''}$ = 2.0, $J_{6''-5''}$ = 8.3 Hz, 1H, H-6″), 7.00 (d, $J_{5''-6''}$ = 8.3 Hz, 1H, H-5″), 6.09 (s, 1H, H-6′), 4.90 (t, $J_{OH-1}$ = 5.5 Hz, 1H, 1-OH), 3.79 (s, 3H, 3′-$OCH_3$), 3.78 (s, 3H, 4″-$OCH_3$), 3.64 (m, 2H, H-1), 3.42 (m, 2H, H-2), 2.52 (s, 3H, 2′-$CH_3$), 2.39 (s, 3H, 5′-$CH_3$). $^{13}C$ NMR (150 MHz, DMSO-$d_6$) $\delta$ (ppm): 158.8 (C-5′), 149.9 (C-2′), 148.6 (C-3″), 146.9 (C-4″), 146.2 (C-7′), 146.0 (C-3′a), 126.3 (C-1″), 120.6 (C-6″), 112.6 (C-2″), 112.2 (C-5″), 105.5 (C-3′), 85.4 (C-6′), 59.5 (C-1), 55.7 and 55.8 (3″-$OCH_3$ and 4″-$OCH_3$), 44.0 (C-2), 25.1 (5′-$CH_3$), 14.7 (2′-$CH_3$). Anal. ($C_{18}H_{22}N_4O_3$) C, H, N. ESI MS, $m/z$ (rel%): 343 (100) [M + H]. HRMS: calcd for [M + H], 343.17647; found, 343.17654.

*4-(3-(3,4-Dimethoxyphenyl)-2,5-dimethylpyrazolo[1,5-a]-pyrimidin-7-yl)morpholine (2g).* Mobile phase: toluene: ethyl acetate 11:9. Crystallized from ethyl acetate. Yield 130 mg (75%); mp 170.5−171 °C. $^1H$ NMR (500 MHz, $CDCl_3$) $\delta$ (ppm): 7.38 (d, $J_{2'-6'}$ = 2.0 Hz, 1H, H-2′), 7.22 (dd, $J_{6'\ 2'}$ = 2.0, $J_{6'\ 5'}$ = 8.3 Hz, 1H, H-6′), 6.97 (d, $J_{5'-6'}$ = 8.3 Hz, 1H, H-5′), 5.97 (s, 1H, H-6), 3.99 (m, 4H, morph-O($CH_2$)$_2$), 3.94 (s, 3H, 3′-$OCH_3$), 3.92 (s, 3H, 4′-$OCH_3$), 3.71 (m, 4H, morph-N($CH_2$)$_2$), 2.59 (s, 3H, 2-$CH_3$), 2.53 (s, 3H, 5-$CH_3$). $^{13}C$ NMR (125 MHz, $CDCl_3$) $\delta$ (ppm): 159.1 (C-5), 151.1 (C-2), 149.7 (C-7), 148.8 (C-3′), 147.4 (C-4′), 125.7 (C-1′), 121.2 (C-6′), 112.6 (C-2′), 111.4 (C-5′), 107.2 (C-3), 93.0 (C-6), 66.3 (morph-O($CH_2$)$_2$), 55.9 and 56.0 (3′-$OCH_3$ and 4′-$OCH_3$), 48.4 (morph-N($CH_2$)$_2$), 25.1 (5-$CH_3$), 14.5 (2-$CH_3$), C-3a was not detected. Anal. ($C_{20}H_{24}N_4O_3$) C, H, N. ESI MS, $m/z$ (rel%): 369 (100) [M + H]. HRMS: calcd for [M + H], 369.19212; found, 369.19215.

*7-(4-Benzhydrylpiperazin-1-yl)-3-(3,4-dimethoxyphenyl)-2,5-dimethylpyrazolo[1,5-a]pyrimidine (2h).* Mobile phase: toluene:ethyl acetate 4:1. Crystallized from ethyl acetate. Yield 193 mg (77%). $^1H$ NMR (500 MHz, $CDCl_3$) $\delta$ (ppm): 7.48−7.45 (m, 4H, Ph-*o*), 7.38 (d, $J_{2'-6'}$ = 2.1 Hz, 1H, H-2′), 7.32−7.28 (m, 4H, Ph-*m*), 7.22−7.19 (m, 2H, Ph-*p*), 7.20 (dd, $J_{6'-2'}$ = 2.1, $J_{6'-5'}$ = 8.3 Hz, 1H, H-6′), 6.95 (d, $J_{5'-6'}$ = 8.3 Hz, 1H, H-5′), 5.94 (s, 1H, H-6), 4.34 (s, 1H, CHPh$_2$), 3.93 (s, 3H, 3′-$OCH_3$), 3.91 (s, 3H, 4′-$OCH_3$), 3.73 (m, 4H, H-1″), 2.68 (t, $J_{2''-1''}$ = 4.7 Hz, 4H, H-2″), 2.59 (s, 3H, 2-$CH_3$), 2.53 (s, 3H, 5-$CH_3$). $^{13}C$ NMR (125 MHz, $CDCl_3$) $\delta$ (ppm): 158.9 (C-5), 150.8 (C-2), 149.8 (C-7), 148.8 (C-3′), 147.9 (C-3a), 147.3 (C-4′), 142.3 (Ph-*i*), 128.6 (Ph-*m*), 127.9 (Ph-*o*), 127.1 (Ph-*p*), 125.9 (C-1′), 121.1 (C-6′), 112.5 (C-2′), 111.4 (C-5′), 106.9 (C-3), 93.1 (C-6), 76.2 (CHPh$_2$), 55.8 and 56.0 (3′-$OCH_3$ and 4′-$OCH_3$), 51.2 (C-2″), 48.3 (C-1″), 25.2 (5-$CH_3$), 14.5 (2-$CH_3$). Anal. ($C_{20}H_{24}N_4O_3 \cdot 0.33EtOAc$) C, H, N. ESI MS, $m/z$ (rel%): 534 (100) [M + H]. HRMS: calcd for [M + H], 534.28635; found, 534.28633.

*3-(3,4-Dimethoxyphenyl)-2,5-dimethylpyrazolo[1,5-a]pyrimidin-7-amine (2i).* Chloro derivative **1** (260 mg, 0.82 mmol) was dissolved in ethanolic ammonia (3.5 M, 5.5 mL) and heated in microwave reactor at 120 °C for 1 h. Reaction mixture was evaporated and chromatographed on silica gel column (75 g) in ethyl acetate:toluene (7:3). Solid was crystallized from ethyl acetate, affording the product **2i**. Yield 181 mg (74%); mp 192−194 °C. $^1H$ NMR (500 MHz, $CDCl_3$) $\delta$ (ppm): 7.39 (d, $J_{2'-6'}$ = 2.0 Hz, 1H, H-2′), 7.22 (dd, $J_{6'-2'}$ = 2.0 Hz, $J_{6'-5'}$ = 8.3 Hz, 1H, H-6′), 6.96 (d, $J_{5'-6'}$ = 8.3 Hz, 1H, H-5′), 5.88 (s, 1H, H-6), 5.63 (s, 2H, $NH_2$), 3.94 (s, 3H, 3′-$OCH_3$), 3.90 (s, 3H, 4′-$OCH_3$), 2.59 (s, 3H, 2-$CH_3$), 2.47 (s, 3H, 5-$CH_3$). $^{13}C$ NMR (125 MHz, $CDCl_3$) $\delta$ (ppm): 159.4 (C-5), 151.4 (C-2), 148.8 (C-3′), 147.2 (C-4′), 146.4 (C-3a), 145.6 (C-7), 125.9 (C-1′), 121.0 (C-6′), 112.4 (C-2′), 111.4 (C-5′), 106.9 (C-3), 88.2 (C-6), 55.9 (4′-$OCH_3$), 55.8 (3′-$OCH_3$), 25.0 (5-$CH_3$), 14.4 (2-$CH_3$). Anal. ($C_{16}H_{18}N_4O_2$) C, H, N. ESI MS, $m/z$ (rel%): 299 (100) [M + H]. HRMS: calcd for [M + H], 299.15025; found, 299.15045.

*N1-(3-(3,4-Dimethoxyphenyl)-2,5-dimethylpyrazolo[1,5-a]-pyrimidin-7-yl)ethane-1,2-diamine (2j).* Chloro derivative **1** (1.81 g, 5.7 mmol) was dissolved in ethanol (100 mL), and ethane-1,2-diamine (7.6 mL, 114 mmol) was added and reaction mixture was heated to 75 °C for 1.5 h and evaporated. Residue was chromatographed (silica gel, 250 g) in ethyl acetate:acetone:ethanol:water (17:3:3:2) + 1% $Et_3N$ to give off the oily product **2j**. Solid powder was obtained after a sonication with ethyl acetate.Yield 1.77 g (91%); mp 183.5−184 °C. $^1H$ NMR (500 MHz, DMSO-$d_6$) $\delta$ (ppm): 7.86 (m, 1H, 7-NH), 7.41 (d, $J_{2''-6''}$ = 1.9 Hz, 1H, H-2″), 7.22 (dd, $J_{6''-2''}$ = 1.9, $J_{6''-5''}$ = 8.3 Hz, 1H, H-6″), 7.01 (d, $J_{5''-6''}$ = 8.3 Hz, 1H, H-5″), 6.27 (s, 1H, C-6′), 3.79 (s, 3H, 3″-$OCH_3$), 3.78 (s, 3H, 4″-$OCH_3$), 3.66 (m, 2H, H-1), 3.04 (t, 2H, $J_{2-1}$ = 6.3 Hz, H-2), 2.53 (s, 3H, 2-$CH_3$), 2.40 (s, 3H, 5-$CH_3$). $^{13}C$ NMR (125 MHz, DMSO-$d_6$) $\delta$ (ppm): 159.0 (C-5′), 149.9 (C-2′), 148.7 (C-3″), 147.0 (C-4″), 146.1 and 146.1 (C-3a′and C-7′), 126.2 (C-1″), 120.6 (C-1″), 112.7 (C-2″), 112.2 (C-5″), 105.6 (C-3′), 85.6 (C-6′), 55.7 and 55.8 (3′-$OCH_3$ and 4′-$OCH_3$), 39.3 (C-1), 38.1 (C-2), 25.1 (5-$CH_3$), 14.7 (2-$CH_3$). Anal. ($C_{18}H_{23}N_5O_2$) C, H, N. ESI MS, $m/z$ (rel%): 342 (100) [M + H]. HRMS: calcd for [M + H], 342.19245; found, 342.19271.

*N1-(3-(3,4-Dimethoxyphenyl)-2,5-dimethylpyrazolo[1,5-a]-pyrimidin-7-yl)propane-1,3-diamine (2k).* Chloro derivative **1** (267 mg, 0.84 mmol) was dissolved in ethanol (20 mL) and propane-1,3-diamine (1.4 mL, 16.8 mmol) was added, and reaction mixture was heated to 75 °C for 1.5 h and evaporated. Residue was chromatographed (silica gel, 75 g) in ethyl acetate:acetone:ethanol:water (17:3:3:2) + 1% $Et_3N$ to give **2k** as an oily product. Solid powder was obtained after sonication with ethyl acetate. Yield: 275 mg (92%); mp 200−204 °C. $^1H$ NMR (500 MHz, DMSO-$d_6$) $\delta$ (ppm): 7.89 (bs, 1H, 7-NH), 7.41 (d, $J_{2''-6''}$ = 2.0 Hz, 1H, H-2″), 7.21 (dd, $J_{6''-2''}$ = 2.0, $J_{6''-5''}$ = 8.3 Hz, 1H, H-6″), 7.01 (d, $J_{5''-6''}$ = 8.3 Hz, 1H, H-5″), 6.15 (s, 1H, C-6′), 3.79 (s, 3H, 3″-$OCH_3$), 3.78 (s, 3H, 4″-$OCH_3$), 3.47 (m, 2H, H-1), 2.85 (m, 2H, H-3), 2.52 (s, 3H, 2-$CH_3$), 2.39 (s, 3H, 5-$CH_3$), 1.92 (m, 2H, H-2). $^{13}C$ NMR (125 MHz, DMSO-$d_6$) $\delta$ (ppm): 158.9 (C-5′), 149.9 (C-2′), 148.6 (C-3″), 146.9 (C-4″), 146.1 (C-3a′), 145.9 (C-7′), 126.6 (C-1″), 120.6 (C-6″), 112.7 (C-2″), 112.2 (C-5″), 105.6 (C-3′), 85.4 (C-6′), 55.7 and 55.8 (3″-$OCH_3$ and 4″-$OCH_3$), 38.4 (C-1), 36.8 (C-3), 26.8 (C-2), 25.1 (5-$CH_3$), 14.7 (2-$CH_3$). Anal. ($C_{19}H_{25}N_5O_2$) C, H, N. ESI MS, $m/z$ (rel%): 356 (100) [M + H]. HRMS: calcd for [M + H], 356.20810; found, 356.20812.

*1-(4-(3-(3,4-Dimethoxyphenyl)-2,5-dimethylpyrazolo[1,5-a]-pyrimidin-7-yl)piperazin-1-yl)ethanone (2l).* Chloro derivative **1** (303 mg, 0.95 mmol) was dissolved in DMF (10 mL), and piperazine (822 mg, 9.5 mmol) was added. Reaction mixture was stirred at rt for 3 h and evaporated. Residue was coevaporated with DMF (3 × 20 mL) and then dissolved in chloroform (70 mL). Organic phase was washed with water (30 mL), and the water phase was re-extracted with chloroform (70 mL). Combined organic phases were dried ($Na_2SO_4$)



DOI: 10.1021/acs.jmedchem.5b00499
J. Med. Chem. 2015, 58, 3767−3793

and evaporated. Crude intermediate was immediately used in the following step. The intermediate was dissolved in $CH_2Cl_2$ (13 mL) and $Et_3N$ (0.4 mL, 2.9 mmol) at 0 °C. Then acetic anhydride (180 μL, 1.9 mmol) and reaction mixture was stirred at 0 °C for 3 h. Reaction was poured into satd aq solution of $NaHCO_3$ (35 mL), and the mixture was extracted with chloroform (2 × 70 mL). The organic phase was dried ($Na_2SO_4$) and evaporated. Chromatography of the residue on silica gel column (75 g) with ethyl acetate → ethyl acetate:toluene:acetone:ethanol (17:4:3:1) afforded the product **2l**. The solid was recrystallized from ethyl acetate. Yield: 348 mg (90%); mp 186.5−187 °C. $^1$H NMR (400 MHz, DMSO-$d_6$) $\delta$ (ppm): 7.37 (d, $J_{2''-6''}$ = 1.8 Hz, 1H, H-2″), 7.20 (dd, $J_{6''-2''}$ = 1.8, $J_{6''-5''}$ = 8.3 Hz, 1H, H-6″), 7.02 (d, $J_{5''-6''}$ = 8.3 Hz, 1H, H-5″), 6.29 (s, 1H, H-6′), 3.79 (s, 3H, 3″-$OCH_3$), 3.78 (s, 3H, 4″-$OCH_3$), 3.77 (m, 2H, H-1a), 3.68−3.63 (m, 6H, H-1b, H-2), 2.52 (s, 3H, 2′-$CH_3$), 2.44 (s, 3H, 5′-$CH_3$), 2.07 (s, 3H, $COCH_3$). $^{13}$C NMR (100 MHz, $CDCl_3$) $\delta$ (ppm): 168.7 (CO), 158.9 (C-5′), 149.9 (C-2′), 148.9 (C-7′), 148.6 (C-3″), 147.5 (C-3a), 147.2 (C-4″), 125.7 (C-1″), 120.9 (C-6″), 112.9 (C-2″), 111.1 (C-5″), 106.0 (C-3), 93.6 (C-6′), 55.7 and 55.8 (3′-$OCH_3$ and 4′-$OCH_3$), 47.6 and 47.8 (2 × C-1), 40.4 and 45.2 (2 × C-2), 24.8 (5′-$CH_3$), 21.4 ($COCH_3$), 14.7 (2′-$CH_3$). Anal. ($C_{22}H_{27}N_5O_3$) C, H, N. ESI MS, $m/z$ (rel%): 432 (100) [M + Na]. HRMS: calcd for [M + H], 410.21867; found, 410.21875.

*N-(2-((3-(3,4-Dimethoxyphenyl)-2,5-dimethylpyrazolo[1,5-a]-pyrimidin-7-yl)amino)ethyl)isobutyramide (3).* Compound **2j** (288 mg, 0.84 mmol) was dissolved in $CH_2Cl_2$ (25 mL), and isobutyric acid (86 μL, 0.92 mmol) was added. The reaction mixture was cooled down to 0 °C, and DCC (209 mg, 1 mmol) was added in one portion. Reaction mixture was slowly allowed to warm to rt and then stirred for 20 h. Precipitated solid was filtered off, and the filtrate was evaporated. Residue was chromatographed on a silica gel column (100 g) with ethyl acetate → ethyl acetate:toluene:acetone:ethanol (17:4:4:1) to obtain product **3**, which was recrystallized from MeOH−$Et_2O$ in a freezer. Yield: 266 mg (74%); mp 135−136 °C. $^1$H NMR (500 MHz, $CDCl_3$) $\delta$ (ppm): 7.40 (d, $J_{2''-6''}$ = 2.0 Hz, 1H, H-2″), 7.22 (dd, $J_{6''-2''}$ = 2.0, $J_{6''-5''}$ = 8.3 Hz, 1H, H-6″), 6.96 (d, $J_{5''-6''}$ = 8.3 Hz, 1H, H-5″), 6.39 (m, 1H, 7′-NH), 5.95 (m, 1H, NHCO), 5.87 (s, 1H, H-6′), 3.94 (s, 3H, 3″-$OCH_3$), 3.91 (s, 3H, 4″-$OCH_3$), 3.57−3.55 (m, 4H, H-1, H-2), 2.57 (s, 3H, 2′-$CH_3$), 2.49 (s, 3H, 5′-$CH_3$), 2.35 (sept, $J_{CH(CH_3)_2\text{-}CH_3}$ = 6.9 Hz, 1H, C**H**$(CH_3)_2$), 1.15 (d, $J_{CH_3-CH(CH_3)_2}$ = 6.9 Hz, 6H, CH(C**H**$_3)_2$). $^{13}$C NMR (125 MHz, $CDCl_3$) $\delta$ (ppm): 177.8 (CO), 159.5 (C-5′), 150.9 (C-2′), 148.8 (C-3″), 147.2 (C-4″), 146.1 (C-3′a), 145.8 (C-7′), 125.9 (C-1″), 120.9 (C-6″), 112.4 (C-2″), 111.4 (C-5″), 107.1 (C-3′), 85.2 (C-6′), 55.8 and 55.9 (3″-$OCH_3$ and 4″-$OCH_3$), 41.5 (C-1), 39.0 (C-2), 35.5 (**C**H$(CH_3)_2$), 25.4 (5′-$CH_3$), 19.5 (CH(C**H**$_3)_2$), 14.4 (2′-$CH_3$). Anal. ($C_{22}H_{29}N_5O_3$) C, H, N. ESI MS, $m/z$ (rel%): 412 (100) [M + H]. HRMS: calcd for [M + H], 412.23432; found, 412.23448.

*N-(2-((3-(3,4-Dimethoxyphenyl)-2,5-dimethylpyrazolo[1,5-a]-pyrimidin-7-yl)amino)ethyl)cyclohexanecarboxamide (4).* To a solution of compound **2j** (257 mg, 0.75 mmol) in $CH_2Cl_2$ (10 mL) and $Et_3N$ (137 μL, 0.98 mmol) at 0 °C was added cyclohexanecarboxylic acid chloride (131 μL, 0.98 mmol), and the reaction mixture was stirred at 0 °C for 2 h. The reaction mixture was poured into a satd aq solution of $NaHCO_3$ (35 mL) and extracted with chloroform (70 mL). The organic phase was dried ($Na_2SO_4$) and evaporated. Chromatography of the residue on a silica gel column (75 g) with ethyl acetate afforded the product **4**. Solid was recrystallized from ethyl acetate. Yield 244 mg (72%); mp 135.5−136 °C. $^1$H NMR (400 MHz, DMSO-$d_6$) $\delta$ (ppm): 7.89 (t, $J_{NH\text{-}1'}$ = 5.3 Hz, 1H, NHCO), 7.75 (t, $J_{NH\text{-}2'}$ = 6.0 Hz, 1H, 7″-NH), 7.41 (d, $J_{2'''-6'''}$ = 1.4 Hz, 1H, H-2‴), 7.22 (dd, $J_{6'''-2'''}$ = 1.4, $J_{6'''-5'''}$ = 8.2 Hz, 1H, H-6‴), 7.01 (d, $J_{5'''-6'''}$ = 8.2 Hz, 1H, H-5‴), 6.07 (s, 1H, H-6″), 3.79 (s, 3H, 3‴-$OCH_3$), 3.78 (s, 3H, 4‴-$OCH_3$), 3.41 (m, 2H, H-2′), 3.29 (m, 2H, H-1′), 2.52 (s, 3H, 2″-$CH_3$), 2.38 (s, 3H, 5″-$CH_3$), 2.04 (m, 1H, H-1), 1.71−1.63 (m, 4H, H-2a, H-3a), 1.59 (m, 1H, H-4a), 1.30 (m, 2H, H-2b), 1.24−1.09 (m, 3H, H-3b, H-4b). $^{13}$C NMR (100 MHz, $CDCl_3$) $\delta$ (ppm): 175.8 (CO), 158.7 (C-5″), 149.8 (C-2″), 148.6 (C-3‴), 146.9 (C-4‴), 146.3 (C-7″), 146.1 (C-3″a), 126.3 (C-1‴), 120.6 (C-6‴), 112.7 (C-2‴), 112.2 (C-5‴), 105.5 (C-3″), 85.3 (C-6″), 55.7 and 55.7 (3‴-$OCH_3$ and 4‴-$OCH_3$), 41.1 (C-2′), 38.2 (C-1′), 29.3 (C-2), 25.7 (C-4), 25.5 (C-3), 25.1 (5″-$CH_3$), 14.6 (2″-$CH_3$). Anal. ($C_{25}H_{33}N_5O_3$) C, H, N. ESI MS, $m/z$ (rel%): 452 (100) [M + H]. HRMS: calcd for [M + H], 452.26562; found, 452.26566.

*N-(2-((3-(3,4-Dimethoxyphenyl)-2,5-dimethylpyrazolo[1,5-a]-pyrimidin-7-yl)amino)ethyl)-2-phenylpropanamide (5).* Compound **2j** (248 mg, 0.73 mmol) was dissolved in $CH_2Cl_2$ (15 mL), and 2-phenylpropanoic acid (100 μL, 0.80 mmol) was added. The reaction mixture was cooled down to 0 °C, and DCC (181 mg, 0.88 mmol) was added in one portion. The reaction mixture was slowly allowed to warm to rt and then stirred for 20 h. Precipitated solid was filtered, and filtrate was evaporated. Residue was chromatographed on silica gel column (100 g) with ethyl acetate:toluene (10:1) to obtain the product **5**, which was recrystallized from ethyl acetate. Yield: 280 mg (81%); mp 154−155 °C. $^1$H NMR (500 MHz, $CDCl_3$) $\delta$ (ppm): 7.42 (d, $J_{2'''-6'''}$ = 2.0 Hz, 1H, H-2‴), 7.29−7.21 (m, 6H, H-6‴, Ph-*o*, Ph-*m*, Ph-*p*), 6.96 (d, $J_{5'''-6'''}$ = 8.4 Hz, 1H, H-5‴), 6.28 (t, $J_{NH\text{-}1'}$ = 5.8 Hz, 7′-NH), 5.83 (s, 1H, H-6″), 5.75 (m, 1H, NHCO), 3.95 (s, 3H, 3‴-$OCH_3$), 3.92 (s, 3H, 4‴-$OCH_3$), 3.55 (q, $J_{COCH\text{-}CH_3}$ = 7.2 Hz, 1H, COC**H**), 3.52−3.49 (m, 4H, H-1′, H-2′), 2.58 (s, 3H, 2″-$CH_3$), 2.49 (s, 3H, 5″-$CH_3$), 1.53 (d, $J_{CH_3\text{-}COCH}$ = 7.2 Hz, 3H, $CH_3$). $^{13}$C NMR (125 MHz, $CDCl_3$) $\delta$ (ppm): 175.1 (CO), 159.5 (C-5″), 150.8 (C-2″), 148.8 (C-3‴), 147.3 (C-4‴), 146.1 (C-3″a), 145.7 (C-7″), 140.9 (Ph-*i*), 128.9 (Ph-*m*), 127.5 (ph-*o*), 127.4 (Ph-*p*), 126.0 (C-1‴), 120.9 (C-6‴), 112.4 (C-2‴), 111.5 (C-5‴), 107.1 (C-3″), 85.1 (C-6″), 56 and 55.8 (3‴-$OCH_3$ and 4‴-$OCH_3$), 47.0 ($COCHCH_3$), 41.3 (C-1′), 39.1 (C-2′), 25.4 (5″-$CH_3$), 18.4 ($CH_3$), 14.4 (2″-$CH_3$). Anal. ($C_{27}H_{31}N_5O_3$) C, H, N. ESI MS, $m/z$ (rel%): 474 (100) [M + H]. HRMS: calcd for [M + H], 474.24997; found, 474.25006.

*1-(2-((3-(3,4-Dimethoxyphenyl)-2,5-dimethylpyrazolo[1,5-a]-pyrimidin-7-yl)amino)ethyl)urea (6).* Starting material **2j** (255 mg, 0.75 mmol) was dissolved in a mixture of methanol (1.5 mL) and aq HCl (3.6 mL, 1 M). The reaction mixture was stirred at rt, and a solution of the KCNO (91 mg, 1.13 mmol) in water (2 mL) was added dropwise. After 2 h at rt, the reaction mixture was heated to 50 °C for 20 h. A second portion of KCNO (200 mg, solid) was added, and heating (50 °C) continued for another 20 h. Reaction mixture was neutralized and diluted with satd aq $NaHCO_3$ (30 mL). This solution was extracted with chloroform (2 × 60 mL). Organic phases were dried ($Na_2SO_4$) and evaporated. Residue was crystallized from acetone to afford of the product **6**. Yield: 216 mg (75%); mp 212−213 °C. $^1$H NMR (500 MHz, DMSO-$d_6$) $\delta$ (ppm): 7.77 (t, $J_{NH\text{-}2}$ = 5.8 Hz, 1H, 7′-NH), 7.42 (d, $J_{2''-6''}$ = 2.0 Hz, 1H, H-2″), 7.22 (dd, $J_{6''-2''}$ = 2.0, $J_{6''-5''}$ = 8.3 Hz, 1H, H-6″), 7.01 (d, $J_{5''-6''}$ = 8.3 Hz, 1H, H-5″), 6.16 (t, $J_{NH\text{-}1}$ = 5.8 Hz, CONH), 6.09 (s, 1H, H-6′), 5.57 (s, 2H, CONH$_2$), 3.79 (s, 3H, 3′-$OCH_3$), 3.78 (s, 3H, 4″-$OCH_3$), 3.37 (m, 2H, H-2), 3.26 (m, 2H, H-1), 2.52 (s, 3H, 2′-$CH_3$), 2.39 (s, 3H, 5′-$CH_3$). $^{13}$C NMR (125 MHz, DMSO-$d_6$) $\delta$ (ppm): 14.7 (2′-$CH_3$), 25.1 (5′-$CH_3$), 38.6 (C-1), 42.3 (C-2), 55.7 and 55.8 (3″-$OCH_3$ and 4″-$OCH_3$), 85.3 (C-6′), 105.5 (C-3′), 112.2 (C-5″), 112.6 (C-2″), 120.6 (C-6″), 126.3 (C-1″), 146.1 (C-3′a), 146.3 (C-7′), 146.9 (C-4″), 148.6 (C-3″), 149.8 (C-2′), 158.8 (C-5′), 159.2 (CO). Anal. ($C_{19}H_{24}N_6O_3{\cdot}0.5CH_3COCH_3$) C, H, N. ESI MS, $m/z$ (rel%): 385 (100) [M + H]. HRMS: calcd for [M + H], 385.19827; found, 385.19850.

*1-(2-((3-(3,4-Dimethoxyphenyl)-2,5-dimethylpyrazolo[1,5-a]-pyrimidin-7-yl)amino)ethyl)-3-phenylurea (7).* Compound **2j** (253 mg, 0.74 mmol) was dissolved in dry $CH_2Cl_2$ (7 mL) under argon atmosphere. Phenyl isocyanate (121 μL, 1.1 mmol) was added, and the reaction mixture was stirred at rt for 24 h. The reaction mixture was evaporated, and residue was chromatographed on silica gel column (75 g) in ethyl acetate:toluene (1:1) → ethyl acetate to obtain the product **7**. Solid was recrystallized from ethyl acetate. Yield: 302 mg (89%); mp 125−127 °C. $^1$H NMR (500 MHz, DMSO-$d_6$) $\delta$ (ppm): 8.55 (s, 1H, NHPh), 7.82 (t, $J_{NH\text{-}2}$ = 5.8 Hz, 1H, 7′-NH), 7.42 (d, $J_{2''-6''}$ = 2.0 Hz, 1H, H-2″), 7.39 (m, 2H, Ph-*o*), 7.20 (m, 3H, H-6″, Ph-*m*), 7.01 (d, $J_{5''-6''}$ = 8.5 Hz, 1H, H-5″), 6.89 (m, 1H, Ph-*p*), 6.16 (t, $J_{NH\text{-}1}$ = 5.8 Hz, CONH), 6.10 (s, 1H, H-6′), 3.79 (s, 3H, 3′-$OCH_3$), 3.78 (s, 3H, 4″-$OCH_3$), 3.47 (m, 2H, H-2), 3.39 (m, 2H, H-1), 2.53 (s,



DOI: 10.1021/acs.jmedchem.5b00499
J. Med. Chem. 2015, 58, 3767−3793

3H, 2′-$CH_3$), 2.33 (s, 3H, 5′-$CH_3$). $^{13}$C NMR (125 MHz, DMSO-$d_6$) $\delta$ (ppm): 158.8 (C-5′), 155.7 (NHCONH), 149.8 (C-2′), 148.6 (C-3″), 146.9 (C-4″), 146.3 (C-7′), 146.1 (C-3′a), 140.6 (Ph-*i*), 128.8 (Ph-*m*), 126.3 (C-1″), 121.3 (Ph-*p*), 120.6 (C-6″), 118.0 (Ph-*o*), 112.6 (C-2″), 112.2 (C-5″), 105.5 (C-3′), 85.3 (C-6′), 55.8 and 55.7 (3″-$OCH_3$ and 4″-$OCH_3$), 41.8 (C-2), 38.6 (C-1), 25.1 (5′-$CH_3$), 14.7 (2′-$CH_3$). Anal. ($C_{25}H_{48}N_6O_3$·0.66EtOAc) C, H, N. ESI MS, *m*/*z* (rel %): 461 (100) [M + H]. HRMS: calcd for [M + H], 461.22957; found, 461.22972.

*Ethyl (2-((3-(3,4-Dimethoxyphenyl)-2,5-dimethylpyrazolo[1,5-a]-pyrimidin-7-yl)amino)ethyl)-carbamate (**8**).* Starting material **2j** (252 mg, 0.79 mmol) was dissolved in $CH_2Cl_2$ (10 mL) and cooled down to 0 °C. To the reaction mixture was then sequentially added $Et_3N$ (143 μL, 1 mmol) followed by ClCOOEt (99 μL, 1 mmol), and the reaction mixture was stirred at 0 °C for 1.5 h and then diluted with chloroform (60 mL). The organic phase was washed with water (35 mL), dried ($Na_2SO_4$), and evaporated. Chromatography of the residue on silica gel column (100 g) with ethyl acetate:toluene (5:1) afforded the product **8**. Crystalline powder was obtained after sonication of the compound from the mixture of ethyl acetate−pentane. Yield: 199 mg (61%); mp 170−171 °C. $^1$H NMR (500 MHz, DMSO-$d_6$) $\delta$ (ppm): 7.76 (t, $J_{NH\text{-}2}$ = 5.9 Hz, 1H, 7′-NH), 7.42 (d, $J_{2''-6''}$ = 1.7 Hz, 1H, H-2″), 7.27 (t, $J_{NH\text{-}1}$ = 5.2 Hz, CONH), 7.22 (dd, $J_{6''-2''}$ = 1.7, $J_{6''-5''}$ = 8.3 Hz, 1H, H-6″), 7.01 (d, $J_{5''-6''}$ = 8.3 Hz, 1H, H-5″), 6.08 (s, 1H, H-6′), 3.99 (q, $J_{OCH_2\text{-}CH_3}$ = 7.0 Hz, 2H, O**C**$H_2$$CH_3$), 3.79 (s, 3H, 3′-$OCH_3$), 3.78 (s, 3H, 4″-$OCH_3$), 3.43 (m, 2H, H-2), 3.23 (m, 2H, H-1), 2.52 (s, 3H, 2′-$CH_3$), 2.38 (s, 3H, 5′-$CH_3$), 1.14 (t, $J_{CH_3\text{-}OCH_2}$ = 7.0 Hz, 3H, $OCH_2$**C**$H_3$). $^{13}$C NMR (125 MHz, DMSO-$d_6$) $\delta$ (ppm): 158.7 (C-5′), 156.7 (CONH), 149.9 (C-2′), 148.6 (C-3″), 146.9 (C-4′), 146.2 and 146.1 (C-7′a and C-3′), 126.3 (C-1″), 120.6 (C-6″), 112.6 (C-2″), 112.2 (C-5″), 105.5 (C-3′), 85.1 (C-6′), 59.9 ($OCH_2CH_3$), 55.8 and 55.7 (4″-$OCH_3$ and 3″-$OCH_3$), 41.1 (C-2), 39.6 (C-1), 25.1 (5′-$CH_3$), 14.8 and 14.7 ($OCH_2CH_3$, 2′-$CH_3$). Anal. ($C_{21}H_{27}N_5O_3$) C, H, N. ESI MS, *m*/*z* (rel%): 414 (100) [M + H]. HRMS: calcd for [M + H], 414.21358; found, 414.21351.

*N-(2-((3-(3,4-Dimethoxyphenyl)-2,5-dimethylpyrazolo[1,5-a]-pyrimidin-7-yl)amino)ethyl)methanesulfonamide (**9**).* To a solution of the compound **2j** (253 mg, 0.74 mmol) in $CH_2Cl_2$ (10 mL) and $Et_3N$ (134 μL, 0.96 mmol) at 0 °C was added mesyl chloride (75 μL, 0.96 mmol), and reaction mixture was stirred at 0 °C for 5 h and then for additional 4 h at rt. Reaction was poured into a satd aq solution of $NaHCO_3$ (35 mL) and extracted with chloroform (70 mL). The organic phase was dried ($Na_2SO_4$) and evaporated. Chromatography of the residue on a silica gel column (75 g) with ethyl acetate afforded the product **9**. Crystalline powder was obtained after sonication of the compound from ether. Yield: 258 mg (83%); mp 208.5−209.5 °C. $^1$H NMR (500 MHz, DMSO-$d_6$) $\delta$ (ppm): 7.75 (t, $J_{NH\text{-}1}$ = 6.3 Hz, 1H, 7′-NH), 7.42 (d, $J_{2''-6''}$ = 2.0 Hz, 1H, H-2″), 7.22 (dd, $J_{6''-2''}$ = 2.0, $J_{6''-5''}$ = 8.4 Hz, 1H, H-6″), 7.21 (t, $J_{NH\text{-}2}$ = 6.0 Hz, 1H, $NHSO_2$), 7.01 (d, $J_{5''-6''}$ = 8.4 Hz, 1H, H-5″), 6.11 (s, 1H, H-6′), 3.79 (s, 3H, 3″-$OCH_3$), 3.78 (s, 3H, 4″-$OCH_3$), 3.49 (m, 2H, H-1), 3.23 (m, 2H, H-2), 2.91 (s, 3H, $SO_2CH_3$), 2.53 (s, 3H, 2′-$CH_3$), 2.40 (s, 3H, 5′-$CH_3$). $^{13}$C NMR (125 MHz, DMSO-$d_6$) $\delta$ (ppm): 158.8 (C-5′), 149.9 (C-2′), 148.6 (C-3″), 146.9 (C-4″), 146.0 (C-3a′, C-7′), 126.2 (C-1″), 120.6 (C-6″), 112.7 (C-2″), 112.2 (C-5″), 105.6 (C-3′), 85.3 (C-6′), 55.8 and 55.7 (4″-$OCH_3$ and 3″-$OCH_3$), 41.6 (C-1), 41.5 (C-2), 39.6 ($SO_2CH_3$), 25.2 (5′-$CH_3$), 14.7 (2′-$CH_3$). Anal. ($C_{19}H_{25}N_5SO_3$) C, H, N. ESI MS, *m*/*z* (rel%): 420 (100) [M + H]. HRMS: calcd for [M + H], 420.17000; found, 420.16994.

*2-((3-(3,4-Dimethoxyphenyl)-2,5-dimethylpyrazolo[1,5-a]-pyrimidin-7-yl)amino)ethyl Acetate Hydrochloride (**10**).* To a solution of the compound **2f** (163 mg, 0.48 mmol) in $CH_2Cl_2$ (12.5 mL) and $Et_3N$ (134 μL, 0.96 mmol) at 0 °C was added acetic anhydride (68 μL, 0.72 mmol), and the reaction mixture was stirred for 20 h at rt. Then same amount of the reagents was added and stirring continued for another 12 h and reaction was evaporated. Chromatography of the residue on silica gel column (75 g) with toluene:ethyl acetate (1:1) afforded the product **10** as viscous oil. Crystalline powder was obtained after conversion of the compound to hydrochloride salt (HCl/ether). Yield: 130 mg (71%); mp 186.5−188.5 °C. $^1$H NMR (600 MHz, DMSO-$d_6$) $\delta$ (ppm): 13.50 (bs, 1H, HCl), 9.81 (bs, 1H, 7′-NH), 7.09 (d, $J_{5''-6''}$ = 8.4 Hz, 1H, H-5″), 7.06 (d, $J_{2''-6''}$ = 1.9 Hz, 1H, H-2″), 7.00 (dd, $J_{6''-2''}$ = 1.9, $J_{6''-5''}$ = 8.4 Hz, 1H, H-6″), 6.68 (s, 1 H, H-6′), 4.29 (t, $J_{1-2}$ = 5.3 Hz, 2H, H-1), 3.84 (q, $J_{2-1}$ = $J_{2\text{-}NH}$ = 5.3 Hz, 2H, H-2), 3.82 (2s, 2 × 3H, 3″-$OCH_3$, 4″-$OCH_3$), 2.56 (s, 3H, 5′-$CH_3$), 2.43 (s, 3H, 2′-$CH_3$), 2.00 (s, 3H, $COCH_3$). $^{13}$C NMR (150 MHz, DMSO-$d_6$) $\delta$ (ppm): 170.5 (CO), 155.3 (C-5′), 153.8 (C-2′), 148.9 (C-3″), 148.8 (C-7′), 148.6 (C-4″), 137.1 (C-3a′), 122.2 (C-6″), 121.6 (C-1″), 113.9 (C-2″), 112.2 (C-5″), 105.5 (C-3′), 85.3 (C-6′), 62.1 (C-1), 55.8 and 55.7 (4″-$OCH_3$ and 3″-$OCH_3$), 41.7 (C-2), 20.9 ($COCH_3$), 20.0 (5′-$CH_3$), 13.4 (2′-$CH_3$). Anal. ($C_{20}H_{25}ClN_4O_4$·$H_2O$) C, H, N. ESI MS, *m*/*z* (rel%): 385 (100) [M + H]. HRMS: calcd for [M + H], 385.18703; found, 385.18714.

*N-(3-((3-(3,4-Dimethoxyphenyl)-2,5-dimethylpyrazolo[1,5-a]-pyrimidin-7-yl)amino)propyl)acetamide Hydrochloride (**11**).* Starting material **2k** (281 mg, 0.79 mmol) was dissolved in chloroform (20 mL) and mixed with a satd aq solution of $NaHCO_3$ (8 mL). To this mixture was added dropwise at 0 °C a solution of $Ac_2O$ (83 μL, 0.87 mmol) in chloroform (3 mL), and reaction mixture was stirred at 0 °C for 2 h. Then the reaction mixture was diluted with water (20 mL) and extracted with chloroform (2 × 70 mL). Combined organic phases were dried ($Na_2SO_4$) and evaporated. Residue was chromatographed on silica gel column (75 g) in ethyl acetate → ethyl acetate:acetone:ethanol:$H_2O$ (20:3:1.2:0.8), and it was obtained an oily product. The oily residue was treated with etheral HCl, and crystalline product **11** was filtered off. Yield 252 mg (80%); mp 174−180 °C. $^1$H NMR (400 MHz, DMSO-$d_6$) $\delta$ (ppm): 13.63 (bs, 1H, HCl), 9.84 (t, $J_{NH\text{-}3}$ = 5.9 Hz, 1H, 7′-NH), 7.76 (t, $J_{NH\text{-}1}$ = 5.8 Hz, 1H, NHCO), 7.10 (d, $J_{5''-6''}$ = 8.2 Hz, 1H, H-5″), 7.03 (d, $J_{2''-6''}$ = 1.7 Hz, 1H, H-2″), 6.98 (dd, $J_{6''-2''}$ = 1.7, $J_{6''-5''}$ = 8.2 Hz, 1H, H-6″), 6.71 (s, 1H, H-6′), 3.82 (s, 3H, 3″-$OCH_3$), 3.81 (s, 3H, 4″-$OCH_3$), 3.16 (m, 2H, H-3), 3.12 (m, 2H, H-3), 2.54 (s, 3H, 5′-$CH_3$), 2.42 (s, 3H, 2′-$CH_3$), 1.83 (s, 3H, $COCH_3$), 1.79 (m, 2H, H-2). $^{13}$C NMR (100 MHz, DMSO-$d_6$) $\delta$ (ppm): 169.6 (CO), 154.8 (C-5′), 153.9 (C-2′), 148.9 (C-3″), 148.7 (C-4″), 148.5 (C-7′), 136.6 (C-3a′), 122.3 (C-6″), 121.4 (C-1″), 113.9 (C-2″), 112.3 (C-5″), 105.4 (C-3′), 87.2 (C-6′), 55.9 and 55.7 (4″-$OCH_3$ and 3″-$OCH_3$), 40.4 (C-3), 36.0 (C-1), 28.7 (C-2), 22.8 ($COCH_3$), 19.7 (5′-$CH_3$), 13.3 (2′-$CH_3$). Anal. ($C_{21}H_{28}ClN_5O_3$) C, H, N. ESI MS, *m*/*z* (rel%): 398 (100) [M + H]. HRMS: calcd for [M + H], 398.21867; found, 398.21894.

*3-(3,4-Dimethoxyphenyl)-2,5-dimethylpyrazolo[1,5-a]-pyrimidine-7-thiol (**12**).* A solution of chloro derivative **1** (160 mg, 0.51 mmol) and thiourea (66 mg, 0.87 mmol) in ethanol (10 mL) was heated to reflux for 15 h, and then the reaction mixture was cooled down to 0 °C. Precipitated solid was filtered and thoroughly washed with ethanol and ether to afford the product **12**. Yield: 136 mg (85%); mp 264.5−266 °C (decomp). $^1$H NMR (500 MHz, DMSO-$d_6$) $\delta$ (ppm): 12.67 (bs, 1H, SH), 7.08 (d, $J_{5'-6'}$ = 8.3 Hz, 1H, H-5′), 7.06 (bs, 1H, H-2′), 6.95 (dd, $J_{6'-2'}$ = 1.7, $J_{6'-5'}$ = 8.2 Hz, 1H, H-6′), 6.63 (s, 1H, H-6), 3.81 (s, 3H, 4′-$OCH_3$), 3.80 (s, 3H, 3′-$OCH_3$), 2.34 (s, 3H, 2-$CH_3$), 2.29 (s, 3H, 5-$CH_3$). $^{13}$C NMR (125 MHz, DMSO-$d_6$) $\delta$ (ppm): 152.1 (C-2), 148.9 (C-3′), 148.3 (C-4′), 144.3 (C-5), 122.8 (C-1′), 122.3 (C-6′), 113.7 (C-2′), 112.3 (C-5′),111.4 (C-6), 103.5 (C-3), 55.8 and 55.7 (4′-$OCH_3$ and 3′-$OCH_3$), 18.3 (5-$CH_3$), 13.3 (2-$CH_3$), carbons 3a and 7 were not detected. Anal. ($C_{16}H_{17}N_3SO_2$) C, H, N. ESI MS, *m*/*z* (rel%): 338 (100) [M + Na]. HRMS: calcd for [M + H], 316.11142; found, 316.11138.

*4-(2-((3-(3,4-Dimethoxyphenyl)-2,5-dimethylpyrazolo[1,5-a]-pyrimidin-7-yl)thio)ethyl)morpholine (**13**).* Thioderivative **12** (100 mg, 0.32 mmol) was combined with 4-(2-chloroethyl)morpholine hydrochloride (89 mg, 0.48 mmol) in DMF (5 mL), and $K_2CO_3$ (132 mg, 0.96 mmol) was added. Resulted mixture was heated for 24 h at 75 °C and evaporated. Residue was partitionated between chloroform (70 mL) and water (50 mL). The organic phase was dried ($Na_2SO_4$) and evaporated. Product was isolated by column chromatography (silica gel, 50 g) with ethyl acetate → ethyl acetate:toluene:acetone:ethanol (17:4:3:1) to afford the product **13**. Solid was recrystallized from ether. Yield: 106 mg (77%); mp 150−152 °C. $^1$H NMR (500 MHz,



DOI: 10.1021/acs.jmedchem.5b00499
J. Med. Chem. 2015, 58, 3767−3793

$CDCl_3$) δ (ppm): 7.35 (d, $J_{2''-6''}$ = 2.0 Hz, 1H, H-2″), 7.22 (dd, $J_{6''-2''}$ = 2.0, $J_{6''-5''}$ = 8.3 Hz, 1H, H-6″), 6.98 (d, $J_{5''-6''}$ = 8.3 Hz, 1H, H-5″), 6.49 (s, 1H, H-6′), 3.94 (s, 3H, 3″-$OCH_3$), 3.92 (s, 3H, 4″-$OCH_3$), 3.75 (m, 4H, morph-O($CH_2$)$_2$), 3.28 (m, 2H, H-1), 2.84 (m, 2H, H-2), 2.64 (s, 3H, 2′-$CH_3$), 2.57 (s, 3H, 5′-$CH_3$), 2.56 (m, 4H, morph-N($CH_2$)$_2$). $^{13}$C NMR (125 MHz, $CDCl_3$) δ (ppm): 157.0 (C-5′), 150.1 (C-2′), 148.9 (C-3″), 147.6 (C-4″), 145.4 (C-7′), 125.2 (C-1″), 121.2 (C-6″), 112.5 (C-2″), 111.4 (C-5″), 108.1 (C-3′), 103.3 (C-6′), 66.8 (morph-O($CH_2$)$_2$), 56.1 (C-2), 55.9 and 56.0 (3″-OCH3, 4″-$OCH_3$), 53.3 (morph-N($CH_2$)$_2$), 28.2 (C-1), 25.1 (5′-$CH_3$), 14.4 (2′-$CH_3$), C-3′a was not detected. Anal. ($C_{22}H_{28}N_4SO_3$) C, H, N. ESI MS, *m/z* (rel%): 451 (100) [M + Na]. HRMS: calcd for [M + H], 429.19549; found, 429.19549.

*4-(4-((3-(3,4-Dimethoxyphenyl)-2,5-dimethylpyrazolo[1,5-a]pyrimidin-7-yl)thio)phenyl)morpholine (14).* 4-(Morpholin-4-yl)-benzenethiol (110 mg, 0.56 mmol) and $K_2CO_3$ (130 mg, 0.94 mmol) were heated at 65 °C in DMF (5 mL) for 0.5 h. Chloro derivative **1** (150 mg, 0.47 mmol) was then added in one portion, and the reaction mixture was heated at 90 °C for 18 h. The reaction mixture was evaporated and partitionated between ethyl acetate (75 mL) and water (50 mL). The water phase was then extracted with ethyl acetate (2 × 70 mL). The combined organic phases were dried ($Na_2SO_4$) and evaporated. Residue was chromatographed (silica gel, 80 g) with toluene−ethyl acetate (2:1). Product **14** was obtained as a solid after a crystallization from ethyl acetate. Yield: 97 mg (43%); mp 214−215 °C. $^1$H NMR (500 MHz, $CDCl_3$) δ (ppm): 7.56 (d, $J_{2-3}$ = 9.0 Hz, 2H, H-2), 7.36 (d, $J_{2''-6''}$ = 2.0 Hz, 1H, H-2″), 7.23 (dd, $J_{6''-2''}$ = 2.0, $J_{6''-5''}$ = 8.3 Hz, 1H, H-6″), 7.02 (d, $J_{3-2}$ = 9.0 Hz, 2H, H-3), 6.98 (d, $J_{5''-6''}$ = 8.3 Hz, 1H, H-5″), 5.87 (s, 1H, H-6′), 3.94 (s, 3H, 3″-$OCH_3$), 3.92 (s, 3H, 4″-$OCH_3$), 3.90 (m, 4H, morph-O($CH_2$)$_2$), 3.30 (m, 4H, morph-N($CH_2$)$_2$), 2.67 (s, 3H, 2′-$CH_3$), 2.41 (s, 3H, 5′-$CH_3$). $^{13}$C NMR (125 MHz, $CDCl_3$) δ (ppm): 157.3 (C-5′), 152.7 (C-4), 152.1 (C-2′), 150.6 (C-1), 148.9 (C-3″), 147.6 (C-4″), 145.5 (C-3′a), 137.5 (C-2), 125.4 (C-1″), 121.2 (C-6″), 116.1 (C-3), 113.9 (C-7′), 112.5 (C-2″), 111.5 (C-5″), 107.8 (C-3′), 103.5 (C-6′), 66.6 (morph-O($CH_2$)$_2$), 56.0 and 55.9 (4″-OCH3, 3″-$OCH_3$), 48.0 (morph-N($CH_2$)$_2$), 25.1 (5′-$CH_3$), 14.4 (2′-$CH_3$). Anal. ($C_{26}H_{28}N_4SO_3$) C, H, N. ESI MS, *m/z* (rel%): 499 (100) [M + Na]. HRMS: calcd for [M + H], 477.19549; found, 477.19544.

*4-(2-((3-(3,4-Dimethoxyphenyl)-2,5-dimethylpyrazolo[1,5-a]pyrimidin-7-yl)oxy)ethyl)morpholine (15).* 4-(2-Hydroxyethyl)-morpholine (0.16 mL, 1.3 mmol) was dissolved in DMF (2 mL), and the solution was cooled to 0 °C. Sodium hydride (46 mg, 1.14 mmol, 60% dispersion in mineral oil) was added, and the reaction mixture was stirred at rt for 0.5 h. A solution of chloroderivative **1** (164 mg, 0.52 mmol) in DMF (2 mL + 1 mL for rinsing of the flask) was slowly added during 30 min, and then the reaction mixture was stirred for 2 h. Reaction was quenched with water (1 mL) and evaporated. Residue was taken into ethyl acetate (80 mL), and the organic phase was washed with water (2 × 30 mL). The organic phase was dried ($Na_2SO_4$) and evaporated. Product **15** was isolated by column chromatography (silica gel, 50 g) with ethyl acetate → ethyl acetate:acetone:ethanol:$H_2O$ (20:3:1.2:0.8) and crystallized from ethyl acetate. Yield: 125 mg (58.3%); mp 139−140 °C. $^1$H NMR (500 MHz, $CDCl_3$) δ (ppm): 7.36 (d, $J_{2''-6''}$ = 2.0 Hz, 1H, H-2″), 7.22 (dd, $J_{6''-2''}$ = 2.0, $J_{6''-5''}$ = 8.3 Hz, 1H, H-6″), 6.97 (d, $J_{5''-6''}$ = 8.3 Hz, 1H, H-5″), 6.05 (s, 1H, H-6′), 4.50 (t, $J_{1-2}$ = 6.1 Hz, H-1), 3.94 (s, 3H, 3″-$OCH_3$), 3.92 (s, 3H, 4″-$OCH_3$), 3.75 (m, 4H, morph-O($CH_2$)$_2$), 3.03 (t, $J_{2-1}$ = 6.1 Hz, 2H, H-2), 2.65 (m, 4H, morph-N($CH_2$)$_2$), 2.62 (s, 3H, 2′-$CH_3$), 2.56 (s, 3H, 5′-$CH_3$). $^{13}$C NMR (125 MHz, $CDCl_3$) δ (ppm): 160.3 (C-5′), 153.9 (C-7′), 152.5 (C-2′), 148.8 (C-3″), 147.6 (C-4′), 125.3 (C-1″), 121.2 (C-6″), 112.4 (C-2″), 111.4 (C-5″), 108.1 (C-3′), 87.4 (C-6′), 67.4 (C-1), 66.7 (morph-O($CH_2$)$_2$), 56.5 (C-2), 55.9 and 55.8 (4″-$OCH_3$ and 3″-$OCH_3$), 54.0 (morph-N($CH_2$)$_2$), 25.5 (5′-$CH_3$), 14.5 (2′-$CH_3$), C-3a was not detected. Anal. ($C_{22}H_{28}N_4O_4{\cdot}H_2O$) C, H, N. ESI MS, *m/z* (rel%): 435 (100) [M + Na]. HRMS: calcd for [M + H], 413.21833; found, 413.21868.

*8-Bromo-3-(3,4-dimethoxyphenyl)-2,6-dimethylimidazo[1,2-a]pyridine (21).* *N*-Iodosuccinimide (2.03 g, 9 mmol) was added to the solution of 8-bromo-3-iodo-2,6-dimethylimidazo[1,2-*a*]pyridine[38] (1.35 g, 6 mmol) in DMF (120 mL), and the reaction mixture was stirred overnight at rt for 1 h. The reaction mixture was diluted with water (400 mL) and extracted with ethyl acetate (3 × 200 mL). Combined organic phases were dried over sodium sulfate and evaporated. Crude product was then directly used in the next step. The intermediate was dissolved in dioxane (88 mL) and water (22 mL), and sodium carbonate (1.77 g, 16.7 mmol) and boronic acid (1.1 g, 6 mmol) were added. Reaction mixture was three times degassed and purged with argon. To the reaction mixture Pd(dppf)$Cl_2$ (220 mg, 0.27 mmol) was added in one portion, and the mixture was stirred at 95 °C overnight under argon atmosphere. After cooling to ambient temperature, the mixture was partitioned between ethyl acetate (400 mL) and brine (200 mL). Organic phase was dried over anhydrous sodium sulfate and evaporated. The crude product was chromatographed on a silica gel column (200 g) in hexanes:ethyl acetate (3:2). It obtained 975 mg (45%, two steps) of an off-white solid. An analytical sample was obtained after recrystallization from hot ethyl acetate. $^1$H NMR (500 MHz, DMSO-$d_6$) δ (ppm): 8.03 (m, 1H, H-5), 7.45 (m, 1H, H-7), 7.14 (d, $J_{5'-6'}$ = 8.4, 1H, H-5′), 7.06 (d, $J_{2'-6'}$ = 1.9, 1H, H-2′), 7.02 (dd, $J_{6'-5'}$ = 8.4, $J_{6'-2'}$ = 1.9, 1H, H-6′), 3.83 (s, 3H, 4′-$OCH_3$), 3.80 (s, 3H, 3′-$OCH_3$), 2.33 (s, 3H, 2-$CH_3$), 2.24 (s, 3H, 6-$CH_3$). $^{13}$C NMR (125 MHz, DMSO-$d_6$DMSO-$d_6$) δ (ppm): 149.31 (C-3′), 149.1 (C-4′), 140.5 (C-2), 140.2 (C-8a), 129.2 (C-7), 122.9 (C-3), 122.3 (C-6′), 121.9 (C-6), 121.1 (C-5), 121.1 (C-1′), 113.1 (C-2′), 112.5 (C-5′), 109.5 (C-8), 55.8 (3′-$OCH_3$), 55.8 (4′-$OCH_3$), 17.5 (6-$CH_3$), 14.0 (2-$CH_3$). HRMS: calcd for [M + H], 361.05462; found, 361.05470.

*3-(3,4-Dimethoxyphenyl)-2,6-dimethyl-N-(2-morpholinoethyl)-imidazo[1,2-a]pyridin-8-amine (16).* Compound **21** (250 mg, 0.69 mmol), Me-DalPhos (42 mg, 0.1 mmol), $Pd_2(dba)_3$ (21 mg, 3% mol), and *t*-BuONa (94 mg, 0.98 mmol) were combined in a microwave vial and purged with argon. To this mixture, a solution of morpholinoethylamine (110 μL, 0.84 mmol) in degassed dioxane (6.5 mL) was added and reaction vessel was heated in microwave reactor for 2 h at 150 °C. Reaction mixture was evaporated and chromatographed on a silica gel column (100 g) in ethyl acetate → ethyl acetate:acetone:ethanol:water (19:3:1.2:0.8). It obtained 113 mg (40%) of the yellowish solid. This compound is rather unstable and difficult to store. $^1$H NMR (500 MHz, DMSO-$d_6$) δ (ppm): 7.30 (m, 1H, H-5), 7.12 (d, $J_{5'-6'}$ = 8.0, 1H, H-5′), 6.97−6.99 (m, 2H, H-2′, H-6′), 5.99 (m, 1H, H-7), 5.70 (t, $J_{NH-1''}$ = 5.5, 1H, NH), 3.82 (s, 3H, 4′-$OCH_3$), 3.79 (s, 3H, 3′-$OCH_3$), 3.60 (m, 4H, morph-O($CH_2$)$_2$), 3.29 (m, 2H, H-1″), 2.61 (t, $J_{2''-1''}$ = 6.3, 2H, H-2″), 2.44 (bs, 4H, morph-N($CH_2$)$_2$), 2.30 (s, 3H, 2-$CH_3$), 2.16 (s, 3H, 6-$CH_3$). $^{13}$C NMR (125 MHz, DMSO-$d_6$) δ (ppm): 149.2 (C-3′), 148.6 (C-4′), 137.3 (C-2), 136.4 (C-8a), 136.2 (C-8), 122.5 (C-6), 122.1 (C-6′), 122.0 (C-1′), 121.7 (C-3), 113.1 (C-2′), 109.5 (C-5), 99.6 (C-7), 66.4 (morph-O($CH_2$)$_2$), 56.7 (C-2″), 55.8 (3′-$OCH_3$), 55.7 (4′-$OCH_3$), 53.4 (morph-N($CH_2$)$_2$), 39.3 (C-1″), 18.7 (6-$CH_3$), 13.9 (2-$CH_3$). HRMS: calcd for [M + H], 411.23907; found, 411.23901.

*6-Chloro-2-methyl-N-(2-morpholinoethyl)imidazo[1,2-b]-pyridazin-8-amine (23).* To a solution of **22** (1.5 g, 7.368 mmol) in $CH_3CN$ (25 mL) were added DIPEA (1.97 mL, 11.31 mmol) and 4-(2-aminoethyl)morpholine (1.25 mL, 9.52 mmol). The reaction mixture was stirred at 80 °C for 16 h and cooled, and the solvent was evaporated. The residue was partitioned between $CHCl_3$ (70 mL) and satd $NH_4Cl$ (70 mL), the layers were separated, and the aqueous layer was extracted with $CHCl_3$ (1 × 70 mL). The combined organic layer was dried over $Na_2SO_4$ and evaporated. The residue was purified by silica gel column chromatography ($CHCl_3$:MeOH = 97:3), affording compound **23**, which was recrystallized from hot EtOAc to obtain an analytical sample. Yield: 2.014 g, (92%). $^1$H NMR (500 MHz, DMSO-$d_6$) δ (ppm): 7.73 (q, $J_{3-CH3}$ = 0.9 Hz, 1H, H-3), 7.48 (t, $J_{NH-1'}$ = 5.7 Hz, 1H, 8-NH), 6.18 (s, 1H, H-7), 3.56 (m, 4H, O-$CH_2$), 3.39 (m, 2H, H-1′), 2.55 (t, $J_{2'-1'}$ = 6.4 Hz, 2H, H-2′), 2.42 (m, 4H, N-$CH_2$), 2.30 (s, 3H, 2-$CH_3$). $^{13}$C NMR (125 MHz, DMSO-$d_6$) δ (ppm): 147.0 (C-6), 142.9 (C-8), 139.8 (C-2), 131.6 (C-9), 114.8 (C-3), 90.8 (C-7), 66.4 (O-$CH_2$), 56.5 (C-2′), 53.4 (N-$CH_2$), 38.3 (C-1′), 14.4 (2-$CH_3$). Anal. ($C_{13}H_{18}ClN_5O$) C, H, N. HRMS: calcd for [M + H], 388.06288; found, 388.06284.



DOI: 10.1021/acs.jmedchem.5b00499
J. Med. Chem. 2015, 58, 3767−3793

*2,6-Dimethyl-N-(2-morpholinoethyl)imidazo[1,2-b]pyridazin-8-amine (24).* To a solution of DABCO (90 mg, 0.8 mmol) in 2 mL of freshly distilled THF, $AlMe_3$ (2 M in hexanes, 0.8 mL, 1.6 mmol) was added dropwise and the mixture was stirred at rt for 30 min. A solution of **23** (296 mg, 1 mmol), $Pd_2(dba)_3$ (46 mg, 0.05 mmol), and X-Phos (48 mg, 0.10 mmol) in 7 mL of freshly distilled THF was subsequently added to the solution, and the reaction mixture was stirred in a sealed tube at 80 °C overnight. The mixture was cooled to 0 °C and quenched with satd $NH_4Cl$ diluted with acetone and MeOH and filtered over Celite. The filtrate was evaporated to near dryness and partitioned between EtOAc and $H_2O$. The aqueous layer was extracted twice with EtOAc, and the combined organic phase was dried over $Na_2SO_4$ and evaporated. The residue was purified by silica gel column chromatography (ethyl acetate:acetone:ethanol:water (20:3:1:1)), and compound **24** was obtained as an off-white solid. Yield: 115 mg (42%). $^1$H NMR (500 MHz, DMSO-$d_6$) $\delta$ (ppm): 7.61 (s, 1H, H-3), 6.83 (s, 1H, 8-NH), 5.94 (s, 1H, H-7), 3.58 (m, 4H, O−$CH_2$), 3.35 (m, 2H, H-1′), 2.56 (t, $J_{2'-1'}$ = 5.6 Hz, 2H, H-2′), 2.43 (m, 4H, N-$CH_2$), 2.30 (s, 3H, 2-$CH_3$), 2.29 (s, 3H, 6-$CH_3$). Anal. ($C_{14}H_{21}N_5O$) C, H, N.

*3-Iodo-2,6-dimethyl-N-(2-morpholinoethyl)imidazo[1,2-b]pyridazin-8-amine (25).* Compound **24** (210 mg, 0.763 mmol) was dissolved in dry $CH_2Cl_2$ (8 mL) and AcOH (320 $\mu$L), and the solution was cooled to 0 °C. *N*-Iodosuccinimide (180 mg, 0.8 mmol) was added in one portion, and the reaction mixture was stirred at 0 °C for 30 min and at rt for 2 h. The reaction mixture was diluted with $CHCl_3$ and treated with satd $Na_2CO_3$:10% aq $Na_2S_2O_3$ = 1:1. The aqueous layer was extracted 1× with $CHCl_3$, and the combined organic phase was dried over $Na_2SO_4$ and evaporated. The residue was purified by silica gel column chromatography (ethyl acetate:acetone:ethanol:water (21:3:0.5:0.5)), affording compound **25** as an off-white solid. Yield: 151 mg (49%). $^1$H NMR (400 MHz, $CDCl_3$) $\delta$ (ppm): 6.13 (bs, 1H, 8-NH), 6.90 (s, 1H, H-7), 3.77 (t, $J_{CH_2\text{-}CH_2}$ = 4.4 Hz, 4H, O-$CH_2$), 3.40 (m, 2H, H-1′), 2.74 (t, $J_{2'-1'}$ = 6.0 Hz, 2H, H-2′), 2.55 (bs, 4H, N-$CH_2$), 2.49 (s, 3H, 2-$CH_3$), 2.46 (s, 3H, 6-$CH_3$). $^{13}$C NMR (125 MHz, CDCl3) $\delta$ (ppm): 153.6 (C-6), 143.3 (C-2), 141.1 (C-8), 134.9 (C-9), 93.4 (C-7), 68.5 (C-3), 66.7 (O-$CH_2$), 56.6 (C-2′), 53.5 (N-$CH_2$), 39.0 (C-1′), 22.4 (6-$CH_3$), 14.9 (2-$CH_3$). Anal. ($C_{14}H_{20}IN_5O$) C, H, N.

**General Procedure for Suzuki Reaction: Preparation of Compounds 17, 28 and 30a−c.** A suspension of iodine derivative **25**, **27**, or **29** (1 equiv) and the corresponding boronic acid (1.1 equiv) in dioxane:1 M $K_2CO_3$ = 4:1 was purged repeatedly with argon, and $Pd(PPh_3)_4$ (5 mol %) was added to the mixture. The reaction mixture was degassed again and subsequently stirred at 95−105 °C between 14 and 22 h. The mixture was allowed to cool and diluted with $CHCl_3$ and $H_2O$. The layers were separated, and the aqueous layer was extracted with $CHCl_3$; the combined organic phase was dried over $Na_2SO_4$ and evaporated. The residue was purified by silica gel column chromatography, and the product was recrystallized to afford an analytically pure sample.

*3-(3,4-Dimethoxyphenyl)-2,6-dimethyl-N-(2-morpholinoethyl)-imidazo[1,2-b]pyridazin-8-amine (17).* This compound has been prepared according to the general procedure described for Suzuki reaction. The following reagents, amounts, and conditions have been employed: compound **25** (149 mg, 0.371 mmol), 3,4-dimethoxyphenylboronic acid (75 mg, 0.412 mmol), and $Pd(PPh_3)_4$ (21 mg, 0.0182 mmol) in 1 M $K_2CO_3$ (1.2 mL) and dioxane (4 mL). The reaction mixture was stirred at 95−100 °C overnight and worked up as described above, including silica gel column chromatography (ethyl acetate:acetone:ethanol:water (20:3:1:1)), yielding compound **17** as a white solid. Recrystallization from hot EtOAc/MeOH afforded an analytically pure sample. Yield: 109 mg (71%); mp 161.3−162.0 °C. $^1$H NMR (500 MHz, DMSO-$d_6$) $\delta$ (ppm): 7.29 (d, $J_{2''-6''}$ = 2.0 Hz, 1H, H-2″), 7.17 (dd, $J_{6''-2''}$ = 2.0, $J_{6''-5''}$ = 8.3 Hz, 1H, H-6″), 7.07 (d, $J_{5''-6''}$ = 8.3 Hz, 1H, H-5″), 6.88 (t, $J_{NH\text{-}1'}$ = 5.6 Hz, 1H, 8-NH), 6.01 (s, 1H, H-7), 3.81, 3.78 (2s, 2 × 3H, 3″-O-$CH_3$, 4″-O-$CH_3$), 3.59 (m, 4H, O-$CH_2$), 3.38 (m, 2H, H-1′), 2.58 (t, $J_{2'-1'}$ = 6.4 Hz, 2H, H-2′), 2.44 (bs, 4H, N-$CH_2$), 2.41 (s, 3H, 2-$CH_3$), 2.31 (s, 3H, 6-$CH_3$). $^{13}$C NMR (125 MHz, DMSO-$d_6$) $\delta$ (ppm): 152.05 (C-6), 148.48 (C-3″), 148.28 (C-4″), 141.63 (C-8), 136.55 (C-2), 131.44 (C-9), 124.22 (C-3), 122.12 (C-1″), 121.91 (C-6″), 113.14 (C-2″), 111.86 (C-5″), 91.46 (C-7), 66.43 (O-$CH_2$), 56.53 (C-2′), 55.75 (3″-O-$CH_3$, 4″-O-$CH_3$), 53.44 (N-$CH_2$), 38.94 (C-1′), 22.03 (6-$CH_3$), 14.81 (2-$CH_3$). Anal. ($C_{22}H_{29}N_5O_3$) C, H, N. HRMS: calcd for [M + H], 412.23432; found, 412.23428.

*2-Methyl-N-(2-morpholinoethyl)imidazo[1,2-b]pyridazin-8-amine (26).* To a solution of compound **23** (590 mg, 2 mmol) in THF (12 mL) and MeOH (12 mL) was added 10% Pd/C (60 mg) and $NEt_3$ (560 $\mu$L, 4 mmol), and the reaction mixture was stirred under a $H_2$ atmosphere (3 atm) in an autoclave at rt for 21 h. The autoclave was flushed with Ar, and then the mixture was filtered over Celite to remove the catalyst and washed with MeOH and acetone. The solvent was evaporated and the residue was partitioned between $CHCl_3$ and satd $NaHCO_3$ (40 mL each), and the layers were separated. The aqueous layer was extracted with $CHCl_3$ (1 × $CHCl_3$), and the combined organic phase was dried over $Na_2SO_4$ and evaporated. The residue was purified by silica gel column chromatography (ethyl acetate:acetone:ethanol:water (21:3:0.5:0.5) → ethyl acetate:acetone:ethanol:water (20:3:1:1)), yielding compound **26** as an off-white solid. Recrystallization from hot EtOAc afforded an analytically pure sample. Yield: 337 mg (64%). $^1$H NMR (500 MHz, DMSO-$d_6$) $\delta$ (ppm): 7.93 (d, $J_{6-7}$ = 5.4 Hz, 1H, H-6), 7.71 (s, 1H, H-3), 6.98 (bs, 1H, 8-NH), 6.02 (d, $J_{7-6}$ = 5.4 Hz, 1H, H-7), 3.57 (bs, 4H, O-$CH_2$), 3.38 (bs, 2H, H-1′), 2.55 (t, $J_{2'-1'}$ = 6.1 Hz, 2H, H-2′), 2.43 (m, 4H, N-$CH_2$), 2.31 (s, 3H, 2-$CH_3$). $^{13}$C NMR (125 MHz, DMSO-$d_6$) $\delta$ (ppm): 144.1 (C-6), 141.9 (C-8), 139.3 (C-2), 133.1 (C-9), 114.2 (C-3), 90.0 (C-7), 66.4 (O-$CH_2$), 56.5 (C-2′), 53.4 (N-$CH_2$), 38.9 (C-1′), 14.4 (2-$CH_3$). Anal. ($C_{13}H_{19}N_5O$) C, H, N. HRMS: calcd for [M + H], 388.06288 (M + H)$^+$; found, 388.06284.

*3-Iodo-2-methyl-N-(2-morpholinoethyl)imidazo[1,2-b]pyridazin-8-amine (27).* To a solution of compound **26** (409 mg, 1.565 mmol) in dry DMF (16 mL), *N*-iodosuccinimide (423 mg, 1.88 mmol) was added in one portion and the reaction mixture was stirred at rt overnight. The solvent was evaporated to near dryness, coevaporated with toluene, and the residue was partitioned between $CHCl_3$ and 10% aq $Na_2S_2O_3$ (25 mL each). The layers were separated, the aqueous layer was extracted with $CHCl_3$ (1 × 25 mL), and the combined organic phase was dried over $Na_2SO_4$ and evaporated. The residue was purified by silica gel column chromatography (ethyl acetate:acetone:ethanol:water (21:3:0.5:0.5)), which furnished compound **27** as an off-white solid. Trituration with ether and filtration/wash yielded an analytically pure sample. Yield: 248 mg (41%); mp 130 °C (decomposed). $^1$H NMR (500 MHz, DMSO-$d_6$) $\delta$ (ppm): 8.06 (d, $J_{6-7}$ = 5.6 Hz, 1H, H-6), 7.12 (t, $J_{NH\text{-}1'}$ = 5.7 Hz, 1H, 8-NH), 6.13 (d, $J_{7-6}$ = 5.6 Hz, 1H, H-7), 3.57 (m, 4H, O-$CH_2$), 3.38 (m, 2H, H-1′), 2.55 (t, $J_{2'-1'}$ = 6.7 Hz, 2H, H-2′), 2.42 (m, 4H, N-$CH_2$), 2.35 (s, 3H, 2-$CH_3$). $^{13}$C NMR (125 MHz, DMSO-$d_6$) $\delta$ (ppm): 144.6 (C-6), 143.1 (C-2), 141.9 (C-8), 135.6 (C-9), 91.0 (C-7), 70.8 (C-3), 66.4 (O-$CH_2$), 56.4 (C-2′), 53.4 (N-$CH_2$), 39.1 (C-1′), 14.8 (2-$CH_3$). Anal. ($C_{13}H_{18}IN_5O$) C, H, N. HRMS calcd for $C_{13}H_{19}IN_5O$ *m*/*z*: HRMS calcd for [M + H], 388.06288; found, 388.06284.

*3-(3,4-Dimethoxyphenyl)-2-methyl-N-(2-morpholinoethyl)-imidazo[1,2-b]pyridazin-8-amine (28).* This compound has been prepared according to the general procedure for Suzuki reaction. The following reagents, amounts, and conditions have been employed: compound **27** (174 mg, 0.449 mmol), 3,4-dimethoxyphenylboronic acid (90 mg, 0.494 mmol), and $Pd(PPh_3)_4$ (26 mg, 0.0225 mmol) in 1 M $K_2CO_3$ (1.5 mL) and dioxane (5 mL). The reaction mixture was stirred at 95−100 °C overnight and worked up as described above, including silica gel column chromatography (ethyl acetate:acetone:ethanol:water (21:3:0.5:0.5)), yielding compound **28** as a white solid. Recrystallization from hot MeOH afforded an analytically pure sample. Yield: 149 mg (83%); mp 169.1−169.9 °C. $^1$H NMR (500 MHz, DMSO-$d_6$) $\delta$ (ppm): 7.99 (d, $J_{6-7}$ = 5.5 Hz, 1H, H-6), 7.24 (d, $J_{2''-6''}$ = 2.0 Hz, H-2″), 7.18 (dd, $J_{6''-2''}$ = 2.0, $J_{6''-5''}$ = 8.2 Hz, 1H, H-6″), 7.07 (d, $J_{5''-6''}$ = 8.2 Hz, 1H, H-5″), 7.04 (t, $J_{NH\text{-}1'}$ = 5.7 Hz, 1H, 8-NH), 6.09 (d, $J_{7-6}$ = 5.5 Hz, 1H, H-7), 3.81 (s, 3H, 4″-O-$CH_3$), 3.78 (s, 3H, 3″-O-$CH_3$), 3.59 (m, 4H, O-$CH_2$), 3.41 (m, 2H, H-1′), 2.58 (t, $J_{2'-1'}$ = 6.5 Hz, 2H, H-2′), 2.44 (m, 4H, *N*-$CH_2$), 2.43 (s, 3H, 2-$CH_3$). $^{13}$C NMR (125 MHz, DMSO-$d_6$) $\delta$ (ppm): 148.5 (C-3″), 148.4 (C-4″),



DOI: 10.1021/acs.jmedchem.5b00499
J. Med. Chem. 2015, 58, 3767−3793

144.0 (C-6), 142.1 (C-8), 136.9 (C-2), 132.3 (C-9), 124.5 (C-3), 122.1 (C-6″), 121.9 (C-1″), 113.2 (C-2″), 111.9 (C-5″), 90.2 (C-7), 66.4 (O-$CH_2$), 56.5 (C-2′), 55.8, 55.8 (3″-O-$CH_3$), 4″-O-$CH_3$), 53.4 (*N*-$CH_2$), 39.0 (C-1′), 14.7 (2-$CH_3$). Anal. ($C_{21}H_{27}N_5O_3$) C, H, N. HRMS: calcd for [M + H], 398.21867; found, 398.21860.

*6-Chloro-3-iodo-2-methyl-N-(2-morpholinoethyl)imidazo[1,2-b]-pyridazin-8-amine (29).*[45] To a solution of compound **23** (705 mg, 2.39 mmol) in $CH_2Cl_2$ (25 mL) and AcOH (1 mL) at 0 °C was added *N*-iodosuccinimide (699 mg, 3.10 mmol), and the reaction mixture was stirred at 0 °C for 5 min and at rt for 2.5 h. The mixture was diluted with $CH_2Cl_2$ (25 mL) and washed with 10% aq $Na_2S_2O_3$ (40 mL). The layers were separated, and the aqueous layer was extracted with $CHCl_3$ (2 × 40 mL). The combined layer was subsequently dried over $Na_2SO_4$ and evaporated to dryness. The crude product was purified by silica gel column chromatography and eluted with Michal 17, which gave compound **29** as an off-white solid. Recrystallization from hot MeOH/$CHCl_3$ afforded an analytical sample. Yield: 412 mg (41%). $^1$H NMR (500 MHz, DMSO-$d_6$) $\delta$ (ppm): 7.59 (t, $J_{NH\text{-}1'}$ = 5.8 Hz, 1H, 8-NH), 6.29 (s, 1H, H-7), 3.56 (m, 4H, O-$CH_2$), 3.40 (m, 2H, H-1′), 2.54 (t, $J_{2'-1'}$ = 6.4 Hz, 2H, H-2′), 2.42 (m, 4H, *N*-$CH_2$), 2.34 (s, 3H, 2-$CH_3$). $^{13}$C NMR (125 MHz, DMSO-$d_6$) $\delta$ (ppm): 147.7 (C-6), 143.7 (C-2), 142.9 (C-8), 134.3 (C-9), 91.8 (C-7), 71.8 (C-3), 66.4 (O-$CH_2$), 56.4 (C-2′), 53.4 (N-$CH_2$), 38.6 (C-1′), 14.9 (2-$CH_3$). Anal. ($C_{13}H_{17}ClIN_5O$) C, H, N. HRMS: calcd for [M + H], 388.06288; found, 388.06284.

*6-Chloro-3-(3,4-dimethoxyphenyl)-2-methyl-N-(2-morpholinoethyl)imidazo[1,2-b]pyridazin-8-amine (30a).* This compound has been prepared according to the general procedure described above. The following reagents, amounts, and conditions have been employed: compound **29** (200 mg, 0.474 mmol), 3,4-dimethoxyphenylboronic acid (95 mg, 0.523 mmol), and $Pd(PPh_3)_4$ (27 mg, 0.0234 mmol) in 1 M $K_2CO_3$ (1.2 mL) and dioxane (4 mL). The reaction mixture was stirred at 100 °C for 16 h and worked up as described above, including silica gel column chromatography ($CHCl_3$:MeOH = 97:3), yielding compound **30a** as a white solid. Recrystallization from hot MeOH/$CHCl_3$ afforded an analytically pure sample. Yield: 157 mg (77%); mp 195.8−196.9 °C. $^1$H NMR (500 MHz, DMSO-$d_6$) $\delta$ (ppm): 7.25 (d, $J_{2''-6''}$ = 1.9 Hz, H-2″), 7.18 (dd, $J_{6''-5''}$ = 8.3, $J_{6''-2''}$ = 1.9 Hz, 1H, H-6″), 7.16 (bs, 1H, NH), 7.11 (d, $J_{5''-6''}$ = 8.3 Hz, 1H, H-5″), 6.21 (s, 1H, H-7), 3.85, 3.82 (2*s*, 6H, 3″-O-$CH_3$, 4″-O-$CH_3$), 3.61 (m, 4H, O-$CH_2$), 3.48 (m, 2H, H-1′), 2.56 (t, $J_{2'-1'}$ = 6.2 Hz, 2H, H-2′), 2.49 (m, 4H, *N*-$CH_2$), 2.43 (s, 3H, 2-$CH_3$). $^{13}$C NMR (125 MHz, DMSO-$d_6$) $\delta$ (ppm): 148.8 and 148.7 (C-3″and C-4″), 146.6 (C-6), 142.8 (C-8), 137.1 (C-2), 130.6 (C-9), 124.8 (C-3), 122.0 (C-6″), 121.1 (C-1″), 113.8 (C-2″), 112.5 (C-5″), 90.8 (C-7), 66.0 (O-$CH_2$), 56.2 (C-2′), 55.8 and 55.73 (3″-O-$CH_3$ and 4″-O-$CH_3$), 53.0 (*N*-$CH_2$), 39.2 (C-1′), 14.2 (2-$CH_3$). Anal. ($C_{21}H_{17}ClIN_5O$) C, H, N. HRMS: calcd for [M + H], 432.17969; found, 432.17957.

*6-Chloro-3-(3-fluoro-4-methoxyphenyl)-2-methyl-N-(2-morpholinoethyl)imidazo[1,2-b]pyridazin-8-amine (30b).* This compound was prepared according to the general procedure described above. The following reagents, amounts, and conditions were employed: compound **29** (200 mg, 0.474 mmol), 3-fluoro-4-methoxyphenylboronic acid (89 mg, 0.523 mmol), and $Pd(PPh_3)_4$ (27 mg, 0.0234 mmol) in 1 M $K_2CO_3$ (1.2 mL) and dioxane (4 mL). The reaction mixture was stirred at 95 °C for 16 h and at 100 °C for 4 h and worked up as described above, including silica gel column chromatography ($CHCl_3$:MeOH = 97:3), yielding compound **30b** as a white solid. Recrystallization from hot MeOH/$CHCl_3$ afforded an analytically pure sample. Yield: 152 mg (76%); mp 195.0−195.8 °C. $^1$H NMR (500 MHz, DMSO-$d_6$) $\delta$ (ppm): 7.49 (dd, $J_{2''-6''}$ = 2.1, $J_{2''\text{-}F}$ = 12.8 Hz, H-2″), 7.42 (ddd, $J_{6''-5''}$ = 8.5, $J_{6''-2''}$ = 2.1, $J_{6''\text{-}F}$ = 1.2 Hz, 1H, H-6″), 7.30 (d, $J_{5''-6''}$ = 8.5, $J_{5''\text{-}F}$ = 9.1 Hz, 1H, H-5″), 7.23 (m, 1H, NH), 6.21 (s, 1H, H-7), 3.93 (s, 3H, 4″-O-$CH_3$), 3.60 (m, 4H, O-$CH_2$), 3.48 (m, 2H, H-1′), 2.63 (t, $J_{2'-1'}$ = 6.4 Hz, 2H, H-2′), 2.48 (m, 4H, *N*-$CH_2$), 2.43 (s, 3H, 2-$CH_3$). $^{13}$C NMR (125 MHz, DMSO-$d_6$) $\delta$ (ppm): 151.2 (d, $J_{3''\text{-}F}$ = 243.9 Hz, C-3″), 146.8 (C-6), 146.64 (d, $J_{4''\text{-}F}$ = 10.8 Hz, C-4″), 142.8 (C-8), 137.5 (C-2), 130.8 (C-9), 125.4 (d, $J_{6''\text{-}F}$ = 3.4 Hz, C-6″), 123.5 (d, $J_{3\text{-}F}$ = 1.7 Hz, C-3), 121.3 (d, $J_{1''\text{-}F}$ = 7.6 Hz, C-1″), 116.3 (d, $J_{2''\text{-}F}$ = 19.4 Hz, C-2″), 114.2 (d, $J_{5''\text{-}F}$ = 2.2 Hz, C-5″), 91.1 (C-7), 66.1 (O−$CH_2$), 56.2 (C-2′), 56.2 (4″-O-$CH_3$), 53.1 (*N*-$CH_2$), 39.2 (C-1′), 14.2 (2-$CH_3$). Anal. ($C_{20}H_{23}ClFN_5O_3$) C, H, N. HRMS: calcd for [M + H], 420.15971; found, 420.15963.

*6-Chloro-3-(pyridin-3-yl)-2-methyl-N-(2-morpholinoethyl)-imidazo[1,2-b]pyridazin-8-amine (30c).* This compound was prepared according to the general procedure described above. The following reagents, amounts, and conditions were employed: compound **29** (229 mg, 0.543 mmol), 3-pyridineboronic acid (73 mg, 0.594 mmol), and $Pd(PPh_3)_4$ (31 mg, 0.027 mmol) in 1 M $K_2CO_3$ (1.5 mL) and dioxane (6 mL). The reaction mixture was stirred at 95 °C overnight and at 105 °C for 8 h and worked up as described above, including silica gel column chromatography (ethyl acetate:acetone:ethanol:water (21:3:0.5:0.5) → ethyl acetate:acetone:ethanol:water (20:3:1:1)), yielding compound **30c** as a white solid. Recrystallization from hot EtOAc/MeOH afforded an analytically pure sample. Yield: 107 mg (53%); mp 179.1−180.0 °C. $^1$H NMR (500 MHz, DMSO-$d_6$) $\delta$ (ppm): 8.84 (dd, $J_{2''\text{-}5''}$ = 0.8, $J_{2''-4''}$ = 2.3 Hz, H-2″), 8.59 (dd, $J_{6''-4''}$ = 1.7, $J_{6''-5''}$ = 4.8 Hz, 1H, H-6″), 8.07 (ddd, $J_{4''-6''}$ = 1.7, $J_{4''-2''}$ = 2.3, $J_{4''-5''}$ = 7.9 Hz, 1H, H-4″), 7.66 (t, $J_{NH\text{-}1'}$ = 5.8 Hz, 1H, 8-NH), 7.56 (ddd, $J_{5''\text{-}2''}$ = 0.8, $J_{5''-6''}$ = 4.8, $J_{5''-4''}$ = 7.9 Hz, 1H, H-5″), 6.31 (s, 1H, H-7), 3.57 (m, 4H, O-$CH_2$), 3.44 (m, 2H, H-1′), 2.57 (t, $J_{2'-1'}$ = 6.3 Hz, 2H, H-2′), 2.46 (m, 4H, *N*-$CH_2$), 2.42 (s, 3H, 2-$CH_3$). $^{13}$C NMR (125 MHz, DMSO-$d_6$) $\delta$ (ppm): 149.6 (C-2″), 148.7 (C-6″), 147.4 (C-6), 143.2 (C-8), 138.7 (C-2), 136.5 (C-4″), 131.7 (C-9), 125.0 (C-3″), 123.8 (C-5″), 122.1 (C-3), 91.6 (C-7), 66.4 (O-$CH_2$), 56.5 (C-2′), 53.4 (*N*-$CH_2$), 38.9 (C-1′), 14.5 (2-$CH_3$). Anal. ($C_{18}H_{21}ClN_6O$) C, H, N. HRMS: calcd for [M + H], 373.15381; found, 373.15371.

**8-(3,4-Dimethoxyphenyl)-2,7-dimethylpyrazolo[1,5-*a*]-[1,3,5]triazin-4(3*H*)-one (32).** A mixture 8-bromo-2,7-dimethylpyrazolo[1,5-*a*][1,3,5]triazin-4(3*H*)-one (**23**) (700 mg, 2.9 mmol), $Na_2CO_3$ (436 mg, 4.4 mmol), boronic acid (757 mg, 4.4 mmol), and Pd(dppf)$Cl_2$ (232 mg, 10%) in deoxygenated dioxane (30 mL) and water (7.5 mL) was heated under argon atmosphere for 16 h at 95 °C. After cooling to ambient temperature, the mixture was partitioned between ethyl acetate (250 mL) and brine (100 mL). Water phase was extracted with ethyl acetate (2 × 200 mL). Organic phases were combined, dried over anhydrous sodium sulfate, and evaporated. The crude product was chromatographed on a silica gel column (200 g) in ethyl acetate → ethyl acetate:toluene:acetone:ethanol (17:4:3:1). Product **24** was obtained after recrystallization from ethyl acetate as an off-white solid. Yield: 653 mg (75%); mp 251.5−252 °C. $^1$H NMR (400 MHz, DMSO-$d_6$) $\delta$ (ppm): 12.36 (bs, 1H, NH), 7.22 (d, $J_{2'-6'}$ = 1.9 Hz, 1H, H-2′), 7.12 (dd, $J_{6'-2'}$ = 1.9, $J_{6'-5'}$ = 8.3 Hz, 1H, H-6′), 7.02 (d, $J_{5'-6'}$ = 8.3 Hz, 1H, H-5′), 3.78 (s, 6H, 4′-$OCH_3$, 3′-$OCH_3$), 2.42 (s, 3H, 7-$CH_3$), 2.32 (s, 3H, 2-$CH_3$). $^{13}$C NMR (100 MHz, DMSO-$d_6$) $\delta$ (ppm): 154.3 (C-2), 152.8 (C-7), 148.7 (C-3′), 147.9 (C-4′), 145.4 (C-8a), 144.1 (C-4), 124.0 (C-1′), 121.2 (C-6′), 112.7 (C-2′), 112.1 (C-5′), 110.3 (C-8), 55.7 (3′-$OCH_3$, 4′-$OCH_3$), 21.2 (2-$CH_3$), 14.5 (7-$CH_3$). Anal. ($C_{15}H_{15}N_4O_3$) C, H, N. ESI MS, *m*/*z* (rel%): 23 (100) [M + Na]. HRMS: calcd for [M + Na], 323.11146; found, 323.11154.

**8-(3,4-Dimethoxyphenyl)-2,7-dimethyl-*N*-(2-morpholinoethyl)pyrazolo[1,5-*a*][1,3,5]triazin-4-amine (18).** Compound **32** (300 mg, 1 mmol) was suspended in $POCl_3$ (7 mL) and dimethylaniline (0.4 mL), and the reaction mixture was heated at 120 °C for 20 h, cooled down, and evaporated to dryness. The residue was dissolved in $CH_2Cl_2$ (20 mL) at 0 °C and 2-morpholinoethanamine (0.92 mL, 7 mmol), and the reaction mixture was stirred for 16 h. Then reaction mixture was diluted with solution of satd aq sodium bicarbonate (50 mL) and extracted with ethyl acetate (2 × 150 mL). Combined organic phases were dried with sodium sulfate and evaporated. Residue was chromatographed on silica gel column (100 g) in ethyl acetate → ethyl acetate:toluene:acetone:ethanol (17:4:3:2) to afford product **18** which was recrystallized from ethyl acetate. Yield: 280 mg (68%); mp 126−126.5 °C. $^1$H NMR (600 MHz, DMSO-$d_6$) $\delta$ (ppm): 8.43 (t, $J_{NH\text{-}2'}$ = 5.8 Hz, 1H, NH), 7.31 (d, $J_{2''-6''}$ = 2.0 Hz, 1H, H-2″), 7.17 (dd, $J_{6''-2''}$ = 2.0, $J_{6''-5''}$ = 8.3 Hz, 1H, H-6″), 7.02 (d, $J_{5''-6''}$ = 8.3 Hz, 1H, H-5″), 3.79 (s, 3H, 3″-$OCH_3$), 3.78 (s, 3H, 4″-$OCH_3$), 3.63 (m, 2H, H-2′), 3.55 (m, 4H, morph-O($CH_2$)$_2$), 2.56 (t, $J_{1'-2'}$ =



DOI: 10.1021/acs.jmedchem.5b00499
J. Med. Chem. 2015, 58, 3767−3793

6.5 Hz, 2H, H-1′), 2.51 (s, 3H, 7-$CH_3$), 2.44 (bs, 4H, morph-N($CH_2$)$_2$), 2.38 (s, 3H, 2-$CH_3$). $^{13}$C NMR (150 MHz, DMSO-$d_6$) $\delta$ (ppm): 163.0 (C-2), 152.1 (C-7), 148.7 (C-3″), 148.2 (C-4), 147.4 (C-4″),146.0 (C-8a), 124.9 (C-1″), 120.9 (C-6″), 112.7 (C-2″), 112.2 (C-5″), 106.9 (C-8), 66.4 (morph-O($CH_2$)$_2$), 57.2 (C-1′), 55.9 and 55.8 (3″-OCH3, 4″-$OCH_3$), 53.4 (morph-N($CH_2$)$_2$), 37.1 (C-2′), 26.0 (2-$CH_3$), 14.5 (7-$CH_3$). Anal. ($C_{21}H_{28}N_6O_3$) C, H, N. ESI MS, *m/z* (rel%): 413 (100) [M + H]. HRMS: calcd for [M + H], 413.22957; found, 413.22980.

***N*-(2-(8-(3,4-Dimethoxyphenyl)-2,7-dimethylpyrazolo[1,5-*a*][1,3,5]triazin-4-ylamino)ethyl)acetamide (33).** Compound **32** (300 mg, 1 mmol) was suspended in $POCl_3$ (7 mL) and dimethylaniline (0.4 mL), and the reaction mixture was heated at 120 °C for 20 h, cooled down, and evaporated to dryness. The residue was dissolved in $CH_2Cl_2$ (20 mL) at 0 °C and *N*-(2-aminoethyl)-acetamide (0.67 mL, 7 mmol), and the reaction mixture was stirred for 16 h. Then reaction mixture was diluted with solution of satd aq sodium bicarbonate (50 mL) and extracted with ethyl acetate (2 × 150 mL). Combined organic phases were dried with sodium sulfate and evaporated. Residue was chromatographed on silica gel column (100 g) in ethyl acetate → ethyl acetate:toluene:acetone:ethanol (17:4:3:2) to afford product **33** as a solid which was recrystallized from ethyl acetate. Yield: 250 mg (65%); mp 203.5 204 °C. $^1$H NMR (600 MHz, DMSO-$d_6$) $\delta$ (ppm): 8.59 (t, $J_{NH\text{-}2}$ = 5.8 Hz, 1H, NH), 7.98 (t, $J_{NH\text{-}1}$ = 5.7 Hz, 1H, NHCO), 7.31 (d, $J_{2''-6''}$ = 2.0 Hz, 1H, H-2″), 7.18 (dd, $J_{6''-2''}$ = 2.0, $J_{6''-5''}$ = 8.3 Hz, 1H, H-6″),7.02 (d, $J_{5''-6''}$ = 8.3 Hz, 1H, H-5″), 3.79 (s, 3H, 3″-$OCH_3$), 3.78 (s, 3H, 4″-$OCH_3$), 3.56 (m, 2H, H-2), 3.32 (m, 2H, H-1), 2.52 (s, 3H, 7′-$CH_3$), 2.39 (s, 3H, 2′-$CH_3$), 1.79 (s, 3H, $COCH_3$). $^{13}$C NMR (150 MHz, DMSO-$d_6$) $\delta$ (ppm): 169.7 (CO), 162.9 (C-2′), 152.0 (C-7′), 148.7 (C-3″), 148.4 (C-4′), 147.4 (C-4″), 146.1 (C-8′a), 124.9 (C-1″), 120.9 (C-6″), 112.7 (C-2″), 112.2 (C-5″), 106.8 (C-8′), 55.7 and 55.8 (3″-OCH3, 4″-$OCH_3$), 40.1 (C-2), 38.3 (C-1), 26.0 (2′-$CH_3$), 22.8 ($COCH_3$), 14.5 (7′-$CH_3$). Anal. ($C_{20}H_{25}N_5O_3$) C, H, N. ESI MS, *m/z* (rel%): 407 (100) [M + Na]. HRMS: calcd for [M + H], 385.19827; found, 385.19833.

**6,8-Dichloro-3-iodo-2-methylimidazo[1,2-*b*]pyridazine (34).** To the suspension of 6,8-dichloro-2-methylimidazo[1,2-*b*]pyridazine (1.155 g, 5.78 mmol) in DMF (8 mL), NIS (1.43 g, 6.36 mmol) was added in one portion, followed by acetic acid (0.5 mL, 8.67 mmol). The reaction mixture was stirred overnight at 65 °C, cooled to rt, and partitioned between DCM/$Na_2S_2O_3$ (100 mL each). The inorganic phase was washed with DCM (2 × 50 mL), and the combined organic phases were dried over sodium sulfate and evaporated. Oily residue was dissolved in minimum amount of DCM, adsorbed onto silica, and purified by flash column chromatography (hexane/EtOAc 15−25%), affording **34** as yellow solid. An analytical sample was obtained after recrystallization from hot acetone. Yield: 1.745 g (93%); mp 127.1−127.7 °C. $^1$H NMR (500 MHz, DMSO-$d_6$) $\delta$ (ppm): 7.81 (s, 1 H, H-7), 2.43 (s, 3 H, 2-$CH_3$). $^{13}$C NMR (125 MHz, DMSO-$d_6$) $\delta$ (ppm): 148.5 (C-2), 145.4 (C-6), 138.0 (C-8), 132.6 (C-9), 118.2 (C-7), 75.1 (C-3), 15.3 (2-$CH_3$). Anal. ($C_7H_4Cl_2N_3I$) C, H, N. HRMS: calcd for [M + H], 327.88997; found, 327.89011.

***N*-(2-((6-Chloro-3-iodo-2-methylimidazo[1,2-*b*]pyridazin-8-yl)amino)ethyl)acetamide (35).** To a solution of **34** (0.43 g, 1.3112 mmol) in EtOH (5 mL), DIPEA (0.365 mL, 1.6 equiv) and *N*-(2-aminoethyl)acetamide (0.2 mL, 1.6 equiv) were subsequently added and the mixture was heated in a microwave reactor at 100 °C for 2 h. Silica gel column chromatography (EtOAc:acetone:EtOH:water, 20:3:1.6:0.4) afforded product **26** as a yellowish solid. Recrystallization from hot MeOH/$CHCl_3$ yielded an analytically pure sample. Yield: 0.465 g (90%). $^1$H NMR (500 MHz, DMSO-$d_6$) $\delta$ (ppm): 8.03 (t, $J_{NH\text{-}1}$ = 5.6 Hz, 1H, NH-CO), 7.87 (t, $J_{NH\text{-}2}$ = 6.0 Hz, 1H, 8′-NH), 6.30 (s, 1H, H-7′), 3.33 (bs, 2H, H-2), 3.23 (m, 2H, H-1), 2.34 (s, 3H, 2′-$CH_3$), 1.79 (s, 3H, $COCH_3$). $^{13}$C NMR (125 MHz, DMSO-$d_6$) $\delta$ (ppm): 170.0 (C═O), 147.7 (C-6′), 143.7 (C-2′), 143.1 (C-8′), 134.3 (C-9′), 91.7 (C-7′), 71.7 (C-3′), 41.9 (C-2), 37.8 (C-1), 22.8 ($COCH_3$), 14.9 (2′-$CH_3$). HRMS: calcd for [M + H], 393.99261; found, 393.99255.

**General Procedure for Suzuki Coupling Reactions: Preparation of Compounds 36a−u.** A round-bottom flask was charged with **34** and appropriate boronic acid derivative (1.1 equiv), 1,4-dioxane:water (4:1), and potassium carbonate (3 equiv). A flask was equipped with stir bar and rubber septum, stirred at RT, and degassed 3 times and purged with argon. To the reaction mixture, Pd($PPh_3$)$_4$ (5 mol %) was added in one portion and the suspension was refluxed for 2 h and then stirred at 95 °C overnight under argon atmosphere. Upon completion of the reaction (monitored by TLC), the mixture was cooled to rt, diluted with water, and extracted with DCM (3 × 50 mL). Combined organic phases were dried over sodium sulfate, evaporated, and purified by column chromatography.

*N-(2-((6-Chloro-3-(3,4-dimethoxyphenyl)-2-methylimidazo[1,2-b]pyridazin-8-yl)amino)ethyl)acetamide (**36a**).* Mobile phase: ethyl acetate:acetone:ethanol:water (21:3:0.5:0.5). Recrystallization from hot MeOH. Yield 237 mg (97%) as an off-white solid; mp 192.4−194.2 °C. $^1$H NMR (500 MHz, DMSO-$d_6$) $\delta$ (ppm): 8.05 (t, $J_{NH\text{-}1}$ = 5.7 Hz, 1H, NH-CO), 7.81 (t, $J_{NH\text{-}2}$ = 6.0 Hz, 1H, 8′-NH), 7.20 (d, $J_{2''-6''}$ = 2.0 Hz, 1H, H-2″), 7.15 (dd, $J_{6''-2''}$ = 2.0, $J_{6''-5''}$ = 8.3 Hz, 1H, H-6″), 7.10 (d, $J_{5''-6''}$ = 8.3 Hz, 1H, H-5″), 6.26 (s, 1H, H-7′), 3.82 (s, 3H, 4″-O-$CH_3$), 3.78 (s, 3H, 3″-O-$CH_3$), 3.36 (m, 2H, H-2), 3.26 (m, 2H, H-1), 2.41 (s, 3H, 2′-$CH_3$), 1.80 (s, 3H, $COCH_3$). $^{13}$C NMR (125 MHz, DMSO-$d_6$) $\delta$ (ppm): 170.0 (C═O), 148.8 (C-4″), 148.6 (C-3″), 147.1 (C-6′), 143.3 (C-8′), 137.4 (C-2′), 130.9 (C-9′), 125.1 (C-3′), 122.2 (C-6″), 121.0 (C-1″), 113.2 (C-2″), 112.0 (C-5″), 90.9 (C-7′), 55.8 (3″-O-$CH_3$, 4″-O-$CH_3$), 41.8 (C-2), 37.9 (C-1), 22.8 ($COCH_3$), 14.6 (2′-$CH_3$). Anal. ($C_{19}H_{22}ClN_5O_3$) C, H, N. HRMS: calcd for [M + H], 404.14839; found, 404.14827.

*N-(2-((6-Chloro-2-methyl-3-(pyridin-3-yl)imidazo[1,2-b]pyridazin-8-yl)amino)ethyl)acetamide (**36b**).* Mobile phase: ethyl acetate:acetone:ethanol:water (21:3:0.5:0.5) → ethyl acetate:acetone:ethanol:water (20:3:1:1). Recrystallization from hot MeOH. Yield: 178 mg (85%) as a white solid; mp 211.1−212.4 °C. $^1$H NMR (500 MHz, DMSO-$d_6$) $\delta$ (ppm): 8.84 (dd, $J_{2''-5''}$ = 0.8, $J_{2''-4''}$ = 2.2 Hz, 1H, H-2″), 8.60 (dd, $J_{6''-5''}$ = 4.8, $J_{6''-4''}$ = 1.6 Hz, 1H, H-6″), 8.07 (ddd, $J_{4''-6''}$ = 1.6, $J_{4''-2''}$ = 2.2, $J_{4''-5''}$ = 7.9 Hz, 1H, H-4″), 8.05 (t, $J_{NH\text{-}1}$ = 5.7 Hz, 1H, NH−CO), 7.94 (t, $J_{NH\text{-}2}$ = 6.1 Hz, 1H, 8′-NH), 7.56 (ddd, $J_{5''-2''}$ = 0.8, $J_{5''-6''}$ = 4.8, $J_{5''-4''}$ = 7.9 Hz, 1H, H-5″), 6.32 (s, 1H, H-7′), 3.37 (m, 2H, H-2), 3.26 (m, 2H, H-1), 2.44 (s, 3H, 2′-$CH_3$), 1.80 (s, 3H, $COCH_3$). $^{13}$C NMR (125 MHz, DMSO-$d_6$) $\delta$ (ppm): 170.0 (C═O), 149.6 (C-2″), 148.7 (C-6″), 147.4 (C-6′), 143.4 (C-8′), 138.7 (C-2′), 136.5 (C-4″), 131.7 (C-9′), 125.0 (C-3″), 123.8 (C-5″), 122.1 (C-3′), 91.5 (C-7′), 41.8 (C-2), 37.8 (C-1), 22.8 ($COCH_3$), 14.5 (2′-$CH_3$). Anal. ($C_{16}H_{17}ClN_6O$) C, H, N. HRMS: calcd for [M + H]: 345.12251, found 345.12254

*N-(2-((6-Chloro-2-methyl-3-(thiophen-3-yl)imidazo[1,2-b]pyridazin-8-yl)amino)ethyl)acetamide (**36c**).* Mobile phase: ethyl acetate:toluene:acetone:ethanol (17:4:4:1) → ethyl acetate:acetone:ethanol:water (21:3:0.5:0.5). Recrystallization from hot MeOH. Yield: 143 mg (67%) as a white solid; mp 197.4−199.0 °C. $^1$H NMR (500 MHz, DMSO-$d_6$) $\delta$ (ppm): 8.05 (t, $J_{NH\text{-}1}$ = 5.6 Hz, 1H, NH-CO), 7.95 (dd, $J_{2''-4''}$ = 1.2, $J_{2''-5''}$ = 3.0 Hz, 1H, H-2″), 7.85 (t, $J_{NH\text{-}2}$ = 6.1 Hz, 1H, 8′-NH), 7.71 (dd, $J_{5''-2''}$ = 3.0, $J_{5''-4''}$ = 5.0 Hz, 1H, H-5″), 7.60 (dd, $J_{4''-2''}$ = 1.2, $J_{4''-5''}$ = 5.0 Hz, 1H, H-4″), 6.29 (s, 1H, H-7′), 3.37 (bs, 2H, H-2), 3.26 (m, 2H, H-1), 2.49 (s, 3H, 2′-$CH_3$), 1.80 (s, 3H, $COCH_3$). $^{13}$C NMR (125 MHz, DMSO-$d_6$) $\delta$ (ppm): 170.0 (C═O), 147.2 (C-6′), 143.3 (C-8′), 137.7 (C-2′), 130.9 (C-9′), 128.7 (C-3″), 127.4 (C-4″), 126.2 (C-5″), 123.7 (C-2″), 121.4 (C-3′), 91.0 (C-7′), 41.8 (C-2), 37.9 (C-1), 22.8 ($COCH_3$), 15.3 (2′-$CH_3$). Anal. ($C_{15}H_{16}ClN_5OS$) C, H, N. HRMS: calcd for [M + H], 350.08369; found, 350.08372.

*N-(2-((6-Chloro-3-(3,5-dimethoxyphenyl)-2-methylimidazo[1,2-b]pyridazin-8-yl)amino)ethyl)acetamide (**36d**).* Mobile phase: ethyl acetate:toluene:acetone:ethanol (17:4:4:1) → ethyl acetate:acetone:ethanol:water (21:3:0.5:0.5). Recrystallization from hot MeOH. Yield: 112 mg (46%) as a white solid; mp 160.5−161.0 °C. $^1$H NMR (500 MHz, DMSO-$d_6$) $\delta$ (ppm): 8.04 (t, $J_{NH\text{-}1}$ = 5.6 Hz, 1H, NH−CO), 7.86 (t, $J_{NH\text{-}2}$ = 6.0 Hz, 1H, 8′-NH), 6.78 (d, $J_{2''-4''}$ = 2.3 Hz, 2H, H-2″), 6.57 (t, $J_{4''-2''}$ = 2.3 Hz, 1H, H-4″), 6.28 (s, 1H, H-7′), 3.79 (s, 6H, 3″-O-$CH_3$), 3.37 (bs, 2H, H-2), 3.26 (m, 2H, H-1), 2.43 (s, 3H, 2′-



DOI: 10.1021/acs.jmedchem.5b00499
J. Med. Chem. 2015, 58, 3767−3793

$CH_3$), 1.80 (s, 3H, $COCH_3$). $^{13}C$ NMR (125 MHz, DMSO-$d_6$) $\delta$ (ppm): 170.0 (C═O), 160.5 (C-3″), 147.1 (C-6′), 143.3 (C-8′), 138.0 (C-2′), 131.2 (C-9′), 130.3 (C-1″), 124.8 (C-3′), 107.5 (C-2″), 99.6 (C-4″), 91.1 (C-7′), 55.5 (3″-O-$CH_3$), 41.8 (C-2), 37.8 (C-1), 22.8 ($COCH_3$), 14.8 (2′-$CH_3$). Anal. ($C_{19}H_{22}ClN_5O_3$) C, H, N. HRMS: calcd for [M + H], 404.14839; found, 404.14815.

*N-(2-((6-Chloro-3-(3-formylphenyl)-2-methylimidazo[1,2-b]pyridazin-8-yl)amino)ethyl)acetamide* ***(36e)***. Mobile phase: ethyl acetate:acetone:ethanol:water (21:3:0.5:0.5). Recrystallization from hot EtOAc. Yield: 234 mg (quant) as a white solid; mp 185.6−186.6 °C. $^1H$ NMR (500 MHz, DMSO-$d_6$) $\delta$ (ppm): 10.09 (s, 1H, CHO), 8.17 (t, $J_{2''-6''} = J_{2''-4''} = 1.7$ Hz, 1H, H-2″), 8.05 (t, $J_{NH\text{-}1} = 5.7$ Hz, 1H, NH-CO), 7.99 (ddd, $J_{6''-4''} = 1.2$, $J_{6''-2''} = 1.7$, $J_{6''-5''} = 7.7$ Hz, 1H, H-6″), 7.94 (dm, $J_{4''-5''} = 7.7$ Hz, 1H, H-4″), 7.92 (t, $J_{NH\text{-}2} = 6.1$ Hz, 1H, 8′-NH), 7.76 (t, $J_{5''-4''} = J_{5''-6''} = 7.7$ Hz, 1H, H-5″), 6.32 (s, 1H, H-7′), 3.38 (m, 2H, H-2), 3.27 (m, 2H, H-1), 2.45 (s, 3H, 2′-$CH_3$), 1.81 (s, 3H, $COCH_3$). $^{13}C$ NMR (125 MHz, DMSO-$d_6$) $\delta$ (ppm): 193.3 (−CHO), 170.0 (HN-C═O), 147.3 (C-6′), 143.4 (C-8′), 138.5 (C-2′), 136.6 (C-3″), 135.0 (C-6″), 131.5 (C-9′), 130.0 (C-2″), 129.6 (C-1″), 129.5 (C-5″), 128.8 (C-4″), 123.8 (C-3′), 91.4 (C-7′), 41.8 (C-2), 37.8 (C-1), 22.8 ($COCH_3$), 14.6 (2′-$CH_3$). Anal. ($C_{18}H_{18}ClN_5O_2$) C, H, N. HRMS: calcd for [M + H], 372.12218; found, 372.12163.

*N-(2-((6-Chloro-2-methyl-3-(3,4,5-trimethoxyphenyl)imidazo[1,2-b]pyridazin-8-yl)amino)ethyl)acetamide* ***(36f)***. Mobile phase: ethyl acetate:toluene:acetone:ethanol (17:4:4:1) → ethyl acetate:acetone:ethanol:water (21:3:0.5:0.5). Recrystallization from hot MeOH. Yield: 285 mg (96%) as a white solid; mp 154.5−155.4 °C. $^1H$ NMR (500 MHz, DMSO-$d_6$) $\delta$ (ppm): 8.04 (t, $J_{NH\text{-}1} = 5.5$ Hz, 1H, NH-CO), 7.85 (t, $J_{NH\text{-}2} = 6.1$ Hz, 1H, 8′-NH), 6.92 (s, 2H, H-2″), 6.28 (s, 1H, H-7′), 3.81 (s, 6H, 3″-O-$CH_3$), 3.73 (s, 3H, 4″-O-$CH_3$), 3.37 (bs, 2H, H-2), 3.26 (m, 2H, H-1), 2.45 (s, 3H, 2′-$CH_3$), 1.80 (s, 3H, $COCH_3$). $^{13}C$ NMR (125 MHz, DMSO-$d_6$) $\delta$ (ppm): 170.0 (C═O), 153.0 (C-3″), 147.1 (C-6′), 143.3 (C-8′), 137.8 (C-2′), 137.5 (C-4″), 131.0 (C-9′), 125.0 (C-3′), 124.0 (C-1″), 107.1 (C-2″), 91.0 (C-7′), 60.3 (4″-O-$CH_3$), 56.2 (3″-O-$CH_3$), 41.8 (C-2), 37.9 (C-1), 22.8 ($COCH_3$), 14.7 (2′-$CH_3$). Anal. ($C_{20}H_{24}ClN_5O_4$) C, H, N. HRMS: calcd for [M + H], 456.14090; found, 456.14077.

*N-(2-((6-Chloro-3-(3-methoxyphenyl)-2-methylimidazo[1,2-b]pyridazin-8-yl)amino)ethyl)acetamide* ***(36g)***. Mobile phase: ethyl acetate:acetone:ethanol:water (21:3:0.5:0.5). Recrystallization from hot MeOH. Yield: 219 mg (96%) as a white solid; mp 186.3−187.0 °C. $^1H$ NMR (500 MHz, DMSO-$d_6$) $\delta$ (ppm): 8.04 (t, $J_{NH\text{-}1} = 5.7$ Hz, 1H, NH-CO), 7.86 (t, $J_{NH\text{-}2} = 6.1$ Hz, 1H, 8′-NH), 7.43 (t, $J_{5''-4''} = J_{5''-6''} = 8.1$ Hz, 1H, H-5″), 7.21−7.19 (m, 2H, H-2″, H-6″), 6.99 (dm, $J_{4''-5''} = 8.1$ Hz, H-4″), 6.29 (s, 1H, H-7′), 3.80 (s, 3H, 3″-O-$CH_3$), 3.37 (m, 2H, H-2), 3.26 (m, 2H, H-1), 2.43 (s, 3H, 2′-$CH_3$), 1.80 (s, 3H, $COCH_3$). $^{13}C$ NMR (125 MHz, DMSO-$d_6$) $\delta$ (ppm): 170.0 (C═O), 159.3 (C-3″), 147.2 (C-6′), 143.3 (C-8′), 138.0 (C-2′), 131.2 (C-9′), 129.9 (C-1″), 129.7 (C-5″), 124.8 (C-3′), 121.6 (C-6″), 115.1 (C-2″), 113.3 (C-4″), 91.1 (C-7′), 55.4 (3″-O-$CH_3$), 41.8 (C-2), 37.9 (C-1), 22.8 ($COCH_3$), 14.7 (2′-$CH_3$). Anal. ($C_{18}H_{20}ClN_5O_2$) C, H, N. HRMS: calcd for [M + H], 396.11977; found, 396.11976.

*N-(2-((6-Chloro-3-(4-cyanophenyl)-2-methylimidazo[1,2-b]pyridazin-8-yl)amino)ethyl)acetamide* ***(36h)***. Mobile phase: ethyl acetate:toluene:acetone:ethanol (17:4:4:1) → ethyl acetate:acetone:ethanol:water (21:3:0.5:0.5). Recrystallization from hot MeOH/$CHCl_3$. Yield: 207 mg (92%) as a white solid; mp 218.0−219.5 °C. $^1H$ NMR (500 MHz, DMSO-$d_6$) $\delta$ (ppm): 8.04 (t, $J_{NH\text{-}1} = 5.6$ Hz, 1H, NH-CO), 7.97 (m, 2H, H-2″), 7.96 (t, $J_{NH\text{-}2} = 6.2$ Hz, 1H, 8′-NH), 7.88 (m, 2H, H-3″), 6.34 (s, 1H, H-7′), 3.36 (m, 2H, H-2), 3.26 (m, 2H, H-1), 2.46 (s, 3H, 2′-$CH_3$), 1.80 (s, 3H, $COCH_3$). $^{13}C$ NMR (125 MHz, DMSO-$d_6$) $\delta$ (ppm): 170.0 (C═O), 147.5 (C-6′), 143.4 (C-8′), 139.5 (C-2′), 133.4 (C-1″), 132.5 (C-2″), 132.0 (C-9′), 129.4 (C-3″), 123.3 (C-3′), 119.1 (C-4″), 109.9 (CN), 91.8 (C-7′), 41.8 (C-2), 37.8 (C-1), 22.8 ($COCH_3$), 14.9 (2′-$CH_3$). Anal. ($C_{18}H_{17}ClN_6O$) C, H, N. HRMS: calcd for [M + H], 369.12251; found, 369.12252.

*N-(2-((6-Chloro-3-(4-formylphenyl)-2-methylimidazo[1,2-b]pyridazin-8-yl)amino)ethyl)acetamide* ***(36i)***. Mobile phase: ethyl acetate:acetone:ethanol:water (21:3:0.5:0.5). Recrystallization from hot MeOH. Yield: 206 mg (91%) as a white solid; mp 193.9−195.2 °C. $^1H$ NMR (500 MHz, DMSO-$d_6$) $\delta$ (ppm): 10.05 (s, 1H, CHO), 8.06−8.02 (m, 3H, H-3″, NH−CO), 7.94 (t, $J_{NH\text{-}2} = 6.0$ Hz, 1H, 8′-NH), 7.91 (m, 2H, H-2″), 6.34 (s, 1H, H-7′), 3.37 (m, 2H, H-2), 3.27 (m, 2H, H-1), 2.48 (s, 3H, 2′-$CH_3$), 1.81 (s, 3H, $COCH_3$). $^{13}C$ NMR (125 MHz, DMSO-$d_6$) $\delta$ (ppm): 192.8 (CHO), 170.0 (HN-C═O), 147.4 (C-6′), 143.4 (C-8′), 139.4 (C-2′), 135.0 (C-4″), 134.6 (C-1″), 131.9 (C-9′), 129.7 (C-3″), 129.2 (C-2″), 123.9 (C-3′), 91.7 (C-7′), 41.8 (C-2), 37.8 (C-1), 22.8 ($COCH_3$), 15.0 (2′-$CH_3$). Anal. ($C_{18}H_{18}ClN_5O_2$) C, H, N. HRMS: calcd for [M + H], 372.12218; found, 372.12207.

*N-(2-((6-Chloro-3-(4-methoxyphenyl)-2-methylimidazo[1,2-b]pyridazin-8-yl)amino)ethyl)acetamide* ***(36j)***. Mobile phase: ethyl acetate:acetone:ethanol:water (21:3:0.5:0.5). Recrystallization from hot MeOH. Yield: 88 mg (39%) as a white solid; mp 210.1−212.0 °C. $^1H$ NMR (500 MHz, DMSO-$d_6$) $\delta$ (ppm): 8.04 (t, $J_{NH\text{-}1} = 5.6$ Hz, 1H, NH-CO), 7.82 (t, $J_{NH\text{-}2} = 6.0$ Hz, 1H, 8′-NH), 7.54 (m, 2H, H-2″), 7.08 (m, 2H, H-3″), 6.26 (s, 1H, H-7′), 3.82 (s, 3H, 4″-O-$CH_3$), 3.36 (bs, 2H, H-2), 3.26 (m, 2H, H-1), 2.39 (s, 3H, 2′-$CH_3$), 1.80 (s, 3H, $COCH_3$). $^{13}C$ NMR (125 MHz, DMSO-$d_6$) $\delta$ (ppm): 170.0 (C═O), 159.0 (C-4″), 147.1 (C-6′), 143.3 (C-8′), 137.2 (C-2′), 130.8 (C-9′), 130.7 (C-2″), 125.0 (C-3′), 120.8 (C-1″), 114.1 (C-3″), 90.8 (C-7′), 55.4 (4″-O-$CH_3$), 41.7 (C-2), 37.9 (C-1), 22.8 ($COCH_3$), 14.5 (2′-$CH_3$). Anal. ($C_{18}H_{20}ClN_5O_2$) C, H, N. HRMS: calcd for [M + H], 374.13783; found, 374.13761.

*N-(2-((6-Chloro-3-(4-chlorophenyl)-2-methylimidazo[1,2-b]pyridazin-8-yl)amino)ethyl)acetamide* ***(36k)***. Mobile phase: ethyl acetate:acetone:ethanol:water (21:3:0.5:0.5). Recrystallization from hot EtOAc/MeOH. Yield: 171 mg (77%) as a white solid; mp 211.5−212.7 °C. $^1H$ NMR (500 MHz, DMSO-$d_6$) $\delta$ (ppm): 8.04 (t, $J_{NH\text{-}1} = 5.7$ Hz, 1H, NH-CO), 7.82 (t, $J_{NH\text{-}2} = 6.0$ Hz, 1H, 8′-NH), 7.67 (m, 2H, H-2″), 7.58 (m, 2H, H-3″), 6.30 (s, 1H, H-7′), 3.37 (m, 2H, H-2), 3.26 (m, 2H, H-1), 2.42 (s, 3H, 2′-$CH_3$), 1.80 (s, 3H, $COCH_3$). $^{13}C$ NMR (125 MHz, DMSO-$d_6$) $\delta$ (ppm): 170.0 (C═O), 147.3 (C-6′), 143.3 (C-8′), 138.2 (C-2′), 132.5 (C-4″), 131.4 (C-9′), 130.9 (C-2″), 128.7 (C-3″), 127.5 (C-1″), 123.8 (C-3′), 91.3 (C-7′), 41.8 (C-2), 37.8 (C-1), 22.8 ($COCH_3$), 14.6 (2′-$CH_3$). Anal. ($C_{17}H_{17}Cl_2N_5O$) C, H, N. HRMS: calcd for [M + H], 378.08829; found, 378.08806.

*Methyl 3-(8-((2-Acetamidoethyl)amino)-6-chloro-2-methylimidazo[1,2-b]pyridazin-3-yl)benzoate* ***(36l)***. Mobile phase: EtOAc:acetone:EtOH:water (20:3:1.2:0.8). Recrystallized from hot MeOH. Yield: 64 mg (40%); mp 181−181.9 °C. $^1H$ NMR (500 MHz, DMSO-$d_6$) $\delta$ (ppm): 8.22 (td, $J_{2-4,2-6} = 1.8$, $J_{2-5} = 0.4$ Hz, 1H, H-2), 8.06 (t, $J_{NH\text{-}2} = 5.6$ Hz, 1H, NH-CO), 7.99 (ddd, $J_{6-5} = 7.8$, $J_{6-2} = 1.8$, $J_{6-4} = 1.2$ Hz, 1H, H-6), 7.92 (ddd, $J_{4-2} = 1.8$, $J_{4-6} = 1.2$, $J_{4-5} = 7.8$ Hz, 1H, H-4), 7.91 (t, $J_{NH\text{-}1} = 6.1$ Hz, 1H, 8′-NH), 7.69 (td, $J_{5-4,\,5-6} = 7.8$, $J_{5-2} = 0.4$ Hz, 1H, H-5), 6.32 (s, 1H, H-7′), 3.89 (s, 3H, 1-$COOCH_3$), 3.38 (m, 2H, H-1″), 3.27 (m, 2H, H-2″), 2.43 (s, 3H, 2′-$CH_3$), 1.81 (s, 3H, $NHCOCH_3$). $^{13}C$ NMR (125 MHz, DMSO-$d_6$) $\delta$ (ppm): 170.0 (C═O), 166.3 (1-CO), 147.4 (C-6′), 143.4 (C-8′), 138.4 (C-2′), 133.9 (C-4), 131.5 (C-9′), 130.1 (C-1), 129.7 (C-2), 129.3 (C-5), 129.3 (C-3), 128.5 (C-6), 123.9 (C-3′), 91.4 (C-7′), 52.6 (CO-O-$CH_3$), 41.8 (C-1″), 37.9 (C-2″), 22.8 (NH-CO-$CH_3$), 14.6 (2′-$CH_3$). Anal. ($C_{19}H_{21}O_3N_5Cl$) C, H, N. HRMS: calcd for [M + H], 402.13274; found, 402.13316.

*N-(2-((3-(Benzo[d][1,3]dioxol-5-yl)-6-chloro-2-methylimidazo[1,2-b]pyridazin-8-yl)amino)ethyl)acetamide* ***(36m)***. Mobile phase: EtOAc:acetone:EtOH:water (20:3:1.2:0.8). Recrystallized from hot MeOH. Yield: 80 mg (40%); mp 183.2−183.9 °C. $^1H$ NMR (500 MHz, DMSO-$d_6$) $\delta$ (ppm): 8.04 (t, $J_{NH\text{-}1} = 5.7$ Hz, 1H, NH-CO), 7.83 (t, $J_{NH\text{-}2} = 6.1$ Hz, 1H, 8′-NH), 7.17 (m, 1H, H-4″), 7.06−7.07 (M, 2H, H-6″, H-7″), 6.26 (s, 1H, H-7′), 6.09 (s, 2H, 2″), 3.35 (m, 2H, H-2), 3.25 (m, 2H, H-1), 2.39 (s, 3H, 2′-$CH_3$), 1.80 (s, 3H, $NHCOCH_3$). $^{13}C$ NMR (125 MHz, DMSO-$d_6$) $\delta$ (ppm): 170.0 (C═O), 147.5 (C-6′), 147.1 (C-1″, C-3″), 143.3 (C-8′), 137.5 (C-2′), 130.9 (C-9′), 124.9 (C-3′), 123.5 (C-6″), 122.2 (C-5″), 109.7 (C-4″), 108.6 (C-7″), 101.5 (C-2″), 91.0 (C-7′), 41.8 (C-2), 37.9 (C-1), 22.8 (NH-CO-$CH_3$), 14.6 (2′-$CH_3$). Anal. ($C_{18}H_{18}ClN_5O_3 \cdot 0.66MeOH$) C, H, N. HRMS: calcd for [M + H], 388.11709; found, 388.11769.



DOI: 10.1021/acs.jmedchem.5b00499
J. Med. Chem. 2015, 58, 3767−3793

*3-(8-((2-Acetamidoethyl)amino)-6-chloro-2-methylimidazo[1,2-b]pyridazin-3-yl)benzamide (**36n**).* Mobile phase: EtOAc:acetone:EtOH:water (20:3:1.2:0.8). Recrystallized from hot MeOH. Yield: 80 mg (40%) as a white solid; mp 263.5−264.6 °C. $^1$H NMR (500 MHz, DMSO-$d_6$) $\delta$ (ppm): 8.09 (td, $J_{2-4,2-6}$ = 1.8, $J_{2-5}$ = 0.4 Hz, 1H, H-2), 8.07 (bs, 2H, CO-$NH_2$), 8.06 (t, $J_{NH\text{-}2}$ = 5.8 Hz, 1H, NH-CO), 7.91 (ddd, $J_{6-5}$ = 7.8, $J_{6-2}$ = 1.8, $J_{6-4}$ = 1.2 Hz, 1H, H-6), 7.89 (t, $J_{NH\text{-}1}$ = 6.1 Hz, 1H, 8′-NH), 7.78 (ddd, $J_{4-2}$ = 1.8, $J_{4-6}$ = 1.2, $J_{4-5}$ = 7.8 Hz, 1H, H-4), 7.61 (td, $J_{5-4,5-6}$ = 7.8, $J_{5-2}$ = 0.4 Hz, 1H, H-5), 7.47 (bs, 2H, CO-$NH_2^B$), 6.31 (s, 1H, H-7′), 3.38 (m, 2H, H-1″), 3.27 (m, 2H, H-2″), 2.43 (s, 3H, 2′-$CH_3$), 1.80 (s, 3H, $NHCOCH_3$). $^{13}$C NMR (125 MHz, DMSO-$d_6$) $\delta$ (ppm): 170.0 (C═O), 167.8 (CO-NH), 147.3 (C-6′), 143.4 (C-8′), 138.1 (C-2′), 134.7 (C-1), 132.1 (C-4), 131.4 (C-9′), 128.8 (C-3), 128.7 (C-5), 127.0 (C-6), 124.6 (C-3′), 91.3 (C-7′), 41.8 (C-1″), 37.9 (C-2″), 22.8 (NH-CO-$CH_3$), 14.5 (2′-$CH_3$). Anal. ($C_{18}H_{19}O_2N_6Cl$) C, H, N. HRMS: calcd for [M + H], 387.13308; found, 387.13363.

*3-(8-((2-Acetamidoethyl)amino)-6-chloro-2-methylimidazo[1,2-b]pyridazin-3-yl)-N,N-dimethylbenzamide (**36o**).* Mobile phase: EtOAc:acetone:EtOH:water (20:3:1.2:0.8). Oily residue triturated with diethyl ether. Yield: 0.206 g (78%) as a pinkish solid; mp 159.5−160.9 °C. $^1$H NMR (500 MHz, DMSO-$d_6$) $\delta$ (ppm): 8.06 (t, $J_{NH\text{-}1}$ = 5.3 Hz, 1H, NH-CO), 7.89 (t, $J_{NH\text{-}2}$ = 5.8 Hz, 1H, 8′-NH), 7.70 (dm, $J_{4-5}$ = 7.9 Hz, H-4), 7.66 (m, 1H, H-2), 7.59 (t, $J_{5-6}$ = $J_{5-4}$ = 7.9 Hz, 1H, H-5), 7.44 (dm, $J_{6-5}$ = 7.9 Hz, 1H, H-6), 6.30 (s, 1H, H-7′), 3.36 (m, 2 H, H-1″), 3.26 (m, 2H, H-2″), 3.01 (s, 6H, *N*-$(CH_3)_2$), 2.44 (s, 3H, 2′-$CH_3$), 1.80 (s, 3H, CO-$CH_3$). $^{13}$C NMR (125 MHz, DMSO-$d_6$) $\delta$ (ppm): 170.1 (C═$OCH_3$), 169.9 (C═$ON(CH_3)_2$), 147.3 (C-6′), 143.4 (C-8′), 138.2 (C-2′), 136.7 (C-1), 131.4 (C-9′), 130.1 (C-4), 128.8 (C-5), 128.5 (C-3), 127.6 (C-2), 126.7 (C-6), 124.4 (C-3′), 91.3 (C-7′), 41.8 (C-1″), 39.3 (N-$CH_3^A$), 37.9 (C-2″), 35.1 (N-$CH_3^B$), 22.8 (NH-CO-$CH_3$), 14.6 (2′-$CH_3$). Anal. ($C_{20}H_{23}O_2N_6Cl$) C, H, N. HRMS: calcd for [M + H], 415.16438; found, 415.16425.

*N-(2-((6-Chloro-3-(4-fluoro-3-formylphenyl)-2-methylimidazo[1,2-b]pyridazin-8-yl)amino)ethyl)acetamide (**36p**).* Mobile phase: EtOAc:acetone:EtOH:water (20:3:1.2:0.8).Yield: 0.140 g (55%) as an off-white solid; mp 177.6−178.9 °C. $^1$H NMR (500 MHz, DMSO-$d_6$) $\delta$ (ppm): 10.27 (CHO), 8.07 (dd, $J_{2''-6''}$ = 2.4, $J_{2''-F}$ = 6.7 Hz, 1H, H-2″), 8.05 (t, $J_{NH\text{-}1}$ = 5.7 Hz, 1H, NH-CO), 8.01 (ddd, $J_{6''-2''}$ = 2.4,$J_{6''-5''}$ = 8.7,$J_{6''-F}$ = 5.1 Hz, 1H, H-6″), 7.92 (t, $J_{NH\text{-}2}$ = 6.0 Hz, 1H, 8′-NH), 7.58 (dd, $J_{5''-6''}$ = 8.7,$J_{5''-F}$ = 10.5 Hz, 1H, H-5″), 6.32 (s, 1H, H-7′), 3.37 (m, 2H, H-2″), 3.26 (m, 2H, H-1″), 2.42 (s, 3H, 2′-$CH_3$), 1.80 (s, 3H, $COCH_3$). $^{13}$C NMR (125 MHz, DMSO-$d_6$) $\delta$ (ppm): 188.0 (d, $J_{C-F}$ = 3.9, CHO), 170.1 (C═O), 162.7 (d, $J_{4'-F}$ = 259.8, C-4″), 147.4 (C-6′), 143.4 (C-8′), 138.4 (C-2′), 137.4 (d, $J_{4'-F}$ = 9.3, C-4″), 131.5 (C-9′), 129.8 (d, $J_{2''-F}$ = 2.1, C-2″), 125.8 ($J_{1''-F}$ = 3.1, C-1″), 124.1 (d, $J_{3''-F}$ = 9.0, C-3″), 123.1 (C-3′), 117.4 (d, $J_{5''-F}$ = 21.1, C-5″), 91.5 (C-7′), 41.8 (C-2″), 37.9 (C-1″), 22.8 (CO-$CH_3$), 14.5 (2′-$CH_3$). Anal. ($C_{18}H_{18}O_2N_5ClF$) C, H, N. HRMS: calcd for [M + H], 390.11276; found, 390.11310.

*N-(2-((6-Chloro-3-(3-cyano-4-fluorophenyl)-2-methylimidazo[1,2-b]pyridazin-8-yl)amino)ethyl)acetamide (**36q**).* Mobile phase: EtOAc:acetone:EtOH:water (20:3:1.2:0.8). Recrystallized from hot MeOH:$CHCl_3$ (10:1). Yield 0.181 g (73%); mp 224.5−225.6 °C. $^1$H NMR (500 MHz, DMSO-$d_6$) $\delta$ (ppm): 8.18 (dd, $J_{2''-6''}$ = 2.2, $J_{2''-F}$ = 6.2 Hz, 1H, H-2″), 8.03−8.07 (m, 2H, NH-CO), 7.94 (t, $J_{NH\text{-}2}$ = 6.0 Hz, 1H, 8′-NH), 7.69 (t, $J_{5''-6'}$ = $J_{5''-F}$ = 9.1 Hz, 1H, H-5″), 6.33 (s, 1H, H-7′), 3.37 (m, 2H, H-2″), 3.26 (m, 2H, H-1″), 2.42 (s, 3H, 2′-$CH_3$), 1.80 (s, 3H, $COCH_3$). $^{13}$C NMR (125 MHz, DMSO-$d_6$) $\delta$ (ppm): 170.1 (C═O), 161.8 (d, $J_{4''-F}$ = 257.5, C-4″), 147.5 (C-6′), 143.4 (C-8′), 138.8 (C-2′), 136.8 (d, $J_{6''-F}$ = 8.8, C-6″), 134.2 (C-2″), 131.6 (C-9′), 126.4 (d, $J_{1''-F}$ = 3.7, C-1″), 122.3 (C-3′), 117.2 (d, $J_{5''-F}$ = 19.9, C-5″), 114.1 (CN), 100.8 (d, $J_{3''-F}$ = 15.6, C-3″), 91.6 (C-7′), 41.8 (C-2″), 37.8 (C-1″), 22.8 (CO-$CH_3$), 14.5 (2′-$CH_3$). Anal. ($C_{18}H_{17}ON_6ClF$) C, H, N. HRMS: calcd for [M + H], 387.11309; found, 387.11368.

*4-(8-((2-Acetamidoethyl)amino)-6-chloro-2-methylimidazo[1,2-b]pyridazin-3-yl)-2-fluorobenzoic Acid (**36r**).* Mobile phase: $CHCl_3$:MeOH:$CH_3COOH$ (9:1:0.1). Triturated with MeOH. Yield: 0.082 g (29%); mp 268.8−270.2 °C. $^1$H NMR (500 MHz, DMSO-$d_6$) $\delta$ (ppm): 8.05 (t, $J_{NH\text{-}2}$ = 5.6 Hz, 1H, NH-CO), 7.99 (t, $J_{6-5}$ = $J_{6-F}$ = 8.1 Hz, 1H, H-6), 7.95 (t, $J_{NH\text{-}1}$ = 5.9 Hz, 1H, 8′-NH), 7.65 (dd, $J_{3-F}$ = 12.3, $J_{3-5}$ = 1.4 Hz, 1H, H-3), 7.62 (dd, $J_{5-3}$ = 1.4, $J_{5-6}$ = 8.1 Hz, 1H, H-5), 6.35 (s, 1H, H-7′), 3.37 (m, 2H, H-1″), 3.26 (m, 2H, H-2″), 2.48 (s, 3H, 2′-$CH_3$), 1.80 (s, 3H, CO-$CH_3$). $^{13}$C NMR (125 MHz, DMSO-$d_6$) $\delta$ (ppm): 170.1 (NH-CO), 165.0 (d, $J_{C-F}$ = 3.1 Hz, COOH), 161.1 (d, $J_{2-F}$ =256.1 Hz, C-2), 147.5 (C-6′), 143.4 (C-8′), 139.6 (C-2′), 134.8 (d, $J_{4-F}$ = 9.7 Hz, C-4), 132.2 (d, $J_{6-F}$ = 1.8 Hz, C-6), 132.0 (C-9′), 124.6 (d, $J_{5-F}$ = 3.4 Hz, C-5), 122.9 (C-3′), 118.2 (d, $J_{1-F}$ = 10.1 Hz, C-1), 116.6 (d, $J_{3-F}$ = 24.1 Hz, C-3), 91.8 (C-7′), 41.8 (C-1″), 37.9 (C-2″), 22.8 (NH-CO-$CH_3$), 15.1 (2′-$CH_3$). Anal. ($C_{18}H_{17}O_3N_5ClF{\cdot}H_2O$) C, H, N. HRMS: calcd for [M + H], 406.10767; found, 406.10802.

*N-(2-((6-Chloro-2-methyl-3-(3-(methylsulfonyl)phenyl)imidazo[1,2-b]pyridazin-8-yl)amino)ethyl)acetamide (**36s**).* Mobile phase: EtOAc:MeOH (10−15%). Recrystallization from hot MeOH:$CHCl_3$ (7:1). Yield: 0.150 g (57%); mp 218.9−219.3 °C. $^1$H NMR (500 MHz, DMSO-$d_6$) $\delta$ (ppm): 8.20 (t, $J_{2''-4''}$ = $J_{2''-6''}$ = 1.7 Hz, 1H, H-2″), 8.06 (t, $J_{NH\text{-}1}$ = 1.7 Hz, 1H, NH−CO), 8.01 (dt, $J_{6''-5''}$ = 7.8, $J_{6''-2''}$ = $J_{6''-4''}$ = 1.7 Hz, 1H, H-6″), 7.95 (dt, $J_{4''-5''}$ = 7.8, $J_{4''-2''}$ = $J_{4''-6''}$ = 1.7 Hz, 1H, H-4″), 7.94 (t, $J_{NH\text{-}2}$ = 5.8 Hz, 1H, 8′-NH), 7.81 (t, $J_{5''-4''}$ = $J_{5''-6''}$ = 7.8 Hz, 1H, H-5″), 6.34 (s, 1H, H-7′), 3.37 (m, 2H, H-2″), 3.27 (m, 2H, H-1″), 2.46 (s, 3H, 2′-$CH_3$), 1.81 (s, 3H, $COCH_3$). $^{13}$C NMR (125 MHz, DMSO-$d_6$) $\delta$ (ppm): 170.1 (C═O), 147.5 (C-6′), 143.4 (C-8′), 141.3 (C-3″), 138.8 (C-2′), 134.0 (C-6″), 131.7 (C-9′), 129.9 (C-1″), 127.1 (C-2″), 126.2 (C-4″), 123.4 (C-3′), 91.6 (C-7′), 43.7 ($SO_2CH_3$), 41.8 (C-2″), 37.9 (C-1″), 22.8 (CO-$CH_3$), 14.7 (2′-$CH_3$). Anal. ($C_{18}H_{20}O_3N_5ClS$) C, H, N. HRMS: calcd for [M + H], 422.10481; found, 422.10486.

*N-(2-((6-Chloro-3-(3-(N,N-dimethylsulfamoyl)phenyl)-2-methylimidazo[1,2-b]pyridazin-8-yl)amino)ethyl)-acetamide (**36t**).* Mobile phase: EtOAc:acetone:EtOH:water (20:3:1.2:0.8). Recrystallized from MeOH:$CHCl_3$ (10:1). Yield 0.791 g (65%) as an off-white solid; mp 240−240.7 °C. $^1$H NMR (500 MHz, DMSO-$d_6$) $\delta$ (ppm): 8.06 (m, 1H, H-2″), 8.05 (t, $J_{NH\text{-}1}$ = 5.6 Hz, 1H, NH-CO), 7.98 (dt, (t, $J_{6''-5''}$ = 7.7, $J_{6''-2''}$ =$J_{6''-4''}$ = 1.4 Hz, 1H, H-6″, 7.95 (t, $J_{NH\text{-}2}$ = 6.0 Hz, 1H, 8′-NH), 7.81 (t, $J_{5''-4''}$ = $J_{5''-6''}$ = 7.8 Hz, 1H, H-5″), 6.34 (s, 1H, H-7′), 3.38 (m, 2H, H-2″), 3.26 (m, 2H, H-1″), 2.69 (s, 6H, $N(CH_3)_2$), 2.48 (s, 3H, 2′-$CH_3$), 1.80 (s, 3H, $COCH_3$). $^{13}$C NMR (125 MHz, DMSO-$d_6$) $\delta$ (ppm): 170.1 (C═O), 147.4 (C-6′), 143.5 (C-8′), 138.7 (C-2′), 134.9 (C-3″), 133.3 (C-6″), 131.7 (C-9′), 129.9 (C-5″), 129.8 (C-1″), 127.7 (C-2″), 126.6 (C-4″), 123.3 (C-3′), 91.6 (C-7′), 41.8 (C-2″), 37.9 (C-1″), 22.8 (CO-$CH_3$), 14.7 (2′-$CH_3$). Anal. ($C_{19}H_{23}ClN_6O_3S$) C, H, N. HRMS: calcd for [M + H], 451.13136; found, 451.13144.

*2-Methoxy-5-(4,4,5,5-tetramethyl-1,3,2-dioxaborolan-2-yl)-aniline.* 5-Bromo-2-methoxyaniline (0.518 mg, 2.56 mmol) was dissolved in DMSO (8 mL). $B_2(pin)_2$ (1.3 g, 5.12 mmol) and AcOK (1.43 g, 14.59 mmol) were added in one portion, and the suspension was degassed 3 times and refilled with argon. Pd(dppf)$Cl_2$·DCM (0.1 g, 5 mol %) was added quickly, and the mixture was degassed once more. The reaction was then heated up to 80 °C and stirred under argon atmosphere overnight. After cooling to rt, the reaction mixture was partitioned between EtOAc/brine and the water phase was extracted twice more with EtOAc. Combined organic phases were dried over sodium sulfate and evaporated, coevaporated with toluene, and then the residue was adsorbed onto silica gel and purified by column chromatography (hexane:EtOAc 4:1) to provide brownish oil. Yield: 370.4 mg (58%). $^1$H NMR (500 MHz, DMSO-$d_6$) $\delta$ (ppm): 7.00 (d, $J_{6-4}$ = 1.6, 1H, H-6), 6.90 (dd, $J_{4-6}$ = 1.6, $J_{4-3}$ = 7.9 Hz, 1H, H-4), 6.77 (d, $J_{3-4}$ = 7.9 Hz, 1H, H-3), 4.66 (bs, 2H, 1-$NH_2$), 3.77 (s, 3H, O−$CH_3$), 1.25 (s, 12H, $CH_3$). $^{13}$C NMR (125 MHz, DMSO-$d_6$) $\delta$ (ppm): 149.2 (C-2), 137.1 (C-1), 128.8 (C-4), 120.2 (C-5), 120.0 (C-6), 109.9 (C-3), 83.2 (C-$(CH_3)_2$), 55.3 (O−$CH_3$), 24.9 ($CH_3$). HRMS: calcd for [M + H], 250.16090; found, 250.16095.

*N-(2-((3-(3-Amino-4-methoxyphenyl)-6-chloro-2-methylimidazo[1,2-b]pyridazin-8-yl)amino)ethyl)acetamide (**36u**).*[46] To the suspension of **35** (0.228 g, 0.58 mmol) in 1,4-dioxane (8 mL) was added solution of 2-methoxy-5-(4,4,5,5-tetramethyl-1,3,2-dioxaborolan-2-yl)-



DOI: 10.1021/acs.jmedchem.5b00499
J. Med. Chem. 2015, 58, 3767−3793

aniline (0.217 g, 0.87 mmol) followed by solution of $K_2CO_3$ (2 mL, 1M). Reaction mixture was degassed 3 times, then $Pd(PPh_3)_4$ (5 mol %) was added quickly and the mixture was degassed once more and stirred under argon atmosphere at 90 °C overnight. After completion of the reaction, it was cooled to rt, diluted with water, and extracted with EtOAc (50 mL). The water phase was extracted twice more with EtOAc (2 × 25 mL), and the combined organic phases were dried over sodium sulfate and evaporated. Oily residue was dissolved in MeOH/$CHCl_3$ mixture and adsorbed onto silica gel and purified by column chromatography (EtOAc:acetone:EtOH:water 20:3:1.6:0.4). Product **36u** was obtained as a brownish powder. Yield: 182 mg (80%); mp 214.7−215.5 °C. $^1$H NMR (500 MHz, DMSO-$d_6$) $\delta$ (ppm): 8.04 (t, $J_{NH\text{-}2}$ = 5.8 Hz, 1H, NH-CO), 7.78 (t, $J_{NH\text{-}1}$ = 6.0 Hz, 1H, 8′-NH), 6.92 (d, $J_{6-5}$ = 8.4 Hz, H-6), 6.87 (d, $J_{3-5}$ = 2.1 Hz, 1H, H-3), 6.75 (dd, $J_{5-3}$ = 2.1, $J_{5-6}$ = 8.4 Hz, 1H, H-5), 6.23 (s, 1H, H-7′), 4.85 (bs, 2H, 2-$NH_2$), 3.82 (s, 3H, 1-O-$CH_3$), 3.33 (m, 2H, H-2″), 3.25 (m, 2H, H-2″), 2.36 (s, 3H, 2′-$CH_3$), 1.80 (s, 3H, CO-$CH_3$). $^{13}$C NMR (125 MHz, DMSO-$d_6$) $\delta$ (ppm): 169.9 (C═O), 146.9 (C-6′), 146.4 (C-1), 143.2 (C-8′), 137.7 (C-2), 137.0 (C-2′), 130.6 (C-9′), 125.9 (C-3′), 121.0 (C-4), 117.8 (C-5), 114.8 (C-3), 110.6 (C-6), 90.6 (C-7′), 55.6 (O-$CH_3$), 41.7 (C-1″), 37.9 (C-2″), 22.8 (CO-$CH_3$), 14.6 (2′-$CH_3$). HRMS: calcd for [M + H], 389.14873; found, 389.14905.

***N*-(2-((3-(3-Acetamido-4-methoxyphenyl)-6-chloro-2-methylimidazo[1,2-*b*]pyridazin-8-yl)amino)ethyl)acetamide (37).** Compound **36u** (201 mg, 0.52 mmol) was dissolved in DCM (5 mL), followed by addition of DIPEA (0.1 mL, 0.62 mmol). Acetanhydride (0.06 mL, 0.62 mmol) was then addend dropwise at 0 °C. After the addition, the mixture was allowed to warm to rt and stirred overnight. Then it was diluted with DCM, washed with $H_2O$, dried over sodium sulfate, evaporated to minimal volume, and adsorbed onto silica gel. Column chromatography (EtOAc:MeOH 6:1) afforded the product **37**. An analytical sample was obtained after recrystallization from MeOH:$CHCl_3$ (10:1) as violet crystals. Yield: 204 mg (92%); mp 145−146.2 °C (decomposed). $^1$H NMR (500 MHz, DMSO-$d_6$) $\delta$ (ppm): 9.27 (s, 1H, 3″-NH), 8.16 (d, 1H, H-2″), 8.03 (t, $J_{NH\text{-}1}$ = 5.6 Hz, 1H, NH-CO), 7.81 (t, $J_{NH\text{-}2}$ = 6.0 Hz, 1H, 8′-NH), 7.36 (dd, $J_{6''-5''}$ = 8.5, $J_{6''-2''}$ = 2.0 Hz, 1H, H-6″), 7.18 (d, $J_{5''-6''}$ = 8.5 Hz, 1H, H-5″), 6.25 (s, 1H, H-7′), 3.90 (s, 3H, 4″-$OCH_3$), 3.36 (m, 2H, H-2), 3.26 (m, 2H, H-1), 2.39 (s, 3H, 2′-$CH_3$), 2.10 (s, 3 H, 3″-NH-CO-$CH_3$), 1.80 (s, 3 H, 1-NH-CO-$CH_3$). $^{13}$C NMR (125 MHz, DMSO-$d_6$) $\delta$ (ppm): 169.9 (1-NH-CO), 168.8 (3″-NH-CO), 149.4 (C-4″), 147.0 (C-6′), 143.3 (C-8″), 137.3 (C-2′), 130.8 (C-9′), 127.4 (C-3″), 125.5 (C-6″), 125.0 (C-3′), 123.2 (C-2″), 120.4 (C-1″), 111.3 (C-5″), 90.8 (C-7′), 57.1 (4″-O-$CH_3$), 41.7 (C-2), 37.9 (C-1), 24.0 (3″-NH-CO-$CH_3$), 22.8 (1-NHCO-$CH_3$), 14.4 (2′-$CH_3$). Anal. ($C_{20}H_{23}ClN_6O_3$) C, H, N. HRMS: calcd for [M + H], 431.15929; found, 431.15935.

***N*-(5-(8-((2-Acetamidoethyl)amino)-6-chloro-2-methylimidazo[1,2-*b*]pyridazin-3-yl)-2-methoxyphenyl)-cyclohexanecarboxamide (38).** Compound **36u** (201 mg, 0.52 mmol) was dissolved in DCM (5 mL), followed by addition of DIPEA (0.1 mL, 0.62 mmol). Cyclohexanoyl chloride (0.07 mL, 0.62 mmol) wad then added dropwise at 0 °C. After the addition, the mixture was allowed to warm to rt and stirred for 1 h. Then it was diluted with DCM, washed with $H_2O$, dried over sodium sulfate, evaporated to minimal volume, and adsorbed onto silica gel. Column chromatography (EtOAc:acetone:EtOH:water 20:3:1.6:0.4) afforded off-white foam, which was triturated with ether, sonicated for a few minutes, and the formed suspension was filtered, washed with ether, and dried, affording the product **38** as an off white solid. Yield: 162 mg (63%); mp 164.6−165.2 °C. $^1$H NMR (500 MHz, DMSO-$d_6$) $\delta$ (ppm): 9.04 (s, 1H, 1′-NH), 8.17 (d, $J_{6'-4'}$ = 2.1 Hz, 1H, H-6′), 8.03 (t, $J_{NH\text{-}2'''}$ = 5.6 Hz, 1H, 2‴-NH−CO), 7.81 (t, $J_{NH\text{-}1''}$ = 6.0 Hz, 1H, 8″-NH), 7.34 (dd, $J_{4'-3'}$ = 8.5, $J_{4'-6'}$ = 2.1 Hz, H-4′), 7.18 (d, $J_{3'-4'}$ = 8.5 Hz, 1H, H-3′), 6.25 (s, 1H, H-7″), 3.90 (s, 3H, 2′-$OCH_3$), 3.36 (m, 2H, H-1‴), 3.26 (m, 2H, H-2‴), 2.54 (m, 2H, H-1), 2.39 (s, 3H, 2″-$CH_3$), 1.81 (s, 3H, NH-CO-$CH_3$), 1.79 (m, 2H, 2a), 1.73 (dm, $J_{GEM}$ = 12.9 Hz, 2H, 3a), 1.64 (dm, $J_{GEM}$ = 12.2 Hz, 4a), 1.38 (m, 2H, 2b), 1.27 (m, 2H, 3b), 1.18 (m, 4b). $^{13}$C NMR (125 MHz, DMSO-$d_6$) $\delta$ (ppm): 174.7 (1′-NH-CO), 169.9 (2″-NH-CO), 149.4 (C-2′), 147.0 (C-6″), 143.3 (C-8″), 137.8 (C-2″), 130.8 (C-9″), 127.6 (C-5′), 125.4 (C-4′), 125.1 (C-3″), 123.0 (C-6′), 120.4 (C-1′), 111.2 (C-3′), 90.8 (C-7″), 56.1 (2′-O-$CH_3$), 44.5 (C-1), 41.7 (C-1‴), 37.9 (C-2‴), 29.5 (C-2), 25.6 (C-4), 25.4 (C-3), 22.8 (NH-CO-$CH_3$), 14.4 (2″-$CH_3$). Anal. ($C_{25}H_{31}ClN_6O_3$·0.5$H_2O$) C, H, N. HRMS: calcd for [M + H], 499.22189; found, 499.22195.

***N*-(5-(8-((2-Acetamidoethyl)amino)-6-chloro-2-methylimidazo[1,2-*b*]pyridazin-3-yl)-2-methoxyphenyl)-pivalamide (39).** Compound **36u** (164 mg, 0.42 mmol) was dissolved in DCM (5 mL) followed by addition of DIPEA (0.1 mL, 0.5 mmol). Pivaloyl chloride (0.078 mL, 0.5 mmol) was then added dropwise at 0 °C. After the addition, the mixture was allowed to warm to rt and stirred overnight. Then the mixture was evaporated to minimal volume, diluted with EtOAc, and washed with water. The water phase was extracted twice more with EtOAc, dried over sodium sulfate, evaporated, and adsorbed onto silica gel from acetone. Column chromatography (EtOAc:acetone:EtOH:water 20:3:1.6:0.4) afforded off-white foam. Yield: 95 mg (48%). $^1$H NMR (500 MHz, DMSO-$d_6$) $\delta$ (ppm): 8.51 (s, 1H, 1-NH), 8.09 (d, $J_{6-4}$ = 2.2 Hz, 1H, H-6), 8.03 (t, $J_{NH\text{-}2''}$ = 5.8 Hz, 1H, 2″-NH-CO), 7.81 (t, $J_{NH\text{-}1}$ = 6.0 Hz, 1H, 8-NH), 7.38 (dd, $J_{4-3}$ = 8.5, $J_{4-6}$ = 2.2 Hz, H-4), 7.21 (d, $J_{3-4}$ = 8.5 Hz, 1H, H-3), 6.26 (s, 1H, H-7′), 3.91 (s, 3H, 2-$OCH_3$), 3.36 (bs, 2H, H-1″), 3.26 (m, 2H, H-2″), 2.40 (s, 3H, 2″-$CH_3$), 1.81 (s, 3H, CO-$CH_3$), 1.24 (s, 9H, $CH(CH_3)_3$. $^{13}$C NMR (125 MHz, DMSO-$d_6$) $\delta$ (ppm): 176.3 (1-NH-CO), 169.9 (2″-NH-CO), 149.9 (C-2), 147.1 (C-6′), 143.3 (C-8′), 137.3 (C-2′), 130.9 (C-9′), 127.4 (C-1), 125.9 (C-4), 125.0 (C-3′), 123.2 (C-6), 120.6 (C-5), 111.3 (C-3), 90.8 (C-7′), 56.3 (2-O-$CH_3$), 41.8 (C-1″), 39.5 ($CH(CH_3)_3$, 37.9 (C-2″), 27.4 ($CH_3$)$_3$, 22.8 (NH-CO-$CH_3$), 14.5 (2′-$CH_3$). Anal. ($C_{23}H_{29}ClN_6O_3$·0.75EtOAc) C, H, N. HRMS: calcd for [M + H]: 473.20624, found 473.20629.

***N*-(2-((6-Chloro-3-(3-(3-isopropylureido)-4-methoxyphenyl)-2-methylimidazo[1,2-*b*]pyridazin-8-yl)amino)ethyl)acetamide (40).** Compound **36u** (178 mg, 0.46 mmol) was dissolved in THF (10 mL), followed by addition of TEA (0.19 mL, 1.38 mmol) and isopropylisocyanate (0.144 mL, 0.92 mmol)). The reaction mixture was refluxed for 6 h. Then the mixture was cooled to rt, evaporated to minimal volume, diluted with EtOAc, and washed with water. The water phase was extracted twice more with EtOAc, dried over sodium sulfate, evaporated, and adsorbed onto silica gel. Column chromatography (EtOAc:acetone:EtOH:water 20:3:1.2:0.8) afforded off-white foam. Yield: 187 mg (86%). $^1$H NMR (500 MHz, DMSO-$d_6$) $\delta$ (ppm): 8.30 (d, $J_{2''-6''}$ = 2.1 Hz, 1H, H-2″), 8.04 (t, $J_{NH\text{-}1}$ = 5.6 Hz, 1H, 1-NH), 7.90 (s, 1H, 3″-NH), 7.80 (t, $J_{NH\text{-}2}$ = 6.1 Hz, 1H, 2-NH−CO), 7.15 (dd, $J_{6''-5''}$ = 8.4, $J_{6''-2''}$ = 2.1 Hz, 1H, H-6″), 7.10 (d, $J_{5''-6''}$ = 8.4 Hz, 1H, H-5″), 6.24 (s, 1H, H-7′), 3.90 (s, 3H, 4″-$OCH_3$), 3.73 (m, 1H, NH-$CH(CH_3)_2$), 3.36 (m, 2H, H-2), 3.26 (m, 2H, H-1), 2.38 (s, 3H, 2′-$CH_3$), 1.80 (s, 3H, NH-CO-$CH_3$), 1.08 (d, $J_{CH-CH_3}$ = 6.5 Hz, 6H, NH-CH-$(CH_3)_2$). $^{13}$C NMR (125 MHz, DMSO-$d_6$) $\delta$ (ppm): 169.9 (NH-CO), 154.6 (CO-NH-Pr), 147.1 (C-4″), 147.0 (C-6′), 143.2 (C-8′), 137.1 (C-2′), 130.7 (C-9′), 129.6 (C-1″), 125.6 (C-3′), 122.2 (C-6″), 120.7 (C-3″), 119.1 (C-2″), 110.6 (C-5″), 90.7 (C-7′), 56.0 (4″-O-$CH_3$), 41.7 (C-2), 41.0 (NH-CH-$(CH_3)_2$), 37.9 (C-1), 23.2 (NH-CH-$(CH_3)_2$), 22.8 (NH-CO-$CH_3$), 14.5 (2′-$CH_3$). Anal. ($C_{22}H_{28}ClN_7O_3$) C, H, N. HRMS: calcd for [M + H], 474.20149; found, 474.20150.

***N*-(2-((6-Chloro-3-(3-(isopropylamino)-4-methoxyphenyl)-2-methylimidazo[1,2-*b*]pyridazin-8-yl)amino)ethyl)acetamide (41).** A round-bottom flask was charged with **36u** (178 mg, 0.46 mmol) and diluted with MeOH (2 mL) and acetone (0.08 mL), followed by an addition of $NaBH_3CN$ (43 mg, 0.69 mmol). Acetic acid (0.065 mL, 1.15 mmol) was added, and the reaction mixture was stirred at rt overnight. Then pH was adjusted to 2 by diluted HCl and stirred for 7 h, after which pH was adjusted to 7 with diluted KOH and the mixture was extracted with chloroform (35 mL). The water phase was extracted with chloroform (2 × 30 mL), and the combined organic phases were dried over sodium sulfate and evaporated. Residue was dissolved in a small amount of DCM, adsorbed on silica gel, and purified by column chromatography (EtOAc:acetone:EtOH:water 20:3:1.2:0.8). Residue was triturated with ether, and the formed suspension was filtered and washed with ether, affording **41** as an off-



DOI: 10.1021/acs.jmedchem.5b00499
J. Med. Chem. 2015, 58, 3767−3793

white solid. Yield: 150 mg (76%); mp 165.2−166.3 °C. $^1$H NMR (500 MHz, DMSO-$d_6$) $\delta$ (ppm): 8.03 (t, $J_{NH\text{-}1}$ = 5.6 Hz, 1H, 1-NH), 7.76 (t, $J_{NH\text{-}2}$ = 6.0 Hz, 1H, 8-NH), 6.94 (d, $J_{5''-6''}$ = 8.2 Hz, 1H, H-5″), 6.79 (d, $J_{2''-6''}$ = 1.9 Hz, 1H, H-2″), 6.77 (dd, $J_{6''-5''}$ = 8.2, $J_{6''-2''}$ = 1.9 Hz, 1H, H-6″), 6.24 (s, 1H, H-7′), 4.46 (d, $J_{NH-CH}$ = 8.2 Hz, 1H, 3″-NH), 3.84 (s, 3H, 4″-OCH$_3$), 3.57 (m, 1H, CH-(CH$_3$)$_2$), 3.36 (bs, 2H, H-2), 3.26 (m, 2H, H-1), 2.41 (s, 3H, 2′-CH$_3$), 1.80 (s, 3H, NH−CO−CH$_3$), 1.19 (d, $J_{CH-CH_3}$ = 6.3 Hz, 6H, CH-(CH$_3$)$_2$). $^{13}$C NMR (125 MHz, DMSO-$d_6$) $\delta$ (ppm): 169.9 (NH-CO), 146.9 (C-6′), 146.2 (C-4′), 143.2 (C-8′), 137.0 and 136.9 (C-2′ and C3″), 130.6 (C-9′), 125.9 (C-3′), 121.2 (C-1″), 116.8 (C-6″), 110.9 (C-2″), 109.8 (C-5″), 90.6 (C-7′), 55.6 (4″-O-CH$_3$), 43.2 (CH-(CH$_3$)$_2$), 41.7 (C-2), 37.9 (C-1), 22.8 (CO-CH$_3$), 22.5 (NH-CH-(CH$_3$)$_2$), 14.6 (2′-CH$_3$). Anal. ($C_{21}H_{27}ClN_6O_2$) C, H, N. HRMS: calcd for [M + H], 431.19568; found, 431.19573.

***N*-(2-((6-Chloro-3-(4-methoxy-3-((2-(methylsulfonamido)ethyl)amino)phenyl)-2-methylimidazo[1,2-*b*]pyridazin-8-yl)amino)ethyl)acetamide (42).** Compound **36u** (0.17 g, 0.437 mmol) was diluted in dry toluene (3 mL), followed by addition of *N*-(2-chloroethyl)methanesulfonamide (0.112 g, 0.554 mmol) in toluene and $K_2CO_3$ (0.06 g, 0.437 mmol). The reaction mixture was stirred at 90 °C overnight. After cooling to rt, the solvent was evaporated and the residue diluted with DCM and washed with water. The organic phase was dried over sodium sulfate, evaporated to minimal volume, adsorbed onto silica gel, and purified by column chromatography (EtOAc:acetone:EtOH:water 20:3:1.2:0.8), affording **42** as an of off-white foam. Yield: 100 mg (45%). $^1$H NMR (500 MHz, DMSO-$d_6$) $\delta$ (ppm): 8.05 (t, $J_{NH\text{-}1}$ = 5.6 Hz, 1H, 1-NH), 7.79 (t, $J_{NH\text{-}2}$ = 6.1 Hz, 1H, 8-NH), 6.98 (d, $J_{5''-6''}$ = 8.3 Hz, 1H, H-5″), 6.83 (dd, $J_{6''-5''}$ = 8.3 Hz, 1H, H-5″), 6.81 (d, $J_{2''-6''}$ = 2.0 Hz, 1H, H-2″), 6.26 (s, 1H, H-7′), 5.37 (t, $J_{NH\text{-}1'''}$ = 6.0 Hz, 1H, 3″-NH), 3.86 (s, 3H, 4″-OCH$_3$), 3.32−3.38 (m, 4H, H-1, H-1‴), 3.26 (m, 2H, H-2), 3.02 (m, 2H, H-2‴), 2.40 (s, 3H, 2′-CH$_3$), 1.80 (s, 3H, NH-CO-CH$_3$). $^{13}$C NMR (125 MHz, DMSO-$d_6$) $\delta$ (ppm): 169.9 (NH-CO), 146.9 (C-6′), 146.6 (C-4″), 143.2 (C-8′), 137.2 (C-3″), 137.0 (C-2′), 130.6 (C-9′), 125.9 (C-3′), 121.2 (C-1″), 117.8 (C-6″), 110.3 (C-2″), 110.1 (C-5″), 90.6 (C-7′), 55.6 (4″-O-CH$_3$), 41.8 (C-1), 40.5 (C-1‴), 38.0 (C-2‴), 22.8 (CO-CH$_3$), 14.6 (2′-CH$_3$). Anal. ($C_{21}H_{28}ClN_7O_4S$·0.5EtOAc) C, H, N. HRMS: calcd for [M + H], 431.19568; found, 431.19573.

***N*-(2-((6-Chloro-3-(3-(hydroxymethyl)phenyl)-2-methylimidazo[1,2-*b*]pyridazin-8-yl)amino)ethyl)acetamide (44).** Compound **36e** (134 mg, 0.36 mmol) was dissolved in $CH_2Cl_2$ (4 mL) and MeOH (1 mL), and $NaBH_4$ (74 mg, 1.95 mmol) was added in one portion. The reaction mixture stirred at rt for 1 h and was subsequently quenched through addition of satd $NH_4Cl$ (1 mL) and $H_2O$ (1 mL), and the resulting suspension was stirred at rt for 10 min before being diluted with $CHCl_3$ (30 mL) and $H_2O$ (15 mL). The layers were separated, and the aqueous layer was extracted twice with $CHCl_3$ (2 × 20 mL) and the organic layer was dried over $Na_2SO_4$ and evaporated. The residue was purified by silica gel column chromatography (ethyl acetate:acetone:ethanol:water (21:3:0.5:0.5)), and the product was recrystallized from hot MeOH to afford compound **33** as a white solid. Yield: 40 mg (30%); mp 185.2−186.4 °C. $^1$H NMR (500 MHz, DMSO-$d_6$) $\delta$ (ppm): 8.05 (t, $J_{NH\text{-}1}$ = 5.7 Hz, 1H, NH-CO), 7.85 (t, $J_{NH\text{-}2}$ = 6.0 Hz, 1H, 8′-NH), 7.55 (m, 1H, H-2″), 7.51−7.45 (m, 2H, H-5″, H-6″), 7.36 (dm, $J_{4''-5''}$ = 6.9 Hz, 1H, H-4″), 6.28 (s, 1H, H-7′), 5.28 (t, $J_{OH\text{-}CH_2}$ = 5.8 Hz, 1H, CH$_2$OH), 4.57 (d, $J_{CH_2\text{-}OH}$ = 5.8 Hz, 2H, CH$_2$-OH), 3.37 (m, 2H, H-2), 3.26 (m, 2H, H-1), 2.41 (s, 3H, 2′-CH$_3$), 1.81 (s, 3H, COCH$_3$). $^{13}$C NMR (125 MHz, DMSO-$d_6$) $\delta$ (ppm): 170.0 (C═O), 147.2 (C-6′), 143.3 (C-8′), 143.0 (C-3″), 137.8 (C-2′), 131.1 (C-9′), 128.4 (C-1″), 128.4 and 127.8 (C-5″and C-6″), 127.3 (C-2″), 126.2 (C-4″), 125.2 (C-3′), 91.1 (C-7′), 63.0 (CH$_2$-OH), 41.8 (C-2), 37.9 (C-1), 22.8 (COCH$_3$), 14.6 (2′-CH$_3$). Anal. ($C_{17}H_{17}Cl_2N_5O$) C, H, N. HRMS: calcd for [M + H], 374.13783; found, 374.13713.

***N*-(2-((6-Chloro-3-(4-(hydroxymethyl)phenyl)-2-methylimidazo[1,2-*b*]pyridazin-8-yl)amino)ethyl)acetamide (45).** Compound **36i** (131 mg, 0.35 mmol) was dissolved in $CH_2Cl_2$ (4 mL) and MeOH (1 mL), and $NaBH_4$ (72 mg, 1.9 mmol) was added in one portion. The reaction mixture stirred at rt for 1 h and was subsequently quenched through addition of satd $NH_4Cl$ (1 mL) and $H_2O$ (1 mL), and the resulting suspension was stirred at rt for 10 min before being diluted with $CHCl_3$ (30 mL) and $H_2O$ (15 mL). The layers were separated, and the aqueous layer was extracted twice with $CHCl_3$ (2 × 20 mL) and the organic layer was dried over $Na_2SO_4$ and evaporated. The residue was purified by silica gel column chromatography (ethyl acetate:acetone:ethanol:water (21:3:0.5:0.5)), and the product was recrystallized from hot MeOH to afford compound **45** as a white solid. Yield: 52 mg (40%); mp 203.8−204.5 °C. $^1$H NMR (500 MHz, DMSO-$d_6$) $\delta$ (ppm): 8.05 (t, $J_{NH\text{-}1}$ = 5.6 Hz, 1H, NH-CO), 7.85 (t, $J_{NH\text{-}2}$ = 6.0 Hz, 1H, 8′-NH), 7.58 (m, 2H, H-2″), 7.46 (m, 2H, H-3″), 6.27 (s, 1H, H-7′), 5.26 (t, $J_{OH\text{-}CH_2}$ = 5.8 Hz, 1H, CH$_2$OH), 4.56 (d, $J_{CH_2\text{-}OH}$ = 5.8 Hz, 2H, CH$_2$-OH), 3.37 (m, 2H, H-2), 3.26 (m, 2H, H-1), 2.41 (s, 3H, 2′-CH$_3$), 1.80 (s, 3H, COCH$_3$). $^{13}$C NMR (125 MHz, DMSO-$d_6$) $\delta$ (ppm): 170.0 (C═O), 147.1 (C-6′), 143.3 (C-8′), 142.4 (C-4″), 137.7 (C-2′), 131.1 (C-9′), 129.1 (C-2″), 127.0 (C-1″), 126.7 (C-3″), 125.1 (C-3′), 91.0 (C-7′), 62.9 (CH$_2$-OH), 41.8 (C-2), 37.9 (C-1), 22.8 (COCH$_3$), 14.6 (2′-CH$_3$). Anal. ($C_{17}H_{17}Cl_2N_5O$) C, H, N. HRMS: calcd for [M + H], 374.13783; found, 374.13785.

**(4-(8-((2-Acetamidoethyl)amino)-6-chloro-2-methylimidazo[1,2-*b*]pyridazin-3-yl)phenyl)methanaminium Chloride (46).** To a solution of compound **36h** (130 mg, 0.352 mmol) in 4 M ethanolic ammonia (10 mL) was added a catalytic amount of Raney-Ni, and the reaction mixture was stirred under $H_2$ (50 psi) at rt for 16 h. The catalyst was filtered off over Celite and washed with MeOH, and the filtrate was concentrated in vacuo. The residue was purified by silica gel column chromatography (ethyl acetate:acetone:ethanol:water (18:3:2.5:1.5) → ethyl acetate:acetone:ethanol:water (17:3:3:2) + 1% NEt$_3$) to give the title compound ,which was converted into its hydrochloride through treatment with ethereal HCl in $CH_2Cl_2$ and a small amount of MeOH. The sticky product thus obtained was triturated with acetone and minute amounts of MeOH, affording title compound **46** as an off-white solid. Yield: 102 mg (71%); mp 254.1−255.3 °C. $^1$H NMR (500 MHz, DMSO-$d_6$) $\delta$ (ppm): 8.70 (m, 1H, 8′-NH), 8.65 (m, 3H, $NH_3^+$), 8.12 (t, $J_{NH\text{-}2''}$ = 5.8 Hz, 1H, NH-CO), 7.71 (s, 2H, H-3), 7.71 (s, 2H, H-2), 6.79 (s, 1H, H-7′), 4.10 (m, 2H, 1-CH$_2$), 3.45 (m, 2H, H-1″), 3.30 (m, 2H, H-2″), 2.49 (s, 3H, 2′-CH$_3$), 1.82 (s, 3H, COCH$_3$). $^{13}$C NMR (125 MHz, DMSO-$d_6$) $\delta$ (ppm): 170.1 (C═O), 149.7 (C-6′), 141.4 (C-8′), 135.3 (C-1), 131.9 (C-2′), 130.1 (C-3), 129.5 (C-2), 129.2 (C-9′), 126.0 (C-4), 125.3 (C-3′), 95.9 (C-7′), 42.1 (C-1″, 1-CH$_2$), 37.4 (C-2″), 22.9 (COCH$_3$), 11.9 (2′-CH$_3$). Anal. ($C_{18}H_{22}Cl_2N_6O$) C, H, N. HRMS: calcd for [M + H], 373.15381; found, 373.15349.

***N*-(2-((3-(3,4-Dimethoxyphenyl)-2-methylimidazo[1,2-*b*]-pyridazin-8-yl)amino)ethyl)acetamide (47).** Compound **36a** (272 mg, 0.67 mmol) was dissolved in THF:MeOH (8 mL, 1:1), and Pd(OH)$_2$ 20%/C (47 mg, 10 mol %) was added followed by addition of TEA (0.187 mL, 1.35 mmol). The mixture was stirred under the atmosphere of $H_2$ in an autoclave (5 bar) overnight. The reaction mixture was then filtrated over pad of Celite, washed with MeOH, and evaporated. Recrystallization from hot MeOH provided the product **47** as an off-white solid. Yield: 156 mg (63%); mp 153.5−154 °C. $^1$H NMR (500 MHz, DMSO-$d_6$) $\delta$ (ppm): 8.05 (t, $J_{NH\text{-}2}$ = 5.5 Hz, 1H, NH-CO), 7.99 (d, $J_{6'-7'}$ = 5.5 Hz, 1H, H-6′), 7.32 (t, $J_{NH\text{-}1}$ = 5.9 Hz, 1H, 8′-NH), 7.24 (d, $J_{2''-6''}$ = 2.0 Hz, H-2″), 7.18 (dd, $J_{6''-5''}$ = 8.3, $J_{6''-2''}$ = 2.0 Hz, 1H, H-6″), 7.07 (d, $J_{5''-6''}$ = 8.3 Hz, 1H, H-5″), 6.12 (d, $J_{7'-6'}$ = 5.5 Hz, 1H, H-7′), 3.81 (s, 3H, 4″-OCH$_3$), 3.78 (s, 3H, 3″-OCH$_3$), 3.35 (m, 2H, H-2), 3.28 (m, 2H, H-1), 2.43 (s, 3H, 2′-CH$_3$), 1.81 (s, 3H, NHCOCH$_3$). $^{13}$C NMR (125 MHz, DMSO-$d_6$) $\delta$ (ppm): 169.9 (C═O), 148.6 (C-3″), 148.4 (C-4″), 144.0 (C-6′), 142.3 (C-8′), 136.9 (C-2′), 132.4 (C-9′), 124.5 (C-3′), 122.1 (C-6″), 121.9 (C-1″), 113.2 (C-2″), 111.9 (C-5″), 90.1 (C-7′), 55.8 (4′-OCH$_3$), 55.8 (3′-OCH$_3$), 41.7 (C-2″), 37.9 (C-1″), 22.9 (CO-CH$_3$), 14.8 (2′-CH$_3$). Anal. ($C_{19}H_{23}ClN_5O_3$) C, H, N. HRMS: calcd for [M + H], 370.18737; found, 370.18749.

**6-Chloro-3-iodo-2-methylimidazo[1,2-*b*]pyridazin-8-amine (48).** Compound **34** (141 mg, 4.3 mmol) was diluted with ethanolic



DOI: 10.1021/acs.jmedchem.5b00499
J. Med. Chem. 2015, 58, 3767−3793

Table 3. Statistics of Crystallographic Data Collection and Refinement[a]

| crystal | PI4K IIIβ + ATP | PI4K IIIβ + MI103 |
|---|---|---|
| space group | P $4_3$ | P $4_3$ |
| cell dimensions (Å) | $a$ = 108.3, $b$ = 108.3, $c$ = 55.1 | $a$ = 108.4, $b$ = 108.4, $c$ = 55.1 |
| X-ray source | BESSY ID 14-1 | BESSY ID 14-1 |
| wavelength (Å) | 0.918409 | 0.918417 |
| resolution (Å) | 48.45−3.318 (3.436−3.318) | 49.14−3.407 (3.529−3.407)[b] |
| no. of unique reflections | 9684 (953) | 8935 (850) |
| $I/\sigma$ ($I$) | 6.59 (2.35) | 5.81 (1.73) |
| $R_{merge}$ | 24.2 | 39.8 |
| data completeness (%) | 99.79 (99.06) | 99.81 (98.15) |
| mltiplicity | 4.5 | 7.5 |
| $R_{work}$ (%) | 18.25 (23.83) | 20.89 (27.77) |
| $R_{free}$ (%) | 24.41 (33.34) | 25.16 (34.40) |
| rms bond angle deviation (deg) | 0.012 | 0.013 |
| rms bond angle deviation (Å) | 1.59 | 1.11 |

[a]Numbers in parentheses refer to the highest resolution shell of the respective data set.

[b]$I/\sigma$ ($I$) = 2 at resolution 3.56 Å.

ammonia (4.5 mL, 4M) and heated in a microwave reactor at 140 °C for 90 min. After completion of the reaction (monitored by TLC, EtOAc:acetone:EtOH:$H_2O$ 20:3:1:1), the reaction mixture was directly adsorbed on silica gel and purified by column chromatography (hexane/EtOAc 3:2 to 1:1). Recrystallization from hot MeOH afforded greenish crystals of **48**. Yield 108 mg (77%); mp 244.4−245.7 °C. $^1$H NMR (500 MHz, DMSO-$d_6$) $\delta$ (ppm): 7.40 (bs, 2H, 8-$NH_2$), 6.18 (s, 1H, H-7), 2.34 (s, 3H, 2-$CH_3$). $^{13}$C NMR (125 MHz, DMSO-$d_6$) $\delta$ (ppm): 147.1 (C-6), 144.3 (C-8), 144.0 (C-2), 134.4 (C-9), 94.5 (C-7), 71.9 (3), 14.9 (2-$CH_3$). Anal. ($C_7H_7ClN_4I$) C, H, N. HRMS: calcd for [M + H], 308.93984; found, 308.93992.

**6-Chloro-3-(3,4-dimethoxyphenyl)-2-methylimidazo[1,2-*b*]-pyridazin-8-amine (49).** Compound **48** (176 mg, 0.57 mmol) was dissolved in 1,4-dioxane (8 mL) and (3,4-dimethoxyphenyl)boronic acid (124 mg, 0.68 mmol) followed by 1 M potassium carbonate solution (2 mL) was added. The reaction mixture was stirred and degassed 3 times, after which Pd($PPh_3$)$_4$ (5 mol %) was added, and the mixture was degassed once more, heated up to 90 °C, and stirred overnight. After cooling to rt, the mixture was diluted with water and extracted with EtOAc (2 × 50 mL), and the combined organic phases were dried over sodium sulfate and evaporated. Residue was dissolved in a minimal volume of DCM/MeOH, adsorbed on silica gel, and purified by column chromatography (EtOAc). Recrystallization from hot MeOH/$CHCl_3$ 6:1 afforded analytical sample **49** as an off-white solid. Yield: 145 mg (80%); mp 230.9−231.7 °C. $^1$H NMR (500 MHz, DMSO-$d_6$) $\delta$ (ppm): 7.31 (bs, 2H, 8-$NH_2$), 7.21 (d, $J_{2'-6'}$ = 2.0, 1H, H-2′), 7.16 (dd, $J_{6'-2'}$ = 2.0, $J_{6'-5'}$ = 8.3, 1H, H-6′), 7.10 (d, $J_{5'-6'}$ = 8.3, 1H, H-5′), 6.15 (s, 1H, H-7), 3.82 (s, 3H, 3′-O-$CH_3$), 3.78 (s, 3H, 4′-O-$CH_3$), 2.42 (s, 3H, 2-$CH_3$). $^{13}$C NMR (125 MHz, DMSO-$d_6$) $\delta$ (ppm): 148.7 and148.6 (C3′ and C4′), 146.5 (C-6), 144.4 (C-8), 137.7 (C-2), 131.0 (C-9), 125.1 (C-3), 122.1 (C-6′), 121.1 (C-1′), 113.2 (C-2′), 112.0 (C-5′), 93.7 (C-7), 55.8 and 55.8 (3′-O-$CH_3$ and 4′-O-$CH_3$), 14.7 (2-$CH_3$). Anal. ($C_{15}H_{15}ClN_4O_2$·0.17$CHCl_3$) C, H, N.

**Protein Expression and Purification.** The PI4K IIIβ was expressed and purified using protocols developed in our laboratory.[4,47,48] Briefly, the protein was affinity purified by using Ni-NTA resin (QIAGEN). Upon cleavage of the 6× His affinity tag, the PI4K IIIβ was further purified at Superdex 200 column (GE Healthcare) in 20 mM citrate, pH = 5.5, 200 mMNaCl, 3 mM β-mercaptoethanol. PI4K IIIβ was concentrated to ∼5 mg/mL, flash frozen in liquid nitrogen, and stored at −80 °C until use.

**Crystallization and Structure Determination.** Before setting up crystal drops, the protein was supplemented with 5 mM ATP and 2 mM $MgCl_2$, or in the case of the structure with MI103 inhibitor bound, the PI4K IIIβ was incubated overnight at 4 °C with 0.5 mM MI103. The crystals grew 5 days at 293 K in sitting drops consisting of a 1:1 mixture of the protein and a well solution (100 mM MOPS/HEPES-Na pH 7.5, 10% w/v PEG 4000, 30 mM diethylene glycol, 30 mM triethylene glycol, 20% v/v glycerol). The crystals were directly frozen in liquid nitrogen, and complete data sets were collected at the MX-14.1 beamLine at BESSY II, Berlin. The structures were solved by molecular replacement using the PI4K IIIβ in complex with PIK93 (PDB code 4D0L) and refined using Phenix[49] to $R_{work}$ = 18.25% and $R_{free}$ = 24.41% for the structure with ATP bound and to $R_{work}$ = 20.89% and $R_{free}$ = 25.16% for the structure with **49** bound as detailed in Table 3.

**Inhibition of the Activity of PI4Ks.** The lipid kinase activity was determined by ADP-Glo kinase assay (Promega) measuring the amount of ADP produced during the kinase reaction. Reactions were carried out in a total volume of 5 μL and contained PI4K enzyme (final concentration for PI4K IIIβ was 4 ng/μL, for PI4K IIIα was 2 ng/μL, and for PI4K IIα was 2 ng/μL) in kinase buffer (20 mM TRIS pH 7.5, 5 mM $MgCl_2$, 0.2% Triton-X, 0.1 mg/mLBSA, 2 mM DTT), PI/PS (lipid kinase substrate) in kinase buffer (final concentration = 50 μM), and inhibitors (10 mM stock solutions in DMSO were diluted with kinase buffer to final concentration dependent on inhibitor's activity, e.g., 400−0.01, 300−0.0001, 150−0.00001 μM for PI4K IIIβ), and the reaction was started by adding ATP in kinase buffer (final concentration 100 μM). This reaction was carried out for 60 min/25 °C, and the amount of hydrolyzed ATP was measured according to the manufacturer's protocol (ADP/Glo reagent was added to terminate the kinase reaction and deplete the remaining ATP, then Kinase Detection Reagent was added to simultaneously convert ADP to ATP and allow the newly synthesized ATP to be measured using a luciferase/luciferin reaction). Luminescence was measured using spectrophotometer TECAN infinite M 1000.

**Screening of Antiviral Activity.** The anticoxsackie activity was measured by determining the extent to which the test compounds inhibited virus-induced cytopathic effect in HeLa cells. Briefly, 3-fold serial dilutions of compounds were added in triplicate in a 96-well plate with 30000 HeLa cells plated a day before in DMEM with L-glutamine supplemented with 2% fetal bovine serum (both GE Healthcare, Little Chalfont, UK), 100 U/mL of penicillin, and 100 μg/mL of streptomycin (Sigma-Aldrich, St. Louis, USA). After 1 h incubation, Coxsackie B3 virus (strain Nancy, ATCC, Manassas, USA) was added at multiplicity of infection at 0.005 IU/cell. Following 3 days incubation at 37 °C in a 5% $CO_2$ incubator, the cell viability was determined by addition of XTT solution (Sigma-Aldrich) for 4 h and the absorbance of newly formed orange formazan solution was measured using Victor X3 plate reader (PerkinElmer). Drug concentrations required to reduce viral cytopathic effect by 50% ($EC_{50}$) were calculated using nonlinear regression analysis from plots of percentage cell viability versus $log_{10}$ drug concentration using GraphPad Prism v.6.02 (GraphPad Software, La Jolla, USA).



DOI: 10.1021/acs.jmedchem.5b00499
J. Med. Chem. 2015, 58, 3767−3793

The antirhinovirus activity of test compounds was measured in H1-HeLa cells. Compounds were prepared in replicate 3-fold serial dilutions in DMSO (384-well format), and 0.1 μL of these dilutions were transferred acoustically to assay plates with an Echo instrument. H1-HeLa cells in RPMI medium supplemented with 10% heat inactivated FBS and antibiotics were premixed in batch with mixture of HRV1A, HRV14, and HRV16 at a $TCID_{90}$ of 4× for each strain. After three day incubation at 33 °C, virus-induced cytopathic effects were determined by a Cell-Titer Glo viability assay (Promega, Madison, WI).

Anti-HCV activity of compounds was determined in multiplex assay using HUH 7-lunet, stably replicating I389luc-ubi-neo/NS3-3′/ET genotype 1b replicon and 2aLucNeo-25 cell line encoding a genotype 2a JFH-1 replicon. Cells were maintained in Dulbecco DMEM medium supplemented with GlutaMAX (Invitrogen), 10% FBS (not heat-inactivated), 1 mg/mL G-418, Pen-Strep, and nonessential amino acids. Cells were plated into 384-well assay plates with 1600 cells per well and treated with serial dilutions of compounds. Following three day incubation, the activity of Renilla luciferase was quantified using the Dual-Glo luciferase assay system from Promega (Promega, Madison, WI).

**Docking.** The 3D structures of the docked molecules were built using ACD/ChemSketch 12.01,[50] and the geometry was optimized with MOPAC2012[51] using the PM7 method. The necessary format conversions were performed using OpenBabel.[52] The preparation of the pdbqt files was done by standard procedure using AutoDock Tools 1.5.6. The docking runs were performed in AutoDock Vina using the default scoring function. Docking of the ligands into the binding pocket was performed in 24 × 34 × 30 $Å^3$ search space centered at 25, 33, and 0.5 Å and exhaustiveness 100.[53] Because the position of several important residues varies in the two crystal structures, we decided to use flexible docking into the structure with MI103 in order to simulate flexibility of the enzyme (4WAG strucute was used for this purpose). We set $Lys^{564}$ and $Tyr^{400}$ as flexible residues that resulted in obtaining the most reliable results of the docking. The docking results of the top five compounds are summarized in Supporting Information.

## ■ ASSOCIATED CONTENT

### Supporting Information

Detailed SAR discussion, results of biochemical assays for remaining compounds, and supplementary figures. The Supporting Information is available free of charge on the ACS Publications website at DOI: 10.1021/acs.jmedchem.5b00499.

### Accession Codes

The atomic coordinates and structure factors have been deposited in the RCSB Protein Data Bank, www.pdb.org (accession codes 4WAE and 4WAG).

## ■ AUTHOR INFORMATION


### Corresponding Authors

*For E.B.: phone, +420-220-183-465; E-mail, boura@uochb.cas.cz.

*For R.N.: phone, +420-220-183-265; E-mail, nencka@uochb.cas.cz.

### Author Contributions

§I.M., D.C. and M.K. contributed equally to this work.


### Notes

The authors declare the following competing financial interest(s): The project was partially founded by a private company Gilead Sciences, Inc.

## ■ ACKNOWLEDGMENTS

We are grateful to Dr. Tamas Balla, Dr. David Murray, Dr. Eric Lansdon, and Michael Downey for critical reading of our manuscript. We are grateful to Eva Zborníková for measurement of HPLC-MS spectra. The project was supported by the Czech Science Foundation (registration no. 15-09310S to I.M., D.C., M.Š., P.P. and R.N. and 15-21030Y to A.B. and E.B) and by the Academy of Sciences Czech Republic (RVO: 61388963). MarieCurie FP7-PEOPLE-2012-CIG project number 333916 and Project InterBioMed LO1302 from Ministry of Education of the Czech Republic are also acknowledged. The work was supported by Gilead Sciences, Inc. The research leading to these results has received funding from the European Community's Seventh Framework Programme (FP7/2007–2013) under BioStruct-X (grant agreement no. 283570). We thank H.Z.B. for the allocation of synchrotron radiation beamtime.

## ■ ABBREVIATIONS USED

ACBD3, Golgi resident protein GCP60; Ade, adenine; AP, clathrin-associated adaptor protein complex; Arf, ADP-ribosylation factor; CVB3, Coxsackievirus B3; Erf3, eukaryotic release factor 3; GBF1, Golgi-specific brefeldin A-resistance guanine nucleotide exchange factor 1; HRV, human rhinovirus; MERS, Middle East respiratory syndrome coronavirus; PI4K, phosphatidylinositol 4-kinase; PI4P, phosphatidylinositol 4-phosphate; SARS, severe acute respiratory syndrome coronavirus; TNG, trans-Golgi network

## ■ REFERENCES


(1) Balla, T. Phosphoinositides: Tiny Lipids with Giant Impact on Cell Regulation. *Phys. Rev.* **2013**, *93*, 1019–1137.

(2) Balla, A.; Balla, T. Phosphatidylinositol 4-kinases: old enzymes with emerging functions. *Trends Cell. Biol.* **2006**, *16*, 351–361.

(3) Minogue, S.; Waugh, M. The Phosphatidylinositol 4-Kinases: Don't Call it a Comeback. In *Phosphoinositides I: Enzymes of Synthesis and Degradation*; Balla, T., Wymann, M., York, J. D., Eds.; Springer Verlag: New York, 2012; Volume *58*, pp 1–24.

(4) Baumlova, A.; Chalupska, D.; Różycki, B.; Jovic, M.; Wisniewski, E.; Klima, M.; Dubankova, A.; Kloer, D. P.; Nencka, R.; Balla, T.; Boura, E. The crystal structure of the phosphatidylinositol 4-kinase IIα. *EMBO Rep.* **2014**, *15*, 1085–1092.

(5) Zhou, Q.; Li, J.; Yu, H.; Zhai, Y.; Gao, Z.; Liu, Y.; Pang, X.; Zhang, L.; Schulten, K.; Sun, F.; Chen, C. Molecular insights into the membrane-associated phosphatidylinositol 4-kinase II alpha. *Nature Commun.* **2014**, *5*, 3552 DOI: 10.1038/ncomms4552.

(6) Burke, J. E.; Inglis, A. J.; Perisic, O.; Masson, G. R.; McLaughlin, S. H.; Rutaganira, F.; Shokat, K. M.; Williams, R. L. Structures of PI4KIIIβ complexes show simultaneous recruitment of Rab11 and its effectors. *Science* **2014**, *344*, 1035–1038.

(7) Wang, Y. J.; Wang, J.; Sun, H. Q.; Martinez, M.; Sun, Y. X.; Macia, E.; Kirchhausen, T.; Albanesi, J. P.; Roth, M. G.; Yin, H. L. Phosphatidylinositol 4 phosphate regulates targeting of clathrin adaptor AP-1 complexes to the golgi. *Cell* **2003**, *114*, 299–310.

(8) Minogue, S.; Waugh, M. G.; De Matteis, M. A.; Stephens, D. J.; Berditchevski, F.; Hsuan, J. J. Phosphatidylinositol 4-kinase is required for endosomal trafficking and degradation of the EGF receptor. *J. Cell Sci.* **2006**, *119*, 571–580.

(9) Jović, M.; Kean, M. J.; Dubankova, A.; Boura, E.; Gingras, A.-C.; Brill, J. A.; Balla, T. Endosomal sorting of VAMP3 is regulated by PI4K2A. *J. Cell Sci.* **2014**, *127*, 3745–3756.

(10) Jović, M.; Kean, M. J.; Szentpetery, Z.; Polevoy, G.; Gingras, A.-C.; Brill, J. A.; Balla, T. Two phosphatidylinositol 4-kinases control lysosomal delivery of the Gaucher disease enzyme, β-glucocerebrosidase. *Mol. Biol. Cell* **2012**, *23*, 1533–1545.

(11) Craige, B.; Salazar, G.; Faundez, V. Phosphatidylinositol-4-kinase type II alpha contains an AP-3-sorting motif and a kinase domain that are both required for endosome traffic. *Mol. Biol. Cell* **2008**, *19*, 1415–1426.

(12) Wieffer, M.; Uhalte, E. C.; Posor, Y.; Otten, C.; Branz, K.; Schutz, L.; Mossinger, J.; Schu, P.; Abdelilah-Seyfried, S.; Krauss, M.; Haucke, V. PI4K2 beta/AP-1-Based TGN-Endosomal Sorting Regulates Wnt Signaling. *Curr. Biol.* **2013**, *23*, 2185−2190.
(13) Wu, X.; Chi, R. J.; Baskin, J. M.; Lucast, L.; Burd, C. G.; De Camilli, P.; Reinisch, K. M. Structural Insights into Assembly and Regulation of the Plasma Membrane Phosphatidylinositol 4-Kinase Complex. *Dev. Cell* **2014**, *28*, 19−29.
(14) Chung, J.; Nakatsu, F.; Baskin, J. M.; De Camilli, P. Plasticity of PI4KIIIalpha interactions at the plasma membrane. *EMBO Rep.* **2015**, *16*, 312−20.
(15) Sasaki, J.; Ishikawa, K.; Arita, M.; Taniguchi, K. ACBD3-mediated recruitment of PI4KB to picornavirus RNA replication sites. *EMBO J.* **2012**, *31*, 754−766.
(16) Godi, A.; Pertile, P.; Meyers, R.; Marra, P.; Di Tullio, G.; Iurisci, C.; Luini, A.; Corda, D.; De Matteis, M. A. ARF mediates recruitment of PtdIns-4-OH kinase-[bgr] and stimulates synthesis of PtdIns(4,5)-P2 on the Golgi complex. *Nature Cell Biol.* **1999**, *1*, 280−287.
(17) Audhya, A.; Emr, S. D. Stt4 PI 4-kinase localizes to the plasma membrane and functions in the Pkc1-mediated MAP kinase cascade. *Dev. Cell* **2002**, *2*, 593−605.
(18) Strahl, T.; Hama, H.; DeWald, D. B.; Thorner, J. Yeast phosphatidylinositol 4-kinase, Pik1, has essential roles at the Golgi and in the nucleus. *J. Cell Sci.* **2005**, *171*, 967−979.
(19) Altan-Bonnet, N.; Balla, T. Phosphatidylinositol 4-kinases: hostages harnessed to build panviral replication platforms. *Trends Cell Biol.* **2012**, *37*, 293−302.
(20) Berger, K. L.; Cooper, J. D.; Heaton, N. S.; Yoon, R.; Oakland, T. E.; Jordan, T. X.; Mateu, G.; Grakoui, A.; Randall, G. Roles for endocytic trafficking and phosphatidylinositol 4-kinase III alpha in hepatitis C virus replication. *Proc. Natl. Acad. Sci. U. S. A.* **2009**, *106*, 7577−7582.
(21) LaMarche, M. J.; Borawski, J.; Bose, A.; Capacci-Daniel, C.; Colvin, R.; Dennehy, M.; Ding, J.; Dobler, M.; Drumm, J.; Gaither, L. A.; Gao, J.; Jiang, X.; Lin, K.; McKeever, U.; Puyang, X.; Raman, P.; Thohan, S.; Tommasi, R.; Wagner, K.; Xiong, X.; Zabawa, T.; Zhu, S.; Wiedmann, B. Anti-Hepatitis C Virus Activity and Toxicity of Type III Phosphatidylinositol-4-Kinase Beta Inhibitors. *Antimicrob. Agents Chemother.* **2012**, *56*, 5149−5156.
(22) Borawski, J.; Troke, P.; Puyang, X. L.; Gibaja, V.; Zhao, S. C.; Mickanin, C.; Leighton-Davies, J.; Wilson, C. J.; Myer, V.; CornellaTaracido, I.; Baryza, J.; Tallarico, J.; Joberty, G.; Bantscheff, M.; Schirle, M.; Bouwmeester, T.; Mathy, J. E.; Lin, K.; Compton, T.; Labow, M.; Wiedmann, B.; Gaither, L. A. Class III Phosphatidylinositol 4-Kinase Alpha and Beta Are Novel Host Factor Regulators of Hepatitis C Virus Replication. *J. Virol.* **2009**, *83*, 10058−10074.
(23) Greninger, A. L.; Knudsen, G. M.; Betegon, M.; Burlingame, A. L.; DeRisi, J. L. The 3A Protein from Multiple Picornaviruses Utilizes the Golgi Adaptor Protein ACBD3 To Recruit PI4KIII beta. *J. Virol.* **2012**, *86*, 3605−3616.
(24) Arita, M.; Kojima, H.; Nagano, T.; Okabe, T.; Wakita, T.; Shimizu, H. Phosphatidylinositol 4-Kinase III Beta Is a Target of Enviroxime-Like Compounds for Antipoliovirus Activity. *J. Virol.* **2011**, *85*, 2364−2372.
(25) Alastruey-Izquierdo, A.; Mellado, E.; Pelaez, T.; Peman, J.; Zapico, S.; Alvarez, M.; Rodriguez-Tudela, J. L.; Cuenca-Estrella, M.; Grp, F. S. Phosphatidylinositol 4-Kinase III Beta Is Essential for Replication of Human Rhinovirus and Its Inhibition Causes a Lethal Phenotype in Vivo. *Antimicrob. Agents Chemother.* **2013**, *57*, 3358−3368.
(26) Mello, C.; Aguayo, E.; Rodriguez, M.; Lee, G.; Jordan, R.; Cihlar, T.; Birkus, G. Multiple Classes of Antiviral Agents Exhibit in Vitro Activity against Human Rhinovirus Type C. *Antimicrob. Agents Chemother.* **2014**, *58*, 1546−1555.
(27) Yang, N.; Ma, P.; Lang, J.; Zhang, Y.; Deng, J.; Ju, X.; Zhang, G.; Jiang, C. Phosphatidylinositol 4-Kinase III$\beta$ Is Required for Severe Acute Respiratory Syndrome Coronavirus Spike-Mediated Cell Entry. *J. Biol. Chem.* **2012**, *287*, 8457−8467.
(28) Berger, K. L.; Kelly, S. M.; Jordan, T. X.; Tartell, M. A.; Randall, G. Hepatitis C Virus Stimulates the Phosphatidylinositol 4-Kinase III Alpha-Dependent Phosphatidylinositol 4-Phosphate Production That Is Essential for Its Replication. *J. Virol.* **2011**, *85*, 8870−8883.
(29) Dorobantu, C. M.; van der Schaar, H. M.; Ford, L. A.; Strating, J. R. P. M.; Ulferts, R.; Fang, Y.; Belov, G.; van Kuppeveld, F. J. M. Recruitment of PI4KIII$\beta$ to Coxsackievirus B3 Replication Organelles Is Independent of ACBD3, GBF1, and Arf1. *J. Virol.* **2014**, *88*, 2725−2736.
(30) Bojjireddy, N.; Botyanszki, J.; Hammond, G.; Creech, D.; Peterson, R.; Kemp, D. C.; Snead, M.; Brown, R.; Morrison, A.; Wilson, S.; Harrison, S.; Moore, C.; Balla, T. Pharmacological and genetic targeting of pPI4KA reveals its important role in maintaining plasma membrane PtdIns4p and PtdIns(4,5)p2 levels. *J. Biol. Chem.* **2014**, *289*, 6120−6132 DOI: 10.1074/jbc.M113.531426.
(31) Vaillancourt, F. H.; Brault, M.; Pilote, L.; Uyttersprot, N.; Gaillard, E. T.; Stoltz, J. H.; Knight, B. L.; Pantages, L.; McFarland, M.; Breitfelder, S.; Chiu, T. T.; Mahrouche, L.; Faucher, A.-M.; Cartier, M.; Cordingley, M. G.; Bethell, R. C.; Jiang, H.; White, P. W.; Kukolj, G. Evaluation of Phosphatidylinositol-4-kinase III alpha as a Hepatitis C Virus Drug Target. *J. Virol.* **2012**, *86*, 11595−11607.
(32) Waring, M. J.; Andrews, D. M.; Faulder, P. F.; Flemington, V.; McKelvie, J. C.; Maman, S.; Preston, M.; Raubo, P.; Robb, G. R.; Roberts, K.; Rowlinson, R.; Smith, J. M.; Swarbrick, M. E.; Treinies, I.; Winter, J. J. G.; Wood, R. J. Potent, selective small molecule inhibitors of type III phosphatidylinositol-4-kinase alpha-but not beta-inhibit the phosphatidylinositol signaling cascade and cancer cell proliferation. *Chem. Commun.* **2014**, *50*, 5388−5390.
(33) Leivers, A. L.; Tallant, M.; Shotwell, J. B.; Dickerson, S.; Leivers, M. R.; McDonald, O. B.; Gobel, J.; Creech, K. L.; Strum, S. L.; Mathis, A.; Rogers, S.; Moore, C. B.; Botyanszki, J. Discovery of Selective Small Molecule Type III Phosphatidylinositol 4-Kinase Alpha (P14KIII alpha) Inhibitors as Anti Hepatitis C (HCV) Agents. *J. Med. Chem.* **2014**, *57*, 2091−2106.
(34) Keaney, E. P.; Connolly, M.; Dobler, M.; Karki, R.; Honda, A.; Sokup, S.; Karur, S.; Britt, S.; Patnaik, A.; Raman, P.; Hamann, L. G.; Wiedmann, B.; LaMarche, M. J. 2-Alkyloxazoles as potent and selective PI4KIII$\beta$ inhibitors demonstrating inhibition of HCV replication. *Bioorg. Med. Chem. Lett.* **2014**, *24*, 3714−3718.
(35) MacLeod, A. M.; Mitchell, D. R.; Palmer, N. J.; de Poel, H. V.; Conrath, K.; Andrews, M.; Leyssen, P.; Neyts, J. Identification of a Series of Compounds with Potent Antiviral Activity for the Treatment of Enterovirus Infections. *ACS Med. Chem. Lett.* **2013**, *4*, 20−24.
(36) Spickler, C.; Lippens, J.; Laberge, M.-K.; Desmeules, S.; Bellavance, É.; Garneau, M.; Guo, T.; Hucke, O.; Leyssen, P.; Neyts, J.; Vaillancourt, F. H.; Décor, A.; O'Meara, J.; Franti, M.; Gauthier, A. Phosphatidylinositol 4-Kinase III Beta Is Essential For Replication of Human Rhinovirus and Its Inhibition Causes a Lethal Phenotype in Vivo. *Antimicrob. Agents Chemother.* **2013**, *57*, 3358−3368.
(37) Chen, C.; Wilcoxen, K. M.; Huang, C. Q.; McCarthy, J. R.; Chen, T.; Grigoriadis, D. E. Optimization of 3-phenylpyrazolo-1,5-*a* pyrimidines as potent corticotropin-releasing factor-1 antagonists with adequate lipophilicity and water solubility. *Bioorg. Med. Chem. Lett.* **2004**, *14*, 3669−3673.
(38) Kazock, J. Y.; Enguehard-Gueiffier, U.; Thery, I.; Gueiffier, A. Evaluation of the 2-substituent effect on the reactivity of the 8-haloimidazo 1,2-*a* pyridine series towards Suzuki-type cross-coupling reaction. *Bull. Chem. Soc. Jpn.* **2005**, *78*, 154−159.
(39) LeClercq, L. C. L., ; Bartolomé-Nebreda, J. M.; Conde-Ceide, S.; Van Gool, M. L. M. Inhibitors of phosphodiesterase 10 enzyme. WO2014009305 A1, 2014.
(40) Cooper, T.; Novak, A.; Humphreys, L. D.; Walker, M. D.; Woodward, S. User-friendly methylation of aryl and vinyl halides and pseudohalides with DABAL-Me-3. *Adv. Synth. Catal.* **2006**, *348*, 686−690.
(41) Zuev, D.; Mattson, R. J.; Huang, H.; Mattson, G. K.; Zueva, L.; Nielsen, J. M.; Kozlowski, E. S.; Huang, X. S.; Wu, D.; Gao, Q.; Lodge, N. J.; Bronson, J. J.; Macor, J. E. Potential CRF1R PET Imaging Agents: *N*-Fluoroalkyl-8-(6-methoxy-2-methylpyridin-3-yl)-2,7-di-


DOI: 10.1021/acs.jmedchem.5b00499
*J. Med. Chem.* 2015, 58, 3767−3793

methyl-*N*-alkylpyrazolo-1,5-*a*-1,3,5 triazin-4-amines. *Bioorg. Med. Chem. Lett.* **2011**, *21*, 2484−2488.
(42) Tai, A. W.; Bojjireddy, N.; Balla, T. A homogeneous and nonisotopic assay for phosphatidylinositol 4-kinases. *Anal. Biochem.* **2011**, *417*, 97−102.
(43) Debreczeni, J. E.; Emsley, P. Handling ligands with Coot. *Acta Crystallogr., Sect. D: Biol. Crystallogr.* **2012**, *68*, 425−430.
(44) Rozycki, B.; Boura, E. Large, dynamic, multi-protein complexes: a challenge for structural biology. *J. Phys.: Condens. Matter* **2014**, *26*, 463103 DOI: 10.1088/0953-8984/26/46/463103.
(45) Pastor-Fernández, J.; Bartolomé-Nebreda, J. M.; MacDonald, G. J.; Conde-Ceide, S.; Delgado-González, Ó.; Vanhoof, G. C. P.; Van Gool, M. L. M.; Martín-Martín, M. L.; Alonso-De Diego, S. A. Imidazo[1,2-*b*]pyridazine derivatives and their use as PDE10 inhibitors. WO 2011/051342 A1, 2011.
(46) Walsh, J. J.; Shah, R.; McCormack, E. M.; Hudson, G. J.; White, M.; Stack, G. D.; Moran, B. W.; Coogan, A.; Breen, E. C. Tubulin binding agents. WO 2013/026942, 2013.
(47) Nemecek, D.; Boura, E.; Wu, W.; Cheng, N.; Plevka, P.; Qiao, J.; Mindich, L.; Heymann, J. B.; Hurley, J. H.; Steven, A. C. Subunit Folds and Maturation Pathway of a dsRNA Virus Capsid. *Structure* **2013**, *21*, 1374−1383.
(48) Boura, E.; Rezabkova, L.; Brynda, J.; Obsilova, V.; Obsil, T. Structure of the human FOXO4−DBD−DNA complex at 1.9 A resolution reveals new details of FOXO binding to the DNA. *Acta Crystallogr., Sect. D: Biol. Crystallogr.* **2010**, *66*, 1351−1357.
(49) Adams, P. D.; Afonine, P. V.; Bunkoczi, G.; Chen, V. B.; Davis, I. W.; Echols, N.; Headd, J. J.; Hung, L. W.; Kapral, G. J.; Grosse-Kunstleve, R. W.; McCoy, A. J.; Moriarty, N. W.; Oeffner, R.; Read, R. J.; Richardson, D. C.; Richardson, J. S.; Terwilliger, T. C.; Zwart, P. H. PHENIX: a comprehensive Python-based system for macromolecular structure solution. *Acta Crystallogr., Sect. D: Biol. Crystallogr.* **2010**, *66*, 213−221.
(50) *ACD/ChemSketch*, 12.01; Advanced Chemistry Development, Inc.: Toronto, Ontario, Canada, 2014; www.acdlabs.com.
(51) Stewart J. P. *MOPAC2012*, version 7.263W; Stewart Computational Chemistry: Colorado Springs, CO, 2012; HTTP://OpenMOPAC.net, .
(52) O'Boyle, N.; Banck, M.; James, C.; Morley, C.; Vandermeersch, T.; Hutchison, G. Open Babel: An open chemical toolbox. *J. Cheminform.* **2011**, 3, 33 DOI: 10.1186/1758-2946-3-33.
(53) Trott, O.; Olson, A. J. Software News and Update AutoDock Vina: Improving the Speed and Accuracy of Docking with a New Scoring Function, Efficient Optimization, and Multithreading. *J. Comput. Chem.* **2010**, *31*, 455−461.



DOI: 10.1021/acs.jmedchem.5b00499
*J. Med. Chem.* 2015, 58, 3767−3793

# 6 Discussion

## 6.1 Structural characterisation of PI4-kinases type II.

PI4K IIα and IIβ were poorly characterised members of the PI4K family. Their substrate specificity, mode of regulation and membrane association, poor sequence similarity with other homologues and different structural motifs make them distinct from type III PI4-kinases belonging to the same family. Their emerging role in fundamental biological processes and human pathologies make them an ever more attractive target for further research. Due to a lack of functional and structural studies elucidating their mechanism of action and regulation, we performed structural characterisation of both isoforms at the atomic level.

We were not able to express the full length protein (1-479 amino acids) of PI4K IIα in the *E.Coli* expression system. Instead, we used secondary structure prediction to design several truncated variants. These variants were further tested and the variant (76-479) with the highest expression yield was used in subsequent experiments. The variant lacking the first 75 amino acids was termed "pseudo-wildtype" in our experiments since it still possessed full enzymatic activity. This variant was used for biochemical analysis but for structural studies it had to be further modified. The palmitoylation motif (173-LCCPCCF-179) was replaced by a three-amino acid linker followed by T4 lysozyme in order to improve protein solubility, crystal growth and diffraction properties. Furthermore, the last 12 C-terminal amino acids were deleted. The final construct containing amino acids 76-467 and inserted T4 lysozyme was co-crystallized with ATP. It formed small but well diffracting crystals (2.8 Å resolution) that belonged to the orthorombic $P2_12_12$ space group. Since PI4K IIα does not bear high sequence similarity with other homologues and no crystal structures of potential homologous candidates were determined at that time, the molecular replacement (MR) method was not sufficient to solve the crystal structure. In order to solve the phase problem, soaking with heavy atoms or preparation of SeMet crystals were tested. Finally, the SeMet crystals provided a sufficient anomalous signal for solving the crystal structure using a combination of MR-SAD (T4 lysozyme provided partial phase information). The crystal structure of PI4K IIα revealed an atypical kinase fold with the catalytic domain distinguished into an N- and C-lobe. The active site with the ATP bound substrate was identified in the groove positioned between these two lobes. The residues defining the ATP binding site held ATP via electrostatic interactions and direct or

water molecule coordinated hydrogen bonds. The relevance of the individual residues for ATP binding was verified using mutagenesis analysis in combination with *in vitro* kinase assay. The unexpected presence of a second ATP molecule was also observed in this structure. The second ATP was identified in the lateral hydrophobic pocket of the C-lobe wherein it was held by interactions with aromatic residues. The precise function of this pocket is not fully understood. In order to provide insight into the putative function of this lateral hydrophobic pocket, we performed enzymatic assay with mutated variants of this enzyme in their natural environment and *in vitro* experiment. Results from these experiments indicate that double mutation of tryptophan residues Trp359,368Ala in the hydrophobic pocket significantly reduced but did not eliminate the kinase activity in the case of the palmitoylated protein. However, significant impairment of the enzymatic activity was observed even for single mutants (Trp359Ala, Trp368Ala) bacterially expressed and thus non palmitoylated. Taken together, these data suggest that the relevance of the hydrophobic pocket increases with the lack of palmitoylation. Since the enzymatic activity of PI4K IIα is determined by its association with the membrane and the mutations in the hydrophobic pocket have impact on the lipid kinase activity, we suppose that this pocket could be important for membrane binding and proper positioning of PI4K IIα with respect to the membrane. Furthermore, we were interested in how the lateral hydrophobic pocket together with the palmitoylation motif affect the membrane binding mode of PI4K IIα. Therefore, molecular dynamic simulations of the membrane bound kinase were performed. Based on these data we proposed that the enzyme affixes to the membrane mainly via palmitoylation, however, also other parts of the protein including the lateral hydrophobic pocket, the amphipathic segment defined as residues Lys165-Lys172, helices H5 and H7 collectively contribute to the correct orientation toward the membrane. To verify our model, certain residues predicted at the membrane-protein interface were subjected to the mutation analysis. Reduction or complete inhibition of the enzymatic activity therefore confirmed the plausibility of our MD structural model.

Our crystallization efforts were also directed toward PI4K IIβ since it is the closet homolog of PI4K IIα and the most poorly investigated member of the PI4K family.

We employed the same strategy to obtain well diffracting crystals of PI4K IIβ as in the case of PI4K IIα. A large N-terminal part and a shorter C-terminal part of the protein were omitted since they were shown to be disordered based on prediction analysis and the crystal structure of PI4K IIα. The truncated variant of PI4K IIβ (90-450 amino acids) with

T4 lysozyme insertion was supplemented with ATP and used for crystallization experiments. Obtained crystals diffracted to 1.9 Å and belonged to the tetragonal $P4_12_12$ space group. The structure was solved by the molecular replacement method with PI4K IIα as a search model. The high resolution crystal structure of PI4K IIβ enabled us to confirm the large structural similarity with PI4K IIα in general. The superposition of the two structures revealed the same atypical kinase fold for both isoforms and highly conserved active sites with the exception of Ser127 (corresponding to Tyr131 in the α isoform) exhibiting a different conformation. However, the importance of this residue seems to be negligible due to its position in the flexible loop where it is pointing out from the ATP binding cavity. The presence of the newly discovered lateral hydrophobic pocket was also confirmed in this structure, however, it was lacking the second ATP. The absence of the second ATP could be explained by different crystal packing where one lateral pocket packs against another lateral pocket from a different molecule. A detailed analysis of this pocket also revealed the conformational flexibility of Trp357 (is not visible in the structure due to its flexibility) and Trp366 (corresponding to Trp359 and Trp368 in the α isoform) which indicated the possibility for putative steric accommodation in the binding of a membrane substrate. Cholesterol serves as an attractive membrane substrate candidate as it has been shown to modulate the enzymatic activity of PI4K IIα [167]. Furthermore, we suppose that the conformational flexibility of the surface-exposed residues (Trp368 and Trp359) in the hydrophobic pocket could be important for membrane binding via immersion of these tryptophan residues into a lipid bilayer. This theory is also supported by the observed blue shift of tryptophan fluorescence upon addition of membrane to the recombinant protein [89].

In summary, structural studies of PI4K type II elucidated a novel non-typical kinase fold, confirmed the structural diversity with type III PI4-kinases and other lipid kinases and highlighted their high evolutionary conservation.

Isoform-specific inhibitors of type II PI4-kinases would be a useful tool to discriminate between these two variants and to examine their functions distinctively.

Therefore, we tested the extent of enzymatic activity inhibition for a series of adenosine analogues and preformed co-crystallization experiments with both protein isoforms. However, we succeeded in obtaining crystals only with PI4K IIα in complex with compound MD59. The crystal structure was solved by the molecular replacement method with PI4K IIα with omitted ATP molecules as a search model. The resulting

structure at 2.6 Å resolution showed conformational changes induced by inhibitor binding into the active site. In particular, a side chain of Asp346 adopts a conformation which allows hydrogen bonding to the hydroxyl group of MD59. Otherwise, this conformation would clash with the α-phosphate of the ATP molecule when ATP bound. The inhibitory potency of this compound against PI4K IIα was also confirmed by *in vitro* enzymatic assay in which MD59 exhibited moderate but still better than other adenosine-based compounds inhibitory activity. No significant inhibitory effect was observed against PI4K IIIβ. To understand why, we docked MD59 in the PI4K IIIβ structure in the same orientation that it has when bound to PI4K IIα. Docking studies revealed that the MD59 adenine ring would be rotated by 60° compared with the ATP adenine ring and thus unable to form the key hydrogen bonds to Lys564 and Glu572. Furthermore, the MD59 hydroxyl group does not form any hydrogen bonds to PI4K IIIβ.

Finally, we demonstrated that nucleoside scaffold-based inhibitors inhibit PI4K IIα potently and selectively.

## 6.2 Highly selective PI4K IIIβ inhibitors

+RNA viruses modulate lipid composition in order to form PtdIns4P enriched membrane platforms indispensable for assembling viral and host proteins into a functional replication complex. In order to achieve this functional state, +RNA viruses hijack type III PI4-kinases to generate so called membranous webs. A huge family of +RNA viruses encompasses animal, plant and notably human pathogenic viruses, most of them inducing cirrhosis and hepatocellular carcinoma (HCV), gastroenteritis (Aichi virus, Poliovirus), herpangina and meningitis (Coxsackie viruses), respiratory diseases (Rhinoviruses) and many others. Therefore, targeting the enzymatic activity of PI4K type III by isoform-specific inhibitors could be a feasible approach to combat different viral infections.

A novel series of PI4K IIIβ inhibitors with differently substituted imidazole-pyridazine moiety was designed using rational drug design. To determine the mechanism of action and the inhibitory potency and specificity, we performed co-crystallization trials and finally solved the crystal structures of PI4K IIIβ either with inhibitor 49 or with ATP. The construct of PI4K IIIβ used for crystallization trials was designed according to the previously solved crystal structure of PI4K IIIβ in complex with its binding partner Rab11 and non-specific lipid kinase inhibitor PIK93 [135].We used the molecular replacement method to solve both structures. Naturally, Rab 11 and PIK93 inhibitor were omitted from

the search model. The electron density for inhibitor 49 was clearly visible but the density for the phosphate moieties of the ATP molecule was missing, because they were disordered. The final crystal structures were at lower resolutions (3.3 Å and 3.5 Å, respectively), but they still provided sufficient structural information. Superposition of the two structures revealed that compound 49 occupied the ATP binding site and showed the extent to which the inhibitor induced conformational changes. The imidazole-pyridazine moiety of compound 49 occupies the same position as the adenine ring does in the active site and the methoxy group of the inhibitor´s aromatic side chain forms a direct hydrogen bond with Lys564 thus displacing Lys564 slightly further away from the active site. Altogether, this family of inhibitors function by providing steric interference for the adenine ring in binding to active site and hence inhibiting the lipid phosphorylation reaction. To confirm the inhibitory mechanism of the whole series of inhibitors, docking studies with selected compounds were performed as well.

The crystal structure of PI4K IIIβ in complex with compound 49 clarified the molecular basis for the specificity of this novel, highly potent class of PI4K IIIβ inhibitors.

# 7 Conclusion

This work significantly contributed to the structural characterisation of type II PI4-kinases, helped elucidate the detailed structural aspects of ligand binding and the role of the unexpected lateral hydrophobic pocket and furthermore, enabled us to outline the mechanism of membrane binding. The juxtaposition of both type II isoforms confirmed an evolutionary conserved non-typical kinase fold and indicated a very similar mode of action and regulation. However, the overall fold does not bear high structural similarity with type III PI4-kinases, instead it is more similar to the fold of Ser/Thr kinases thus indicating the protein kinases as structural relatives. We were not able to obtain crystals with inositol or inositol 1-phosphate bound, however, we were able to use docking and modelling to identify the putative phosphatidylinositol binding pocket.

Additionally, the crystal structures of PI4-kinases in complex with isoform-specific inhibitors provided structural information about the mechanism of inhibition and steric preferences necessary for selective inhibitor binding. The currently available inhibitors of PI4-kinases originate from inhibitors of the PI3-kinases class. Therefore, the structural studies of PI4-kinases either in complex with ATP or inhibitor provided the basis for the design of PI4K-specific inhibitors with potential implications in anti-viral therapy.

# 8 Abbreviations

| | |
|---|---|
| ACBD3 | acyl-CoA binding domain containing 3 |
| AP | adaptor protein |
| Arf1 | ADP-ribosylation factor 1 |
| ARM | armadillo repeat domain |
| ATGs | autophagy related proteins |
| CCVs | clathrin-coated vesicles |
| CERT | ceramide transfer protein |
| DAG | diacylglycerol |
| Dvl | Dishevelled protein |
| EGF | epidermal growth factor |
| ENTH domain | epsin N-terminal homology domain |
| ER | endoplasmic reticulum |
| FAPP1/FAPP2 | four-phosphate adaptor protein 1/2 |
| FERM domain | named according to: **F** for 4.1 protein, **E**zrin, **R**adixin, **M**oesin |
| FYVE domain | named according to: **F**ab1 (yeast orthologue of PIKfyve), **Y**OTB, **V**ac1 (vesicle transport protein), **E**EA1 |
| Fz | Frizzled protein |
| GABARAP | γ-aminobutyric acid receptor-associated protein |
| GBA | β-glucocerebrosidase |
| GBF1 | Golgi-specific brefeldin A-resistance guanine nucleotide exchange factor 1 |
| GGA2 | the **G**olgi-localised, **γ**-ear containing, **A**DP-ribosylation factor binding protein 2 |
| GlcCer | glucosylceramide |
| HCV | Hepatitis C virus |
| Hom2 | homology region 2 |
| ILVs | intraluminal vesicles |
| Ins(1,4,5)$P_3$/$IP_3$ | inositol (1,4,5) trisphosphate |
| IRES | internal ribosome entry site |
| Itch-E3 | E3 ubiquitin-protein ligase Itchy homolog |
| LCV | *Legionela*-containing vesicles |
| LIMP-2 | lysosomal integral membrane protein type 2 |

| | |
|---|---|
| LKU domain | lipid kinase unique domain |
| LRP6 | low-density lipoprotein receptor-related protein 6 |
| MD simulations | molecular dynamic simulations |
| MR-SAD | molecular replacement in combination with single wavelength anomalous dispersion |
| MTM | myotubularin lipid phosphatase |
| MTMT | myotubularin-related lipid phosphatase |
| MVBs | multivesicular bodies |
| MWs | membranous webs |
| NCS-1 | neuronal calcium sensor-1 |
| NES | nuclear export signals |
| NLS | nuclear localisation signal |
| NTR | non-translated region |
| ORF | open reading frame |
| ORPL | OSBP-related protein like |
| OSBP | oxysterol-binding protein |
| PA | phosphatidic acid |
| PH domain | pleckstrin homology domain |
| PI4K | phosphatidylinositol 4-kinase |
| PI5PK / PIKfyve | phosphatidylinositol-3-phosphate 5-kinase |
| PKD | protein kinase D |
| PLC | phospholipase C |
| PM | plasma membrane |
| PS | phosphatidylserine |
| PtdIns | phosphatidylinositol |
| PtdIns4P | phosphatidylinositol 4-phosphate |
| PX domain | Phox homology domain |
| Rab11a | Ras-related protein Rab11a |
| RdRp 3Dpol | RNA-dependent RNA-polymerase 3D |
| Sac1/Sac2 | Suppressor of actin mutations 1/2 |
| SH3 domain | SRC homology 3 domain |
| siRNA | small interfering RNA |
| SidC | synonym to interaptin |
| SidM | synonym to DrrA, Defect in Rab1 recruitment protein A |

| | |
|---|---|
| SM | sphingomyelin |
| TfR | transferrin receptor |
| TGN | *trans*-Golgi network |
| VAMP | (vesicle-associated membrane protein) associated protein-A |
| Wnt | results from a fusion of the name of the Drosophila segment polarity gene *wingless* and the name of the vertebrate homolog, *integrated or int-1* |
| +RNA | plus sense single strand RNA |

# References


1. Micheva KD (2001) Regulation of presynaptic phosphatidylinositol 4,5-biphosphate by neuronal activity. *J Cell Biol* **154**: 355–368.
2. Holz RW, Hlubek MD, Sorensen SD, Fisher SK, Balla T, Ozaki S, Prestwich GD, Stuenkel EL, Bittner MA (2000) A Pleckstrin Homology Domain Specific for Phosphatidylinositol 4,5-Bisphosphate (PtdIns-4,5-P2) and Fused to Green Fluorescent Protein Identifies Plasma Membrane PtdIns-4,5-P2 as Being Important in Exocytosis. *J Biol Chem* **275**: 17878–17885.
3. Ellson CD, Anderson KE, Morgan G, Chilvers ER, Lipp P, Stephens LR, Hawkins PT (2001) Phosphatidylinositol 3-phosphate is generated in phagosomal membranes. *Curr Biol CB* **11**: 1631–1635.
4. Burd CG, Emr SD (1998) Phosphatidylinositol(3)-phosphate signaling mediated by specific binding to RING FYVE domains. *Mol Cell* **2**: 157–162.
5. Balla T, Varnai P (2002) Visualizing Cellular Phosphoinositide Pools with GFP-Fused Protein-Modules. *Sci Signal* **2002**: pl3–pl3.
6. Levine TP, Munro S (2002) Targeting of Golgi-Specific Pleckstrin Homology Domains Involves Both PtdIns 4-Kinase-Dependent and -Independent Components. *Curr Biol* **12**: 695–704.
7. Shisheva A, Rusin B, Ikonomov OC, DeMarco C, Sbrissa D (2001) Localization and insulin-regulated relocation of phosphoinositide 5-kinase PIKfyve in 3T3-L1 adipocytes. *J Biol Chem* **276**: 11859–11869.
8. Krauß M, Haucke V (2007) Phosphoinositides: Regulators of membrane traffic and protein function. *FEBS Lett* **581**: 2105–2111.
9. Brombacher E, Urwyler S, Ragaz C, Weber SS, Kami K, Overduin M, Hilbi H (2009) Rab1 Guanine Nucleotide Exchange Factor SidM Is a Major Phosphatidylinositol 4-Phosphate-binding Effector Protein of Legionella pneumophila. *J Biol Chem* **284**: 4846–4856.
10. Weber SS, Ragaz C, Reus K, Nyfeler Y, Hilbi H (2006) Legionella pneumophila exploits PI(4)P to anchor secreted effector proteins to the replicative vacuole. *PLoS Pathog* **2**: e46.
11. DiNitto JP, Cronin TC, Lambright DG (2003) Membrane recognition and targeting by lipid-binding domains. *Sci STKE Signal Transduct Knowl Environ* **2003**: re16.
12. Roth MG (2004) Phosphoinositides in Constitutive Membrane Traffic. *Physiol Rev* **84**: 699–730.
13. Griffiths G, Simons K (1986) The trans Golgi network: sorting at the exit site of the Golgi complex. *Science* **234**: 438–443.
14. Nemoto Y, Kearns BG, Wenk MR, Chen H, Mori K, Alb JG, De Camilli P, Bankaitis VA (2000) Functional characterization of a mammalian Sac1 and mutants exhibiting substrate-specific defects in phosphoinositide phosphatase activity. *J Biol Chem* **275**: 34293–34305.
15. Cheong FY, Sharma V, Blagoveshchenskaya A, Oorschot VMJ, Brankatschk B, Klumperman J, Freeze HH, Mayinger P (2010) Spatial regulation of Golgi phosphatidylinositol-4-phosphate is required for enzyme localization and glycosylation fidelity. *Traffic Cph Den* **11**: 1180–1190.
16. Whitters EA, Cleves AE, McGee TP, Skinner HB, Bankaitis VA (1993) SAC1p is an integral membrane protein that influences the cellular requirement for phospholipid transfer protein function and inositol in yeast. *J Cell Biol* **122**: 79–94.
17. Liu Y, Boukhelifa M, Tribble E, Morin-Kensicki E, Uetrecht A, Bear JE, Bankaitis VA (2008) The Sac1 phosphoinositide phosphatase regulates Golgi membrane

morphology and mitotic spindle organization in mammals. *Mol Biol Cell* **19**: 3080–3096.
18. Hanada K, Kumagai K, Tomishige N, Yamaji T (2009) CERT-mediated trafficking of ceramide. *Biochim Biophys Acta* **1791**: 684–691.
19. Kawano M, Kumagai K, Nishijima M, Hanada K (2006) Efficient trafficking of ceramide from the endoplasmic reticulum to the Golgi apparatus requires a VAMP-associated protein-interacting FFAT motif of CERT. *J Biol Chem* **281**: 30279–30288.
20. Hanada K, Kumagai K, Yasuda S, Miura Y, Kawano M, Fukasawa M, Nishijima M (2003) Molecular machinery for non-vesicular trafficking of ceramide. *Nature* **426**: 803–809.
21. Fugmann T, Hausser A, Schöffler P, Schmid S, Pfizenmaier K, Olayioye MA (2007) Regulation of secretory transport by protein kinase D-mediated phosphorylation of the ceramide transfer protein. *J Cell Biol* **178**: 15–22.
22. D'Angelo G, Polishchuk E, Di Tullio G, Santoro M, Di Campli A, Godi A, West G, Bielawski J, Chuang C-C, van der Spoel AC, et al. (2007) Glycosphingolipid synthesis requires FAPP2 transfer of glucosylceramide. *Nature* **449**: 62–67.
23. Godi A, Di Campli A, Konstantakopoulos A, Di Tullio G, Alessi DR, Kular GS, Daniele T, Marra P, Lucocq JM, De Matteis MA (2004) FAPPs control Golgi-to-cell-surface membrane traffic by binding to ARF and PtdIns(4)P. *Nat Cell Biol* **6**: 393–404.
24. Raychaudhuri S, Im YJ, Hurley JH, Prinz WA (2006) Nonvesicular sterol movement from plasma membrane to ER requires oxysterol-binding protein-related proteins and phosphoinositides. *J Cell Biol* **173**: 107–119.
25. Ngo M, Ridgway ND (2009) Oxysterol binding protein-related Protein 9 (ORP9) is a cholesterol transfer protein that regulates Golgi structure and function. *Mol Biol Cell* **20**: 1388–1399.
26. Mayinger P (2009) Regulation of Golgi function via phosphoinositide lipids. *Semin Cell Dev Biol* **20**: 793–800.
27. Wang YJ, Wang J, Sun HQ, Martinez M, Sun YX, Macia E, Kirchhausen T, Albanesi JP, Roth MG, Yin HL (2003) Phosphatidylinositol 4 phosphate regulates targeting of clathrin adaptor AP-1 complexes to the Golgi. *Cell* **114**: 299–310.
28. Odorizzi G, Babst M, Emr SD (2000) Phosphoinositide signaling and the regulation of membrane trafficking in yeast. *Trends Biochem Sci* **25**: 229–235.
29. Ortiz D, Medkova M, Walch-Solimena C, Novick P (2002) Ypt32 recruits the Sec4p guanine nucleotide exchange factor, Sec2p, to secretory vesicles; evidence for a Rab cascade in yeast. *J Cell Biol* **157**: 1005–1015.
30. Mizuno-Yamasaki E, Medkova M, Coleman J, Novick P (2010) Phosphatidylinositol 4-phosphate controls both membrane recruitment and a regulatory switch of the Rab GEF Sec2p. *Dev Cell* **18**: 828–840.
31. Santiago-Tirado FH, Legesse-Miller A, Schott D, Bretscher A (2011) PI4P and Rab inputs collaborate in myosin-V-dependent transport of secretory compartments in yeast. *Dev Cell* **20**: 47–59.
32. Medkova M, France YE, Coleman J, Novick P (2006) The rab exchange factor Sec2p reversibly associates with the exocyst. *Mol Biol Cell* **17**: 2757–2769.
33. Cao X, Coskun U, Rössle M, Buschhorn SB, Grzybek M, Dafforn TR, Lenoir M, Overduin M, Simons K (2009) Golgi protein FAPP2 tubulates membranes. *Proc Natl Acad Sci U S A* **106**: 21121–21125.

34. Ren X, Farías GG, Canagarajah BJ, Bonifacino JS, Hurley JH (2013) Structural basis for recruitment and activation of the AP-1 clathrin adaptor complex by Arf1. *Cell* **152**: 755–767.
35. Demmel L, Gravert M, Ercan E, Habermann B, Müller-Reichert T, Kukhtina V, Haucke V, Baust T, Sohrmann M, Kalaidzidis Y, et al. (2008) The clathrin adaptor Gga2p is a phosphatidylinositol 4-phosphate effector at the Golgi exit. *Mol Biol Cell* **19**: 1991–2002.
36. Wang J, Sun H-Q, Macia E, Kirchhausen T, Watson H, Bonifacino JS, Yin HL (2007) PI4P promotes the recruitment of the GGA adaptor proteins to the trans-Golgi network and regulates their recognition of the ubiquitin sorting signal. *Mol Biol Cell* **18**: 2646–2655.
37. Hurley JH, Boura E, Carlson L-A, Różycki B (2010) Membrane Budding. *Cell* **143**: 875–887.
38. Muthusamy B-P, Natarajan P, Zhou X, Graham TR (2009) Linking phospholipid flippases to vesicle-mediated protein transport. *Biochim Biophys Acta* **1791**: 612–619.
39. Natarajan P, Liu K, Patil DV, Sciorra VA, Jackson CL, Graham TR (2009) Regulation of a Golgi flippase by phosphoinositides and an ArfGEF. *Nat Cell Biol* **11**: 1421–1426.
40. Lenoir M, Coskun Ü, Grzybek M, Cao X, Buschhorn SB, James J, Simons K, Overduin M (2010) Structural basis of wedging the Golgi membrane by FAPP pleckstrin homology domains. *EMBO Rep* **11**: 279–284.
41. Berridge MJ, Irvine RF (1984) Inositol trisphosphate, a novel second messenger in cellular signal transduction. *Nature* **312**: 315–321.
42. Berridge MJ, Irvine RF (1989) Inositol phosphates and cell signalling. *Nature* **341**: 197–205.
43. Orrenius S, Zhivotovsky B, Nicotera P (2003) Calcium: Regulation of cell death: the calcium–apoptosis link. *Nat Rev Mol Cell Biol* **4**: 552–565.
44. Boni LT, Rando RR (1985) The nature of protein kinase C activation by physically defined phospholipid vesicles and diacylglycerols. *J Biol Chem* **260**: 10819–10825.
45. Madison DV, Malenka RC, Nicoll RA (1986) Phorbol esters block a voltage-sensitive chloride current in hippocampal pyramidal cells. *Nature* **321**: 695–697.
46. Stefan CJ, Manford AG, Baird D, Yamada-Hanff J, Mao Y, Emr SD (2011) Osh proteins regulate phosphoinositide metabolism at ER-plasma membrane contact sites. *Cell* **144**: 389–401.
47. Balla A, Tuymetova G, Tsiomenko A, Várnai P, Balla T (2005) A plasma membrane pool of phosphatidylinositol 4-phosphate is generated by phosphatidylinositol 4-kinase type-III alpha: studies with the PH domains of the oxysterol binding protein and FAPP1. *Mol Biol Cell* **16**: 1282–1295.
48. Ketel K, Krauss M, Nicot A-S, Puchkov D, Wieffer M, Müller R, Subramanian D, Schultz C, Laporte J, Haucke V (2016) A phosphoinositide conversion mechanism for exit from endosomes. *Nature* **529**: 408–412.
49. Hartwig JH, Bokoch GM, Carpenter CL, Janmey PA, Taylor LA, Toker A, Stossel TP (1995) Thrombin receptor ligation and activated Rac uncap actin filament barbed ends through phosphoinositide synthesis in permeabilized human platelets. *Cell* **82**: 643–653.
50. Lodish HF, ed. (2000) *Molecular cell biology*. W.H. Freeman, New York.
51. Jost M, Simpson F, Kavran JM, Lemmon MA, Schmid SL (1998) Phosphatidylinositol-4,5-bisphosphate is required for endocytic coated vesicle formation. *Curr Biol CB* **8**: 1399–1402.

52. Mao Y, Chen J, Maynard JA, Zhang B, Quiocho FA (2001) A novel all helix fold of the AP180 amino-terminal domain for phosphoinositide binding and clathrin assembly in synaptic vesicle endocytosis. *Cell* **104**: 433–440.
53. Ford MG, Pearse BM, Higgins MK, Vallis Y, Owen DJ, Gibson A, Hopkins CR, Evans PR, McMahon HT (2001) Simultaneous binding of PtdIns(4,5)P2 and clathrin by AP180 in the nucleation of clathrin lattices on membranes. *Science* **291**: 1051–1055.
54. Itoh T, Koshiba S, Kigawa T, Kikuchi A, Yokoyama S, Takenawa T (2001) Role of the ENTH domain in phosphatidylinositol-4,5-bisphosphate binding and endocytosis. *Science* **291**: 1047–1051.
55. Cremona O, Di Paolo G, Wenk MR, Lüthi A, Kim WT, Takei K, Daniell L, Nemoto Y, Shears SB, Flavell RA, et al. (1999) Essential role of phosphoinositide metabolism in synaptic vesicle recycling. *Cell* **99**: 179–188.
56. Hill E, van Der Kaay J, Downes CP, Smythe E (2001) The role of dynamin and its binding partners in coated pit invagination and scission. *J Cell Biol* **152**: 309–323.
57. Di Paolo G, De Camilli P (2006) Phosphoinositides in cell regulation and membrane dynamics. *Nature* **443**: 651–657.
58. Takasuga S, Sasaki T (2013) Phosphatidylinositol-3,5-bisphosphate: metabolism and physiological functions. *J Biochem (Tokyo)* **154**: 211–218.
59. Balla T (2016) Cell biology: Lipid code for membrane recycling. *Nature* **529**: 292–293.
60. Wang H, Sun H-Q, Zhu X, Zhang L, Albanesi J, Levine B, Yin H (2015) GABARAPs regulate PI4P-dependent autophagosome:lysosome fusion. *Proc Natl Acad Sci U S A* **112**: 7015–7020.
61. Mizushima N, Komatsu M (2011) Autophagy: renovation of cells and tissues. *Cell* **147**: 728–741.
62. Singh R, Cuervo AM (2011) Autophagy in the cellular energetic balance. *Cell Metab* **13**: 495–504.
63. Knævelsrud H, Simonsen A (2012) Lipids in autophagy: Constituents, signaling molecules and cargo with relevance to disease. *Biochim Biophys Acta BBA - Mol Cell Biol Lipids* **1821**: 1133–1145.
64. Mizushima N (2007) Autophagy: process and function. *Genes Dev* **21**: 2861–2873.
65. Hamasaki M, Shibutani ST, Yoshimori T (2013) Up-to-date membrane biogenesis in the autophagosome formation. *Curr Opin Cell Biol* **25**: 455–460.
66. Graef M, Friedman JR, Graham C, Babu M, Nunnari J (2013) ER exit sites are physical and functional core autophagosome biogenesis components. *Mol Biol Cell* **24**: 2918–2931.
67. Carlos Martín Zoppino F, Damián Militello R, Slavin I, Álvarez C, Colombo MI (2010) Autophagosome Formation Depends on the Small GTPase Rab1 and Functional ER Exit Sites. *Traffic* **11**: 1246–1261.
68. Axe EL, Walker SA, Manifava M, Chandra P, Roderick HL, Habermann A, Griffiths G, Ktistakis NT (2008) Autophagosome formation from membrane compartments enriched in phosphatidylinositol 3-phosphate and dynamically connected to the endoplasmic reticulum. *J Cell Biol* **182**: 685–701.
69. Teter SA, Eggerton KP, Scott SV, Kim J, Fischer AM, Klionsky DJ (2001) Degradation of Lipid Vesicles in the Yeast Vacuole Requires Function of Cvt17, a Putative Lipase. *J Biol Chem* **276**: 2083–2087.
70. Anding AL, Baehrecke EH (2015) Autophagy in Cell Life and Cell Death. *Curr Top Dev Biol* **114**: 67–91.

71. Shibutani ST, Yoshimori T (2014) A current perspective of autophagosome biogenesis. *Cell Res* **24**: 58–68.
72. Méresse S, Steele-Mortimer O, Moreno E, Desjardins M, Finlay B, Gorvel JP (1999) Controlling the maturation of pathogen-containing vacuoles: a matter of life and death. *Nat Cell Biol* **1**: E183–E188.
73. Büttner D, Bonas U (2002) Port of entry--the type III secretion translocon. *Trends Microbiol* **10**: 186–192.
74. Ireton K, Payrastre B, Cossart P (1999) The Listeria monocytogenes protein InlB is an agonist of mammalian phosphoinositide 3-kinase. *J Biol Chem* **274**: 17025–17032.
75. Pizarro-Cerdá J, Payrastre B, Wang Y-J, Veiga E, Yin HL, Cossart P (2007) Type II phosphatidylinositol 4-kinases promote Listeria monocytogenes entry into target cells. *Cell Microbiol* **9**: 2381–2390.
76. Kagan JC, Roy CR (2002) Legionella phagosomes intercept vesicular traffic from endoplasmic reticulum exit sites. *Nat Cell Biol* **4**: 945–954.
77. Luo X, Wasilko DJ, Liu Y, Sun J, Wu X, Luo Z-Q, Mao Y (2015) Structure of the Legionella Virulence Factor, SidC Reveals a Unique PI(4)P-Specific Binding Domain Essential for Its Targeting to the Bacterial Phagosome. *PLoS Pathog* **11**: e1004965.
78. Szentpetery Z, Szakacs G, Bojjireddy N, Tai AW, Balla T (2011) Genetic and functional studies of phosphatidyl-inositol 4-kinase type IIIα. *Biochim Biophys Acta* **1811**: 476–483.
79. Wong K, Cantley LC (1994) Cloning and characterization of a human phosphatidylinositol 4-kinase. *J Biol Chem* **269**: 28878–28884.
80. Nakagawa T, Goto K, Kondo H (1996) Cloning, expression, and localization of 230-kDa phosphatidylinositol 4-kinase. *J Biol Chem* **271**: 12088–12094.
81. Balla A, Kim YJ, Varnai P, Szentpetery Z, Knight Z, Shokat KM, Balla T (2008) Maintenance of hormone-sensitive phosphoinositide pools in the plasma membrane requires phosphatidylinositol 4-kinase IIIalpha. *Mol Biol Cell* **19**: 711–721.
82. Nakatsu F, Baskin JM, Chung J, Tanner LB, Shui G, Lee SY, Pirruccello M, Hao M, Ingolia NT, Wenk MR, et al. (2012) PtdIns4P synthesis by PI4KIIIα at the plasma membrane and its impact on plasma membrane identity. *J Cell Biol* **199**: 1003–1016.
83. Baird D, Stefan C, Audhya A, Weys S, Emr SD (2008) Assembly of the PtdIns 4-kinase Stt4 complex at the plasma membrane requires Ypp1 and Efr3. *J Cell Biol* **183**: 1061–1074.
84. Kakuk A, Friedländer E, Vereb G, Kása A, Balla A, Balla T, Heilmeyer LMG, Gergely P, Vereb G (2006) Nucleolar localization of phosphatidylinositol 4-kinase PI4K230 in various mammalian cells. *Cytom Part J Int Soc Anal Cytol* **69**: 1174–1183.
85. Kakuk A, Friedländer E, Vereb G, Lisboa D, Bagossi P, Tóth G, Gergely P, Vereb G (2008) Nuclear and nucleolar localization signals and their targeting function in phosphatidylinositol 4-kinase PI4K230. *Exp Cell Res* **314**: 2376–2388.
86. Balla A, Vereb G, Gülkan H, Gehrmann T, Gergely P, Heilmeyer LM, Antal M (2000) Immunohistochemical localisation of two phosphatidylinositol 4-kinase isoforms, PI4K230 and PI4K92, in the central nervous system of rats. *Exp Brain Res* **134**: 279–288.
87. Baumlova A, Chalupska D, Różycki B, Jovic M, Wisniewski E, Klima M, Dubankova A, Kloer DP, Nencka R, Balla T, et al. (2014) The crystal structure of the phosphatidylinositol 4-kinase IIα. *EMBO Rep* **15**: 1085–1092.

88. Klima M, Baumlova A, Chalupska D, Hřebabecký H, Dejmek M, Nencka R, Boura E (2015) The high-resolution crystal structure of phosphatidylinositol 4-kinase IIβ and the crystal structure of phosphatidylinositol 4-kinase IIα containing a nucleoside analogue provide a structural basis for isoform-specific inhibitor design. *Acta Crystallogr D Biol Crystallogr* **71**: 1555–1563.
89. Zhou Q, Li J, Yu H, Zhai Y, Gao Z, Liu Y, Pang X, Zhang L, Schulten K, Sun F, et al. (2014) Molecular insights into the membrane-associated phosphatidylinositol 4-kinase IIα. *Nat Commun* **5**: 3552.
90. Gehrmann T, Heilmeyer LM (1998) Phosphatidylinositol 4-kinases. *Eur J Biochem FEBS* **253**: 357–370.
91. Cohen GB, Ren R, Baltimore D (1995) Modular binding domains in signal transduction proteins. *Cell* **80**: 237–248.
92. Heilmeyer LMG, Vereb G, Vereb G, Kakuk A, Szivák I (2003) Mammalian phosphatidylinositol 4-kinases. *IUBMB Life* **55**: 59–65.
93. Harak C, Radujkovic D, Taveneau C, Reiss S, Klein R, Bressanelli S, Lohmann V (2014) Mapping of Functional Domains of the Lipid Kinase Phosphatidylinositol 4-Kinase Type III Alpha Involved in Enzymatic Activity and Hepatitis C Virus Replication. *J Virol* **88**: 9909–9926.
94. Balla A, Tuymetova G, Toth B, Szentpetery Z, Zhao X, Knight ZA, Shokat K, Steinbach PJ, Balla T (2008) Design of drug-resistant alleles of type-III phosphatidylinositol 4-kinases using mutagenesis and molecular modeling. *Biochemistry (Mosc)* **47**: 1599–1607.
95. Wong K, Meyers ddR null, Cantley LC (1997) Subcellular locations of phosphatidylinositol 4-kinase isoforms. *J Biol Chem* **272**: 13236–13241.
96. Shoji-Kawaguchi M, Izuta S, Tamiya-Koizumi K, Suzuki M, Yoshida S (1995) Selective inhibition of DNA polymerase epsilon by phosphatidylinositol. *J Biochem (Tokyo)* **117**: 1095–1099.
97. Moradpour D, Penin F, Rice CM (2007) Replication of hepatitis C virus. *Nat Rev Microbiol* **5**: 453–463.
98. Tsukiyama-Kohara K, Iizuka N, Kohara M, Nomoto A (1992) Internal ribosome entry site within hepatitis C virus RNA. *J Virol* **66**: 1476–1483.
99. Henke JI, Goergen D, Zheng J, Song Y, Schüttler CG, Fehr C, Jünemann C, Niepmann M (2008) microRNA-122 stimulates translation of hepatitis C virus RNA. *EMBO J* **27**: 3300–3310.
100. Jopling CL, Yi M, Lancaster AM, Lemon SM, Sarnow P (2005) Modulation of hepatitis C virus RNA abundance by a liver-specific MicroRNA. *Science* **309**: 1577–1581.
101. Hijikata M, Kato N, Ootsuyama Y, Nakagawa M, Shimotohno K (1991) Gene mapping of the putative structural region of the hepatitis C virus genome by in vitro processing analysis. *Proc Natl Acad Sci U S A* **88**: 5547–5551.
102. Dubuisson J (2007) Hepatitis C virus proteins. *World J Gastroenterol* **13**: 2406–2415.
103. Lee C (2012) Roles of phosphoinositides and phosphoinositides kinases in hepatitis C virus RNA replication. *Arch Pharm Res* **35**: 1701–1711.
104. Lindenbach BD, Rice CM (2005) Unravelling hepatitis C virus replication from genome to function. *Nature* **436**: 933–938.
105. Egger D, Wölk B, Gosert R, Bianchi L, Blum HE, Moradpour D, Bienz K (2002) Expression of hepatitis C virus proteins induces distinct membrane alterations including a candidate viral replication complex. *J Virol* **76**: 5974–5984.

106. Gosert R, Egger D, Lohmann V, Bartenschlager R, Blum HE, Bienz K, Moradpour D (2003) Identification of the Hepatitis C Virus RNA Replication Complex in Huh-7 Cells Harboring Subgenomic Replicons. *J Virol* **77**: 5487–5492.
107. Hsu N-Y, Ilnytska O, Belov G, Santiana M, Chen Y-H, Takvorian PM, Pau C, van der Schaar H, Kaushik-Basu N, Balla T, et al. (2010) Viral reorganization of the secretory pathway generates distinct organelles for RNA replication. *Cell* **141**: 799–811.
108. Reiss S, Rebhan I, Backes P, Romero-Brey I, Erfle H, Matula P, Kaderali L, Poenisch M, Blankenburg H, Hiet M-S, et al. (2011) Recruitment and activation of a lipid kinase by hepatitis C virus NS5A is essential for integrity of the membranous replication compartment. *Cell Host Microbe* **9**: 32–45.
109. Tai AW, Salloum S (2011) The role of the phosphatidylinositol 4-kinase PI4KA in hepatitis C virus-induced host membrane rearrangement. *PloS One* **6**: e26300.
110. Quinkert D, Bartenschlager R, Lohmann V (2005) Quantitative Analysis of the Hepatitis C Virus Replication Complex. *J Virol* **79**: 13594–13605.
111. Berger KL, Kelly SM, Jordan TX, Tartell MA, Randall G (2011) Hepatitis C virus stimulates the phosphatidylinositol 4-kinase III alpha-dependent phosphatidylinositol 4-phosphate production that is essential for its replication. *J Virol* **85**: 8870–8883.
112. Berger KL, Cooper JD, Heaton NS, Yoon R, Oakland TE, Jordan TX, Mateu G, Grakoui A, Randall G (2009) Roles for endocytic trafficking and phosphatidylinositol 4-kinase III alpha in hepatitis C virus replication. *Proc Natl Acad Sci U S A* **106**: 7577–7582.
113. Roulin PS, Lötzerich M, Torta F, Tanner LB, van Kuppeveld FJM, Wenk MR, Greber UF (2014) Rhinovirus uses a phosphatidylinositol 4-phosphate/cholesterol counter-current for the formation of replication compartments at the ER-Golgi interface. *Cell Host Microbe* **16**: 677–690.
114. May ER, Narang A, Kopelevich DI (2007) Role of molecular tilt in thermal fluctuations of lipid membranes. *Phys Rev E Stat Nonlin Soft Matter Phys* **76**: 021913.
115. den Boon JA, Ahlquist P (2010) Organelle-like membrane compartmentalization of positive-strand RNA virus replication factories. *Annu Rev Microbiol* **64**: 241–256.
116. Vaillancourt FH, Brault M, Pilote L, Uyttersprot N, Gaillard ET, Stoltz JH, Knight BL, Pantages L, McFarland M, Breitfelder S, et al. (2012) Evaluation of Phosphatidylinositol-4-Kinase III as a Hepatitis C Virus Drug Target. *J Virol* **86**: 11595–11607.
117. Borawski J, Troke P, Puyang X, Gibaja V, Zhao S, Mickanin C, Leighton-Davies J, Wilson CJ, Myer V, Cornellataracido I, et al. (2009) Class III phosphatidylinositol 4-kinase alpha and beta are novel host factor regulators of hepatitis C virus replication. *J Virol* **83**: 10058–10074.
118. Tai AW, Benita Y, Peng LF, Kim S-S, Sakamoto N, Xavier RJ, Chung RT (2009) A functional genomic screen identifies cellular cofactors of hepatitis C virus replication. *Cell Host Microbe* **5**: 298–307.
119. Trotard M, Lepère-Douard C, Régeard M, Piquet-Pellorce C, Lavillette D, Cosset F-L, Gripon P, Le Seyec J (2009) Kinases required in hepatitis C virus entry and replication highlighted by small interference RNA screening. *FASEB J Off Publ Fed Am Soc Exp Biol* **23**: 3780–3789.
120. Ahn J, Chung K-S, Kim D-U, Won M, Kim L, Kim K-S, Nam M, Choi S-J, Kim H-C, Yoon M, et al. (2004) Systematic identification of hepatocellular proteins interacting with NS5A of the hepatitis C virus. *J Biochem Mol Biol* **37**: 741–748.

121. Reiss S, Harak C, Romero-Brey I, Radujkovic D, Klein R, Ruggieri A, Rebhan I, Bartenschlager R, Lohmann V (2013) The lipid kinase phosphatidylinositol-4 kinase III alpha regulates the phosphorylation status of hepatitis C virus NS5A. *PLoS Pathog* **9**: e1003359.
122. Lim Y-S, Hwang SB (2011) Hepatitis C virus NS5A protein interacts with phosphatidylinositol 4-kinase type IIIalpha and regulates viral propagation. *J Biol Chem* **286**: 11290–11298.
123. Shepard CW, Finelli L, Alter MJ (2005) Global epidemiology of hepatitis C virus infection. *Lancet Infect Dis* **5**: 558–567.
124. Meyers R, Cantley LC (1997) Cloning and characterization of a wortmannin-sensitive human phosphatidylinositol 4-kinase. *J Biol Chem* **272**: 4384–4390.
125. Balla T, Downing GJ, Jaffe H, Kim S, Zólyomi A, Catt KJ (1997) Isolation and molecular cloning of wortmannin-sensitive bovine type III phosphatidylinositol 4-kinases. *J Biol Chem* **272**: 18358–18366.
126. Saito T, Seki N, Ishii H, Ohira M, Hayashi A, Kozuma S, Hori T (1997) Complementary DNA cloning and chromosomal mapping of a novel phosphatidylinositol kinase gene. *DNA Res Int J Rapid Publ Rep Genes Genomes* **4**: 301–305.
127. Suzuki K, Hirano H, Okutomi K, Suzuki M, Kuga Y, Fujiwara T, Kanemoto N, Isono K, Horie M (1997) Identification and characterization of a novel human phosphatidylinositol 4-kinase. *DNA Res Int J Rapid Publ Rep Genes Genomes* **4**: 273–280.
128. Godi A, Pertile P, Meyers R, Marra P, Di Tullio G, Iurisci C, Luini A, Corda D, De Matteis MA (1999) ARF mediates recruitment of PtdIns-4-OH kinase-beta and stimulates synthesis of PtdIns(4,5)P2 on the Golgi complex. *Nat Cell Biol* **1**: 280–287.
129. Weisz OA, Gibson GA, Leung SM, Roder J, Jeromin A (2000) Overexpression of frequenin, a modulator of phosphatidylinositol 4-kinase, inhibits biosynthetic delivery of an apical protein in polarized madin-darby canine kidney cells. *J Biol Chem* **275**: 24341–24347.
130. Hilfiker S (2003) Neuronal calcium sensor-1: a multifunctional regulator of secretion. *Biochem Soc Trans* **31**: 828–832.
131. Sasaki J, Ishikawa K, Arita M, Taniguchi K (2012) ACBD3-mediated recruitment of PI4KB to picornavirus RNA replication sites: Picornaviral protein/ACBD3/PI4KB complex. *EMBO J* **31**: 754–766.
132. Klima M, Tóth DJ, Hexnerova R, Baumlova A, Chalupska D, Tykvart J, Rezabkova L, Sengupta N, Man P, Dubankova A, et al. (2016) Structural insights and in vitro reconstitution of membrane targeting and activation of human PI4KB by the ACBD3 protein. *Sci Rep* **6**: 23641.
133. de Graaf P, Klapisz EE, Schulz TKF, Cremers AFM, Verkleij AJ, van Bergen en Henegouwen PMP (2002) Nuclear localization of phosphatidylinositol 4-kinase beta. *J Cell Sci* **115**: 1769–1775.
134. Balla A, Balla T (2006) Phosphatidylinositol 4-kinases: old enzymes with emerging functions. *Trends Cell Biol* **16**: 351–361.
135. Burke JE, Inglis AJ, Perisic O, Masson GR, McLaughlin SH, Rutaganira F, Shokat KM, Williams RL (2014) Structures of PI4KIIIβ complexes show simultaneous recruitment of Rab11 and its effectors. *Science* **344**: 1035–1038.
136. Ngo MH, Colbourne TR, Ridgway ND (2010) Functional implications of sterol transport by the oxysterol-binding protein gene family. *Biochem J* **429**: 13–24.

137. Hausser A, Storz P, Märtens S, Link G, Toker A, Pfizenmaier K (2005) Protein kinase D regulates vesicular transport by phosphorylating and activating phosphatidylinositol-4 kinase IIIβ at the Golgi complex. *Nat Cell Biol* **7**: 880–886.
138. Hausser A (2006) Phospho-specific binding of 14-3-3 proteins to phosphatidylinositol 4-kinase III protects from dephosphorylation and stabilizes lipid kinase activity. *J Cell Sci* **119**: 3613–3621.
139. Szivak I, Lamb N, Heilmeyer LMG (2006) Subcellular localization and structural function of endogenous phosphorylated phosphatidylinositol 4-kinase (PI4K92). *J Biol Chem* **281**: 16740–16749.
140. Yang N, Ma P, Lang J, Zhang Y, Deng J, Ju X, Zhang G, Jiang C (2012) Phosphatidylinositol 4-kinase IIIβ is required for severe acute respiratory syndrome coronavirus spike-mediated cell entry. *J Biol Chem* **287**: 8457–8467.
141. Arita M, Kojima H, Nagano T, Okabe T, Wakita T, Shimizu H (2011) Phosphatidylinositol 4-kinase III beta is a target of enviroxime-like compounds for antipoliovirus activity. *J Virol* **85**: 2364–2372.
142. Greninger AL, Knudsen GM, Betegon M, Burlingame AL, Derisi JL (2012) The 3A protein from multiple picornaviruses utilizes the golgi adaptor protein ACBD3 to recruit PI4KIIIβ. *J Virol* **86**: 3605–3616.
143. Wessels E, Duijsings D, Niu T-K, Neumann S, Oorschot VM, de Lange F, Lanke KHW, Klumperman J, Henke A, Jackson CL, et al. (2006) A Viral Protein that Blocks Arf1-Mediated COP-I Assembly by Inhibiting the Guanine Nucleotide Exchange Factor GBF1. *Dev Cell* **11**: 191–201.
144. Niu T-K, Pfeifer AC, Lippincott-Schwartz J, Jackson CL (2005) Dynamics of GBF1, a Brefeldin A-sensitive Arf1 exchange factor at the Golgi. *Mol Biol Cell* **16**: 1213–1222.
145. Altan-Bonnet N, Sougrat R, Lippincott-Schwartz J (2004) Molecular basis for Golgi maintenance and biogenesis. *Curr Opin Cell Biol* **16**: 364–372.
146. Sohda M, Misumi Y, Fujiwara T, Nishioka M, Ikehara Y (1994) Molecular cloning and sequence analysis of a human 372-kDA protein localized in the Golgi complex. *Biochem Biophys Res Commun* **205**: 1399–1408.
147. Delang L, Paeshuyse J, Neyts J (2012) The role of phosphatidylinositol 4-kinases and phosphatidylinositol 4-phosphate during viral replication. *Biochem Pharmacol* **84**: 1400–1408.
148. Balla A, Tuymetova G, Barshishat M, Geiszt M, Balla T (2002) Characterization of type II phosphatidylinositol 4-kinase isoforms reveals association of the enzymes with endosomal vesicular compartments. *J Biol Chem* **277**: 20041–20050.
149. Minogue S, Anderson JS, Waugh MG, dos Santos M, Corless S, Cramer R, Hsuan JJ (2001) Cloning of a human type II phosphatidylinositol 4-kinase reveals a novel lipid kinase family. *J Biol Chem* **276**: 16635–16640.
150. Han G-S, Audhya A, Markley DJ, Emr SD, Carman GM (2002) The Saccharomyces cerevisiae LSB6 gene encodes phosphatidylinositol 4-kinase activity. *J Biol Chem* **277**: 47709–47718.
151. Mueller-Roeber B, Pical C (2002) Inositol phospholipid metabolism in Arabidopsis. Characterized and putative isoforms of inositol phospholipid kinase and phosphoinositide-specific phospholipase C. *Plant Physiol* **130**: 22–46.
152. Flanagan CA, Schnieders EA, Emerick AW, Kunisawa R, Admon A, Thorner J (1993) Phosphatidylinositol 4-kinase: gene structure and requirement for yeast cell viability. *Science* **262**: 1444–1448.

153. Garcia-Bustos JF, Marini F, Stevenson I, Frei C, Hall MN (1994) PIK1, an essential phosphatidylinositol 4-kinase associated with the yeast nucleus. *EMBO J* **13**: 2352–2361.
154. Cutler NS, Heitman J, Cardenas ME (1997) STT4 is an essential phosphatidylinositol 4-kinase that is a target of wortmannin in Saccharomyces cerevisiae. *J Biol Chem* **272**: 27671–27677.
155. Barylko B, Gerber SH, Binns DD, Grichine N, Khvotchev M, Südhof TC, Albanesi JP (2001) A novel family of phosphatidylinositol 4-kinases conserved from yeast to humans. *J Biol Chem* **276**: 7705–7708.
156. Jung G, Wang J, Wlodarski P, Barylko B, Binns DD, Shu H, Yin HL, Albanesi JP (2008) Molecular determinants of activation and membrane targeting of phosphoinositol 4-kinase IIbeta. *Biochem J* **409**: 501–509.
157. Wei YJ, Sun HQ, Yamamoto M, Wlodarski P, Kunii K, Martinez M, Barylko B, Albanesi JP, Yin HL (2002) Type II phosphatidylinositol 4-kinase beta is a cytosolic and peripheral membrane protein that is recruited to the plasma membrane and activated by Rac-GTP. *J Biol Chem* **277**: 46586–46593.
158. Barylko B, Wlodarski P, Binns DD, Gerber SH, Earnest S, Sudhof TC, Grichine N, Albanesi JP (2002) Analysis of the catalytic domain of phosphatidylinositol 4-kinase type II. *J Biol Chem* **277**: 44366–44375.
159. Craige B, Salazar G, Faundez V (2008) Phosphatidylinositol-4-kinase type II alpha contains an AP-3-sorting motif and a kinase domain that are both required for endosome traffic. *Mol Biol Cell* **19**: 1415–1426.
160. Minogue S, Waugh MG, De Matteis MA, Stephens DJ, Berditchevski F, Hsuan JJ (2006) Phosphatidylinositol 4-kinase is required for endosomal trafficking and degradation of the EGF receptor. *J Cell Sci* **119**: 571–581.
161. Salazar G, Craige B, Wainer BH, Guo J, De Camilli P, Faundez V (2005) Phosphatidylinositol-4-kinase type II alpha is a component of adaptor protein-3-derived vesicles. *Mol Biol Cell* **16**: 3692–3704.
162. Pan W, Choi S-C, Wang H, Qin Y, Volpicelli-Daley L, Swan L, Lucast L, Khoo C, Zhang X, Li L, et al. (2008) Wnt3a-mediated formation of phosphatidylinositol 4,5-bisphosphate regulates LRP6 phosphorylation. *Science* **321**: 1350–1353.
163. Qin Y, Li L, Pan W, Wu D (2009) Regulation of phosphatidylinositol kinases and metabolism by Wnt3a and Dvl. *J Biol Chem* **284**: 22544–22548.
164. Mössinger J, Wieffer M, Krause E, Freund C, Gerth F, Krauss M, Haucke V (2012) Phosphatidylinositol 4-kinase IIα function at endosomes is regulated by the ubiquitin ligase Itch. *EMBO Rep* **13**: 1087–1094.
165. Jović M, Kean MJ, Szentpetery Z, Polevoy G, Gingras A-C, Brill JA, Balla T (2012) Two phosphatidylinositol 4-kinases control lysosomal delivery of the Gaucher disease enzyme, β-glucocerebrosidase. *Mol Biol Cell* **23**: 1533–1545.
166. Jung G, Barylko B, Lu D, Shu H, Yin H, Albanesi JP (2011) Stabilization of phosphatidylinositol 4-kinase type IIbeta by interaction with Hsp90. *J Biol Chem* **286**: 12775–12784.
167. Lu D, Sun H, Wang H, Barylko B, Fukata Y, Fukata M, Albanesi JP, Yin HL (2012) Phosphatidylinositol 4-kinase IIα is palmitoylated by Golgi-localized palmitoyltransferases in cholesterol-dependent manner. *J Biol Chem* **287**: 21856–21865.
168. Wetzker R, Klinger R, Hsuan J, Fry MJ, Kauffmann-Zeh A, Müller E, Frunder H, Waterfield M (1991) Purification and characterization of phosphatidylinositol 4-kinase from human erythrocyte membranes. *Eur J Biochem FEBS* **200**: 179–185.

169. Kang MS, Baek S-H, Chun YS, Moore AZ, Landman N, Berman D, Yang HO, Morishima-Kawashima M, Osawa S, Funamoto S, et al. (2013) Modulation of lipid kinase PI4KIIα activity and lipid raft association of presenilin 1 underlies γ-secretase inhibition by ginsenoside (20S)-Rg3. *J Biol Chem* **288**: 20868–20882.
170. Wu B, Kitagawa K, Zhang N-Y, Liu B, Inagaki C (2004) Pathophysiological concentrations of amyloid beta proteins directly inhibit rat brain and recombinant human type II phosphatidylinositol 4-kinase activity. *J Neurochem* **91**: 1164–1170.

# List of figures

Figure 1.: Intracellular distribution of phosphoinositides in mammalian cells. ..... 10
Figure 2.: Schematic representation of PtdIns4P effectors..... 12
Figure 3.: Signal transduction into the cell. ..... 14
Figure 4.: Cartoon representation of an endocytosed receptor and its further derivatization into recycling or late endosomes. ..... 16
Figure 5.: Autolysosome formation. ..... 17
Figure 6.: Schematic representation of the predicted domain organisation of PI4K IIIα. .. 21
Figure 7.: Schematic representation of the HCV genome. ..... 23
Figure 8.: Schematic representation of the predicted domain organisation of PI4K IIIβ. .. 27
Figure 9.: The crystall structure of human PI4K IIIβ in complex with Rab 11a (Q70L)-GTPγS and inhibitor Pik93. ..... 27
Figure 10.: Schematic representation of different strategies to hijack human PI4 kinases type III. ..... 30
Figure 11.: The crystal structure of PI4K IIα..... 37
Figure 12.: Superposition of ATP binding sites and lateral hydrophobic pockets of PI4K IIα and IIβ. ..... 47
Figure 13.: Detailed view of the ATP binding site of PI4K IIα with bound inhibitor MD59 from a series of adenosine analogues. ..... 48
Figure 14.: The crystal structures of inhibitor 49 and ATP bound to PI4K IIIβ..... 60